IAEA
International Atomic Energy Agency

INDC(CCP)-0448
Distr. Web only

INDC International Nuclear Data Committee

Measurements of the neutron field characteristics inside and on the surface of the Pb target micromodel exposed to 0.8 GeV protons

Prepared by

Yu. E. Titarenko
Institute for Theoretical and Experimental Physics (ITEP)

Co-authors: V.F. Batyaev, V.M. Zhivun,
A.Yu. Titarenko, M.A. Butko, K.V. Pavlov, S.N. Florya
Institute for Theoretical and Experimental Physics (ITEP)
and
W. Gudowski
Kungliga Tekniska Högskolan, Lindstedtvgen 30, Stockholm, Sweden

October 2009

Selected INDC documents may be downloaded in electronic form from
http://www-nds.iaea.org/indc_sel.html or sent as an e-mail attachment.
Requests for hardcopy or e-mail transmittal should be directed to *services@iaeand.iaea.org*
or to:
Nuclear Data Section
International Atomic Energy Agency
Vienna International Centre
PO Box 100
A-1400 Vienna
Austria

Printed by the IAEA in Austria

October 2009

INDC(CCP)-0448
Distr. Web only

Measurements of the neutron field characteristics inside and on the surface of the Pb target micromodel exposed to 0.8 GeV protons

Prepared by
Yu.E. Titarenko
Institute for Theoretical and Experimental Physics (ITEP)
Co-authors: V.F. Batyaev, V.F. Batyaev, V.M. Zhivun,
A.Yu. Titarenko, M.A. Butko, K.V. Pavlov, S.N. Florya
Institute for Theoretical and Experimental Physics (ITEP)
and
W. Gudowski
Kungliga Tekniska Högskolan, Lindstedtvgen 30, Stockholm, Sweden

Abstract

The work presents the results of experimental determining the threshold reaction rates in 79 ^{209}Bi, ^{nat}Pb, ^{197}Au, ^{181}Ta, ^{169}Tm, ^{nat}In, ^{93}Nb, ^{64}Zn, ^{65}Cu, ^{63}Cu, ^{59}Co, ^{19}F, and ^{12}C samples and in 127 ^{27}Al samples. The samples are arranged along the proton beam axis inside and outside the collapsible 920-mm thick Pb target of 50-mm diameter. The target is assembled of 23 40-mm thick discs.

The samples are placed at 12 points on odd target discs to reproduce the longitudinal distributions of protons and neutrons along the target axis. The target was exposed for 18 hours to 800 MeV proton beam from the ITEP U-10 accelerator. The proton fluence and the proton beam shape are determined using ^{27}Al(p,x)^{22}Na and ^{27}Al(p,x)^{7}Be monitor reactions which were measured in three Al monitors. One of the monitors of 169.6-mm diameter is cut into 36 fragments. In all, (6.0±0.5)·1015 protons hit the target.

The reaction rates are determined by direct γ-spectrometry techniques. The measurements are made using a GC-2518 detector of 1.8 keV resolution and a DGDK-60V detector of 2.9 keV resolution in ^{60}Co 1332 keV ^{60}Co γ-line. The γ-lines measured are processed by the GENIE2000 code system. In all, 1196 γ-spectra have been measured and processed, and 2467 reaction rates determined (monitor reactions included).

The results obtained will be used to verify the transport codes and the databases used to design the Pb target units for ADS facilities.

October 2009

Title of the Project:	Experimental researches into nuclear-phesics chsracteristics of the materials that are of major importance in utilizing weapon plutonium and in transmuting radioactive wastes
Commencement Date:	1 April 2005
Duration:	24 months
Leading Institute:	Federal Nuclear Center of Russia – VNIIEF N.Novgorod region, 607188 Sarov, 34, Mira avenue +7 (83130)45373 rvg@vniief.ru
Participating Institutes:	State Scientific Center of Russian Federation - Institute for Theoretical and Experimental Physics Address: Bol'shaya Cheremushkinskaya Street, 25, 117218 Moscow +7 495 129 9691 director@itep.ru www.itep.ru
Foreign Collaborators:	Toshihiko Kawano, Mark Chadwick, Richard E. Prael MS B283, Los Alamos, NM 87545, США 505-664-0513 kawano@lanl.gov www.lanl.gov

Keywords: ADS facility, target, nuclear reaction, high-energy transport code

CONTENTS

I. Brief description of Workplan; aims of task 5; expected results, engineering approach to implementing the Workplan.

Task 5 of the Project is aimed at consistent studying the target characteristics of ADS intended for transmuting radioactive wastes.

Implementing the task will result in activation-aided determination of the threshold reaction rates in 92 ^{209}Bi, ^{nat}Pb, ^{197}Au, ^{181}Ta, ^{169}Tm, ^{nat}In, ^{93}Nb, ^{64}Zn, ^{65}Cu, ^{63}Cu, ^{59}Co, ^{19}F, and ^{12}C samples and in 121 ^{27}Al samples arranged along the proton beam axis inside and on the surface of the sectional 920-mm deep Pb target of a 150-mm diameter. The target has been assembled of 23 discs of 40-mm depth each.

The samples are positioned at 12 points on the target to reproduce the proton and neutron distributions along the target axis. In June, 2006, the target was exposed for 18 hours to a 800 MeV proton beam extracted from the ITEP U-10 accelerator. The proton fluence and the proton beam shape were determined via ^{27}Al(p,x)^{7}Be monitor reaction. In total, the target was exposed to $(6.0\pm0.5)\cdot10^{15}$ protons.

The reaction rates were determined by direct γ-spectrometry. The measurements were made using GC-2518 and DGDK-60V detectors of 1.8 and 2.9 keV resolution, respectively, in the 1332 keV ^{60}Co γ-line. The γ-spectra measured were processed by the GENIE -2000 code system. In total, 1196 γ-spectra have been measured and processed, and 2498 reaction (including monitor ones) rates determined.

The reaction rates measured were simulated by the MCNPX code using the ENDF/B6 database for 20-100 MeV neutrons together with the MENDL2 and MENDL2P databases for 20-100 MeV protons and neutrons. An acceptable agreement was found between the experimental and calculated data. Nevertheless, the subsequent researches must be aimed at improving the simulation of reproduction of secondary protons and high-energy neutrons, especially in the lateral and reverse directions with respect to the beam. The results must permit some conclusions concerning the validity of the transport codes and the databases used when designing the Pb target units for ADS facilities.

II. Tasking.

Conforming to the Project#2405 Workplan, Task 5 (Measurements of the neutron field characteristics inside and on the surface of the Pb or Pb-Bi target micromodel exposed to 0.6-1.2 GeV protons) involved

1. Manufacture of the target micromodel,
2. Mounting the target micromodel on the extracted proton beam,
3. A few runs of target micromodel exposures to 0.6-1.2 GeV protons,
4. Recording and analysing the γ-spectra,
5. Processing the measurement resuts.

Primarily, the activation detectors of the compositions employed earlier in Project#1145 to monitor the W-Na target exposed to 0.8 GeV protons (the ^{209}Bi, ^{197}Au, ^{181}Ta, ^{169}Tm, ^{nat}In, ^{93}Nb, ^{64}Zn, ^{65}Cu, ^{63}Cu, ^{59}Co, ^{19}F, and ^{12}C samples) were suggested to use. Under the reported Project, the proton energies were decided to preserve with the view to comparison between the sets of reaction rates obtained under the two Projects. Besides, the list of experimental samples was decided to extend by adding 12 ^{nat}Pb samples on the target surface. Besides, Pb was sampled at the central points of odd rulers. Measuring the resultant Pb samples permits the activation and the reaction rates to be estimated directly in the material of the lengthy Pb target. It should be noted, however, that the measurements of the said samples fall on the surface of the Workplan, so they were considered a lower priority compared with the planned sample measurements. As a result, the Pb data reported here may be but tentative and are aimed at appraising a feasibility of the full-scale measurements of the type.

III. Experimental study of the Pb target parameters.

3.1. Techniques for determining reaction rates.

Using the concepts of independent nuclide production rate R_i^{ind}, when a product (Z_1,A_1) is generated in a nuclear reaction, and of cumulative production rate R_i^{cum}, when a product (Z_2,A_2) is generated in all processes (in the course of both the reaction proper and the decays of its independently produced **precursors**, for example Z_1,A_1), they may be presented [1,2] as

$$R_i^{cum/ind} = \sigma_i^{cum/ind} \cdot \hat{\Phi} \qquad i=1,2,st \qquad (1)$$

where $\sigma_1^{cum/ind}$ and $\sigma_2^{cum/ind}$ are, respectively, cumulative and independent cross sections for production of nuclides N_1 and N_2, in experimental sample N_{Tag} exposed to protons or neutrons, [barn]; $\sigma_{st}^{cum/ind}$ are, respectively, cumulative and independent cross sections of the monitor reactions used to calculate the mean proton flux density [barn]; $\hat{\Phi}$ is the area- and time-averaged neutron or proton flux density [particle/(cm^2 s)].

The reaction rate definition (1) permits the double-link radioactive transformation chain under irradiation to be described by the set of differential equations

$$\begin{cases} \dfrac{dN_1(t)}{dt} = N_{Tag} \cdot R_1^{cum/ind} - \lambda_1 N_1(t), \\ \dfrac{dN_2(t)}{dt} = N_{Tag} \cdot R_2^{ind} + \upsilon_{1,2} \cdot \lambda_1 N_1(t) - \lambda_2 N_2(t), \end{cases} \qquad (2)$$

with initial conditions $N_1(0)=N_2(0)=0$. Here, $N_1(t)$, $N_2(t)$ are numbers of nuclei in an irradiated sample; $R_1^{cum/ind}$ and R_2^{ind} are, respectively, their cumulative and independent production rates; λ_1 and λ_2 are decay constants; $v_{1,2}$ is a probability for the 1st nuclide to turn into the 2nd nuclide; N_{Tag} is the number of nuclei of element ${}_Z^A Tag$ in an experimental sample; t is current time measured from the beginning to the end of irradiation.

The given experiments make use of the pulsed (i.e. cyclic) irradiation that consists of K pulses of duration τ and pulse repletion rate T each (see Fig. 1).

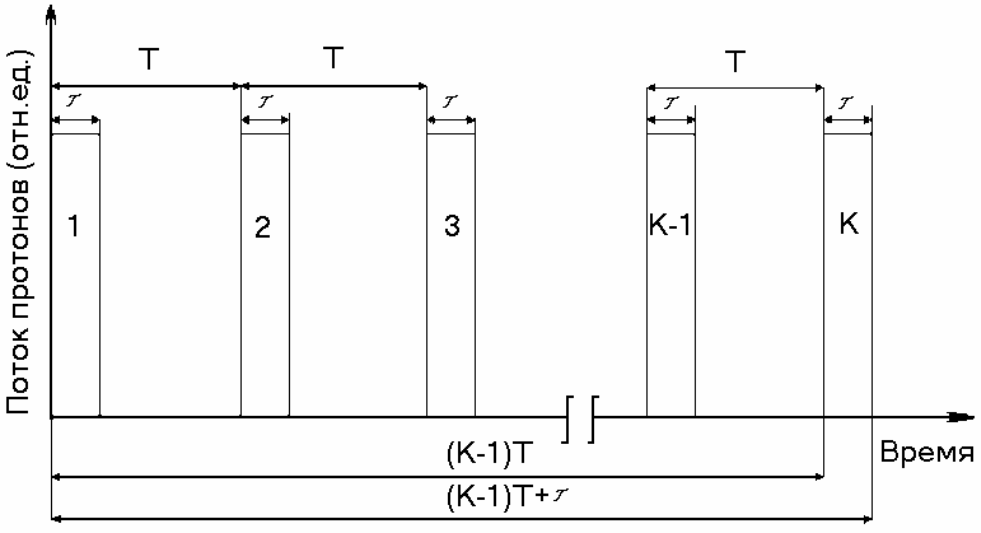

Fig. 1. Characteristics of the pulsed irradiation mode.

Solution for set (2) by the irradiation end moment $t_{irr}= (K-1)\cdot T+\tau$ can be presented as

$$\begin{cases} N_1 = ((K-1)\cdot T+\tau) = \dfrac{N_{Tag}\cdot R_1\cdot F_1}{\lambda_1} \\ N_2 = ((K-1)\cdot T+\tau) = N_{Tag}\cdot R_1\cdot \nu_1\cdot \dfrac{1}{\lambda_2-\lambda_1}\cdot F_1 + \dfrac{N_{Tag}}{\lambda_2}\cdot\left[R_2 - \dfrac{\lambda_1}{\lambda_2-\lambda_1}\cdot\nu_1\cdot R_1\right]\cdot F_2 \end{cases} \quad (3)$$

Irradiation having ended, the decays of the nuclides produced is described by the set

$$\begin{cases} \dfrac{dN_1}{dt} = -\lambda_1\cdot N_1(t) \\ \dfrac{dN_2}{dt} = \nu_1\cdot\lambda_1\cdot N_1(t) - \lambda_2\cdot N_2(t) \end{cases} \quad (4)$$

With initial conditions $N_1(0) = N_{1_0}$ и $N_2(0) = N_{2_0}$, where N_{1_0} and N_{2_0} are numbers of nuclei produced by the cooling start (irradiation end) moment: t is current time measured from irradiation end.

Solution for set (4) at any moment of the cooling time t is

$$\begin{cases} N_1(t) = N_{1_0}\cdot e^{-\lambda_1\cdot t} \\ N_2(t) = \dfrac{\lambda_1}{\lambda_2-\lambda_1}\cdot N_{1_0}\cdot\nu_{1,2}\cdot e^{-\lambda_1\cdot t} + \left(N_{2_0} + \dfrac{\lambda_1}{\lambda_1-\lambda_2}\cdot\nu_{1,2}\cdot N_{1_0}\right)\cdot e^{-\lambda_2\cdot t} \end{cases} \quad (5)$$

The reaction rates in the irradiated samples were measured by direct γ-spectroscopy without pre-separating them. The least squares technique was used to fit the measured dots of the decay curves of the 1st and 2nd nuclides by the cooling start (irradiation end) moment. The condition of equal numbers of nuclei of the 1st and 2nd nuclides in the samples irradiated by irradiation end moment and at cooling start moment permits the sought reaction rates to be inferred from (3) and (5) as

$$R_1^{cum/ind} = \frac{\hat{A}_1}{N_{Tag}\cdot\eta_1\cdot\varepsilon_1}\cdot\frac{1}{F_1} \quad (6)$$

$$R_1^{cum/ind} = \frac{\hat{A}_2^1}{N_{Tag}\cdot\eta_2\cdot\varepsilon_2\cdot\nu_{12}}\cdot\frac{\lambda_2-\lambda_1}{\lambda_2}\cdot\frac{1}{F_1} \quad (7),$$

$$R_2^{ind} = \left(\frac{\hat{A}_2^2}{F_2} + \frac{\hat{A}_2^1}{F_1}\cdot\frac{\lambda_1}{\lambda_2}\right)\cdot\frac{1}{N_{Tag}\cdot\eta_2\cdot\varepsilon_2} \quad (8),$$

$$R_2^{cum} = R_2^{ind} + \nu_{12}\cdot R_1^{cum/ind} = \left(\frac{\hat{A}_2^1}{F_1} + \frac{\hat{A}_2^2}{F_2}\right)\cdot\frac{1}{N_{Tag}\cdot\eta_2\cdot\varepsilon_2} \quad (9),$$

where $\hat{A}_1 = A_1\cdot k_{\mu_1}$, $\hat{A}_2^1 = A_2^1\cdot k_{\mu_2}$ and $\hat{A}_2^2 = A_2^2\cdot k_{\mu_2}$ are the parameters determined by fitting the experimental points of the decay curves of the parent and daughter nuclides via least squares techniques (sub- and super-scripts 1 are for parent, sub- and super-scripts 2 are for daughter); η_1, and η_2 are absolute γ-yields; λ_1 and λ_2 are decay constants; ε_1 and ε_2 are absolute spectrometer effectivenesses at γ-energies E_1 (the 1st nuclide) and E_2 (the 2nd nuclide); ν is the branching factor,

i.e. a probability for mother to turn into daughter; F_1 and F_2 are functionals calculated as $F_i = 1 - e^{-\lambda_i \cdot t_{irr}}$, where $I = 1,2,st$; t_{irr} is irradiation time.

The corrections k_μ that allow for γ-quantum absorption in a sample are determined as

$$k_{\mu_j} = \frac{k \cdot \sigma_{tot_j} \cdot h}{1 - e^{k \cdot \sigma_{tot_j} \cdot h}} \qquad (10),$$

$$\frac{\Delta k_{\mu_j}}{k_{\mu_j}} = \left(1 - k_{\mu_j} \cdot e^{-k \cdot \sigma_{tot_j} \cdot h}\right) \cdot \frac{\Delta \sigma_{tot_j}}{\sigma_{tot_j}} \qquad (11),$$

where h is experimental sample depth (g/cm^2); σ_{tot_j} is cross section for interaction of γ-quanta of the j-th energy with matter (barn/atom); $k = \frac{N_{A_v}}{M} \cdot 10^{-24}$ is scale factor between dimension-[barn/atom] and dimension [cm^2/g], wherein N_{A_v} is Avogadro number; M is molecular weight. The values of cross sections for interactions of γ-quanta of the j-the energy with matter were borrowed from [3].

As recommended in [3], the relative errors in the cross sections for γ-quantum interactions with matter within 100-2600 keV range were broken into two groups, namely, at energies below and above 200 keV the errors were taken to be 10% and 5% respectively.

Since a few values of $(R_{ij}^{ind/cum} \pm \Delta R_{ij}^{ind/cum})$ calculated for k γ-lines $(i = 1,2; \quad 1 < j < k)$ may be averaged later when calculating their production rates, it is expedient to introduce the definitions of relative γ-yield and of relative spectrometer effectiveness hat are related to their absolute values as

$$\eta_{ij} = k_{\gamma_i} \cdot \eta_{ij}^{rel} \qquad \varepsilon_{ij} = k_\varepsilon \cdot \varepsilon_{ij}^{rel} \qquad (12)$$

The values of factors $k_{\gamma i} \pm \Delta k_{\gamma i}$ were borrowed from [4], while the procedure of determining the $k_\varepsilon \pm \Delta k_\varepsilon$ values is described in [2]. In this case, the relative reaction rate of each nuclide expressed via factors $k_{\gamma i}$ and k_ε, as well as the absolute reaction rates calculated by formulas (6)-(9), can be presented as

$$^{rel}R_{ij}^{cum/ind} = R_{ij}^{cum/ind} \cdot k_{\gamma j} \cdot k_\varepsilon \cdot N_{tag}, \qquad (13)$$

The errors $\Delta\,^{rel}R_1^{cum/ind}$, $\Delta\,^{rel}R_2^{cum/ind}$, $\Delta\,^{rel}R_2^{ind}$, and $\Delta\,^{rel}R_2^{cum}$ in the relative reaction rates are calculated using the error transfer formula with due allowance for errors in all the values that enter expressions (6)-(9) and (12):

$$\Delta\,^{rel}R_1^{cum/ind} = {}^{rel}R_1^{cum/ind} \cdot \sqrt{\left(\frac{\Delta A_1}{A_1}\right)^2 + \left(\frac{\Delta k_{\mu_1}}{k_{\mu_1}}\right)^2 + \left(\frac{\Delta \eta_1^{rel}}{\eta_1^{rel}}\right)^2 + \left(\frac{\Delta \varepsilon_1^{rel}}{\varepsilon_1^{rel}}\right)^2} \qquad (14)$$

$$\Delta^{rel}R_2^{cum/ind} = {}^{rel}R_2^{cum/ind} \cdot \sqrt{\left(\frac{\Delta A_2^1}{A_2^1}\right)^2 + \left(\frac{\Delta k_{\mu_2}}{k_{\mu_2}}\right)^2 + \left(\frac{\Delta \eta_2^{rel}}{\eta_2^{rel}}\right)^2 + \left(\frac{\Delta \varepsilon_2^{rel}}{\varepsilon_2^{rel}}\right)^2} \tag{15}$$

$$\Delta^{rel}R_2^{cum/ind} = {}^{rel}R_2^{cum/ind} \cdot \sqrt{\left(\frac{\Delta G_{A_2^1}}{G_{A_2^1}}\right)^2 + \left(\frac{\Delta k_{\mu_2}}{k_{\mu_2}}\right)^2 + \left(\frac{\Delta \eta_2^{rel}}{\eta_2^{rel}}\right)^2 + \left(\frac{\Delta \varepsilon_2^{rel}}{\varepsilon_2^{rel}}\right)^2} \tag{16}$$

$$\Delta^{rel}R_2^{cum} = {}^{rel}R_2^{cum} \cdot \sqrt{\left(\frac{\Delta G_{A_2^2}}{G_{A_2^2}}\right)^2 + \left(\frac{\Delta k_{\mu_2}}{k_{\mu_2}}\right)^2 + \left(\frac{\Delta \eta_2^{rel}}{\eta_2^{rel}}\right)^2 + \left(\frac{\Delta \varepsilon_2^{rel}}{\varepsilon_2^{rel}}\right)^2} \tag{17}$$

The errors in functions

$$G_{A_2^1}(\vec{A}_2) = \frac{A_2^2}{F_2} + \frac{A_2^1}{F_1} \cdot \frac{\lambda_1}{\lambda_2} \tag{18}$$

$$G_{A_2^2}(\vec{A}_2) = \frac{A_2^1}{F_1} + \frac{A_2^2}{F_2} \tag{19}$$

of parameters A_2^1 and A_2^2 were determined as

$$\Delta G_{A_2^i}^2 = gradG_{A_2^i} \cdot M_{A_2}^{-1} \cdot (gradG_{A_2^i})^T, \quad i = 1,2 \tag{20}$$

$$gradG_{A_2^1} = \left\{\frac{1}{F_1} \cdot \frac{\lambda_1}{\lambda_2}, \frac{1}{F_2}\right\} \tag{21}$$

$$gradG_{A_2^2} = \left\{\frac{1}{F_1}, \frac{1}{F_2}\right\} \tag{22}$$

The means of the relative independent or cumulative rates of the *i*-th nuclide production inferred from *j* γ-lines were calculated as

$${}^{rel}\overline{R}_i^{cum/ind} = \frac{\sum_{j=1}^{k} {}^{rel}R_{ij}^{cum/ind} \cdot {}^{rel}W_{ij}}{\sum_{j=1}^{k} {}^{rel}W_{ij}} \qquad {}^{rel}W_{ij} = \frac{1}{\left(\Delta^{rel}R_{ij}^{cum/ind}\right)^2} \tag{23}$$

$$\Delta^{rel}\overline{R}_i^{cum/ind} = \max\left\{\left(\Delta^{rel}\overline{R}_i^{cum/ind}\right)'; \left(\Delta^{rel}\overline{R}_i^{cum/ind}\right)''\right\} \tag{24}$$

$$\left(\Delta\,{}^{rel}\overline{R}_i^{cum/ind}\right)' = \sqrt{\frac{\sum_{j=1}^{k} {}^{rel}W_{ij}\left({}^{rel}\overline{R}_i^{cum/ind} - {}^{rel}\overline{R}_{ij}\right)^2}{(k-1)\sum_{j=1}^{k} {}^{rel}W_{ij}}} \tag{25}$$

$$\left(\Delta\,{}^{rel}\overline{R}_i^{cum/ind}\right)'' = \sqrt{\frac{1}{\sum_{j=1}^{k} {}^{rel}W_{ij}}} \tag{26}$$

The means of the absolute independent or cumulative rates of the *i*-th nuclide production inferred from *j* γ-lines, as well as their errors, were calculated from their relative values as

$$\overline{R}_i^{cum/ind} = \frac{{}^{rel}\overline{R}_{ij}^{cum/ind}}{k_{\gamma_i} \cdot k_\varepsilon \cdot N_{tag}} \tag{27}$$

$$\Delta\overline{R}_i^{cum/ind} = \overline{R}_i^{cum/ind} \cdot \sqrt{\left(\frac{\Delta\,{}^{rel}\overline{R}_i^{cum/ind}}{{}^{rel}\overline{R}_i^{cum/ind}}\right)^2 + \left(\frac{\Delta k_{\gamma_i}}{k_{\gamma_i}}\right)^2 + \left(\frac{\Delta k_\varepsilon}{k_\varepsilon}\right)^2 + \left(\frac{\Delta N_{tag}}{N_{tag}}\right)^2} \tag{28}$$

In case but a single γ-line is involved in calculating the reaction rate (a single γ-line may be selected among *j* γ-lines, or else a nuclide has but a single γ-line, *j* = 1), use was made, according to (6)-(9)-(12), of the absolute γ-yield in that line $\left(\eta_i \pm \Delta\eta_i\right)$ and of the absolute detection effectiveness $\left(\varepsilon_i \pm \Delta\varepsilon_i\right)$.

Since

$$\left(\frac{\Delta\eta_{ij}}{\eta_{ij}}\right)^2 = \left(\frac{\Delta k_{\gamma i}}{k_{\gamma i}}\right)^2 + \left(\frac{\Delta\eta_{ij}^{rel}}{\eta_{ij}^{rel}}\right)^2 \tag{29}$$

$$\left(\frac{\Delta\varepsilon_{ij}}{\varepsilon_{ij}}\right)^2 = \left(\frac{\Delta k_\varepsilon}{k_\varepsilon}\right)^2 + \left(\frac{\Delta\eta_{ij}^{rel}}{\eta_{ij}^{rel}}\right)^2 \tag{30}$$

then, allowing for (14)-(17), expression (27) gets transformed to calculate the error in the reaction rate calculated for a single γ-line.

The ^{27}Al(p,x)^{7}Be and ^{27}Al(p,x)^{22}Na reaction rates are calculated to determine the number of protons onto the Pb target. The mean proton flux density and its error for each of the reactions are calculated as

$$\hat{\Phi} = \frac{R_{st}^{cum/ind}}{\sigma_{st}^{cum/ind}} \tag{31}$$

$$\frac{\Delta\hat{\Phi}}{\hat{\Phi}} = \sqrt{\left(\frac{\Delta R_{st}^{cum/ind}}{R_{st}^{cum/ind}}\right)^2 + \left(\frac{\Delta\sigma_{st}^{cum/ind}}{\sigma_{st}^{cum/ind}}\right)^2} \tag{32}$$

Величина The $R_{st}^{cum/ind}$ value is calculated by expression (6).

To get the correct comparison between the measured and calculated reaction rates, they were normalized to the beam power W.

3.2. Description of the external proton beam extraction

The characteristics of the neutron fields outside and inside the 0.8 GeV proton-irradiated thick Pb target were studied using the proton beam extracted from the ITEP U-10 synchrotron, which is a ring accelerator with a 25-MeV energy of proton injection to a rung and a 9.3-GeV maximum energy of accelerated protons. The proton beam accelerated up to a given energy (within a 40-9300 MeV range) and consisting of four bunches of 250 ns duration each gets transferred from the accelerator ring to the transport channel that provides proton beam ejection with a ~$2 \cdot 10^{11}$ proton/pulse intensity, ellipse-shaped cross section with ~10x15 mm axes, a 1 μs total duration, and a ~15 pulse/min pulse repetition rate

Fig. 2 is a schematic of the transport channel for irradiating experimental samples. Also shown are elements of the proton beam fast extraction system.

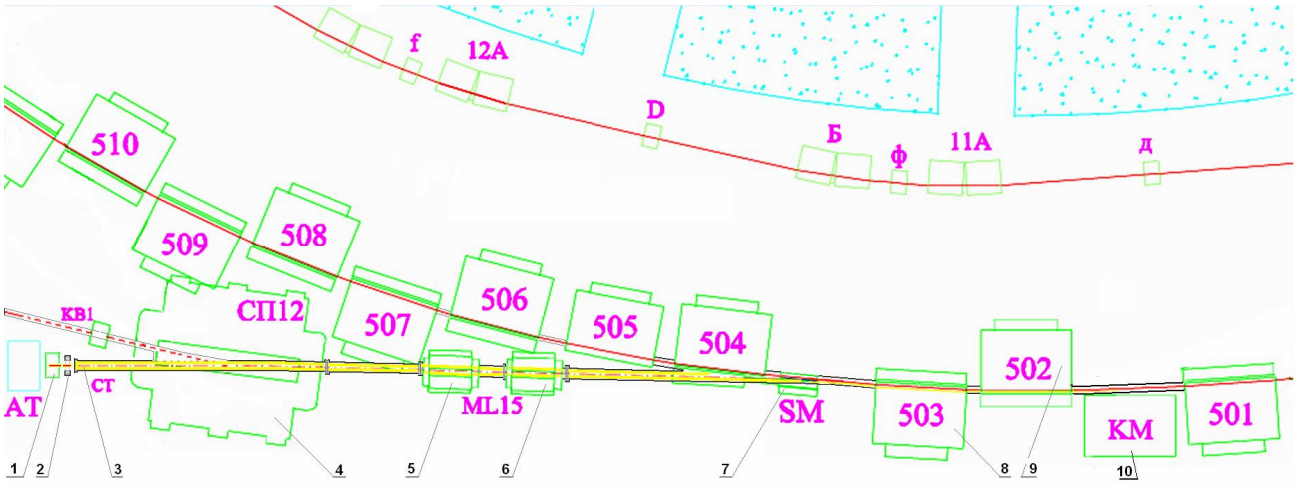

Fig. 2. The facility schematic and the fast extraction units: 1. Table to place the samples to be irradiated. 2. Current transformer. 3. Outlet flange of vacuumized proton guide. 4. Bending magnet. 5, 6. Doublet of quadrupole lenses. 7. Septum magnet. 8, 9. Magnetic units of accelerating ring. 10. Kicker-magnet.

3.3. Description of the Pb target micromodel

The target to be irradiated was assembled of 23 lead discs (see Figs 3 and 4). The target is 920-mm long to provide proton beam stoppage.

The all-metal Pb discs of 150-mm diameter and 40-mm depth were manufactured by founding them in a graphite mold with subsequent machining. The Pb disc parameters are presented in Table 1, and the input material composition in Table 4. Pending irradiations of samples inside the discs, the disc design includes task-oriented “rulers”. Figs. 5 and 6 show general views of a disc and of a ruler, respectively.

Table 1

Parameters of Pb discs

Position number	Disc number	Weight of an assembled disc, g	Weight, free of ruler, g	Weight of a ruler, g	Samples on the disc
1	5	8045.9	7636.1	409.9	present
2	9	8045.2	7635.1	409.9	
3	20	8043.4	7634.5	408.7	present
4	3	8043.2	7633.8	409.5	
5	6	8042.8	7634.2	408.5	present
6	7	8040.8	7630.5	410.3	
7	23	8040.7	7631.4	409.3	present
8	25	8037.2	7629.3	407.8	
9	14	8036.3	7626.1	410.3	present
10	18	8035.2	7627.6	407.7	
11	13	8035.9	7626.7	409.2	present
12	15	8032.6	7623.2	409.6	
13	19	8032.3	7621.9	410.6	present
14	22	8027.1	7617.8	409.3	
15	12	8025.7	7615.2	410.5	present
16	10	8024.2	7610.8	413.4	
17	24	8017.5	7608.6	409	present
18	8	8017.2	7606.5	410.7	
19	4	8016.4	7606.2	409.9	present
20	11	8009.7	7601.7	407.9	
21	16	7995.4	7584.6	410.8	present
22	26.2	8019.4	7610.8	408.7	
23	26.1	7996.8	7586.5	410.3	present

Pending irradiations, the target was placed on the task-oriented table composed of a cradle and of a massive support equipped with micrometric adjustment screws to provide accurate positioning of the cradle and of the target therein with respect to the proton beam axis.

The target was adjusted as follows. The task-oriented round rests of a 150-mm outer diameter were fastened to the front and rear butts of the cradle. The centers of the rests carried ceramic plates that get phosphorescent when affected by the proton beam. The light flash was monitored by a video camera.

The table was initially positioned so that the proton beam would hit the center of the first plate on the front butt of the cradle in correspondence with the center of the first Pb disc. After that, the rest with a plate thereon was removed, whereupon the cradle position was so corrected that the proton beam would hit the center of the second plate mounted on the cradle rear butt, which corresponds to the center of the last Pb disc. Later, the first rest was mounted in the cradle again, whereupon the proton beam position with respect to the first Pb disc was corrected. The procedure recurred repeatedly until the cradle takes the position for the proton beam to hit the centers of the first and last Pb discs. The proton beam positions on the front and rear butts of the cradle are show in Figs. 7A, 7B and 8A, 8B, respectively.

The adjustment of the cradle having been finished, all 23 Pb discs with rulers were so mounted in the cradle that they abutted on each other. The geometric position of the rulers with the

samples in their grooves relative to vertical axis was fixed with a semicircular template. The target was covered on top with a task-oriented protective case made of whatman paper, to which the experimental samples were fastened with a sticky tape. To reduce the contribution from radiative capture, some of the samples were placed inside Cd jackets. Irradiations having ended, the whatman case permitted remote-controlled removal of the samples. The rulers with experimental samples therein were also removed remotely using a task-oriented hooked rod.

Fig. 3. General view of the Pb target.

Fig. 4. General view of the Pb target together with experimental samples.

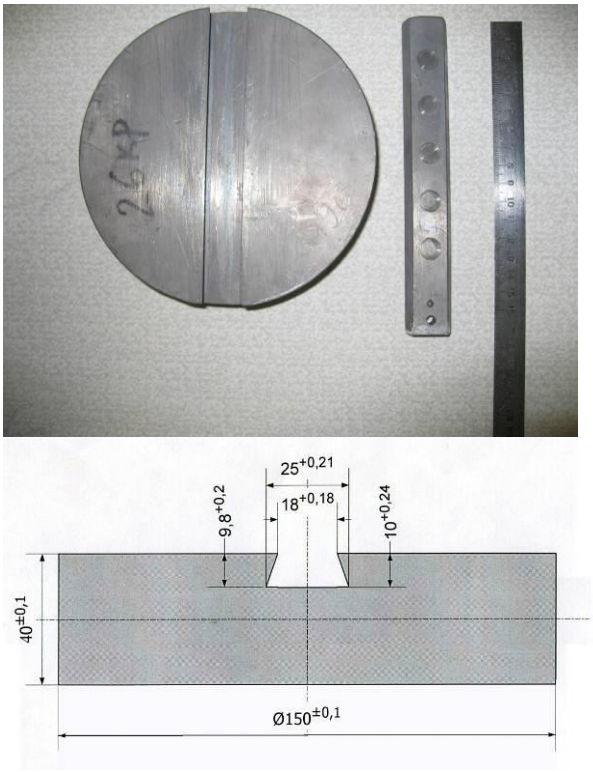

Fig. 5. The general view and the drawing of a Pb disc.

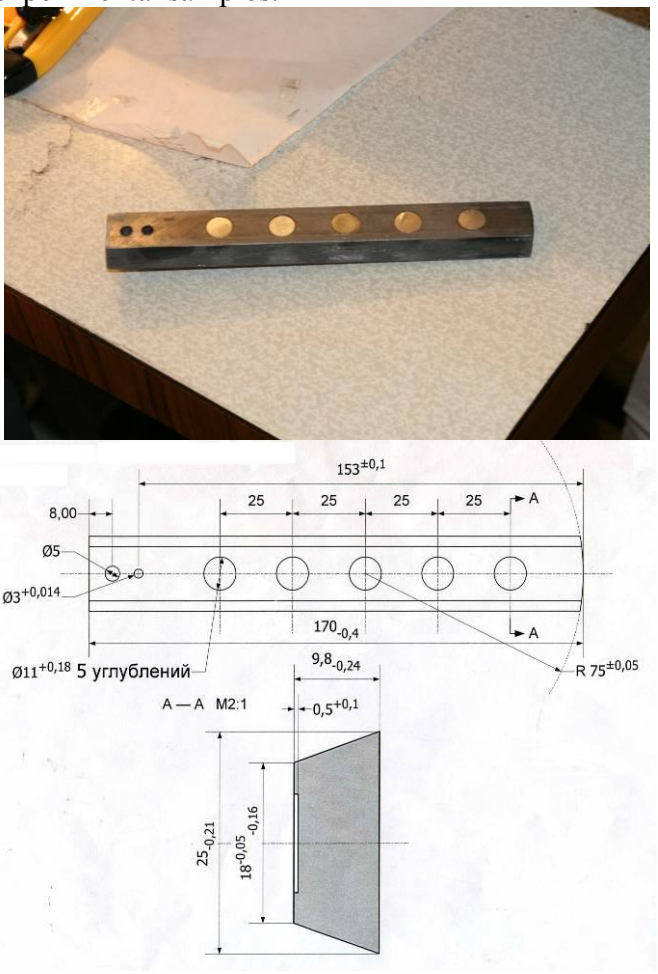

Fig. 6. The general view and the drawing of a ruler.

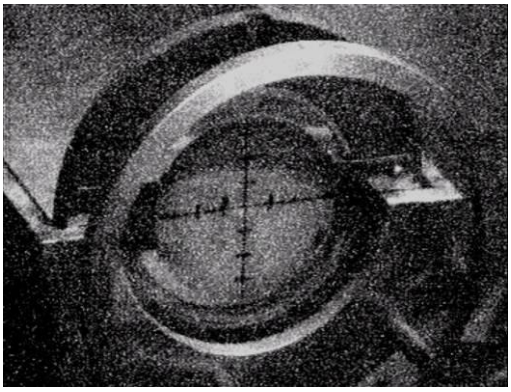

Fig. 7A. Position of the front rest center.

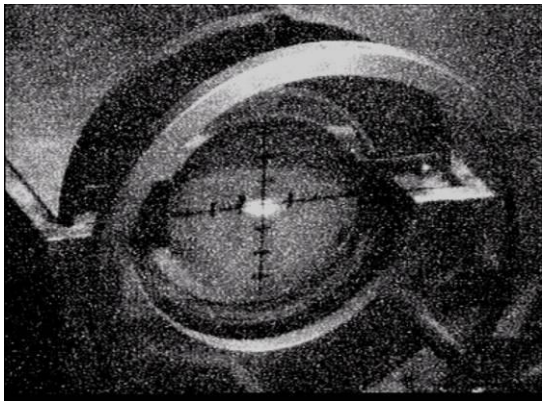

Fig. 7B. Position of proton beam on the front rest.

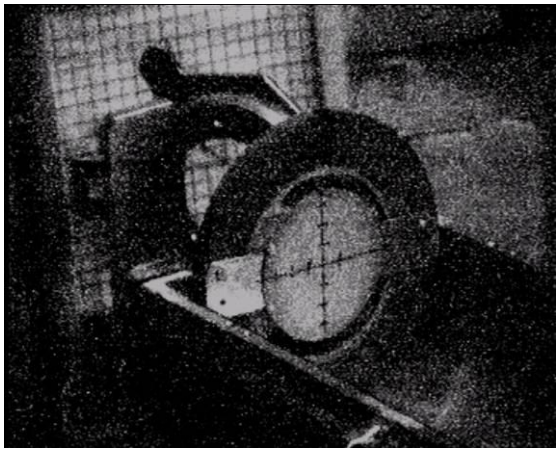

Fig. 8A. Position of the rear rest center.

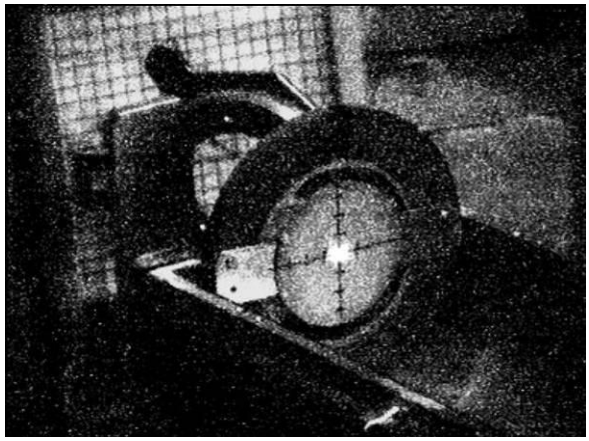

Fig. 8B. Position of proton beam on the rear rest.

3.4. EXPERIMENTAL SAMPLES

In the experiments, the absolute reaction rates are determined on ^{209}Bi, ^{nat}Pb, ^{197}Au, ^{181}Ta ^{169}Tm, ^{nat}In, ^{93}Nb, ^{65}Cu, ^{64}Zn, ^{63}Cu, ^{59}Co, ^{27}Al, ^{19}F, and ^{12}C. Table 2 presents the parameters the experimental samples. The data on the sample compositions are presented in Tables 3 and 4. The arrangement of the samples on the target is presented in Figs. 9 and 10 and in Table 2. The samples were placed either on the lateral surfaces of Pb discs or in the task-oriented grooves on the Pb rulers. The sample loci are marked as S (0˚ from a vertical), M (45˚ clockwise from the vertical), L (90˚), K (135˚), J (180˚), I (225˚), O (270˚), and N (315˚) on the surface of the discs and as A, B, C, D, E in the rulers. The guide marks are strictly coaxial in all discs, i.e. the identical marks on different discs lie on the same straight line parallel to the target axis.

Table 2

Parameters of the samples used in the Pb target

Disc No.	On the surface of the disc				Inside the disc			
	Sample	Weigh t g	Depth, mm	Diameter mm	Sample	Weigh t g	Depth, mm	Diameter mm
1	^{209}Bi	1.5006	1.86	10.5	^{27}Al(A)	0.2039	0.25	10.5
	^{197}Au	0.4720	0.44	10.5	^{27}Al(B)	0.4318	0.46	10.5
	^{nat}In	0.5011	0.81	10.5	^{59}Co(C)	0.1240	0.5	10.5
	^{nat}Pb(S)	1.5180	1.61	10.5	^{nat}Pb(C)	0.1196	0.5	10.5
	^{181}Ta	0.1253	0.10	10.5	^{27}Al(C)	0.0581	0.25	10.5

	^{27}Al (S)	0.3543	1.50	10.5	^{27}Al(D)	0.1195	0.5	10.5
	^{27}Al(I)	0.1196	0.50	10.5	^{27}Al(E)	0.1199	0.5	10.5
	^{27}Al(J)	0.1237	0.50	10.5				
	^{27}Al(K)	0.1238	0.50	10.5				
	^{27}Al(L)	0.3483	1.50	10.5				
	^{27}Al(M)	0.3501	1.50	10.5				
	^{27}Al(N)	0.3481	1.50	10.5				
	^{27}Al(O)	0.3465	1.50	10.5				
3	^{209}Bi	1.4982	1.85	10.5	^{59}Co(C)	0.2021	0.25	10.5
	^{197}Au	0.4713	0.40	10.5	^{nat}Pb(C)	0.6826	0.72	10.5
	^{nat}In	0.4931	0.83	10.5	^{27}Al(A)	0.1245	0.5	10.5
	^{nat}Pb(S)	1.5421	1.59	10.5	^{27}Al(B)	0.1236	0.5	10.5
	^{181}Ta	0.1264	0.10	10.5	^{27}Al(C)	0.0584	0.25	10.5
	^{27}Al (S)	0.3519	1.50	10.5	^{27}Al(D)	0.1235	0.5	10.5
	^{59}Co	0.8064	1.00	10.5	^{27}Al(E)	0.1239	0.5	10.5
	^{64}Zn	0.2250	0.40	10.5				
	^{63}Cu	0.4116	0.55	10.5				
	^{65}Cu	0.5304	0.72	10.5				
	^{93}Nb	0.2114	0.30	10.5				
	^{169}Tm	0.4868	0.95	10.5				
	^{12}C	0.2867	1.95	10.5				
	^{19}F	0.7639	4.00	10.5				
5	^{209}Bi	1.4495	1.84	10.5	^{59}Co(C)	0.2023	0.25	10.5
	^{197}Au	0.4864	0.42	10.5	^{nat}Pb(C)	0.6700	0.72	10.5
	^{nat}In	0.4754	0.78	10.5	^{27}Al(A)	0.1244	0.5	10.5
	^{nat}Pb(S)	1.5078	1.57	10.5	^{27}Al(B)	0.1240	0.5	10.5
	^{181}Ta	0.1257	0.10	10.5	^{27}Al(C)	0.0580	0.25	10.5
	^{27}Al (S)	0.3490	1.50	10.5	^{27}Al(D)	0.1260	0.5	10.5
	^{27}Al(I)	0.1198	0.50	10.5	^{27}Al(E)	0.1247	0.5	10.5
	^{27}Al(J)	0.1239	0.50	10.5				
	^{27}Al(K)	0.1233	0.50	10.5				
	^{27}Al(L)	0.3514	1.50	10.5				
	^{27}Al(M)	0.3476	1.50	10.5				
	^{27}Al(N)	0.3498	1.50	10.5				
	^{27}Al(O)	0.3513	1.50	10.5				
7	^{209}Bi	1.4988	1.84	10.5	^{59}Co(C)	0.2004	0.25	10.5
	^{197}Au	0.4787	0.42	10.5	^{nat}Pb(C)	0.4964	0.54	10.5
	^{nat}In	0.4538	0.74	10.5	^{27}Al(A)	0.1230	0.5	10.5
	^{nat}Pb(S)	1.5144	1.59	10.5	^{27}Al(B)	0.1193	0.5	10.5
	^{181}Ta	0.1230	0.10	10.5	^{27}Al(C)	0.0580	0.25	10.5
	^{27}Al (S)	0.3495	1.50	10.5	^{27}Al(D)	0.1193	0.5	10.5
					^{27}Al(E)	0.1245	0.5	10.5
9	^{209}Bi	1.5024	1.82	10.5	^{59}Co(C)	0.2011	0.25	10.5
	^{197}Au	0.4669	0.41	10.5	^{nat}Pb(C)	0.6163	0.67	10.5
	^{nat}In	0.4033	0.66	10.5	^{27}Al(A)	0.1278	0.5	10.5
	^{nat}Pb(S)	1.5144	1.60	10.5	^{27}Al(B)	0.1249	0.5	10.5
	^{181}Ta	0.1268	0.10	10.5	^{27}Al(C)	0.0584	0.25	10.5

	^{27}Al (S)	0.3467	1.50	10.5	^{27}Al(D)	0.1185	0.5	10.5
	^{27}Al(I)	0.1254	0.50	10.5	^{27}Al(E)	0.1199	0.5	10.5
	^{27}Al(J)	0.1216	0.50	10.5				
	^{27}Al(K)	0.1194	0.50	10.5				
	^{27}Al(L)	0.3523	1.50	10.5				
	^{27}Al(M)	0.3533	1.50	10.5				
	^{27}Al(N)	0.3484	1.50	10.5				
	^{27}Al(O)	0.3561	1.50	10.5				
11	^{209}Bi	1.5031	1.89	10.5	^{59}Co(C)	0.2027	0.25	10.5
	^{197}Au	0.4461	0.39	10.5	^{nat}Pb(C)	0.6510	0.68	10.5
	^{nat}In	0.5040	0.83	10.5	^{27}Al(A)	0.1193	0.5	10.5
	^{nat}Pb(S)	1.5191	1.60	10.5	^{27}Al(B)	0.1195	0.5	10.5
	^{181}Ta	0.1249	0.10	10.5	^{27}Al(C)	0.0583	0.25	10.5
	^{27}Al (S)	0.3503	1.50	10.5	^{27}Al(D)	0.1206	0.5	10.5
					^{27}Al(E)	0.1205	0.5	10.5
13	^{209}Bi	1.4961	1.83	10.5	^{59}Co(C)	0.2020	0.25	10.5
	^{197}Au	0.4450	0.33	10.5	^{nat}Pb(C)	0.6986	0.74	10.5
	^{nat}In	0.5072	0.83	10.5	^{27}Al(A)	0.1187	0.5	10.5
	^{nat}Pb(S)	1.4911	1.60	10.5	^{27}Al(B)	0.1261	0.5	10.5
	^{181}Ta	0.1292	0.10	10.5	^{27}Al(C)	0.0589	0.25	10.5
	^{27}Al (S)	0.3508	1.50	10.5	^{27}Al(D)	0.1237	0.5	10.5
	^{27}Al(I)	0.1207	0.50	10.5	^{27}Al(E)	0.1241	0.5	10.5
	^{27}Al(J)	0.1194	0.50	10.5				
	^{27}Al(K)	0.1196	0.50	10.5				
	^{27}Al(L)	0.3514	1.50	10.5				
	^{27}Al(M)	0.3497	1.50	10.5				
	^{27}Al(N)	0.3514	1.50	10.5				
	^{27}Al(O)	0.3532	1.50	10.5				
15	^{209}Bi	1.4983	1.86	10.5	^{59}Co(C)	0.2011	0.25	10.5
	^{197}Au	0.4720	0.41	10.5	^{nat}Pb(C)	0.8912	0.92	10.5
	^{nat}In	0.4592	0.76	10.5	^{27}Al(A)	0.1193	0.5	10.5
	^{nat}Pb(S)	1.5179	1.58	10.5	^{27}Al(B)	0.1209	0.5	10.5
	^{181}Ta	0.1238	0.10	10.5	^{27}Al(C)	0.0582	0.25	10.5
	^{27}Al (S)	0.3527	1.50	10.5	^{27}Al(D)	0.1199	0.5	10.5
					^{27}Al(E)	0.1247	0.5	10.5
17	^{209}Bi	1.5028	1.83	10.5	^{59}Co(C)	0.2017	0.25	10.5
	^{197}Au	0.4809	0.39	10.5	^{nat}Pb(C)	0.8799	0.92	10.5
	^{nat}In	0.4583	0.75	10.5	^{27}Al(A)	0.1249	0.5	10.5
	^{nat}Pb(S)	1.5069	1.57	10.5	^{27}Al(B)	0.1210	0.5	10.5
	^{181}Ta	0.1252	0.10	10.5	^{27}Al(C)	0.0588	0.25	10.5
	^{27}Al (S)	0.3493	1.50	10.5	^{27}Al(D)	0.1242	0.5	10.5
	^{27}Al(I)	0.1170	0.50	10.5	^{27}Al(E)	0.1194	0.5	10.5
	^{27}Al(J)	0.1193	0.50	10.5				
	^{27}Al(K)	0.1200	0.50	10.5				
	^{27}Al(L)	0.3509	1.50	10.5				
	^{27}Al(M)	0.3509	1.50	10.5				
	^{27}Al(N)	0.3495	1.50	10.5				

	^{27}Al(O)	0.3531	1.50	10.5				
19	^{209}Bi	1.5008	1.84	10.5	^{59}Co(C)	0.2024	0.25	10.5
	^{197}Au	0.4355	0.34	10.5	^{nat}Pb(C)	1.1266	1.17	10.5
	^{nat}In	0.5022	0.84	10.5	^{27}Al(A)	0.1182	0.5	10.5
	^{nat}Pb(S)	1.5161	1.56	10.5	^{27}Al(B)	0.1195	0.5	10.5
	^{181}Ta	0.1279	0.10	10.5	^{27}Al(C)	0.0580	0.25	10.5
	^{27}Al (S)	0.3494	1.50	10.5	^{27}Al(D)	0.1202	0.5	10.5
					^{27}Al(E)	0.1254	0.5	10.5
21	^{209}Bi	1.4998	1.90	10.5	^{59}Co(C)	0.2025	0.25	10.5
	^{197}Au	0.4770	0.36	10.5	^{nat}Pb(C)	0.8673	0.91	10.5
	^{nat}In	0.4775	0.78	10.5	^{27}Al(A)	0.1203	0.5	10.5
	^{nat}Pb(S)	1.5390		10.5	^{27}Al(B)	0.1193	0.5	10.5
	^{181}Ta	0.1240	0.10	10.5	^{27}Al(C)	0.0583	0.25	10.5
	^{27}Al (S)	0.3515	1.50	10.5	^{27}Al(D)	0.1245	0.5	10.5
	^{27}Al(I)	0.1240	0.50	10.5	^{27}Al(E)	0.1213	0.5	10.5
	^{27}Al(J)	0.1204	0.50	10.5				
	^{27}Al(K)	0.1251	0.50	10.5				
	^{27}Al(L)	0.3512	1.50	10.5				
	^{27}Al(M)	0.3542	1.50	10.5				
	^{27}Al(N)	0.3475	1.50	10.5				
	^{27}Al(O)	0.3447	1.50	10.5				
23	^{209}Bi	1.5007	1.86	10.5	^{59}Co(C)	0.2025	0.25	10.5
	^{197}Au	0.4732	0.41	10.5	^{nat}Pb(C)	1.5593	1.62	10.5
	^{nat}In	0.5011	0.82	10.5	^{27}Al(A)	0.1242	0.5	10.5
	^{nat}Pb(S)	1.5160	1.57	10.5	^{27}Al(B)	0.1242	0.5	10.5
	^{181}Ta	0.1271	0.10	10.5	^{27}Al(C)	0.0582	0.25	10.5
	^{27}Al (S)	0.3454	1.50	10.5	^{27}Al(D)	0.1259	0.5	10.5
					^{27}Al(E)	0.1232	0.5	10.5

Table 3

Composition of isotope-enriched experimental samples

No.	Sample	Composition (the components whose fraction exceeds 0.1%)	Certificate
1	^{63}Cu	63Cu-99.46%,65Cu-0.50%	[14]
3	^{65}Cu	65Cu-99.665%,63Cu-0.30%	[15]
2	^{64}Zn	64Zn-99.3%,66Zn-0.39%,	[16]

In case certificates are absent, the samples were examined additionally. The total admixture composition was determined via spark mass-spectrometry using a JEOL Co. (Japan)-manufactured JMS-01-BM2 double-focusing mass spectrometer. The mass-spectra of a high mass-spectrum resolution were recorded on Ilford-Q photoplates. The mass-spectra were quantitatively interpreted using a Joyce Loebl Co. (UK)-manufactured MDM6 microdensitometer together with a US-made NOVA-4 minicomputer. The admixture fractions were calculated using software developed at MS Lab. The random error in the analysis results is characterized by a 0.15-3.0 relative standard deviation. The content of noble gases and transuranics in the tested samples is below their detection limit of 0.1 ppm.

Table 4 presents the analysis results in mass parts per million (1 ppm = 0,0001%).

Table 4

Composition of chemical admixtures in experimental samples.

Эле-мент	ppm													
	C[5]	Al[6]	Al[7]*	In[8]	Ta[9]	Au[10]	Pb(C) [11]	Bi[12]	Pb(S) [13]	Nb[14]	^{63}Cu[15]	^{65}Cu[16]	^{64}Zn[17]	Co[18]*
H	---	---	---	---	---	---	---	---	---	---	---	---	---	<3
Li	< 0.002	<0.01	<0.005	< 0.002	< 0.002	<0.01	< 0.002	< 0.002	< 0.002	<0.07	---	---	---	<0.001
Be	< 0.001	< 0.01	<0.005	< 0.001	< 0.001	< 0.01	< 0.001	< 0.001	< 0.003	<0.05	---	---	---	<0.001
B	0.07	< 0.01	0.02	0.02	< 0.002	0.07	0.003	< 0.01	0.005	0.1	---	---	---	<0.001
C	Base	---	---	---	---	---	---	---	---	---	---	---	---	<33
N	---	---	---	---	---	---	---	---	---	---	---	---	---	13
O	---	---	---	---	---	---	---	---	---	---	---	---	---	<13
F	0.03	5	<0.005	0.2	0.2	0.08	0.09	0.06	0.6	1	---	---	---	<0.01
Na	0.2	2	0.25	<0.02	<0.02	0.5	0.02	<0.02	<0.06	<1	---	---	10	1.4
Mg	<0.01	400	3	0.01	< 0.01	3	0.01	0.008	0.05	3	---	---	<10	0.006
Al	0.01	Base	Base	0.2	0.2	4	0.08	0.2	0.2	10	---	---	7	0.02
Si	30	<0.5	6.5	0.2	0.06	6	0.07	0.04	0.1	20	---	---	<10	0.13
P	0.6	0.6	0.19	<0.01	< 0.01	0.2	0.06	0.1	<0.03	---	---	---	---	<0.005
S	1	2	0.5	0.1	0.05	9	0.3	1	0.06	8	50	50	---	<20
Cl	0.3	20	0.5	0.09	0.2	60	0.6	0.08	0.3	4	---	---	---	1.6
K	0.8	10	0.05	<0.05	<0.05	10	0.05	<0.05	<0.08	<1	---	---	<10	<0.01
Ca	0.1	6	0.25	0.1	0.03	9	0.04	0.03	1	2	---	---	5	<0.05
Sc	< 0.01	<0.1	0.007	< 0.01	< 0.01	< 0.01	< 0.01	< 0.01	<0.3	<0.6	---	---	---	<0.001
Ti	0.02	1	0.25	< 0.01	< 0.01	0.5	0.004	< 0.005	<0.04	6	---	---	---	1.1
V	< 0.01	<0.1	0.01	< 0.01	< 0.01	0.03	< 0.006	< 0.001	<0.03	<0.3	---	---	---	<0.001
Cr	0.01	0.6	0.15	0.3	<0.03	2	< 0.007	0.01	0.2	3	---	---	---	0.02
Mn	0.04	<0.1	0.05	< 0.01	< 0.01	0.2	< 0.01	< 0.002	<0.03	0.9	---	---	---	<0.005

Fe	0.1	30	1.1	0.04	<0.04	10	0.08	0.02	2	200	50	12	20	5.6
Co	< 0.006	<0.1	0.05	< 0.01	< 0.01	0.05	< 0.01	< 0.003	<0.02	0.2	---	---	---	OCHOBA
Ni	< 0.01	<0.1	0.5	<0.03	<0.03	0.2	< 0.01	0.04	0.09	0.4	100	27	9	230
Cu	< 0.01	20	4.5	<0.05	<0.05	5	1	0.01	0.2	4	---	---	30	37
Zn	<0.02	10	0.5	<0.1	<0.1	1	<0.02	0.03	<0.06	2	<40	<40	---	0.07
Ga	<0.01	<0.5	0.01	<0.06	<0.06	<005	<0.02	< 0.01	<0.05	20	---	---	---	<0.05
Ge	<0.02	<0.2	<0.01	<0.05	<0.05	<0.04	<0.03	<0.02	<0.1	<0.5	---	---	---	<0.05
As	0.1	<0.1	<0.05	<0.02	<0.02	0.2	<0.01	< 0.01	<0.03	<0.2	<5	<5		0.11
Se	<0.04	<0.1	<0.03	<0.03	<0.03	0.2	<0.03	<0.03	<0.08	<0.4	---	---	---	<0.05
Br	<0.05	<0.1	<0.005	<0.03	<0.03	<0.2	<0.01	< 0.01	<0.04	<0.4	---	---	---	<0.01
Rb	<0.03	<0.1	<0.001	<0.02	<0.02	< 0.01	<0.02	<0.02	<0.2	<0.5	---	---	---	<0.005
Sr	<0.03	<0.3	<0.005	<0.03	<0.03	0.04	<0.01	<0.01	<0.06	<0.2	---	---	---	<0.005
Y	< 0.01	<0.1	<0.005	<0.02	<0.02	<0.02	< 0.01	<0.01	<0.06	<0.6	---	---	---	<0.005
Zr	<0.07	<0.2	0.05	<0.2	<0.2	<0.05	<0.02	<0.02	<0.2	7	---	---	---	0.05
Nb	<0.05	<0.3	0.01	<0.2	200	< 0.05	<0.04	<0.02	<0.4	Base	---	---	---	<0.01
Mo	<0.1	<0.5	0.11	<0.3	0.5	<0.1	<0.06	<0.03	<0.3	30	---	---	---	0.25
Ru	<0.06	<0.2	<0.005	<0.1	<0.1	0.3	<0.03	<0.02	<0.2	<0.4	---	---	---	<0.05
Rh	< 0.01	<0.1	<0.5	<0.1	<0.1	1	<0.01	<0.01	<0.2	<0.6	---	---	---	<0.05
Pd	<0.1	<0.5	<0.005	<0.2	<0.2	3	<0.07	<0.03	<0.2	<7	---	---	---	<0.05
Ag	<0.05	<0.3	<0.005	<0.06	<0.06	400	3	0.1	<0.1	<4	---	---	---	<0.05
Cd	<0.2	<0.4	<0.01	<0.1	<0.1	0.2	1	<0.04	<0.3	<2	---	---	< 3	<0.05
In	<0.03	<0.2	<0.005	OCHOBA	<0.1	<0.4	<0.03	<0.02	<0.1	<0.4	---	---	---	<0.05
Sn	<0.03	<0.3	<0.01	<0.2	<0.2	0.4	<0.03	<0.04	<0.2	<2	60	30	---	<0.05
Sb	<0.04	<0.3	<0.005	<0.2	<0.2	0.2	<0.04	<0.04	<0.2	<2	<60	<60	---	<0.05
Te	<0.2	<0.4	<0.01	<0.3	<0.3	0.8	0.2	0.03	3	<3	---	---	---	<0.01
I	<0.05	<0.1	<0.001	<0.05	<0.05	<0.1	<0.05	<0.05	<0.08	<0.5	---	---	---	<0.005
Cs	<0.1	<0.3	<0.005	< 0.1	<0.1	<0.3	<0.1	<0.1	<0.09	<0.5	---	---	---	<0.005
Ba	<0.2	<0.3	<0.001	<0.2	<0.2	0.5	<0.2	<0.2	<0.1	<1	---	---	---	<0.005
La	<0.1	<0.2	<0.01	<0.2	<0.2	0.1	<0.1	<0.1	<0.1	<0.4	---	---	---	<0.005

Ce	<0.1	<0.1	0.001	<0.1	<0.1	<0.02	<0.1	<0.1	<0.1	<0.5	---	---	---	<0.005
Pr	<0.05	<0.1	<0.005	<0.1	<0.1	<0.05	<0.05	<0.05	<0.09	<0.4	---	---	---	<0.005
Nd	<0.2	<0.5	<0.005	<0.4	<0.4	<0.1	<0.2	<0.2	<0.2	<0.8	---	---	---	<0.005
Sm	<0.4	<0.5	<0.005	<0.5	<0.5	<0.2	<0.4	<0.4	<0.2	<0.9	---	---	---	<0.005
Eu	<0.1	<0.4	<0.005	<0.4	<0.4	<0.1	<0.1	<0.1	<0.1	<0.5	---	---	---	<0.005
Gd	<0.3	<0.6	<0.005	<0.3	<0.3	<0.4	<0.3	<0.3	<0.3	<0.8	---	---	---	<0.005
Tb	<0.2	<0.4	<0.005	<0.4	<0.4	<0.2	<0.2	<0.2	<0.1	<0.4	---	---	---	<0.005
Dy	<0.3	<0.4	<0.005	<0.3	<0.3	<0.5	<0.3	<0.3	<0.3	<0.8	---	---	---	<0.005
Ho	<0.05	<0.2	<0.005	<0.2	<0.2	<0.06	<0.05	<0.05	<0.2	<0.5	---	---	---	<0.005
Er	<0.1	<0.6	<0.005	<0.5	<0.5	<0.1	<0.1	<0.1	<0.3	<0.9	---	---	---	<0.005
Tm	<0.04	<0.2	<0.005	<0.3	<0.3	<0.05	<0.04	<0.04	<0.2	<0.5	---	---	---	<0.005
Yb	<0.05	<0.6	<0.005	<0.5	<0.5	<0.3	<0.05	<0.05	<0.4	<0.9	---	---	---	<0.005
Lu	<0.04	<0.4	<0.005	<0.4	<0.4	<0.2	<0.04	<0.04	<0.2	<0.5	---	---	---	<0.005
Hf	<0.1	<0.7	<0.005	<0.5	<0.5	<0.3	<0.1	<0.1	<0.3	<1	---	---	---	<0.9
Ta**	---	<0.5	<5	---	Base	<0.4	---	---	---	300	---	---	---	---
W	<0.2	<0.6	0.09	<0.4	6	<0.3	<0.2	<0.2	<0.3	20	---	---	---	0.03
Re	<0.1	<0.4	<0.001	<0.4	<0.4	<0.2	<0.1	<0.1	<0.5	<0.9	---	---	---	<0.05
Os	<0.3	<0.8	<0.001	<0.5	<0.5	<0.5	<0.3	<0.3	<0.6	<0.8	---	---	---	<0.05
Ir	<0.2	<0.5	<0.001	<0.4	<0.4	1	<0.2	<0.2	<0.4	<0.6	---	---	---	<0.05
Pt	<0.4	<0.7	<0.01	<0.8	<0.8	8	<0.4	<0.4	<0.5	<0.8	---	---	---	<0.01
Au	<0.2	<0.4	<0.05	<0.4	<0.4	Base	<0.2	<0.2	<0.2	<0.6	---	---	---	<0.05
Hg	<0.3	<0.8	<0.01	<0.7	<0.7	<0.6	<0.3	<0.3	<0.5	<1	---	---	---	<0.01
Tl	<0.05	<0.3	<0.01	<0.3	<0.3	<0.1	0.8	0.8	<0.4	<0.7	---	---	---	<0.001
Pb	<0.3	<0.6	0.01	1	<0.5	20	Base	10	Base	<2	<10	30	<10	1.8
Bi	<0.1	<0.3	<0.005	< 0.2	<0.2	2	10	Base	<1	<0.7	<10	<10	---	<0.005
Th	<0.1	<0.2	0.005	< 0.2	<0.2	<0.2	<0.1	<0.1	<0.3	<0.9	---	---	---	<0.001
U	<0.1	<0.2	<0.001	< 0.2	<0.2	<0.2	<0.1	<0.1	<0.3	<0.9	---	---	---	<0.001

* - The admixture contents in Al[7] and Co[18] is in nuclear ppm.

** - Ta is structural material of ion source

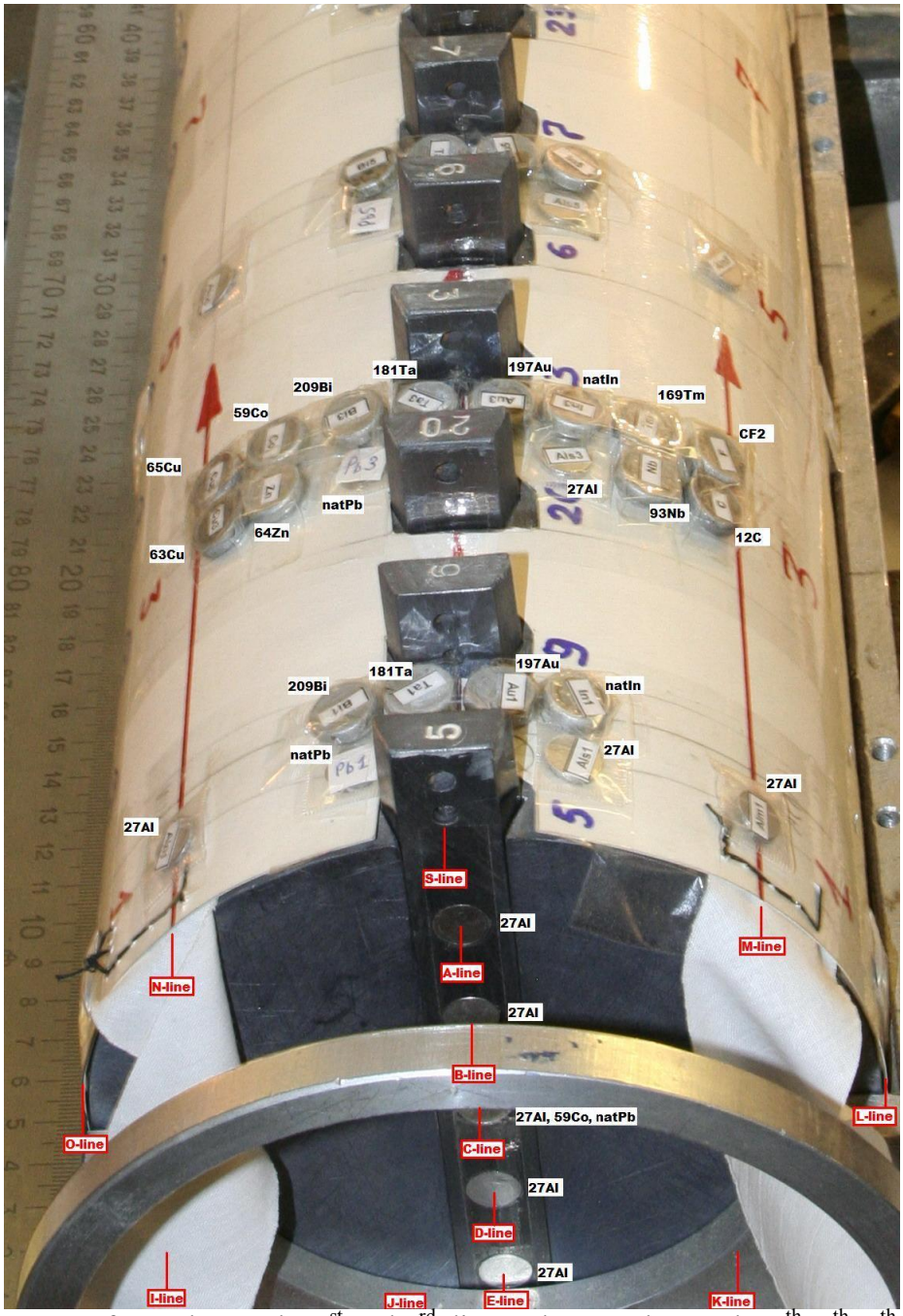

Fig. 9. Arrangement of samples on the 1st and 3rd discs. The samples on the 5th, 7th, 9th , 11th, 13th, 15th, 17th, 19th, 21st, and 23rd discs are arranged similarly to the 1st disc.

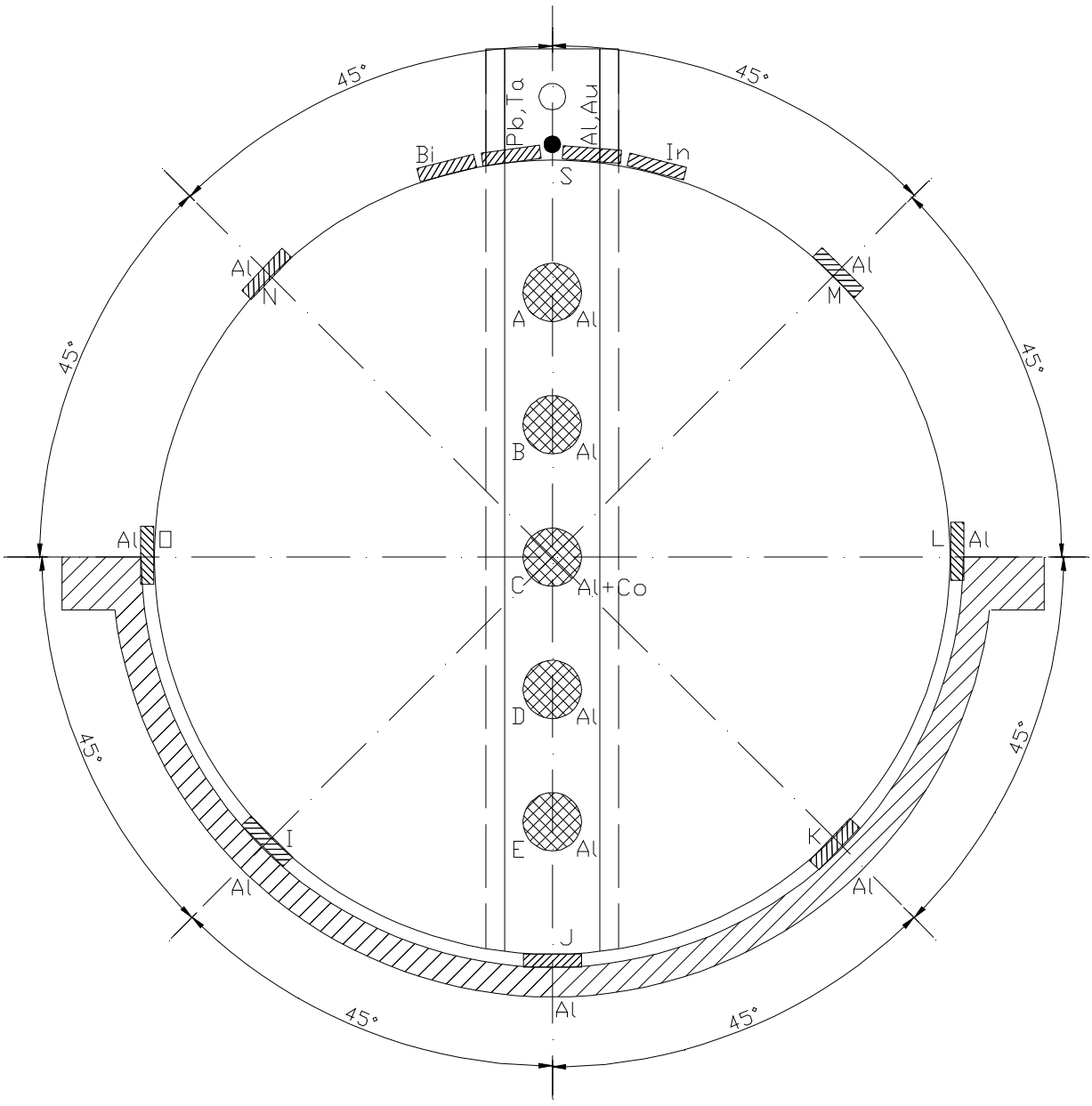

Fig. 9. Arrangement of samples on the 1st, 5th, 9th, 13th, 17th, and 21st discs. The samples on the 7th, 11th, 15th, 19th, and 23rd discs are arranged similarly, except for the samples on lines I, J, K, L, M, N, and O.

3.5. Irradiation of the Pb target micromodel.

The target was exposed to the 0.8 GeV proton beam for t_{irr}= 64800 s (start at 22:40 on 9 June 2006, end at 16:40 on 10 June 2006).

3.6. Monitoring of proton beam

The total number of protons incident onto the Pb target and the proton beam shape were determined using three Al monitors placed to intercept the beam. The first (M_1) and the second (M_2) were square plates (50x50 mm and 72x72 mm, respectively) were fastened to one another with a Scotch tape and were placed on a task-oriented rest at 220 mm from the outlet flange of a vacuumized proton guide. The third (M_3) of 169.6-mm diameter was fastened to a ring placed at 50 mm before the 1st disc (445 mm from the outlet flange of the vacuumized proton guide). After irradiation, the first and second monitors were folded repeatedly to get two ~15x15 mm plates of ~3 and ~4 mm thicknesses. The third monitor was cut into 36 fragments, most of which were 20x20 mm squares. The resulting fragments were also folded to get ~o.4-mm thick 10x10 mm plates. Fig. 11 shows the monitor cut pattern.

Fig. 11. Monitor cutting layout

The measurements have shown that, due to the significant thickness of the fist two monitors, alternation of their positions **[“top” – “bottom”]** results in varying count rates in the total absorption peaks ^{7Be}SPA (E_γ = 477.6 keV) and ^{22Na}SPA (E_γ = 1274.5 keV) by 10 -16%. The effect arises from the dependence of the absolute spectrometer effectiveness on the height of a measured sample above the detector because the multiple folding of the monitors leads to an uncertain position of the central sector under proton beam impact.

Therefore, the experimental ^{7Be}SPA and ^{22Na}SPA values and their errors $\Delta^{7Be}SPA$ and $\Delta^{22Na}SPA$, which are used to fit the former to the irradiation end as shown in Figs. 12 and 13 and which enter expression (4) in calculating the ^{7}Be and ^{22}Na reaction rates, were calculated as

$$^{7Be}SPA = \frac{^{7Be}SPA_{низ} + {}^{7Be}SPA_{верх}}{2} \quad (33)$$

$$\Delta\,^{7Be}SPA = \frac{\sqrt{\Delta\left(^{7Be}SPA_{низ}\right)^2 + \Delta\left(^{7Be}SPA_{верх}\right)^2}}{2} \quad (34)$$

$$^{22Na}SPA = \frac{^{22Na}SPA_{низ} + {}^{22Na}SPA_{верх}}{2} \quad (35)$$

$$\Delta\,^{22Na}SPA = \frac{\sqrt{\Delta\left(^{22Na}SPA_{низ}\right)^2 + \Delta\left(^{22Na}SPA_{верх}\right)^2}}{2} \quad (36)$$

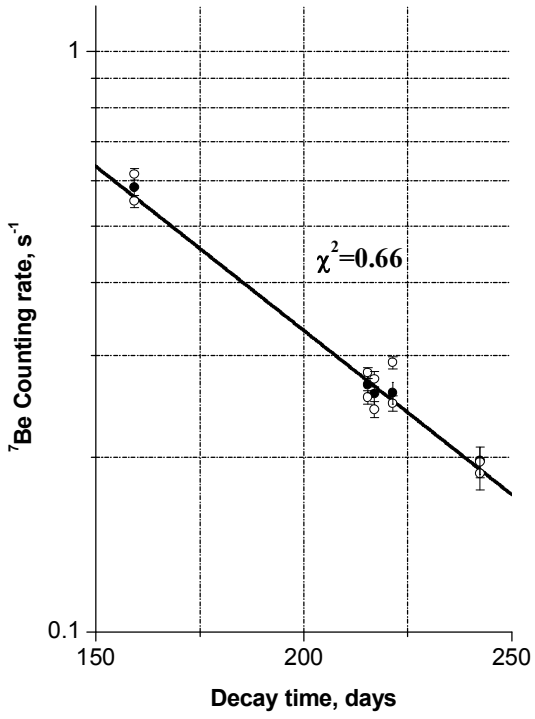

Fig.12. The ^{7}Be decay curve measured for monitor M_2. (he open circles are for the up and down **["top" – "bottom"]** position; the filled circles are the mean values).

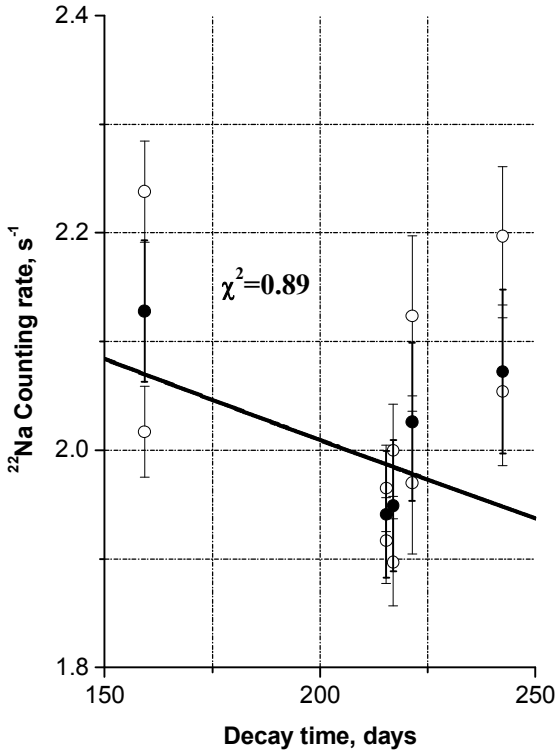

Fig.13. The ^{22}Na decay curve measured for monitor M_2. (he open circles are for the up and down **["top" – "bottom"]** position; the filled circles are the mean values).

The effects of absolute spectrometer effectiveness variations and of γ-absorption in the sample materials that arise from differences in the sample thicknesses were quantified during the latest stage (in a year after irradiation) via dissolving all of 36 fragments of monitor M_3 and monitor pair M_2 and M_1 in alkali to measure ^{22}Na content therein.

In dissolving the solid-state samples, the Al amphotericity properties that permit Al to be solved in both acids and alkali were allowed for. Since operations with alkali are more convenient and safe (the solutions do not evolve any harmful corrosion-active vapors), the Al plates were dissolved in the alkali in the form of a water solution of NaOH, inducing the chemical reaction

$$Al + NaOH + 5H_2O = Na\,[Al\,(OH)_4\,(H_2O)_2] + 3/2H_2 \quad (37)$$

The reaction formula (37) was used to calculate the required alkali concentration with due allowance for the test tube volume and the Al sample masses. The solution was prepared in polypropylene-made test tubes of a 50-ml maximum volume with screw-on caps (the ^{22}Na activity

was measured in the test tubes too. The solution volume was 40 ml to preclude any possible overflow under dissolving accompanied by a weak airing.

The alkali concentration was calculated and experimentally proved using nonexposed Al samples and allowing for real dissolution time (4-5 hours at a 0.2-g mean Al sample mass and the room temperature) to be about 12-13-fold surplus as compared with stoichiometry. A more rapid dissolution under heating or a higher alkali concentration resulted in a significant aerosol carryover, so the heating had to be effected in a glass cup with subsequent carrying the solution to a polymeric test tube. This procedure may have involved a significant relative loss of sample nuclei due to a small solution volume. As a result, a 100 g/l solution of analytically pure NaOH in desalinated water was prepared. Also used in the experiment were two samples of ~1.5-g and ~0.7-g masses that were dissolved in an alkali solution of a higher (300 g NaOH/l) concentration (alkali excess of ~5 and ~11, respectively). Besides, a test tube with 40 ml of pure NaOH solution in water (100 g/l) was prepared to become a background sample.

To determine the absolute volume effectiveness of the spectrometer, the «VNIIFTRI» team prepared a task-oriented source with the attested ^{22}Na quantity (5300±190 Bq) [19]. The solution weight in the test tube was 40.0 g to provide a conformity between the geometries of measuring the alkali solutions of Al monitors and the certified γ-source.

In terms of expression (6), the ^{27}Al(p,x)^{24}Na, ^{27}Al(p,x)^{22}Na, and ^{27}Al(p,x)^{7}Be reaction rates were determined in each of the fragments by γ-spectrometry techniques. The results are presented in Table 5.

Since the numbers of ^{24}Na, ^{22}Na, and ^{7}Be nuclei produced in each of the fragments are proportional to the number of protons that traversed a fragment, the measured results make it possible to determine the proton number through each fragment using the ^{27}Al(p,x)^{24}Na, ^{27}Al(p,x)^{22}Na, and ^{27}Al(p,x)^{7}Be reaction rates:

$$N_p^{ij} = \hat{\Phi}_{ij} \cdot S_{ij} \cdot t_{irr} \qquad i = {}^{24}Na,\ {}^{22}Na,\ {}^{7}Be; \qquad j = 1, 36, M_1, M_2, \tag{38}$$

.

$$\Delta N_p^i = N_p^i \cdot \sqrt{\left(\frac{\Delta\hat{\Phi}_{ij}}{\hat{\Phi}_{ij}}\right)^2 + \left(\frac{\Delta S_{ij}}{S_{ij}}\right)^2} \tag{39}$$

where N_p^{ij} is the proton number through the *j*-th fragment; $\hat{\Phi}_{ij}$ is the mean proton density for the *j*-th sample; S_{ij} is the *j*-th sample surface area.

The numbers of protons N_p^{ij} that hit each *j*-th fragment having been calculated together with their errors ΔN_p^i, the total proton number onto the target throughout the irradiation time and its errors were calculated as

$$N_p^i = \sum_{j=1}^{36} N_{j,i} \tag{40}$$

$$\Delta N_i = \sqrt{\Delta N_{1,i}^2 + \Delta N_{2,i}^2 + \ldots + \Delta N_{36,i}^2} \tag{41}$$

Table 6 presents the results of determining the proton numbers through each fragment and through monitors M_1 and M_2. The ^{27}Al(p,x)^{24}Na, ^{27}Al(p,x)^{22}Na, and ^{27}Al(p,x)^{7}Be reaction cross

sections for 800 MeV protons presented in Table 7 have been taken from [2]. Since the presented ^{27}Al(p,x)^{24}Na and ^{27}Al(p,x)^{7}Be reaction cross sections were measured with respect to the ^{27}Al(p,x)^{22}Na reaction cross section, thei errors are shown as a fraction, whose numerator and denominator are, respectively the total error and the statistical error only, with the total error only being presented for ^{22}Na conforming to [20] (the statistical error is conventionally taken to be zero)

Analyzing the results obtained permits the following conclusions:

- the data obtained using ^{27}Al(p,x)^{24}Na monitor reaction have to be henceforth disregarded because the additional ^{24}Na production due to neutrons ejected backwards from the target reaches 30%;
- in the case of ^{22}Na, the correction homogenizing the samples irradiated reaches $^{22Na}k_{M_3}^{гом.}$ = (1.02±0.06) and $^{22Na}k_{M_2}^{гом.}$ = (0.98±0.08) for monitors M_3 and M_2. The same values can be therefore used for ^{7}Be;
- monitor M_1 is expedient to disregard (see Fig. 14) because of its insufficient area.

With the above approach, in the case of M_2 and M_3, excluding the ^{27}Al(p,x)^{22}Na data measured in foils and retaining the ^{27}Al(p,x)^{7}Be data measured in foils and the ^{27}Al(p,x)^{22}Na data measured in solutions, the total proton number can be obtained as

$$\overline{N}=\frac{^{7Be}N_{M_2}^{foil}\cdot{}^{22Na}k_{M_2}^{\text{hom}}+{}^{7Be}N_{M_3}^{foil}\cdot{}^{22Na}k_{M_3}^{\text{hom}}+{}^{22Na}N_{M_2}^{solution}+{}^{22Na}N_{M_3}^{solution}}{4} \quad (42)$$

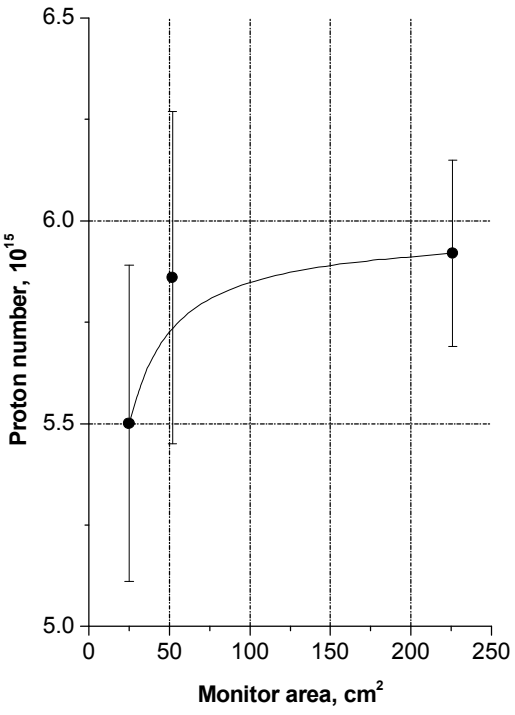

Fig. 14. The number of protons through the monitors as a function of monitor area.

Since the statistical errors in the ^{27}Al(p,x)^{24}Na, ^{27}Al(p,x)^{22}Na, and ^{27}Al(p,x)^{7}Be cross sections were only used during the previous calculation stages, the error in $\Delta\overline{N}$ can be calculated as

$$\Delta\overline{N}=\overline{N}\cdot\sqrt{\left(\frac{\Delta\overline{N}'}{\overline{N}}\right)^2+\left(\frac{\Delta\,{}^{22Na}\sigma}{{}^{22Na}\sigma}\right)^2} \tag{43}$$

The $\Delta\overline{N}'$ value is calculated as

$$\Delta\left(\overline{N}\right)'=\frac{\sqrt{(\Delta({}^{7Be}N_{M_2}^{foil})')^2+(\Delta({}^{7Be}N_{M_3}^{foil})')^2+(\Delta\,{}^{22Na}N_{M_2}^{foil})^2+(\Delta\,{}^{22Na}N_{M_3}^{foil})^2}}{4}, \tag{44}$$

wherein $\Delta({}^{7Be}N_{M_2}^{foil})'$ and $\Delta({}^{7Be}N_{M_3}^{foil})'$ are determined to be

$$\Delta({}^{7Be}N_{M_2}^{foil})'=({}^{7Be}N_{M_2}^{foil})'\cdot\sqrt{\left(\frac{\Delta\,{}^{7Be}N_{M_2}^{foil}}{{}^{7Be}N_{M_2}^{foil}}\right)^2+\left(\frac{\Delta\,{}^{22Na}k_{M_2}^{\hom}}{{}^{22Na}k_{M_2}^{\hom}}\right)^2} \tag{45}$$

$$\Delta({}^{7Be}N_{M_3}^{foil})'=({}^{7Be}N_{M_3}^{foil})'\cdot\sqrt{\left(\frac{\Delta\,{}^{7Be}N_{M_3}^{foil}}{{}^{7Be}N_{M_3}^{foil}}\right)^2+\left(\frac{\Delta\,{}^{22Na}k_{M_3}^{\hom}}{{}^{22Na}k_{M_3}^{\hom}}\right)^2} \tag{46}$$

Table 5

The $^{27}Al(p,x)^{24}Na$, $^{27}Al(p,x)^{22}Na$ and $^{27}Al(p,x)^{7}Be$ reaction rates in the segments of Al-monitor.

		Foils			Solutions
Segment Nos.	Weight, g	$^{27}Al(p,x)^{24}Na$ reaction rate ($10^{-20}s^{-1}$)	$^{27}Al(p,x)^{22}Na$ reaction rate ($10^{-20}s^{-1}$)	$^{27}Al(p,x)^{7}Be$ reaction rate ($10^{-20}s^{-1}$)	$^{27}Al(p,x)^{22}Na$ reaction rate ($10^{-20}s^{-1}$)
1	0.2013	306 ± 15	24.3 ± 1.6	7.30 ± 0.46	23.6 ± 3.1
2	0.2182	302 ± 21	23.8 ± 4.0	10.1 ± 1.4	28.6 ± 3.9
3	0.2465	330 ± 15	25.9 ± 3.2	9.34 ± 1.68	25.5± 3.8
4	0.2502	341 ± 15	24.4 ± 5.9	16.3 ± 1.9	25.6 ± 3.5
5	0.2137	333 ± 20	26.0 ± 3.9	10.3 ± 1.5	27.4 ± 4.5
6	0.2026	293 ± 16	22.9 ± 4.0	10.6 ± 2.0	23.4 ± 4.1
7	0.2249	307 ± 14	31.1 ± 4.0	7.52 ± 1.39	23.4 ± 3.7
8	0.1128	401 ± 22	36.4 ± 5.9	12.4 ± 4.2	41.7 ± 7.1
9	0.1093	432 ± 26	36.8 ± 7.4	35.4 ± 4.4	53.5 ± 7.2
10	0.1081	460 ± 20	48.3 ± 8.0	61.7 ± 6.2	48.8 ± 7.5
11	0.1098	430 ± 17	40.2 ± 6.9	22.6 ± 3.3	34.7 ± 10.1
12	0.2150	343± 12	29.6 ± 3.5	9.65 ± 2.17	22.3± 3.6
13	0.2339	307 ± 12	30.4 ± 3.9	7.33 ± 1.43	32.3 ± 3.3
14	0.1078	428 ± 38	46.1 ± 7.7	23.0 ± 3.3	55.4± 8.6
15	0.1064	5180 ± 191	5846 ± 198	2528 ± 89	6206 ± 438
16	0.1090	12613 ± 439	16079 ± 544	6626 ± 232	16187 ± 1138
17	0.1035	530 ± 24	89.5 ± 8.9	74.3 ± 5.0	73.8 ± 12.6
18	0.2409	338 ± 14	26.5 ± 3.8	14.3 ± 1.7	27.5 ± 4.1
19	0.2526	296 ± 12	33.3 ± 4.9	9.34 ± 1.97	34.3 ± 5.5
20	0.1168	426 ± 22	54.8 ± 6.7	25.4 ± 3.1	38.4 ± 8.2

21	0.1136	1739 ± 60	1698 ± 61	818 ± 30	1739 ± 125
22	0.1207	8011 ± 267	9334 ± 313	3990 ± 139	9455 ± 666
23	0.1140	501 ± 29	73.8 ± 21.5	39.7 ± 14.8	81.5 ± 12.1
24	0.2560	343 ± 14	28.6 ± 3.7	8.51 ± 1.69	25.8 ± 3.2
25	0.2212	309 ± 13	27.7 ± 3.8	8.54 ± 2.89	23.4± 5.9
26	0.1113	410 ± 25	40.1 ± 6.4	17.1 ± 3.5	41.1 ± 10.6
27	0.1142	429 ± 29	35.9 ± 6.6	18.7 ± 3.4	35.1 ± 10.6
28	0.1100	442 ± 33	42.4 ± 5.3	21.9 ± 4.9	48.3 ± 7.4
29	0.1126	418 ± 21	39.7 ± 7.3	13.3 ± 4.4	41.7 ± 5.7
30	0.2120	339 ± 20	23.2 ± 4.2	7.07 ± 2.14	32.3 ± 4.7
31	0.2121	262 ± 20	22.4 ± 3.7	6.20 ± 2.14	20.0 ± 3.7
32	0.2057	303 ± 18	24.3 ± 2.8	7.15 ± 1.83	20.9 ± 4.1
33	0.2491	304 ± 17	23.9 ± 3.8	8.72 ± 1.67	31.3 ± 4.9
34	0.2475	320 ± 19	25.3 ± 3.6	8.61 ± 1.73	30.3 ± 5.3
35	0.2157	312 ± 13	23.8 ± 3.6	6.13 ± 4.32	17.5 ± 4.7
36	0.2049	274 ± 13	35.9 ± 5.4	13.4 ± 2.9	33.1± 6.4
50x50	0.7145	-	5372 ± 178	2289 ± 79	5260 ± 370
72x72	1.4185	-	2807 ± 98	1151 ± 42	2704 ± 190

Table 6

Numbers of protons through the segments of of Al-monitor.

		Foils			Solutions
Segment Nos.	Weight, g	Proton number (10^{13}) measured via $^{27}Al(p,x)^{24}Na$ rate	Proton number (10^{13}) measured via $^{27}Al(p,x)^{22}Na$ rate	Proton number (10^{13}) measured via $^{27}Al(p,x)^{7}Be$ rate	Proton number (10^{13}) measured via $^{27}Al(p,x)^{22}Na$ rate
1	0.2013	10.7 ± 1.0	0.73 ± 0.07 (0.05)	0.54 ± 0.05 (0.04)	0.71 ± 0.11 (0.09)
2	0.2182	11.4 ± 1.2	0.78 ± 0.14 (0.13)	0.81 ± 0.13 (0.11)	0.94 ± 0.14 (0.13)
3	0.2465	14.1 ± 1.3	0.96 ± 0.14 (0.12)	0.84 ± 0.17 (0.15)	0.94 ±0.16 (0.14)
4	0.2502	14.8 ± 1.3	0.91 ± 0.23 (0.22)	1.50 ± 0.21 (0.18)	0.96 ± 0.15 (0.13)
5	0.2137	12.3 ± 1.2	0.83 ± 0.14 (0.13)	0.81 ± 0.13 (0.12)	0.88 ± 0.16 (0.14)
6	0.2026	10.3 ± 1.0	0.69 ± 0.13 (0.12)	0.79 ± 0.16 (0.15)	0.71 ± 0.14 (0.13)
7	0.2249	12.0 ± 1.1	1.05 ± 0.15 (0.13)	0.62 ± 0.12 (0.12)	0.79 ± 0.14 (0.12)
8	0.1128	7.8 ± 0.7	0.61 ± 0.11 (0.10)	0.51 ± 0.18 (0.17)	0.71 ± 0.13 (0.12)
9	0.1093	8.2 ± 0.8	0.60 ± 0.13 (0.12)	1.42 ± 0.21 (0.18)	0.88 ± 0.13 (0.12)
10	0.1081	8.6 ± 0.8	0.78 ± 0.14 (0.13)	2.45 ± 0.31 (0.26)	0.79 ± 0.13 (0.12)
11	0.1098	8.2 ± 0.7	0.66 ± 0.12 (0.11)	0.91 ± 0.15 (0.13)	0.57 ± 0.17 (0.17)
12	0.2150	12.8 ± 1.1	0.95 ± 0.13 (0.11)	0.76 ± 0.18 (0.17)	0.72 ± 0.13 (0.12)
13	0.2339	12.4 ± 1.1	1.07 ± 0.16 (0.14)	0.63 ± 0.13 (0.12)	1.13 ± 0.14 (0.12)
14	0.1078	8.0 ± 0.9	0.74 ± 0.14 (0.12)	0.91 ± 0.15 (0.13)	0.89 ± 0.15 (0.14)
15	0.1064	95.5 ± 8.2	93.2 ± 7.3 (3.2)	98.7 ± 8.4 (4.8)	98.9 ± 9.9 (7.0)
16	0.1090	238 ± 20	263 ± 21 (9)	265 ± 23 (13)	264 ± 26 (19)
17	0.1035	9.5 ± 0.8	1.39 ± 0.17 (0.14)	2.82 ± 0.29 (0.21)	1.14 ± 0.21 (0.20)
18	0.2409	14.1 ± 1.2	0.96 ± 0.15 (0.14)	1.26 ± 0.18 (0.16)	0.99 ± 0.16 (0.15)
19	0.2526	13.0 ± 1.1	1.26 ± 0.21 (0.19)	0.87 ± 0.19 (0.18)	1.30 ± 0.23 (0.21)
20	0.1168	8.6 ± 0.8	0.96 ± 0.14 (0.12)	1.09 ± 0.16 (0.14)	0.67 ± 0.15 (0.14)
21	0.1136	34.2 ± 2.9	28.9 ± 2.3 (1.0)	34.1 ± 2.9 (1.7)	29.6 ± 3.0 (2.1)
22	0.1207	168 ± 14	169 ± 13 (6)	177 ± 15 (9)	171 ± 17 (12)
23	0.1140	9.9 ± 1.0	1.26 ± 0.38 (0.37)	1.66 ± 0.63 (0.62)	1.39 ± 0.23 (0.21)
24	0.2560	15.2 ± 1.3	1.10 ± 0.16 (0.14)	0.80 ± 0.17 (0.16)	0.99 ± 0.14 (0.12)
25	0.2212	11.8 ± 1.0	0.92 ± 0.14 (0.13)	0.69 ± 0.24 (0.24)	0.78 ± 0.20 (0.20)

26	0.1113	7.9 ± 0.8	0.67 ± 0.12 (0.11)	0.70 ± 0.15 (0.15)	0.69 ± 0.18 (0.18)
27	0.1142	8.5 ± 0.9	0.61 ± 0.12 (0.11)	0.78 ± 0.16 (0.15)	0.60 ± 0.19 (0.18)
28	0.1100	8.4 ± 0.9	0.70 ± 0.10 (0.09)	0.88 ± 0.21 (0.20)	0.80 ± 0.13 (0.12)
29	0.1126	8.2 ± 0.8	0.67 ± 0.13 (0.12)	0.55 ± 0.19 (0.18)	0.70 ± 0.11 (0.10)
30	0.2120	12.5 ± 1.2	0.74 ± 0.14 (0.13)	0.55 ± 0.17 (0.17)	1.03 ± 0.17 (0.15)
31	0.2121	9.6 ± 1.1	0.71 ± 0.13 (0.12)	0.48 ± 0.17 (0.17)	0.64 ± 0.13 (0.12)
32	0.2057	10.8 ± 1.0	0.75 ± 0.10 (0.09)	0.54 ± 0.14 (0.14)	0.65 ± 0.14 (0.13)
33	0.2491	13.1 ± 1.3	0.89 ± 0.15 (0.14)	0.80 ± 0.16 (0.15)	1.17 ± 0.20 (0.18)
34	0.2475	13.7 ± 1.3	0.94 ± 0.15 (0.13)	0.78 ± 0.17 (0.16)	1.12 ± 0.21 (0.20)
35	0.2157	11.7 ± 1.0	0.77 ± 0.13 (0.12)	0.49 ± 0.34 (0.34)	0.57 ± 0.16 (0.15)
36	0.2049	9.7 ± 0.9	1.10 ± 0.18 (0.17)	1.01 ± 0.23 (0.22)	1.02 ± 0.21 (0.20)
Total proton number		**883 ± 72**	**581 ± 46 (28)**	**605 ± 52 (37)**	**592 ± 48 (23)**
M_2	1.4185	-	597 ± 47 (21)	599 ± 51 (30)	586 ± 59 (41)
M_1	0.7145	-	575 ± 45 (19)	600 ± 51 (29)	550 ± 55 (39)
The summary total proton number (10^{13})					**600 ± 50**

Table 7

The $^{27}Al(p,x)^{24}Na$, $^{27}Al(p,x)^{22}Na$, and $^{27}Al(p,x)^{7}Be$ cross sections for 800 MeV protons.

Reaction	$^{27}Al(p,x)^{24}Na$,	$^{27}Al(p,x)^{22}Na$	$^{27}Al(p,x)^{7}Be$
Cross section, mbarn	13.40 ± 1.04 (0.42)	15.5 ± 1.1 (0)	6.33 ± 0.49 (0.21)

Since the monitor fragments are sufficiently large, (any smaller dimensions raise the error of count rate in total absorption peak), the beam shape was restored by the least squares techniques under the assumption that in either of coordinates *x,y* the beam shape is described by Gaussian. In this case, the number, N_p, of protons that hit the *i-th* fragment of round monitor can be determined as

$$N_{p_i}(\vec{P}) = \iint\limits_{S_i} \frac{P_5}{2\pi P_2 P_4} e^{-\frac{(x-P_1)^2}{2P_2^2}} e^{-\frac{(y-P_3)^2}{2P_4^2}} dxdy \qquad (47)$$

where $(\vec{P}) = \{P_1, P_2, P_3, P_4, P_5\}$ is the vector of input parameters– вектор исходных параметров; S_i is the surface of the i-th fragment.

The parameters $(\vec{P})$ are determined from the least squared functional

$$R = \sum_{i=1}^{N} \frac{1}{\sigma^2_{\tilde{N}_{p_i}}} \cdot \left(\tilde{N}_{p_i} - \frac{P_5}{2\pi P_2 P_4} \cdot \iint\limits_{S_i} e^{-\frac{(x-P_1)^2}{2P_2^2}} e^{-\frac{(y-P_3)^2}{2P_4^2}} dxdy \right)^2 \qquad (48)$$

where $\sigma_{\tilde{N}_{p_i}}$ is the error in $\tilde{N}_{p_i}$; N is the number of monitor fragments.

Since the parameters $(\vec{P})$ enter function (47) nonlinearly, they were determined by successive approximations. With that purpose, the approximating function (47) was expanded in a Taylor series in the vicinities of point $(\vec{P}_0)$, which is the first approximation of the parameters $(\vec{P})$. By minimizing the expression

$$R_i = \sum_{i=1}^{N} \frac{1}{\sigma^2_{\tilde{N}_{p_i}}} \cdot \left(\tilde{N}_{p_i} - \tilde{N}_{p_i}(\vec{P}_0) - \sum_{j=1}^{5} \left. \frac{\partial N_{p_i}}{\partial P_j} \right|_{\vec{P}=\vec{P}_0} \cdot \Delta P_j \right)^2, \tag{49}$$

we find the addends $\Delta\vec{P}$ to the parameters $\vec{P}$ from the conditions

$$\frac{\partial R_1}{\partial P_k} = 0 \qquad \text{k = 1, 2, 3, 4, 5.} \tag{50}$$

This leads to the ordinary set of linear equations, wherein the addends $\Delta\vec{P}$ to parameters $\vec{P}$ are unknowns:

$$M \cdot \Delta\vec{P} = \vec{b} \tag{51}$$

where

$$M_{ij} = \sum_{k=1}^{N} \frac{1}{\sigma^2_{\tilde{N}_{pk}}} \cdot \left. \frac{\partial N_{p_k}}{\partial P_i} \right|_{\vec{P}=\vec{P}_0} \left. \frac{\partial N_{p_k}}{\partial P_j} \right|_{\vec{P}=\vec{P}_0} \tag{52}$$

$$b_i = \sum_{k=1}^{N} \frac{1}{\sigma^2_{\tilde{N}_{pk}}} \cdot \left(\tilde{N}_{p_k} - \tilde{N}_{p_k}(\vec{P}_0) \right) \left. \frac{\partial N_{p_k}}{\partial P_i} \right|_{\vec{P}=\vec{P}_0} \tag{53}$$

After that, the entire procedure recurs in the vicinities of point $\vec{P}_1 = \vec{P}_0 + \Delta\vec{P}$, etc. The iteration process come to end when the condition $\left|\Delta\vec{P}\right| << \sigma_{p_i}$ gets satisfied for all parameters (σ_{p_i} is an error in determining the parameter P_i).

Table 8 presents the results of determining the proton beam shape parameters.

Table 8

The proton beam shape parameters.

Parameter	Value
Proton number	(6.0 ± 0.5) 10^{15}
Beam shape parameters (cm)	
P_1	0.27 ± 0.10
P_2	0.80 ± 0.06
P_3	0.44 ± 0.15
P_4	0.70 ± 0.09
P_5	(3.9 ± 1.0) 10^{15}

3.7. Determination of proton beam power

The proton beam power under irradiation can be calculated as

$$W = \frac{N}{T} \cdot E \cdot k, \tag{54}$$

where E is proton beam energy (0.8 GeV);
N is the total number of protons that hit the target throughout the irradiation time, $(6.0\pm0.5)\cdot10^{15}$;
T is the total irradiation time (64800c), k – system factor that is $1.60206\cdot10^{-19}$J/eV.

Allowing for the values of the parameters *N, E, T,* the resulting power is

$$W = (11.87\pm0.99)\text{W} \qquad (55)$$

Since the experimental reaction rates are of dimension [1/s] , they can be renormalized to be [1/s·W] by introducing the normalization factor $R_{norm}^{\exp} = R^{\exp}/W$. The LAHET code system generates the flux densities of particles produced in a single proton interaction with target in units of [1/cm^2]. Therefore, the calculated reaction rate $R^{calc} = \int_0^\infty \sigma(E)\cdot\phi(E)dE$ is dimensionless. By introducing the normalization factor $R_{norm}^{calc} = R^{calc}/E$, we can also renormalize the calculated reaction rates to become [1/s·W]. In this case, the conversion factor for E_p = 0.8 GeV is

$$K = 0.8\cdot10^{9}\left[eV\right]\times1.60206\cdot10^{-19}\left[J/eV\right] = 1.2816\cdot10^{-10}\left[J\right] = 1.2816\cdot10^{-10}\left[s\cdot W\right] \qquad (56)$$

3.8 Experimental results

3.8.1. Space distributions of the nuclide reaction rates inside the Pb target.

3.8.1.1. Rates of reactions on ^{59}Co.

Table 9 presents the nuclear-physics characteristics of the nuclides produced in twelve ^{59}Co samples during interactions of different-energy protons and neutrons, which are used to calculate the reaction rates. Table 10 and Fig. 15 present the rates of residual nuclide production in ^{59}Co samples rradiated at the Pb disc centers along line C at 0, 80, 160, 240, 320, 400, 480, 560, 640, 720, 800, and 880 mm from the target front edge.

Table 9

The nuclear-physics characteristics of the nuclides produced in a ^{59}Co sample in interactions with high-energy neutrons and protons [4,21].

Nuclide	Half-lives	γ-energy (E_γ , keV) and yield (Y_γ , %)
^{57}Ni	35.60h	*1919.5(12.3), 1377.6(81.7), 127.2(16.7)*
^{60}Co	5.2714y	*1332.5(99.99), 1173.2(99.97)*
^{58}Co	70.86d	*1674.7(0.52), 864(0.68), 810.8(99.45)*
^{58m}Co	9.04h	*810.8(*)*
^{57}Co	271.74d	*136.5 (10.68), 122.1 (85.60)*
^{56}Co	77.233d	*2598.5 (17.3), 2034.8 (7.89), 2015.2 (3.04), 1810.8(0.64), 1771.3 (15.47), 1360.2 (4.29), 1238.3 (66.9), 1175.1(2.29), 1037.8 (14.17), 977.4(1.45), 846.8 (99.94),*
^{55}Co	17.53h	*1408.5 (16.9),1370.0(2.9), 1316(7.1), 931.1 (75.0), 803.7(1.87), 477.2 (20.2)*
^{59}Fe	44.472d	*1291.6(43.2),1099.2(56.5),192.4(3.08),168.9(43.2), 142.6(0.05)*
^{52}Fe	8.275h	*168.7 (99.0)*
^{56}Mn	2.5789h	*2113.1 (14.3), 1810.7 (27.2), 846.8 (98.),*
^{54} Mn	312.11d	*834.8 (99.98)*

^{52} Mn	5.591d	*1434.1 (100.0), 1333.7 (5.07), 1246.3 (4.21), 935.5 (94.5), 848.2 (3.32), 744.2 (90.0), 647.5(0.40), 600.2(0.39), 346.0(0.98)*
^{51} Cr	27.7025d	*320.1 (9.92)*
^{48} Cr	21.56h	*308.2 (100.0), 112.3 (96.0),*
^{48} V	15.9735d	*2240.4(2.41), 1312.1 (97.5), 983.5 (100.0), 944.1(7.76), 928.3 (0.77),*
^{48} Sc	43.67h	*1312.1 (100.1), 1037.5 (97.6), 983.5 (100.1),175.4 (7.48)*
^{47} Sc	3.3492d	*159.4 (68.3)*
^{46} Sc	83.79d	*1120.5 (99.9870), 889.3 (99.9840)*
^{44m} Sc	58.61h	*1499.5(98.61), 1157.0(98.61), 1126.1 (1.20), 1001.8 (1.20), 270.9 (86.7)*
^{44}Sc	3.97h	*1499.5 (0.908), 1157.0(99.9)*
^{43}Sc	3.891h	*372.8 (22.5),*
^{47}Ca	4.536d	*1297.1 (71.0), 159,4(D)*
^{43}K	22.3h	*617.5 (79.2), 593.4 (11.26), 396.9 (11.85), 372.8 (86.80), 220.6(4.80)*
^{42}K	12.360h	*1525.0 (18.08)*
^{28}Mg	20.915h	*1778.8(100.20)1342.3(52.6), 400.7(36.6).*
^{24}Na	14.9590h	*1369.0 (100.0)*
^{22}Na	2.6019y	*1274.5 (99.944)*
^{7}Be	53.29d	*477.6 (10.52)*

Table 10 Residual production rates in ^{59}Co inside Pb target $\left[10^{-20}, \frac{1}{s \cdot nucleus \cdot W}\right]$

Pro-duct	Yield type	$T_{1.2}$	Distance from target front (mm)											
			0	80	160	240	320	400	480	560	640	720	800	880
^{57}Ni	i	35.60h	88(11)	88.9(9.0)	32.6(3.2)	10.3(1.3)	4.34(0.43)	5.61(0.55)	-	-	-	-	-	-
^{60}Co	i(m+g)	5.2714y	960(94)	1260(120)	720(66)	417(38)	290(27)	203(19)	172(16)	171(15)	173(16)	189(17)	214(20)	246(22)
^{58m}Co	i(m)	9.04h	19300(2500)	12800(1700)	5650(740)	1930(300)	791(99)	234(28)	24.9(10.0)	12.2(3.6)	-	-	-	-
^{58}Co	i(m+g)	70.86d	28000(2500)	24000(2100)	9050(810)	2900(260)	990(90)	415(37)	43.3(3.9)	16.3(1.5)	6.89(0.63)	3.34(0.32)	1.80(0.18)	0.95(0.11)
^{58}Co	i	70.86d	8700(1900)	11100(1600)	3430(610)	970(260)	202(72)	182(25)	18.4(9.9)	4.1(3.4)	-	-	-	-
^{57}Co	c	271.74d	13000(1200)	10540(950)	3850(350)	1290(120)	461(41)	270(24)	14.9(1.4)	5.80(0.59)	2.67(0.26)	1.22(0.13)	0.633(0.089)	0.46(0.11)
^{56}Co	c	77.233d	3410(310)	2550(230)	867(78)	287(26)	106.4(9.6)	67.2(6.0)	-	-	-	-	-	-
^{55}Co	c	17.53h	449(44)	333(33)	125(12)	39.7(3.9)	14.1(1.4)	7.55(0.76)	-	-	-	-	-	-
^{59}Fe	c	44.472d	1170(110)	1510(140)	592(64)	228(21)	74.7(7.6)	19.4(1.8)	4.42(0.51)	1.67(0.18)	0.81(0.16)	0.42(0.13)	-	-
^{52}Fe	c	8.275h	-	42.2(5.5)	15.1(2.0)	5.70(0.68)	1.77(0.20)	0.294(0.046)	-	-	-	-	-	-
^{56}Mn	c	2.5789h	2060(240)	1790(220)	780(89)	258(26)	76.3(7.4)	19.9(2.0)	3.86(0.51)	1.27(0.22)	-	-	-	-
^{54}Mn	i	312.11d	12500(1100)	8360(750)	2800(250)	881(79)	288(26)	82.0(7.5)	6.50(0.72)	2.73(0.34)	1.27(0.19)	0.82(0.24)	-	-
^{52}Mn	c	5.591d	4340(390)	2710(240)	929(84)	260(24)	81.0(7.3)	17.2(1.6)	0.979(0.097)	0.350(0.043)	0.116(0.030)	-	-	-
^{51}Cr	c	27.7025d	14300(1300)	8580(780)	2700(250)	799(72)	238(22)	31.7(3.1)	3.22(0.61)	1.41(0.32)	-	-	-	-
^{48}Cr	c	21.56h	205(19)	114(11)	37.4(3.5)	9.75(0.92)	2.30(0.21)	0.106(0.035)	-	-	-	-	-	-
^{48}V	c	15.9735d	7130(640)	3910(350)	1150(100)	307(27)	75.5(6.8)	3.98(0.37)	0.64(0.12)	-	-	-	-	-
^{48}Sc	i	43.67h	335(32)	177(17)	55.9(6.4)	11.9(1.1)	2.19(0.23)	0.22(0.11)	-	-	-	-	-	-
^{47}Sc	i	3.3492d	1600(150)	851(78)	257(24)	59.7(5.4)	12.7(1.2)	1.002(0.092)	-	-	-	-	-	-
^{47}Sc	c	3.3492d	1650(150)	868(79)	264(24)	61.7(5.6)	13.0(1.2)	1.056(0.096)	0.171(0.024)	-	-	-	-	-
^{46}Sc	i(m+g)	83.79d	4220(380)	2190(200)	611(55)	145(13)	30.1(2.7)	1.41(0.44)	-	-	-	-	-	-
^{44m}Sc	i(m)	58.61h	3260(290)	1610(150)	469(42)	97.9(8.9)	17.3(1.6)	0.537(0.062)	0.178(0.024)	0.099(0.023)	0.071(0.022)	-	-	-
^{44}Sc	i(m+g)	3.97h	5680(520)	2830(250)	886(81)	193(18)	33.6(3.1)	-	-	-	-	-	-	-
^{44}Sc	i	3.97h	2460(240)	1230(110)	429(42)	98(11)	16.9(1.6)	-	-	-	-	-	-	-
^{43}Sc	c	3.891h	1430(240)	800(140)	198(43)	50.7(9.8)	7.5(1.6)	-	-	-	-	-	-	-
^{47}Ca	c	4.536d	37.3(8.6)	16.8(2.6)	4.9(1.3)	1.46(0.53)	0.29(0.13)	0.054(0.020)	-	-	-	-	-	-
^{43}K	c	22.3h	612(56)	292(27)	77.4(7.1)	15.2(1.4)	2.16(0.22)	-	-	-	-	-	-	-
^{42}K	i	12.360h	1550(250)	811(79)	226(23)	46.3(6.1)	6.98(0.85)	-	-	-	-	-	-	-
^{28}Mg	c	20.915h	36.0(7.6)	14.1(2.4)	2.31(0.53)	-	0.89(0.27)	-	-	-	-	-	-	-
^{24}Na	c	14.9590h	371(37)	136(15)	30.0(3.0)	4.87(0.59)	0.87(0.16)	-	-	-	-	-	-	-
^{22}Na	c	2.6019y	218(31)	114(21)	-	-	-	-	-	-	-	-	-	-
^{7}Be	i	53.29d	1320(130)	634(85)	106(14)	-	-	-	-	-	-	-	-	-

.

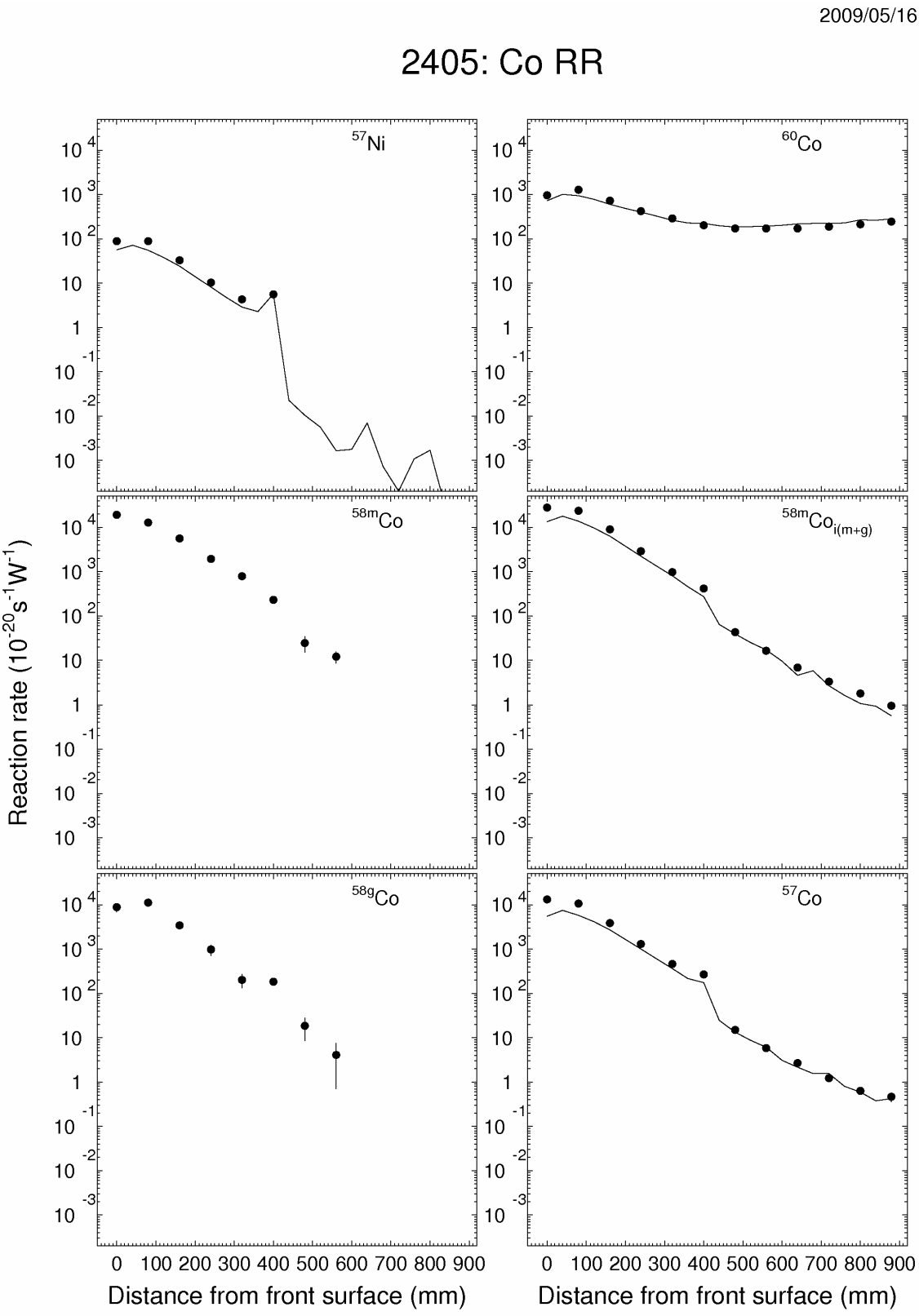

Fig. 15. Experimental and calculated distributions of ^{59}Co reaction products inside Pb target (^{57}Ni, ^{60}Co, ^{58m}Co, ^{58m}Co$_{i(m+g)}$, ^{58g}Co, ^{57}Co).

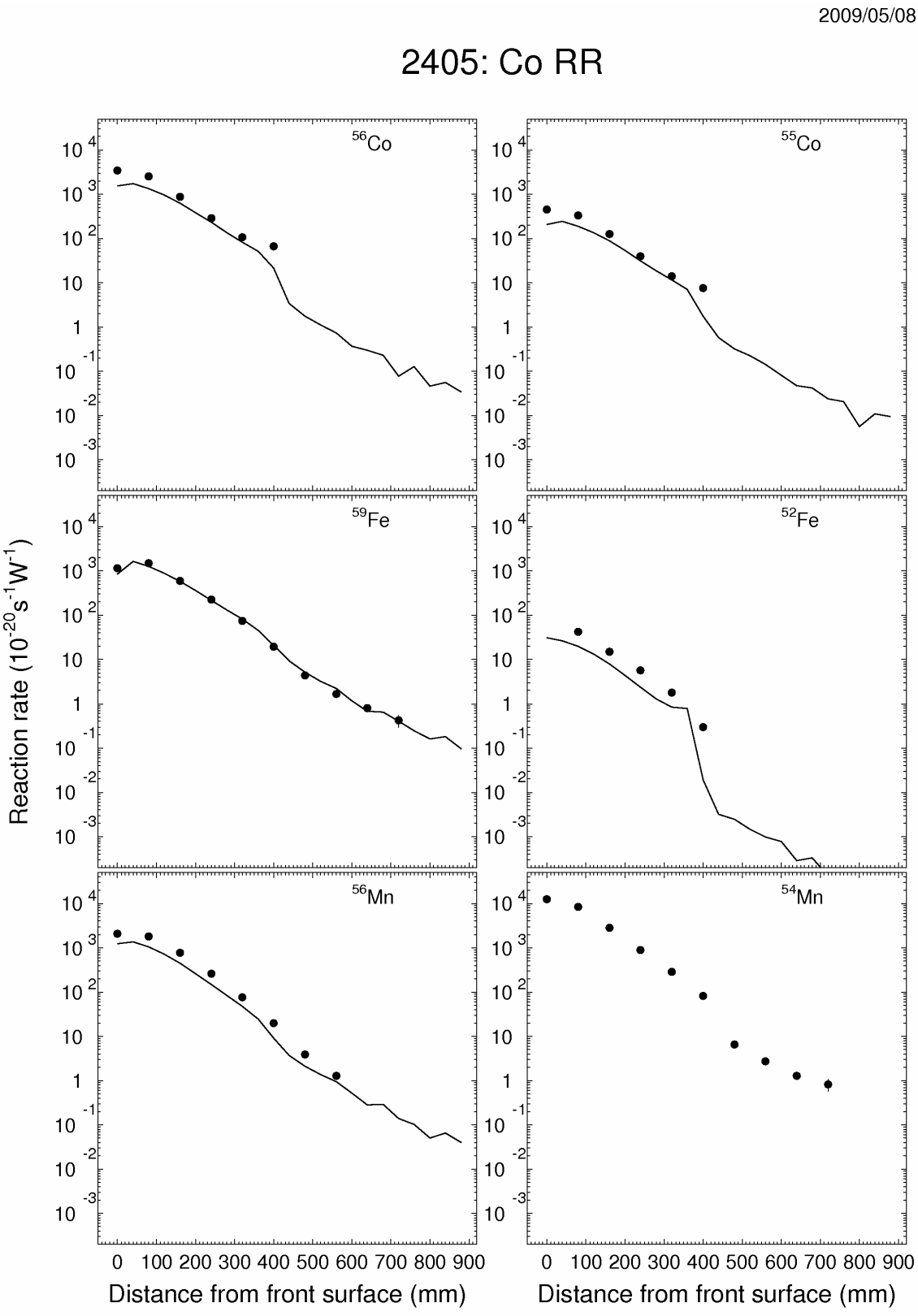

Fig. 15 (cont'd.). The experimental and calculated distributions of ^{59}Co reaction products inside Pb target (^{56}Co, ^{55}Co, ^{59}Fe, ^{52}Fe, ^{56}Mn, ^{54}Mn).

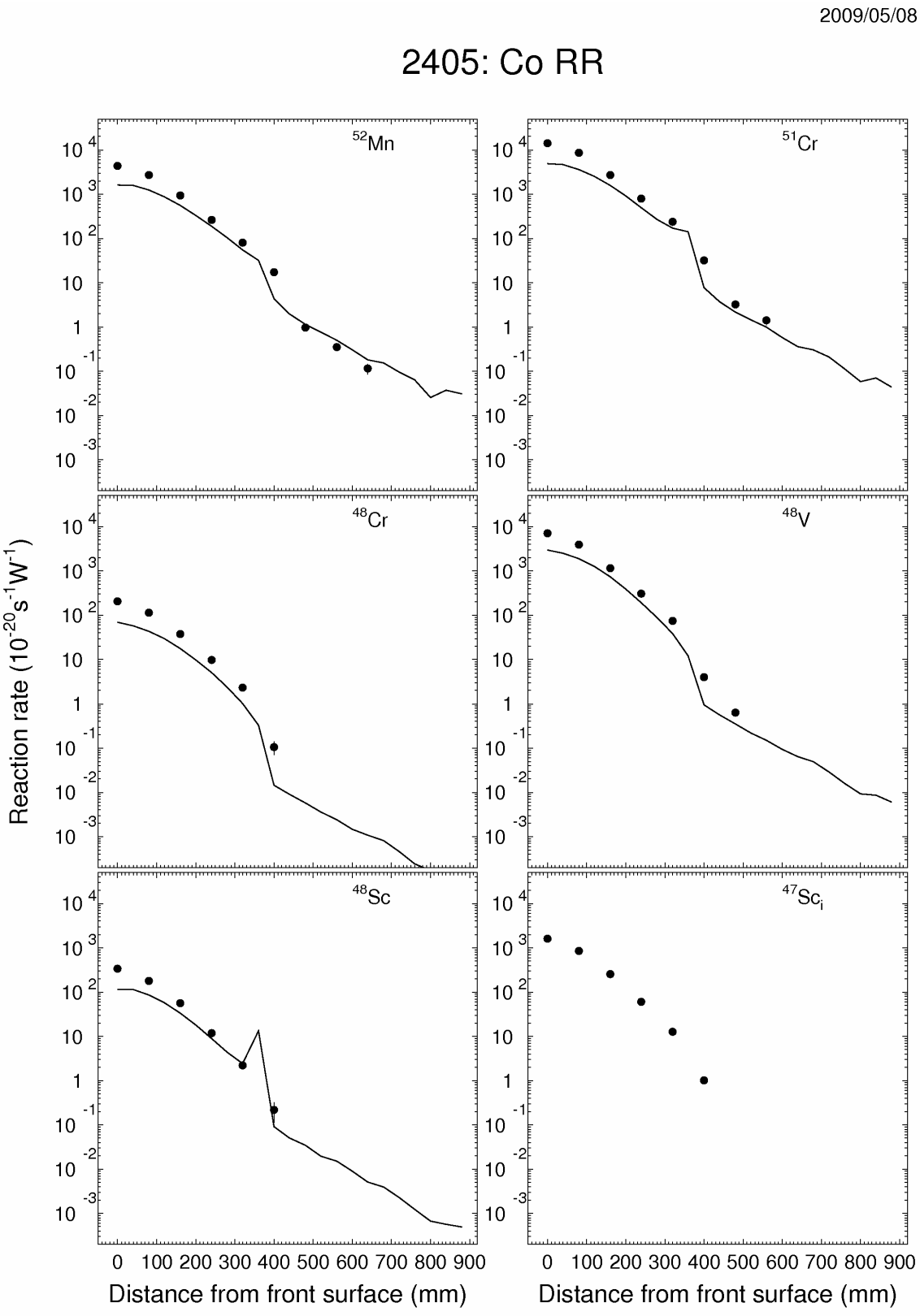

Fig. 15 (cont'd.). The experimental and calculated distributions of ^{59}Co reaction products inside Pb target (^{52}Mn, ^{51}Cr, ^{48}Cr, ^{48}V, ^{48}Sc, ^{47}Sc$_i$).

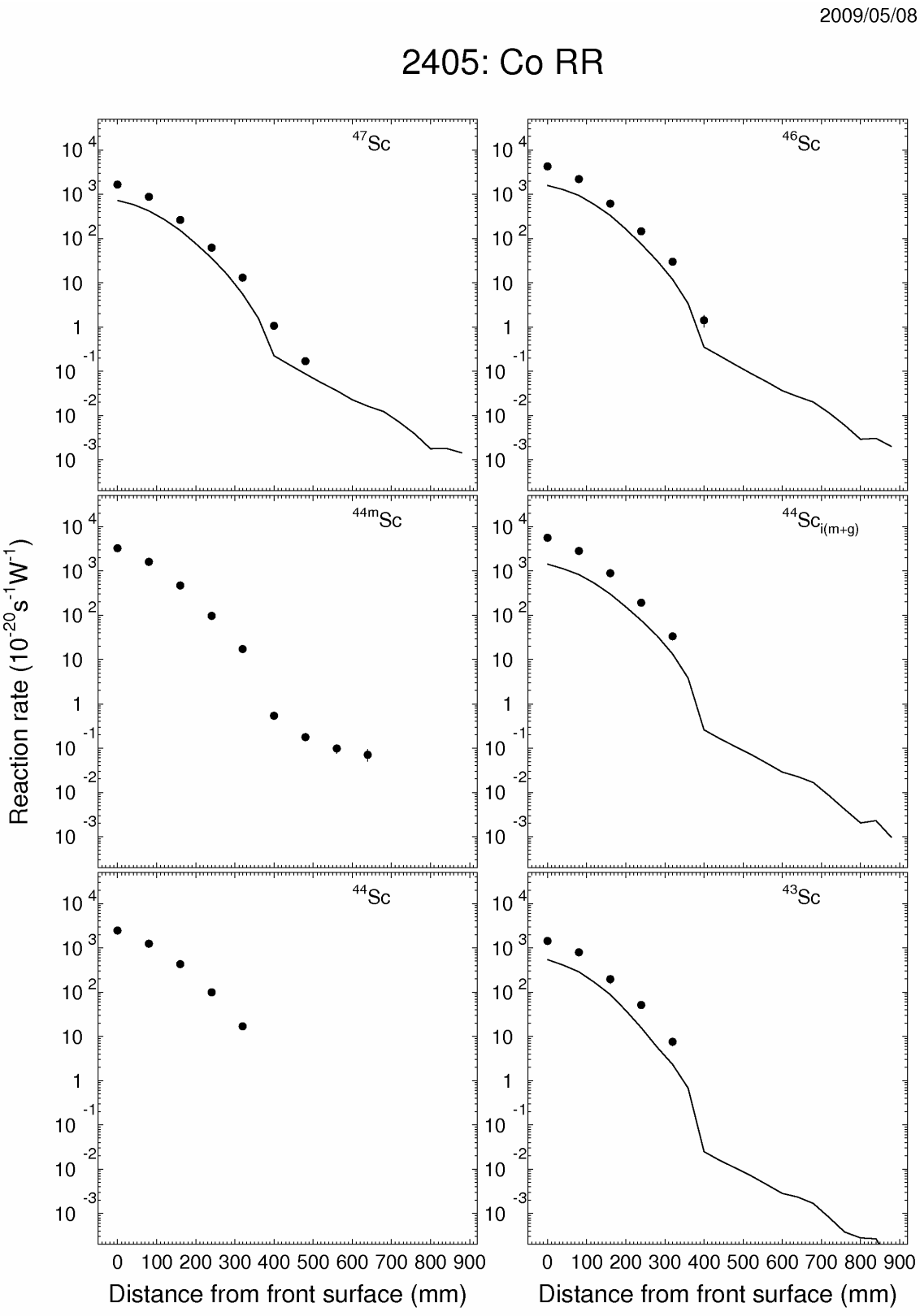

Fig. 15 (cont'd.). The experimental and calculated distributions of ^{59}Co reaction products inside Pb target (^{47}Sc, ^{46}Sc, ^{44m}Sc, $^{44}Sc_{i(m+g)}$, ^{44}Sc, ^{43}Sc).

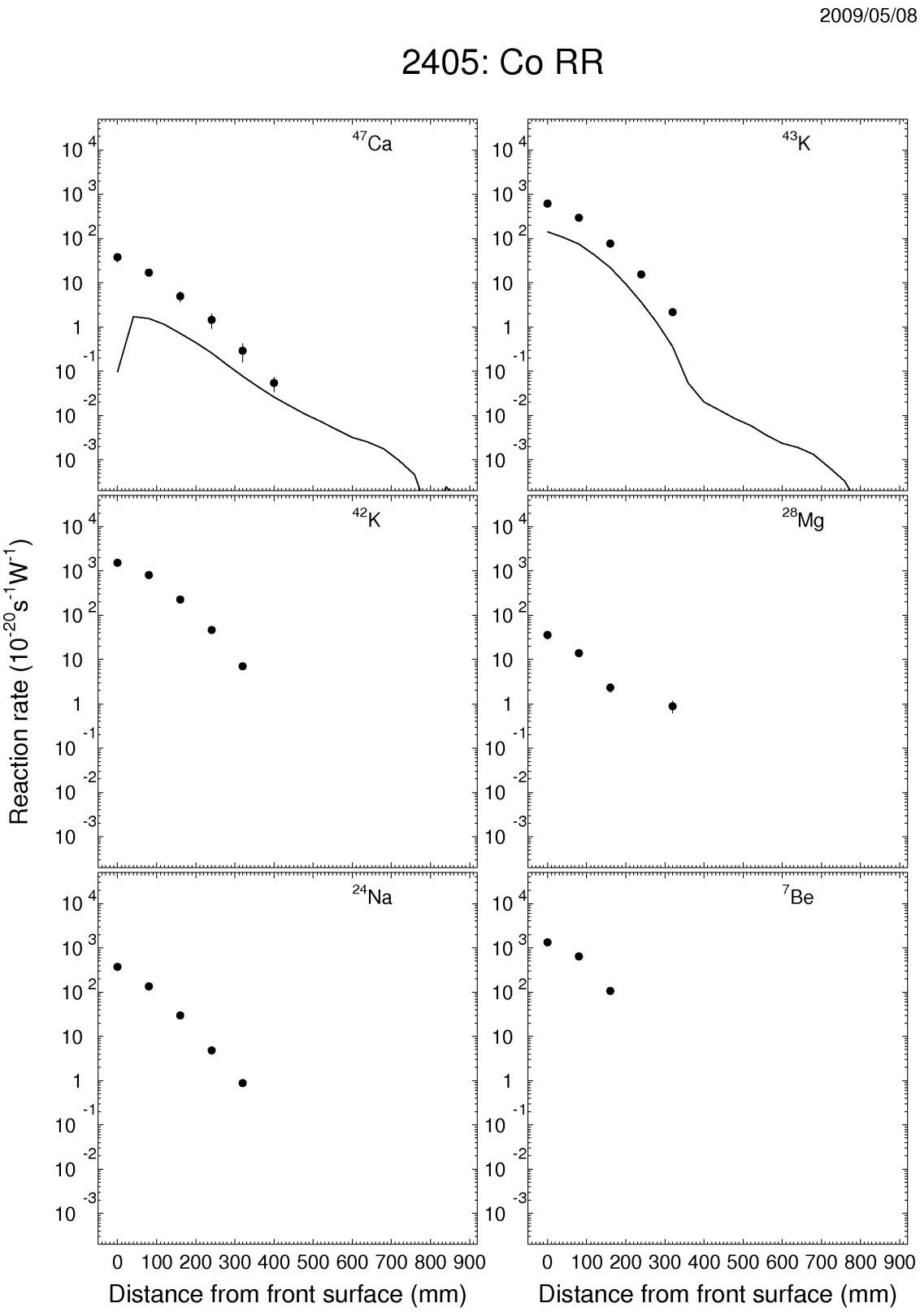

Fig. 15 (cont'ed.). The experimental and calculated distributions of ^{59}Co reaction products inside Pb target (^{47}Ca, ^{43}K, ^{42}K, ^{28}Mg, ^{24}Na, ^{7}Be).

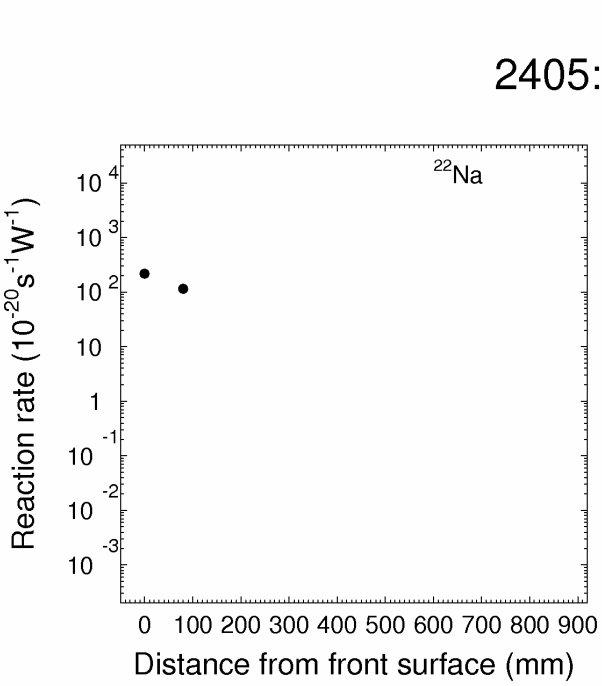

Fig. 15 (cont'ed.). The experimental and calculated distributions of ^{59}Co reaction products inside Pb target (^{22}Na).

3.8.1.2. Rates of reactions on ^{27}Al.

Table 11 presents the nuclear-physics characteristics of the nuclides produced in sixty ^{27}Al samples in interaction of different-energy protons and neutrons, which are used to calculate the reaction rates. Table 12 and Figs. 16-18 present the rates of residual nuclide production in ^{27}Al samples irradiated in the centers and periphery of Pb discs along lines «A», «B», «C», «D», «E» at 0, 80, 160, 240, 320, 400, 480, 560, 640, 720, 800, and 880 mm from the target front butt end

Table 11

Nuclear-physics characteristics of the nuclides produced by high-energy proton and neutron interactions in ^{27}Al sample [4,21].

Nuclide	Half-life	γ-quantum energy (E_γ, keV) and yield (Y_γ , %)
^{27}Mg	9.458m	*843.8(99.944), 1014.4(28.0)*
^{22}Na	2.6019y	*1274.5(99.944)*
^{24}Na	14.9590h	*1369.0(100.0)*
^{7}Be	53.29 d	*477.6(10.52)*

Table 12

Residual production rates in ^{27}Al along lines «A», «B», «C», «D», «E», inside Pb target $\left[10^{-20}, \frac{1}{s \cdot nucleus \cdot W}\right]$.

Posi-tion	Nuclide	T1/2	Yield type	Distance from target front (mm)											
				0	80	160	240	320	400	480	560	640	720	800	880
A	^{24}Na	14.959 h	c	48.4(4.5)	163(15)	134(12)	80.9(7.4)	48.2(4.4)	18.7(1.7)	5.68(0.50)	2.18(0.27)	1.06(0.10)	0.462(0.046)	0.260(0.029)	0.165(0.020)
	^{22}Na	2.6019y	c	8.0(1.0)	19.9(2.3)	26.9(2.8)	20.9(2.3)	8.1(1.5)							
B	^{24}Na	14.959 h	c	62.0(5.5)	432(38)	321(28)	206(19)	115(10)	32.7(3.0)	6.90(0.61)	2.86(0.44)	1.12(0.11)	0.578(0.063)	0.377(0.066)	0.178(0.019)
	^{22}Na	2.6019y	c	5.23(0.56)	87.4(7.8)	79.7(7.2)	82.3(7.5)	59.2(5.5)	25.8(2.7)		4.1(1.2)				
C	^{24}Na	14.959 h	c	6190(570)	4610(410)	1800(160)	559(49)	172(15)	48.3(4.8)	6.96(0.64)	3.04(0.52)	1.28(0.12)	0.668(0.065)	0.314(0.034)	0.195(0.026)
	^{22}Na	2.6019y	c	6120(530)	3810(330)	1170(100)	374(33)	95.1(9.3)	50.8(5.5)	7.8(2.8)					
	^{7}Be	53.29d	i	2470(210)	1180(100)	279(24)	71.9(6.6)	11.2(2.0)	5.8(1.7)						
D	^{24}Na	14.959 h	c	233(21)	498(45)	337(30)	230(21)	116(10)	33.4(3.1)	7.02(0.62)	2.66(0.24)	1.52(0.34)	0.633(0.061)	0.287(0.050)	0.166(0.023)
	^{22}Na	2.6019y	c	14.7(2.6)	109(10)	77.2(7.0)	77.4(7.1)	54.0(5.2)	23.0(2.6)	3.22(0.27)					
E	^{24}Na	14.959 h	c	79.4(9.8)	180(17)	131(12)	81.3(7.7)	49.8(4.5)	21.4(2.0)	6.48(0.58)	2.69(0.25)	1.14(0.11)	0.55(0.08)	0.352(0.037)	0.187(0.029)
	^{22}Na	2.6019y	c	1.98(1.40)	32.2(3.2)	25.2(2.7)	22.4(2.2)	19.3(2.2)	16.0(2.0)	5.78(1.00)					

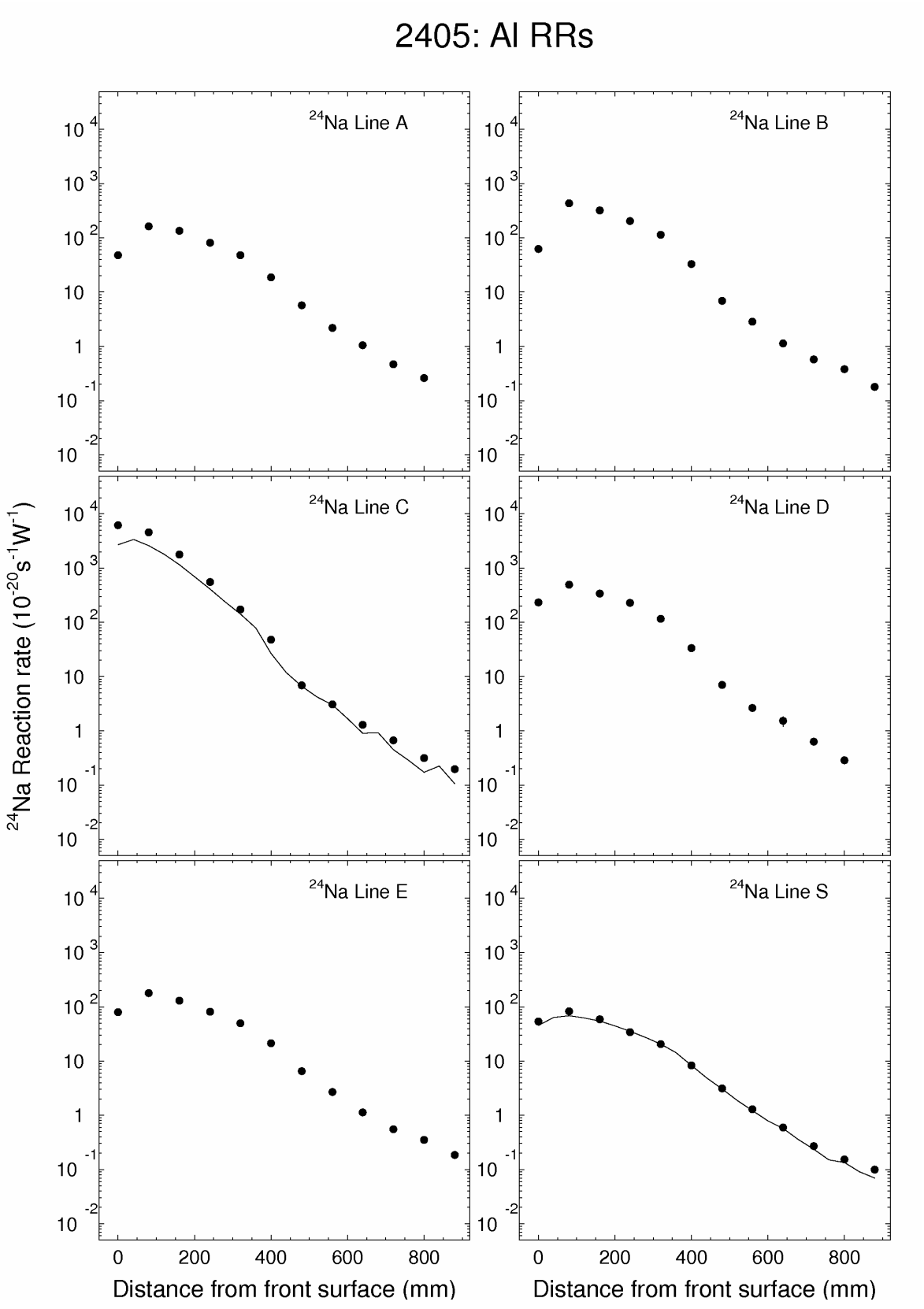

Fig. 16. The experimental and calculated distributions of ^{24}Na in ^{27}Al inside (lines A,B,C,D,E) and outside (line S) the target.

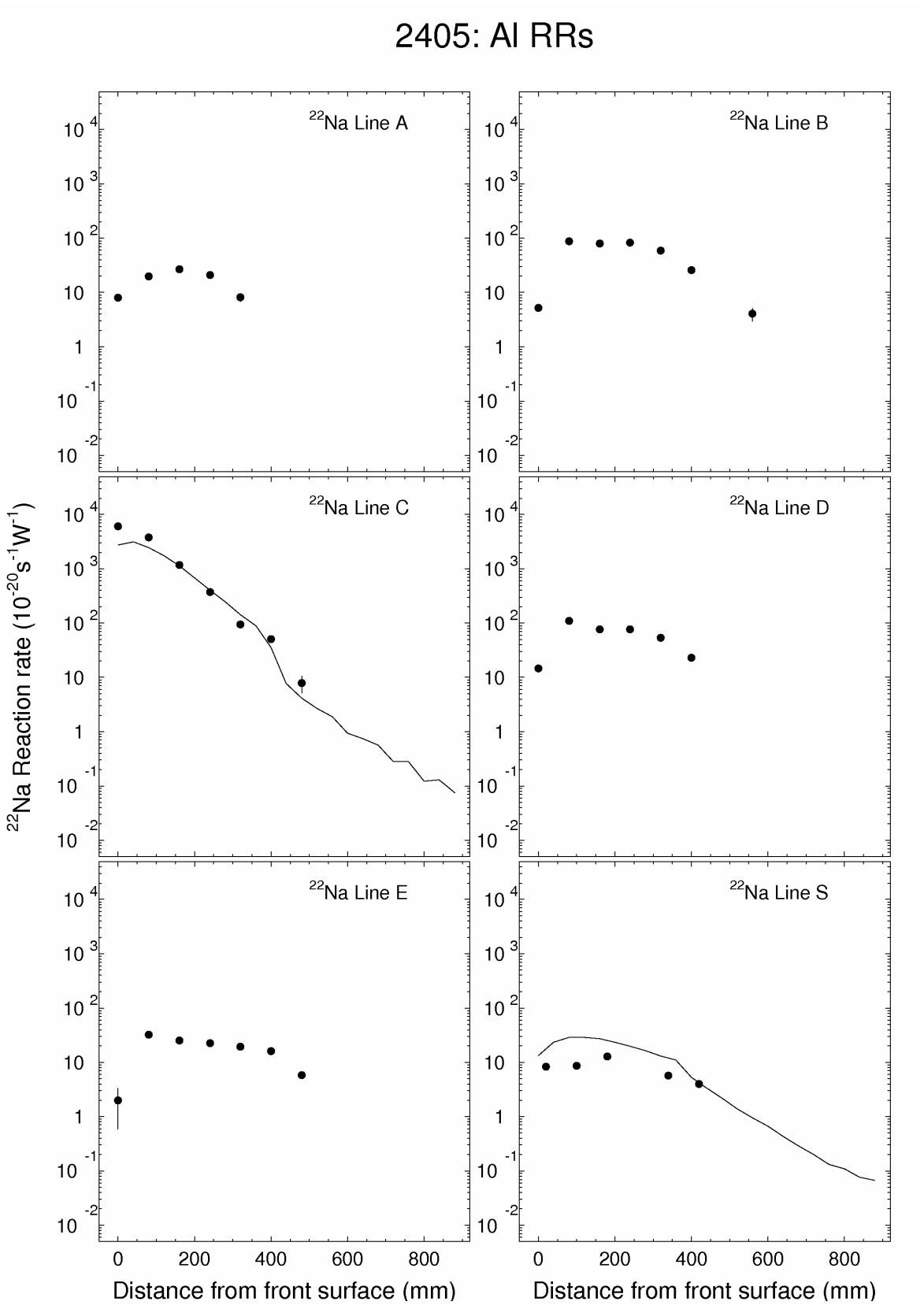

Fig. 17. The experimental and calculated distributions of ^{22}Na in ^{27}Al inside (lines A,B,C,D,E) and outside (line S) the target.

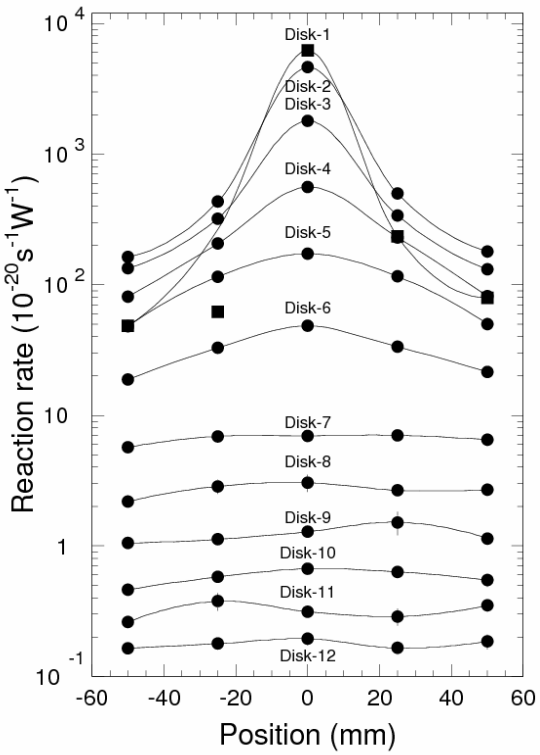

Fig. 18. Experimental distributions of ^{24}Na in 27Al along the odd disc rulers (on lines A, B, C, D).

3.8.2. Space distributions of nuclide reaction rates on the surface of the Pb target

3.8.2.1. Rates of reactions on ^{209}Bi

Table 13 presents the nuclear-physics characteristics of the nuclides produced in twelve ^{209}B samples in interactions with different-energy neutrons and protons, which used to calculate reaction rates. Table 14 and Fig. 19 present the rates of residual nuclide production in ^{209}Bi samples irradiated on the surface of the Pb target at 20, 100, 180, 260, 340, 420, 500, 580, 660, 740, 820, and 900 mm from the target front butt end.

Table 13

The nuclear-physics characteristics of the nuclides produced in ^{209}B sample in interactions with high-energy neutrons and protons [4,21]

^{207}Po	5.80h	*992.3(59.3), 742.6(28.2), 405.8(9.7)*
^{206}Po	8.8d	*1318.7(0.65), 1032.3(33), 980.2(7.1),881.0(94.5), 860.9(3.5), 807.4(23), 803.1(94.5), 632.2(94.5), 620.5(94.5), 516.2(94.5), 286.4(24), 184.0(94.5)*
^{207}Bi	31.55y	*1770.2(6.87), 1063.7(74.5), 569.7(97.74)*
^{206}Bi	6.243d	*1903.6(0.35), 1878.7(2.01), 1844.5(0.57), 1718.7(31.8), 1595.3(5.01), 1565.3(0.3), 1560.3(0.38), 1405(1.43), 1332.3(0.28), 1098.3(13.5), 1018.6(7.6), 895.1(15.66), 881(66.2), 803.1(98.9), 784.6(0.54), 755(0.53), 739.2(0.16),664.2(0.10), 657.2(1.91), 632.2(4.47), 620.5(5.76), 582(0.48), 576.4(0.11), 537.5(30.5), 516.2(40.7), 497.1(15.31), 398(10.74), 386.2(0.52), 343.5(23.4), 262.7(3.02), 234.2(0.24), 184(15.8)*
^{205}Bi	15.31d	*1903.4(2.47), 1861.7(6.17), 1775.8(3.99), 1764.3(32.5), 1614.3(2.28), 1551(0.97), 1548.7(0.28), 1521.2(0.2), 1501.4(0.23), 1351.5(1.06), 1264.6(0.05), 1208.7(0.51),*

		1208.7(0.51), 1199.6(0.19), 1190(2.26), 1072.4(0.3), 1043.8(7.51), 1013.8(0.06), 1014.3(0.91), 1001.6(0.26), 992.7(0.09), 987.7(16.13), 971.6(0.28), 894.6(0.62), 890.2(0.68), 872(0.42), 828.2(0.29), 813.8(0.47), 788.1(0.1), 780.9(0.57), 761.3(0.68), 759.1(1.04), 744.7(0.7), 717.4(0.31), 703.5(31.1), 688.5(0.23), 661.4(0.03), 646(0.07), 626.7(0.58), 579.8(5.44), 576.3(0.19), 573.8(0.62), 570.6(4.34), 549.8(2.95), 493.6(0.37), 361.2(0.03), 349.5(0.56), 284.1(1.69), 282.4(0.43), 262.8(0.36), 260.5(1.09), 259.5(0.05)
^{204}Bi	11.22h	*1896.3(1.29), 1826.4(0.56), 1818.1(0.52), 1755.3(1.22), 1703.3(1.99), 1652.1(0.56), 1689.1(0.58), 1524.1(0.96), 1351.7(0.48), 1274.8(2.14), 1211.7(3), 1043.6(1.27), 984(59), 918.3(10.8), 899.2(98), 821.1(0.6), 791.2(3.3),753.8(1.08), 718.4(0.91), 709.1(1.43), 670.7(11.4), 661.6(2.54), 532.7(1.35), 501.7(0.84), 440.5(2.5), 421.6(1.13), 374.8(82), 291.4(0.95), 289.3(2.86), 248.9(2.14), 222.1(0.94), 219.4(2.3), 216.1(1.43)*
^{203}Bi	11.76h	*2011(1.76), 2001(0.83), 1893(8.2), 1888(1.94), 1847.3(11.4), 1748(1.89), 1719.6(3.4), 1679.6(8.8),1551(0.77), 1536.5(7.5), 1506.7(3.7), 1421(0.25), 1034(8.8), 1000.3(0.98), 936(0.74), 896.8(13.1), 866.5(1.49), 847.2(8.5), 825.2(14.6), 820.2(29.6), 816.3(4.03), 657.9(0.22), 468.8(0.23), 401.3(*), 381.7(1.28), 279.2(*)), 264.2(5.2), 186.6(3.11)*
^{202}Bi	1.72h	*960.7(99.28), 657.5(60.6), 422.1(83.7)*
^{201}Bi	108m	*1014.1(10.7)*
^{203}Pb	51.873h	*680.5(0.75), 401.3(3.35), 279.2(80.8)*
^{202m}Pb	3.53h	*960.7(92), 787.0(49.8),657.5(32.4), 422.1(86)*
^{201}Pb	9.33h	*946(7.4), 907.6(5.7), 767.3(3.16), 692.4(4.27), 584.5(3.56), 406(2.01), 361.3(9.9), 331.2(79)*
^{200}Pb	21.5h	*1205.7(*), 450.53.33), 367.9(*)), 268.4(3.96), 257.2(4.46), 235.6(4.3), 147.6(37.7), 142.3(3.16)*
^{198}Pb	2.4h	*865.3(5.9)*
^{202}Tl	12.23d	*439.6(91.4)*
^{201}Tl	72.912h	*167.4(10), 135.3(2.56)*
^{200}Tl	26.1h	*1514.9(4), 1362.9(3.4), 1273.5(3.31), 1263(0.78), 1225.5(3.36), 1205.7(29.9), 886.2(2.02), 828.3(10.8) 787.1(1.03), 661.3(2.28), 628.6(1), 579.3(13.8), 367.9(87.2)*
^{199}Tl	7.42h	*455.5(12.4), 247.3(9.3), 208.2(12.3)*
^{198}Tl	5.3h	*2040.2(8.4), 1832.6(4.3), 636.7(10.1), 411.8(82)*
^{197}Tl	2.84h	*425.8(13)*
^{196m}Tl	1.41h	*426.3(91)*
^{203}Hg	46.612d	*279.2(81.46)*
^{197m}Hg	23.8h	*134.0(33.3)*
^{192}Hg	4.85h	*274.8(50.2)*
^{200m}Au	18.7h	*759.5(66), 497.8(497.8)*
^{194}Au	38.02h	*328.5(61.)*
^{188}Pt	10.2d	*187.6(19.4)*
^{185}Os	93.6d	*646.1(78.)*
^{110m}Ag	249.76d	*657.8(94.3)*
^{103}Ru	39.26d	*497.1(91)*
^{99}Mo	65.94h	*140.5(90.27)*
^{96}Nb	23.35h	*1200.2(19.97), 778.2(96.45), 568.9(58)*

^{95}Nb	34.975d	*765.8(99.81)*
^{95}Zr	64.02d	*765.8(99.1),756.7(54.46)*
^{88}Y	106.65d	*898(93.7)*
^{82}Br	35.30h	*776.5(83.5)*

Table14

The rates of residual production in ^{209}Bi on the surface of the Pb target $\left[10^{-20}, \frac{1}{s \cdot nucleus \cdot W}\right]$.

Nuclide	Yield type	T1/2	Spacing between sample center and target front butt (mm)											
			20	100	180	260	340	420	500	580	660	740	820	900
^{207}Po	i(m+g)	5.80h	5.0(3.7)	3.1(1.8)	5.24(0.71)	3.74(0.98)	2.72(0.49)	0.57(0.14)	-	-	-	-	-	-
^{206}Po	i	8.8d	1.41(0.13)	4.11(0.37)	4.18(0.37)	3.97(0.35)	3.18(0.28)	0.463(0.041)	0.159(0.014)	0.28(0.28)	-	-	-	-
^{207}Bi	c	31.55y	345(32)	469(44)	395(38)	257(24)	139(13)	62.7(6.2)	25.9(3.5)	12.1(2.8)	3.8(2.0)	-	-	-
^{206}Bi	i	6.243d	209(21)	257(24)	219(20)	144(13)	85.0(7.8)	36.0(3.4)	14.8(1.4)	7.61(0.82)	-	-	-	-
^{206}Bi	c	6.243d	176(16)	258(23)	222(20)	145(13)	86.6(7.8)	37.4(3.4)	14.6(1.3)	6.37(0.58)	2.86(0.28)	1.32(0.14)	0.720(0.067)	0.411(0.039
^{205}Bi	c	15.31d	117(11)	182(16)	162(14)	110.9(10.0)	66.7(6.0)	29.4(2.7)	12.3(1.1)	5.21(0.48)	2.48(0.24)	1.09(0.11)	0.555(0.078)	0.367(0.063
^{204}Bi	c*	11.22h	70.8(6.7)	123(12)	106(10)	77.4(7.7)	47.2(4.5)	19.1(1.8)	7.91(0.80)	3.34(0.32)	1.48(0.16)	0.816(0.089)	0.374(0.049)	0.220(0.024
^{203}Bi	c	11.76h	42.3(3.9)	73.1(7.7)	73.0(7.2)	53.8(5.0)	33.0(3.2)	14.8(1.4)	6.21(0.60)	2.77(0.26)	1.53(0.16)	0.556(0.073)	0.340(0.047)	0.172(0.038
^{202}Bi	c*	1.72h	28.9(3.3)	57.3(6.0)	51.7(5.6)	36.5(4.0)	27.5(2.8)	10.6(1.6)	4.93(0.68)	2.18(0.25)	1.29(0.23)	-	-	-
^{201}Bi	c*	108m	75(58)	52(15)	-	-	-	-	-	-	-	-	-	-
^{203}Pb	i(m1+m2+g)	51.873h	19.8(2.6)	52(26)	25.5(6.1)	22.3(2.3)	9.6(2.5)	5.64(0.88)	2.48(0.28)	1.16(0.20)	0.303(0.062)	-	0.119(0.031)	-
^{203}Pb	c*	51.873h	62.0(5.8)	120(11)	110(10)	80.6(7.8)	50.5(4.7)	21.8(2.0)	9.38(0.87)	4.30(0.53)	1.98(0.19)	-	0.493(0.046)	0.327(0.057
^{202m}Pb	i(m)	3.53h	5.77(0.83)	15.9(2.1)	14.5(3.2)	9.3(1.5)	5.5(1.1)	3.54(0.47)	1.46(0.39)	0.61(0.15)	0.423(0.081)	-	-	-
^{201}Pb	c*	9.33h	27.0(3.6)	60.4(6.5)	63.9(6.3)	45.2(4.8)	28.3(3.0)	12.0(1.3)	5.23(0.57)	2.50(0.26)	1.27(0.14)	0.675(0.076)	0.327(0.046)	0.222(0.029
^{200}Pb	c	21.5h	12.6(1.2)	46.1(6.2)	36.1(4.3)	26.3(3.1)	20.4(2.0)	9.3(1.0)	3.54(0.35)	1.73(0.19)	0.864(0.080)	0.421(0.040)	0.229(0.026)	0.119(0.012
^{198}Pb	c	2.4h	-	-	-	5.4(3.7)	-	-	-	-	-	-	-	-
^{202}Tl	c	12.23d	2.90(0.30)	5.96(0.56)	6.18(0.59)	4.22(0.41)	2.76(0.27)	1.39(0.14)	0.648(0.067)	0.293(0.034)	0.179(0.028)	-	-	-
^{201}Tl	c*	72.912h	30.5(3.3)	75.5(7.9)	74.8(8.3)	56.7(6.8)	37.7(5.3)	15.4(3.0)	6.8(1.1)	3.73(0.54)	1.31(0.26)	0.84(0.25)	-	0.44(0.17)
^{200}Tl	i	26.1h	4.23(0.58)	14.0(7.4)	13.3(3.2)	8.1(2.3)	2.61(0.73)	-	0.83(0.12)	0.350(0.063)	0.136(0.023)	0.084(0.018)	0.039(0.020)	0.025(0.005
^{200}Tl	c	26.1h	16.9(1.6)	43.0(5.3)	47.8(6.8)	36.6(4.4)	23.8(2.4)	12.5(1.4)	4.35(0.43)	2.09(0.23)	1.001(0.091)	0.505(0.046)	0.266(0.026)	0.144(0.013
^{199}Tl	c*	7.42h	14.7(2.3)	33.6(4.7)	40.7(5.7)	28.6(4.8)	21.4(2.6)	8.2(1.0)	3.98(0.50)	1.92(0.25)	0.85(0.19)	0.43(0.17)	-	-
^{198}Tl	c	5.3h	10.4(1.6)	26.0(3.9)	33.6(4.8)	25.7(3.3)	16.3(2.4)	7.4(1.2)	2.81(0.36)	1.60(0.26)	0.67(0.16)	0.69(0.29)	0.34(0.13)	0.205(0.075
^{197}Tl	c*	2.84h	-	34(19)	76(33)	44(19)	42(18)	13.0(5.7)	3.6(1.7)	2.4(1.1)	1.22(0.64)	-	-	-
^{196m}Tl	i(m)	1.41h	-	11.4(4.5)	6.6(4.4)	10.4(3.4)	3.9(2.1)	2.71(0.83)	2.10(0.45)	0.72(0.21)	0.37(0.12)	-	-	-
^{203}Hg	c	46.612d	0.32(0.12)	0.231(0.037)	0.230(0.041)	0.27(0.12)	0.134(0.031)	0.044(0.015)	0.044(0.022)	-	-	-	-	-
^{197m}Hg	i(m)	23.8h	-	-	-	-	3.82(0.89)	1.36(0.32)	0.76(0.32)	-	-	-	-	-
^{192}Hg	c	4.85h	-	5.4(1.0)	5.0(1.0)	6.4(1.1)	2.91(0.57)	1.20(0.19)	0.67(0.14)	0.341(0.051)	0.187(0.040)	-	-	-
^{200m}Au	i(m)	18.7h	1.22(0.31)	1.05(0.99)	0.56(0.49)	0.86(0.52)	0.42(0.12)	0.295(0.076)	-	-	-	-	-	-
^{194}Au	i(m1+m2+g)	38.02h	-	-	-	0.29(0.11)	0.250(0.066)	0.244(0.061)	-	-	-	-	-	-
^{188}Pt	c	10.2d	-	-	2.23(0.43)	1.93(0.45)	1.39(0.49)	0.74(0.25)	0.65(0.18)	0.46(0.16)	-	-	-	-
^{185}Os	c	93.6d	0.286(0.050)	0.88(0.18)	1.10(0.12)	0.99(0.11)	0.625(0.075)	0.416(0.048)	0.114(0.060)	-	-	-	-	-
^{110m}Ag	i(m)	249.76d	-	0.57(0.17)	0.24(0.10)	-	-	-	-	-	-	-	-	-
^{103}Ru	c	39.26d	0.475(0.054)	1.52(0.15)	1.87(0.18)	1.43(0.15)	1.14(0.14)	0.322(0.043)	0.144(0.016)	-	-	-	-	-
^{99}Mo	c	65.94h	0.67(0.32)	1.24(0.26)	2.47(0.49)	1.58(0.26)	1.34(0.20)	0.60(0.13)	0.264(0.066)	0.088(0.033)	-	-	-	-
^{96}Nb	i	23.35h	0.31(0.41)	1.19(0.40)	0.66(0.21)	0.86(0.35)	0.53(0.11)	-	0.45(0.10)	0.07(0.11)	-	-	-	-

^{95}Nb	i(m+g)	34.975d	0.066(0.006)	0.466(0.049)	0.633(0.076)	0.544(0.055)	0.233(0.043)	0.010(0.001)	-	-	-	-	-	-
^{95}Nb	c	34.975d	0.444(0.040)	1.50(0.14)	1.82(0.17)	1.43(0.13)	0.956(0.088)	0.352(0.032)	0.124(0.021)	-	-	-	-	-
^{95}Zr	c	64.02d	0.381(0.034)	1.053(0.094)	1.20(0.11)	0.912(0.081)	0.691(0.061)	0.344(0.031)	-	-	-	-	-	-
^{88}Y	c	106.65d	-	0.108(0.042)	0.148(0.038)	-	-	-	-	-	-	-	-	-
^{82}Br	i(m+g)	35.30h	0.382(0.088)	0.42(0.36)	-	-	-	-	-	-	-	-	-	-

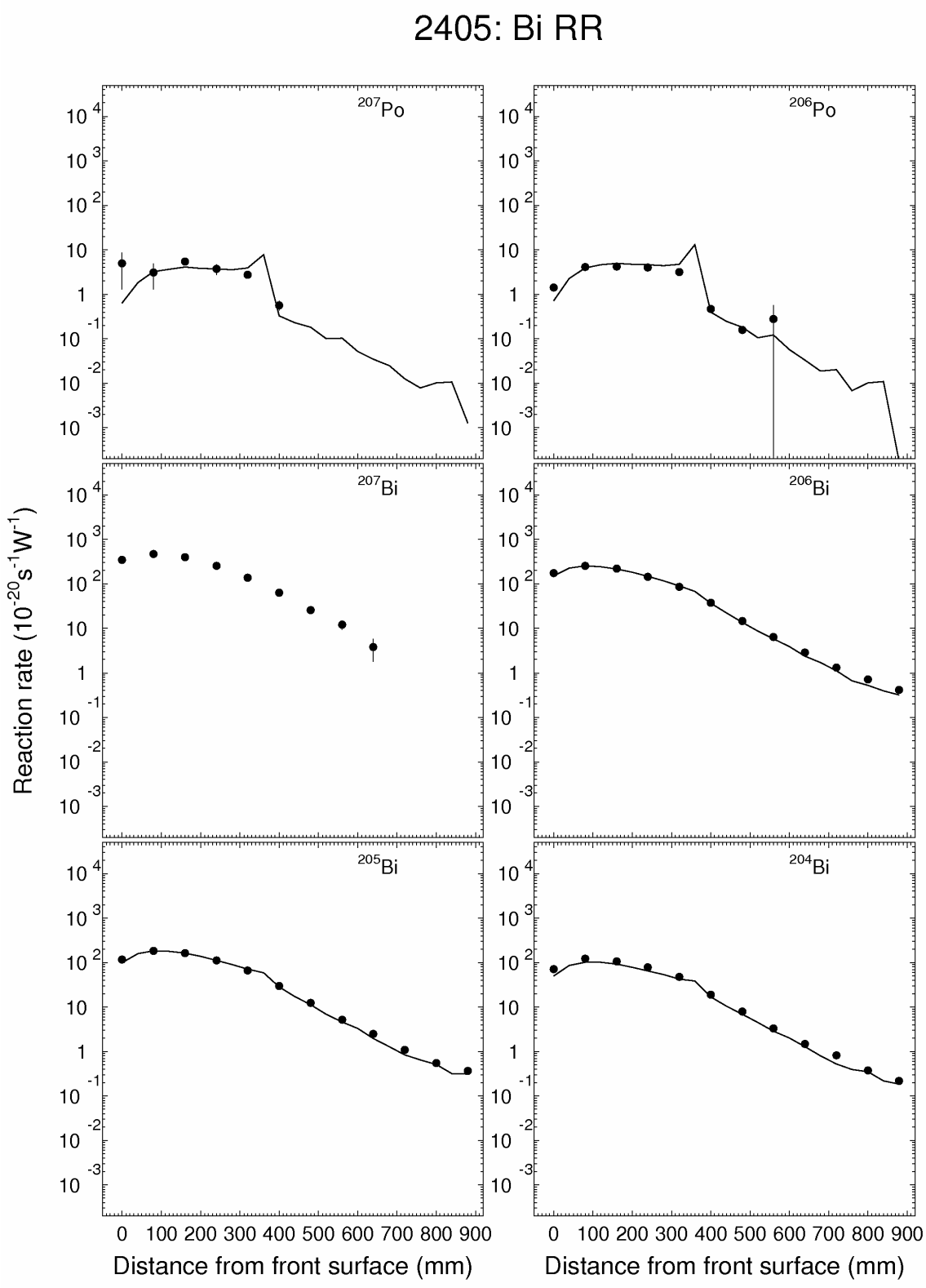

Fig. 19. Experimental and calculated distributions of ^{209}Bi reaction products on the surface of the Pb target (line S, ^{207}Po, ^{206}Po, ^{207}Bi, ^{206}Bi, ^{205}Bi, ^{204}Bi).

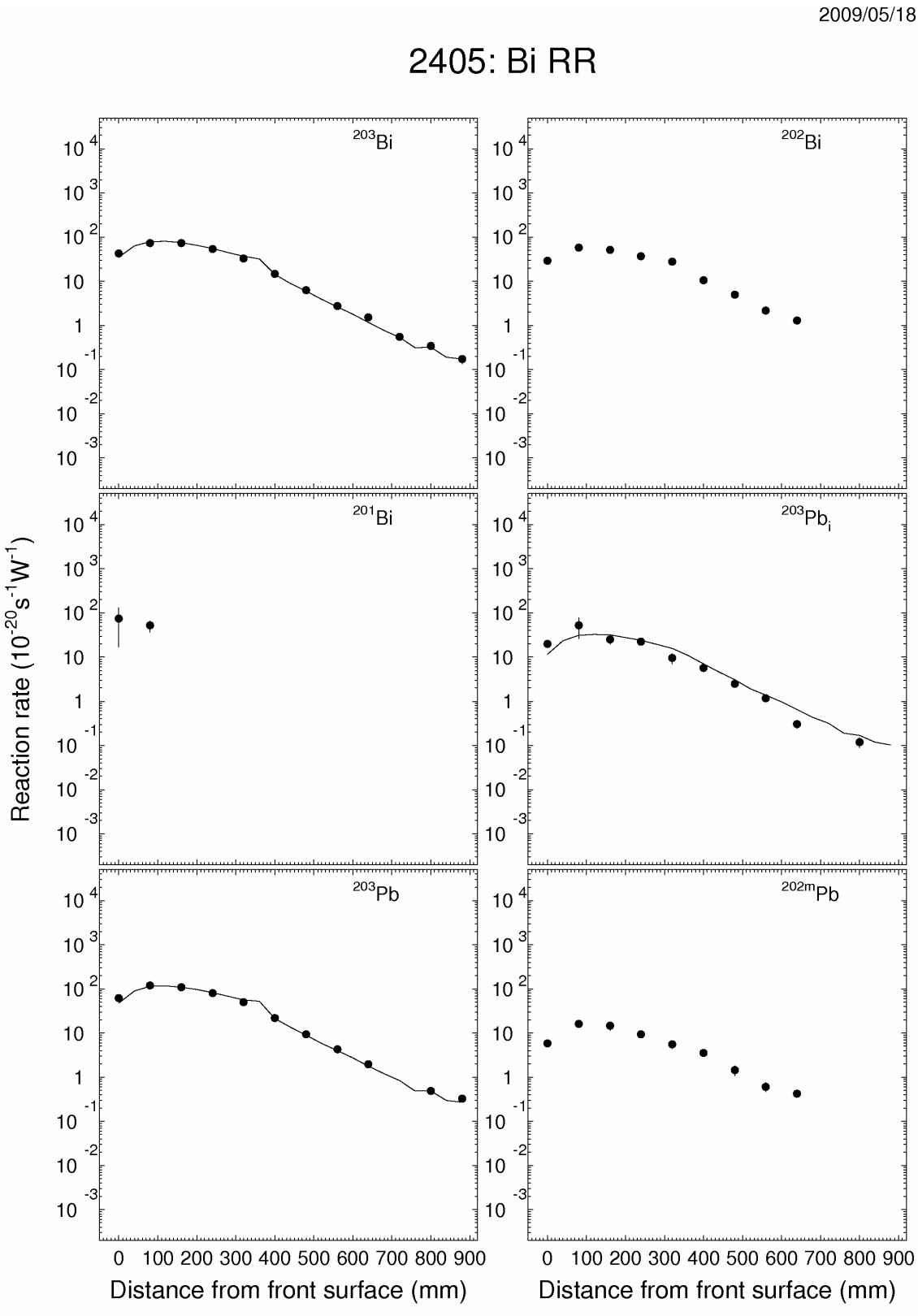

Fig. 19 (cont'd). Experimental and calculated distributions of ^{209}Bi reaction products on the surface of the Pb target (line S, ^{203}Bi, ^{202}Bi, ^{201}Bi, ^{203}Pb$_i$, ^{203}Pb, ^{202m}Pb)

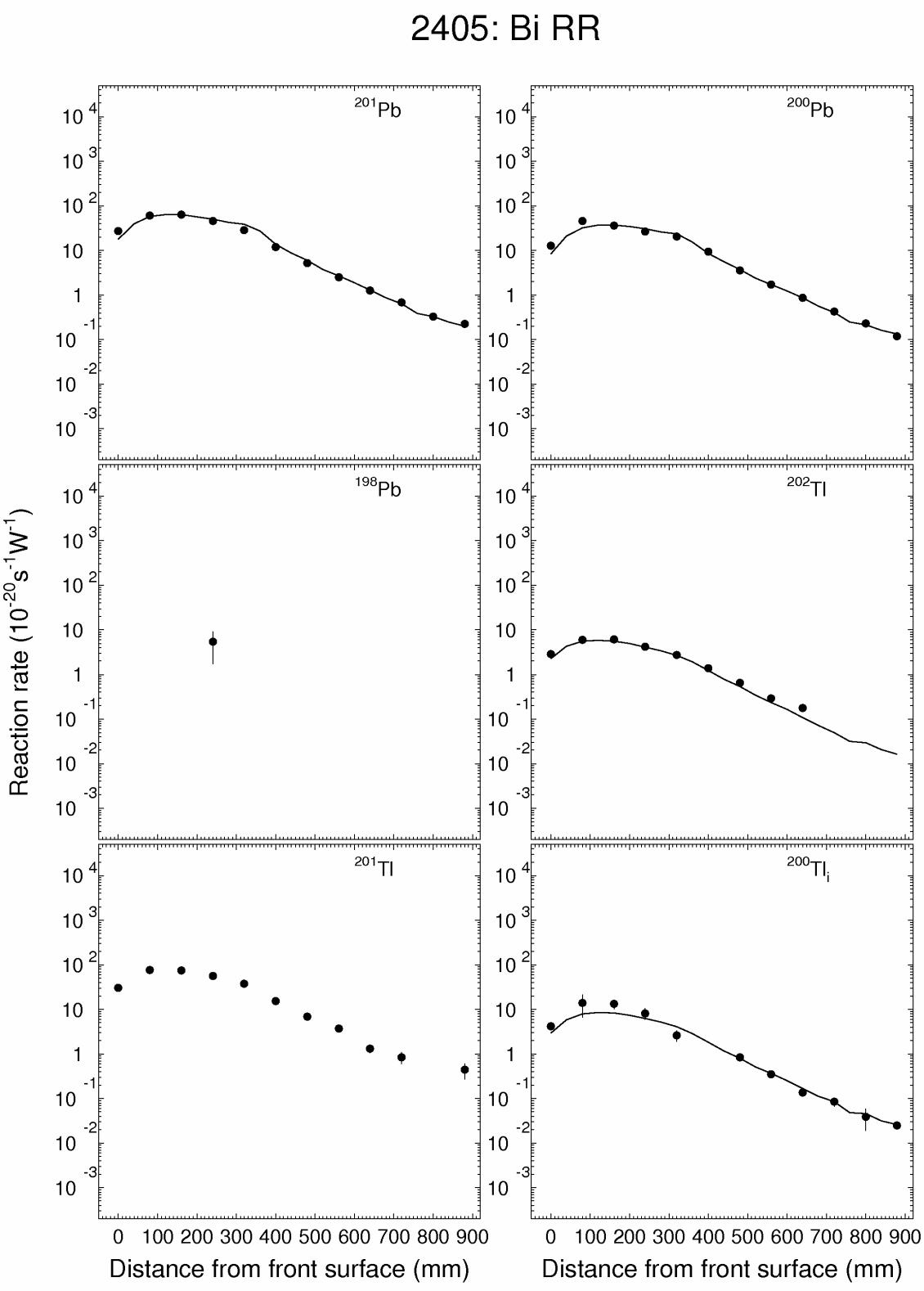

Fig. 19 (cont'd). Experimental and calculated distributions of ^{209}Bi reaction products on the surface of the Pb target (line S, ^{201}Pb, ^{200}Pb, ^{198}Pb, ^{202}Tl, ^{201}Tl, ^{200}Tl$_i$)

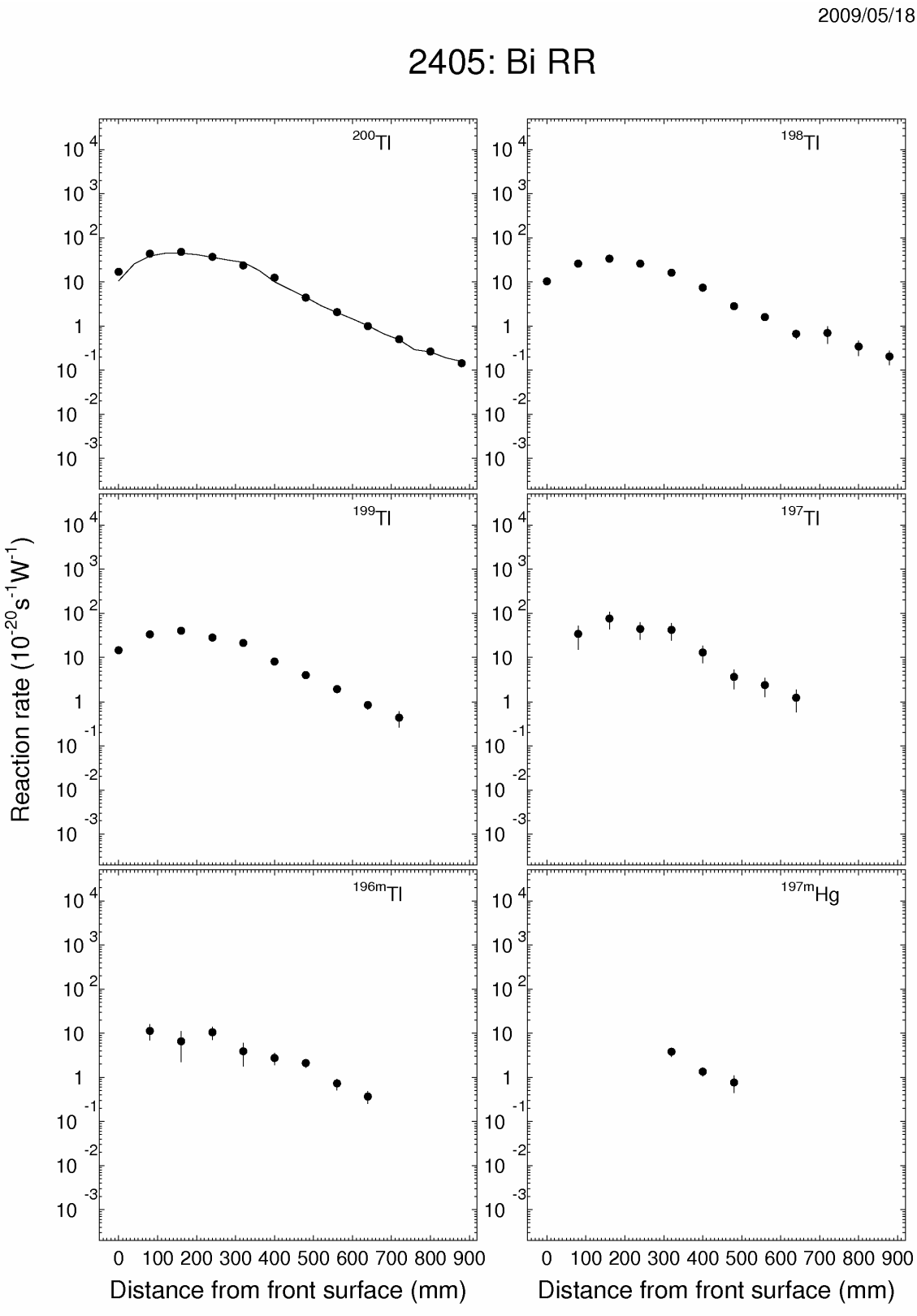

Fig. 19 (cont'd). Experimental and calculated distributions of ^{209}Bi reaction products on the surface of the Pb target (line S, ^{200}Tl, ^{198}Tl, ^{199}Tl, ^{197}Tl, ^{196m}Tl, ^{197m}Hg$_i$).

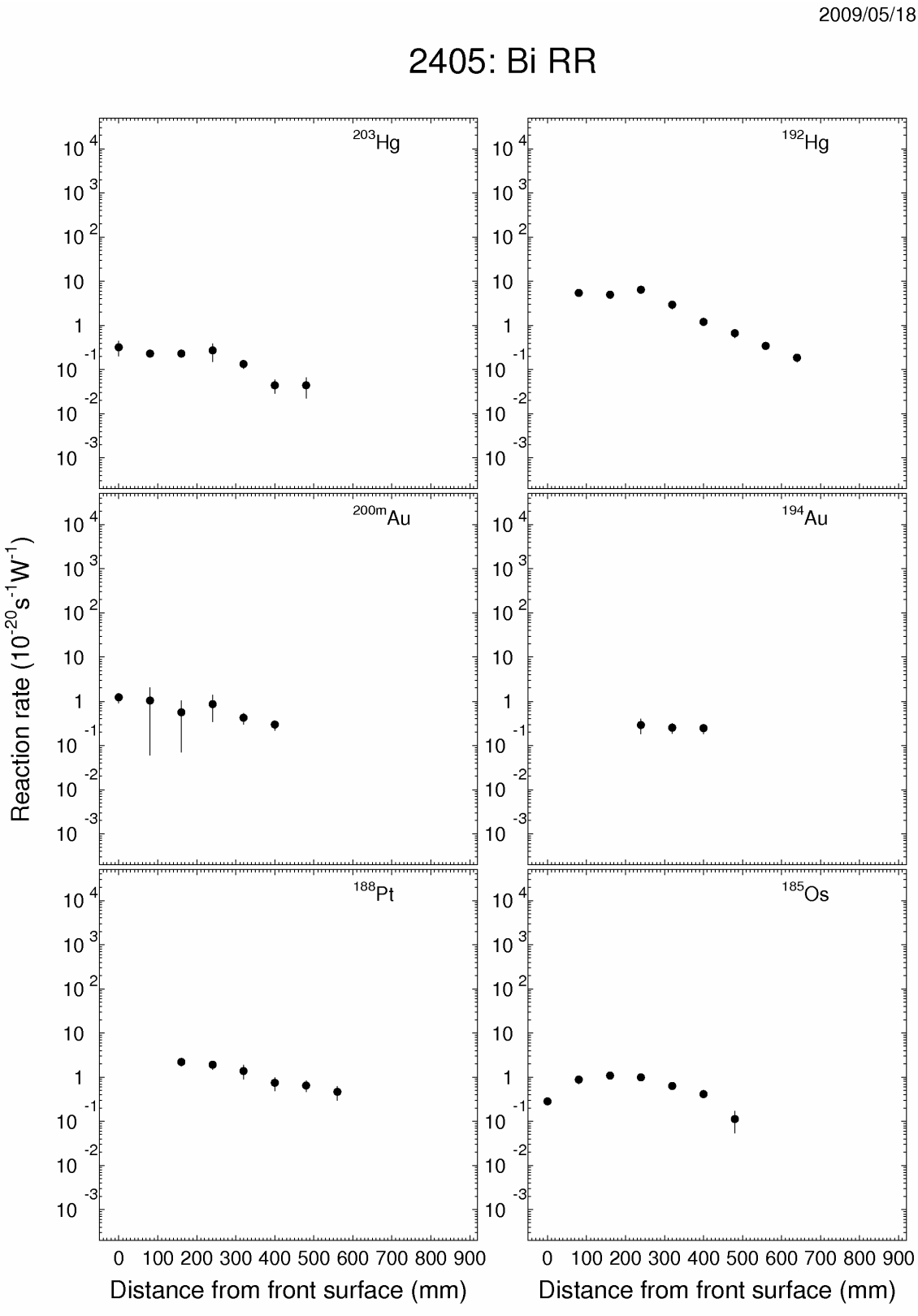

Fig. 19 (cont'd). Experimental and calculated distributions of ^{209}Bi reaction products on the surface of the Pb target (line S, ^{203}Hg, ^{192}Hg, ^{200m}Au, ^{194}Au, ^{188}Pt, ^{185}Os)

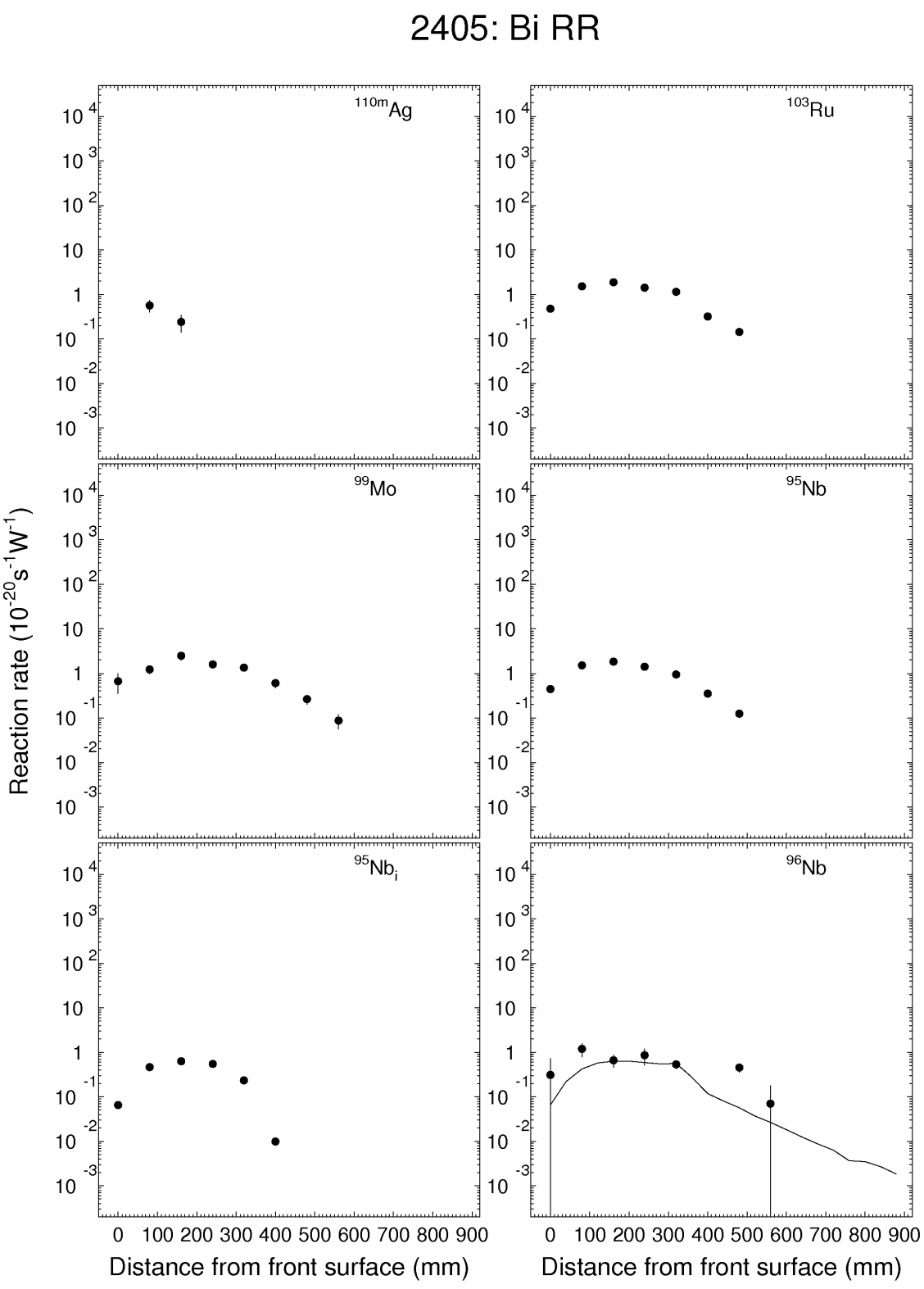

Fig. 19 (cont'd). Experimental and calculated distributions of ^{209}Bi reaction products on the surface of the Pb target (line S, ^{110m}Ag, ^{103}Ru, ^{99}Mo, ^{95}Nb, ^{95}Nb$_i$, ^{96}Nb)

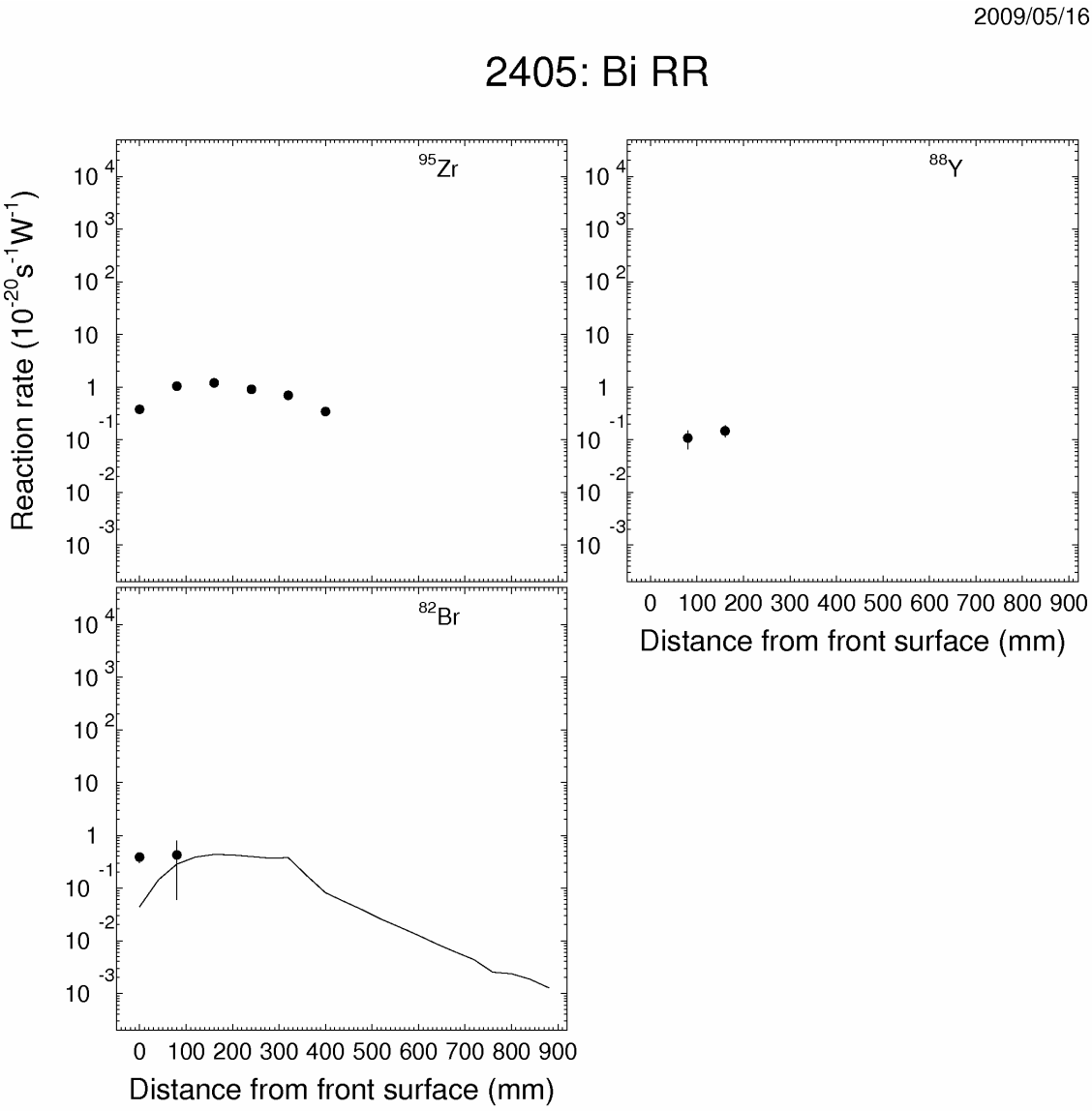

Fig. 19 (cont'd). Experimental and calculated distributions of ^{209}Bi reaction products on the surface of the Pb target (line S, ^{95}Zr, ^{88}Y, ^{82}Br,)

3.8.2.2. Rates of reaction on ^{197}Au

Table 15 presents the nuclear-physics characteristics of the nuclides produced in twelve ^{197}Au samples in interactions with different-energy neutrons and protons, which are used to calculate reaction rates. Table 16 and Fig. 20 present the rates of residual nuclide production in ^{209}Bi samples irradiated on the surface of the Pb target at 20, 100, 180, 260, 340, 420, 500, 580, 660, 740, 820, and 900 mm from the target front butt end.

Table 15

Nuclear-physics characteristics of nuclides produced in ^{197}Au sample exposed to high-energy neutrons and protons [4,21].

Nuclide	Half-life	γ-quantum energy (E_γ, кэВ) and yield (Y_γ, %)
^{198}Au	2.69517d	*1087.7(0.1590), 675.9(0.804), 411.8(95.58)*

^{196}Au	6.183d	*1091.4(0.15), 759.1(0.0444), 426.1(6.6), 355.7(87), 333(22.9)*
^{196m}Au	9.6h	*285.5(4.3), 188.3(37), 168.4(7.7), 147.8(43)*
^{195}Au	186.098d	*129.8(0.82)*
^{194}Au	38.02h	*2113.9(0.26), 2043.7(3.6), 1969.7(0.44), 1958.7(0.17), 1924.2(2.01), 1835.3(0.37), 1797.3(0.61), 1785.5(0.38), 1735.3(0.29), 1602(0.26), 1595.8(1.71), 1468.9(6.4), 1421.7(0.35), 1342.2(1.22), 1302.3(0.27), 1218.8(1.1), 1183.5(0.63), 1175.3(2.01), 1156.6(0.45), 1150.8(1.39), 1104.1(2.01), 1048.6(0.86), 948.3(2.2), 938.7(1.1), 703.5(0.46), 645.2(2.14), 622(2.32), 607.5(0.29), 593.3(0.46), 589.2(0.25), 529.9(0.61), 528.8(1.65), 482.8(1.13), 364.9(1.51), 328.5(61), 300.8(0.85), 293.6(10.4)*
^{193}Au	17.65h	*491.3(0.65), 439(1.78), 268.2(3.6), 255.6(6.2), 173.5(2.7)*
^{192}Au	4.94h	*2216.4(0.53), 1832.8(3.2), 1423(3), 1140.4(2.6), 1127(0.7), 1061.5(0.93), 759.1(1.65), 612.5(4.3), 604.4(1.01), 468.1(1.75), 316.5(58), 308.5(3.4), 296(22)*
^{191}Au	3.18h	*586.4(17.0), 399.8(4.7)*
^{191}Pt	2.802d	*624.1(1.41), 538.9(13.7), 456.5(3.4), 409.4(8.096), 359.9(6), 268.7(2.43), 172.2(3.5), 129.4(3.2)*
^{189}Pt	10.87h	1423(0.04), 721.4(9.3), 607.6(8.1), 568.8(7.1), 544.9(5.8), 317.6(3.3), 300.5(3.7), 243.5(7), 141.2(4.2)
^{188}Pt	10.2d	*1209.8(D), 1174.6(D), 987.4(D), 824.3(D), 634.9(D), 633.0(D), 423.3(4.4), 381.4(7.5), 195.1(18.6), 187.6(19.4), 155.1(D)*
^{192}Ir	73.827d	*588.6(4.52), 468.1(47.81), 308.5(29.68), 296(28.72)*
^{190}Ir	11.78d	*829(3.5), 690(0.28), 605.1(39.9), 569.3(28.5), 558(30.1), 518.5(34), 407.2(23.9), 371.2(22.8)*
^{188}Ir	41.5h	*1209.8(6.9), 1174.6(1.32), 634.9(5), 633.0(18), 155.1(30)*
^{187}Ir	10.5h	*987.3(2.8), 912.9(4.79), 610.9(3.93)*
^{186}Ir	16.64h	*933.3(5.3), 773.3(8.9), 636.4(6.1), 622.3(3.17), 296.9(62.3), 137.2(41.4)*
^{186m}Ir	1.90h	*773.2(11.7), 137.1(23.0)*
^{185}Ir	14.4h	*1829(10.1), 254.2(13.3)*
^{184}Ir	3.09h	*390.4(25.9), 264(68)*
^{185}Os	93.6d	*880.5(5.17), 874.8(6.29), 717.4(3.94), 646.1(78)*
^{183}Os	13.0h	*381.8(89.6)*
^{183m}Os	9.9h	*1107.9(22.4), 1101.9(49)*
^{182}Os	22.10h	*180.2(33.5)*
^{183}Re	70.0d	*162.3(23.3)*
^{182}Re	64.0h	*1221.4(17.4), 1189(9), 1121.3(22), 100.1(16.4)*
^{182m}Re	12.7h	*1221.5(24.8), 1189.2(15), 1121.4(31.8), 100.1(14.3)*

Table 16

Residual production rates in ^{197}Au outside Pb target $\left[10^{-20}, \frac{1}{s \cdot nucleus \cdot W}\right]$.

Nuclide	Yield Type	T1/2	Distance from the target front (mm)											
			20	100	180	260	340	420	500	580	660	740	820	900
^{198}Au	i(m+g)	2.69517d	1160(100)	1420(130)	1150(100)	795(71)	538(48)	351(31)	277(25)	245(22)	253(23)	271(24)	275(25)	308(27)
^{196}Au	i(m1+m2+g)	6.183d	797(72)	959(85)	719(65)	446(40)	247(22)	98.6(8.9)	36.2(3.3)	14.7(1.3)	6.75(0.62)	3.25(0.30)	1.81(0.19)	1.17(0.12)
^{196}Au	i(m)	9.6h	52.6(8.8)	64.3(8.2)	51.7(7.2)	32.2(3.6)	19.0(2.3)	7.39(0.87)	2.92(0.37)	1.12(0.20)	0.63(0.19)	-	-	-
^{195}Au	c	186.098d	410(120)	617(79)	475(85)	260(110)	179(47)	78(37)	-	-	-	-	-	-
^{194}Au	i(m1+m2+g)	38.02h	205(19)	290(27)	246(23)	162(15)	100.9(9.9)	42.8(4.0)	17.3(1.7)	7.10(0.74)	3.21(0.37)	1.62(0.22)	1.00(0.15)	0.331(0.068)
^{193}Au	c	17.65h	100(13)	150(18)	127(17)	73(11)	48.6(6.3)	24.0(3.2)	6.9(1.5)	-	-	-	-	-
^{192}Au	c	4.94h	75.0(9.7)	132(16)	141(20)	92(12)	41.6(7.8)	23.9(3.5)	10.2(2.3)	-	-	-	-	-
^{191}Au	c*	3.18h	43.0(5.2)	77.9(6.9)	60.1(5.4)	43.2(3.8)	36.3(3.2)	12.7(1.7)	5.2(1.3)	1.74(0.60)	-	-	-	-
^{191}Pt	c	2.802d	44.6(5.3)	92.9(9.5)	90.1(9.3)	60.2(6.4)	40.3(4.7)	18.0(2.0)	7.4(1.0)	4.75(0.77)	2.73(0.54)	-	-	-
^{189}Pt	c	10.87h	21.6(2.3)	55.8(5.5)	52.1(5.6)	36.8(3.6)	29.3(2.8)	12.2(1.3)	6.58(0.78)	2.59(0.38)	1.57(0.55)	-	-	-
^{188}Pt	c	10.2d	15.4(2.1)	37.3(3.3)	36.6(3.6)	27.9(2.5)	21.7(1.9)	9.07(0.81)	3.88(0.56)	1.60(0.28)	1.24(0.47)	-	-	-
^{192}Ir	i(m1+g)	73.827d	1.62(0.36)	2.89(0.37)	3.24(0.61)	1.84(0.31)	1.20(0.48)	-	-	-	-	-	-	-
^{190}Ir	i(m1+g)	11.78d	1.58(0.19)	3.20(0.44)	3.11(0.32)	2.29(0.41)	1.35(0.17)	0.86(0.14)	-	-	-	-	-	-
^{188}Ir	i	41.5h	1.1(1.5)	5.1(3.0)	9.7(4.8)	2.8(1.7)	1.57(0.43)	1.29(0.21)	0.594(0.080)	0.25(0.34)	-	-	-	-
^{188}Ir	c	41.5h	15.4(2.5)	44(12)	50(11)	31.8(3.8)	23.6(2.7)	9.6(1.1)	4.7(1.0)	2.39(0.54)	-	-	-	-
^{187}Ir	c*	10.5h	-	52.0(7.2)	59(13)	19.9(3.6)	21.3(3.6)	6.7(1.5)	-	-	-	-	-	-
^{186m}Ir	i(m)	1.90h	-	64(23)	57(18)	49(12)	52(11)	12.3(4.4)	-	-	-	-	-	-
^{186}Ir	c	16.64h	3.86(0.74)	11.8(1.3)	14.3(1.8)	11.1(1.2)	6.6(1.1)	3.56(0.39)	1.59(0.26)	0.93(0.19)	0.561(0.095)	-	-	-
^{185}Ir	c	14.4h	5.5(2.7)	17.8(4.0)	23.3(4.9)	11.6(2.6)	8.5(1.6)	2.8(1.0)	-	-	-	-	-	-
^{184}Ir	c*	3.09h	3.85(0.86)	21.0(4.3)	18.7(3.6)	12.4(1.9)	9.7(2.8)	3.80(0.54)	1.60(0.28)	0.67(0.45)	-	-	-	-
^{185}Os	c	93.6d	4.95(0.65)	19.3(2.3)	21.2(2.3)	16.1(1.6)	12.9(1.3)	5.33(0.65)	2.18(0.34)	1.01(0.24)	-	-	-	-
^{183m}Os	c*	9.9h	-	5.7(1.9)	7.7(1.6)	6.5(1.2)	5.5(1.1)	2.26(0.29)	-	-	-	-	-	-
^{183}Os	c	13.0h	-	6.42(0.86)	8.05(0.90)	7.03(0.73)	4.42(0.53)	1.67(0.21)	0.99(0.13)	-	-	-	-	-
^{182}Os	c	22.10h	-	12.6(2.2)	12.7(2.3)	8.0(1.0)	5.82(0.97)	2.46(0.35)	1.09(0.27)	-	-	-	-	-
^{183}Re	c	70.0d	3.4(1.0)	11.6(1.2)	13.5(2.1)	12.1(1.5)	8.3(1.0)	4.09(0.65)	2.35(0.54)	-	-	-	-	-
^{182m}Re	c	12.7h	1.48(0.90)	7.0(1.5)	6.2(4.2)	5.9(2.1)	5.7(1.7)	1.33(0.35)	0.51(0.36)	-	-	-	-	-
^{182}Re	c	64.0h	5.2(1.3)	8.2(4.5)	18.6(5.5)	5.7(3.3)	4.1(1.8)	5.28(0.66)	2.09(0.43)	-	-	-	-	-

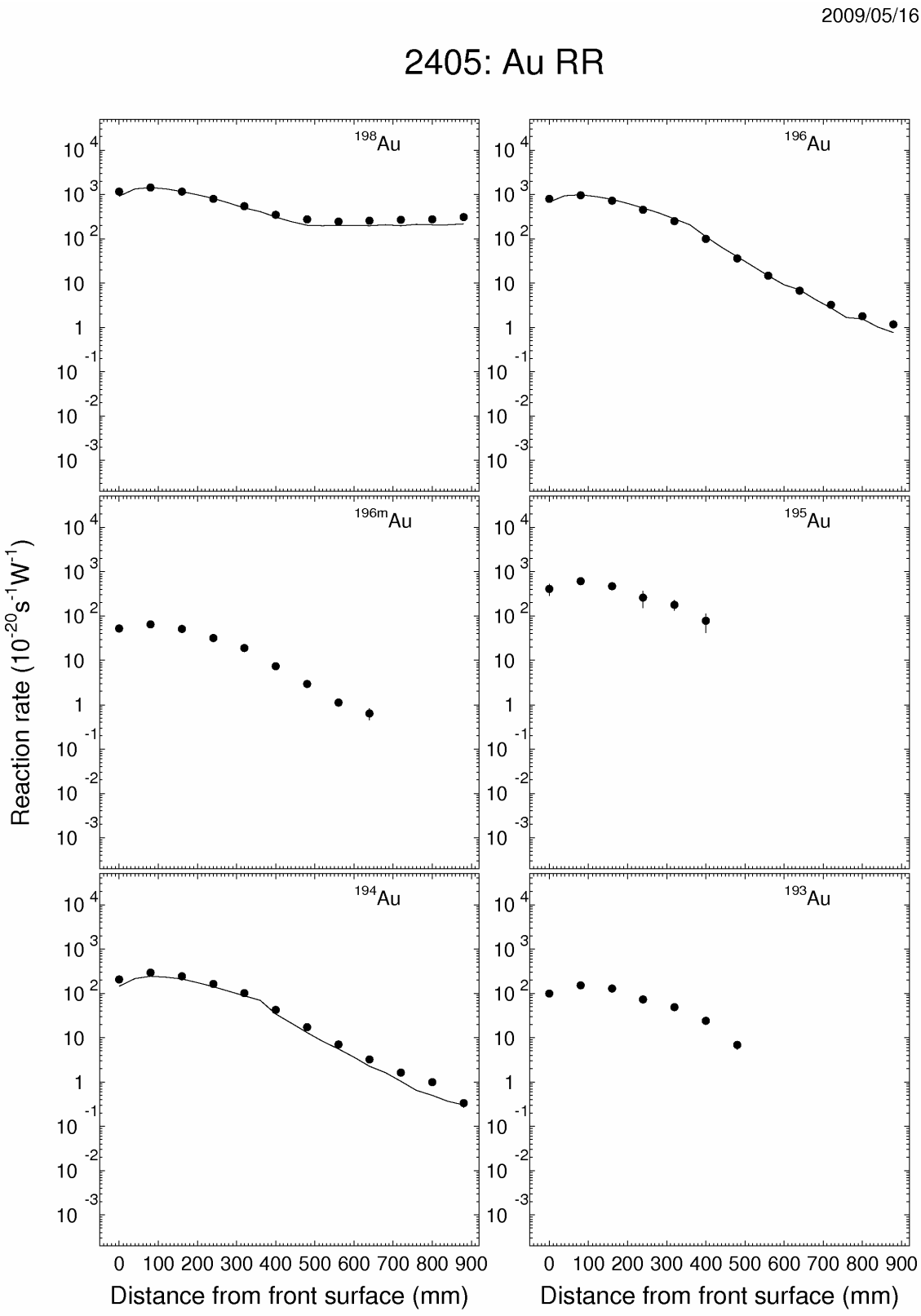

Fig. 20. Experimental and calculated distributions of ^{197}Au reaction products on the surface of the Pb target (line S, ^{198}Au, ^{196}Au, ^{196m}Au, ^{195}Au, ^{194}Au, ^{193}Au).

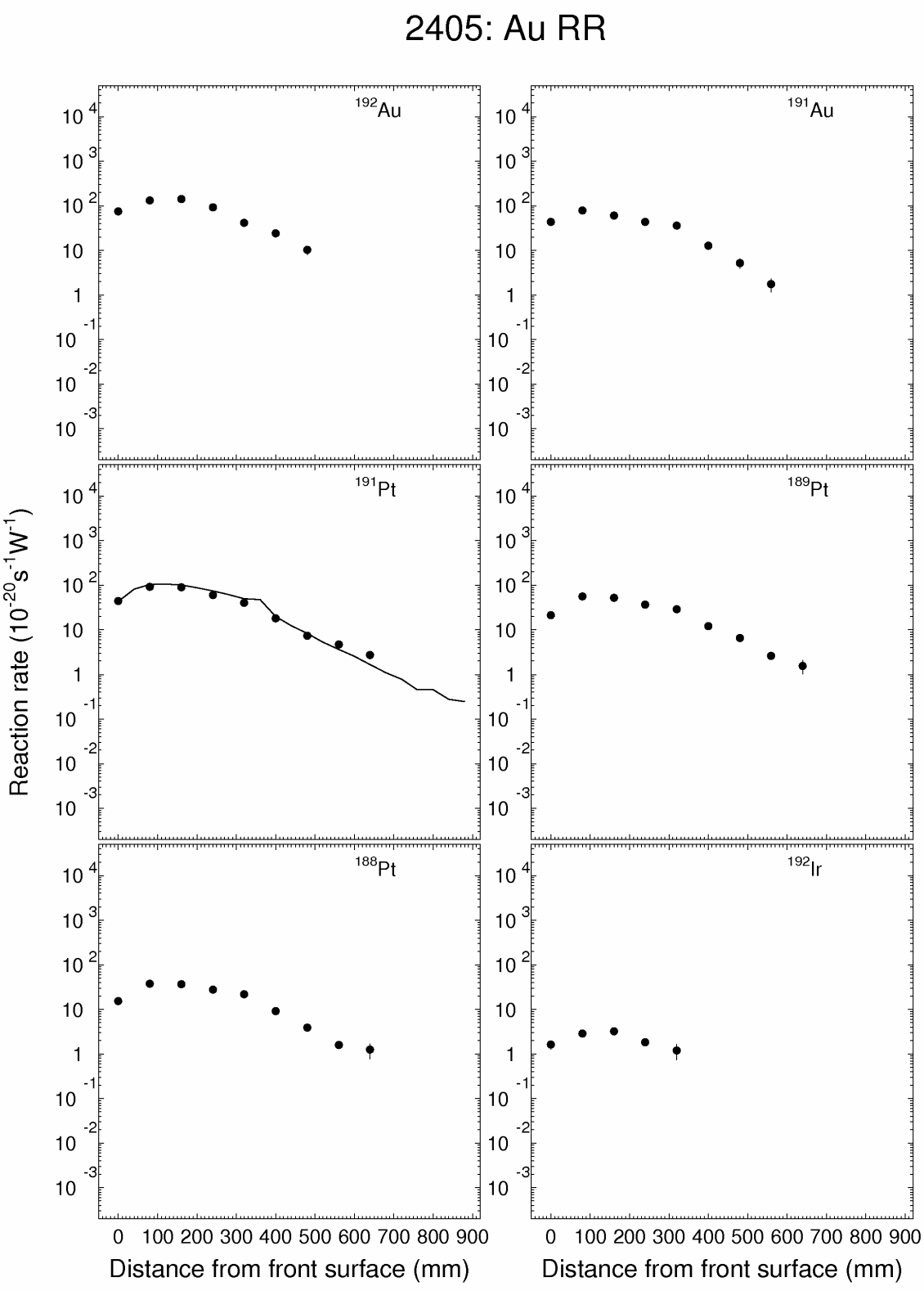

Fig. 20 (cont'd). Experimental and calculated distributions of ^{197}Au reaction products on the surface of the Pb target (line S, ^{192}Au, ^{191}Au, ^{191}Pt, ^{189}Pt, ^{188}Pt, ^{192}Ir).

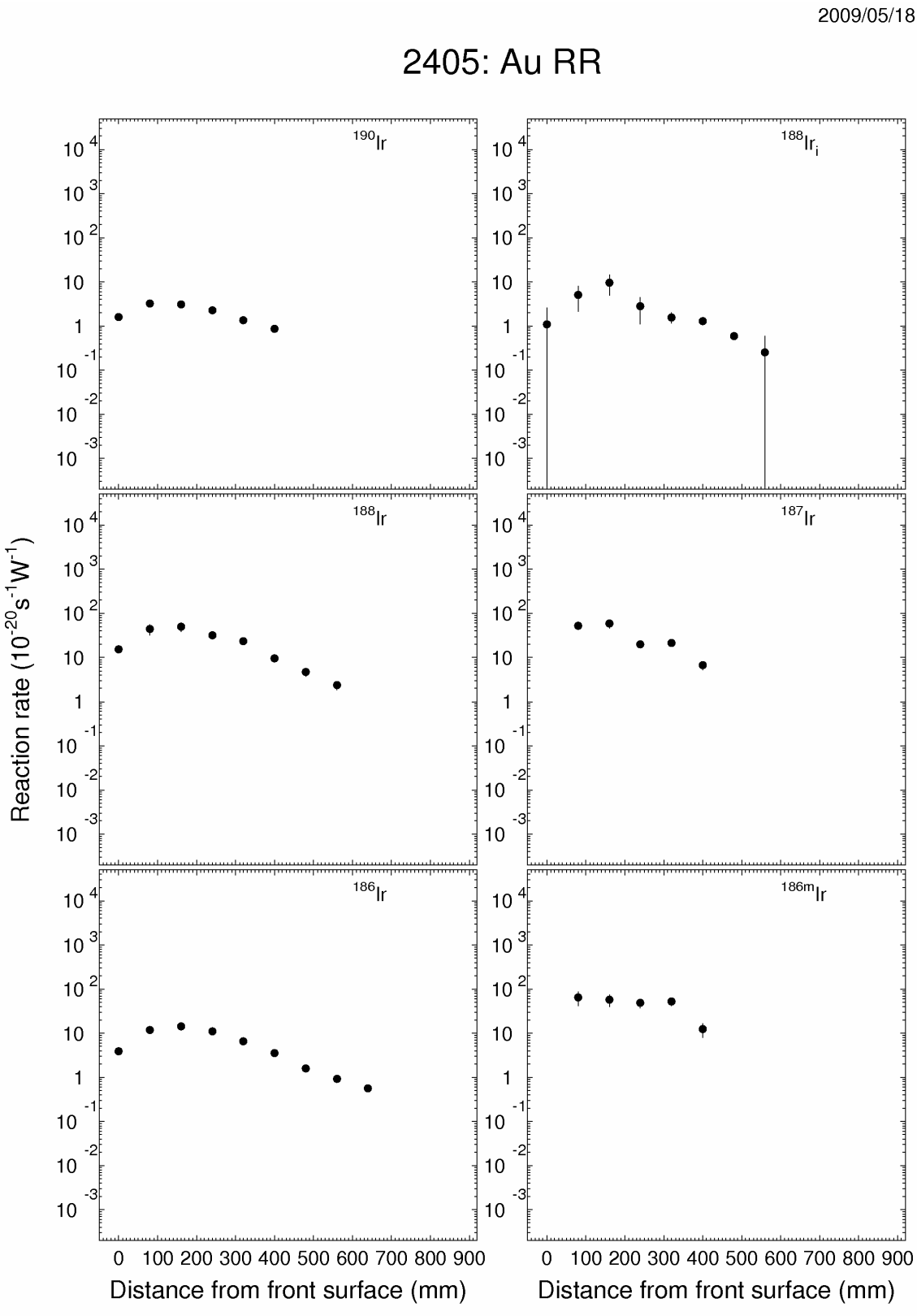

Fig. 20 (cont'd). Experimental and calculated distributions of ^{197}Au reaction products on the surface of the Pb target (line S: ^{190}Ir, ^{188}Ir$_i$, ^{188}Ir, ^{187}Ir, ^{186}Ir, ^{186m}Ir)

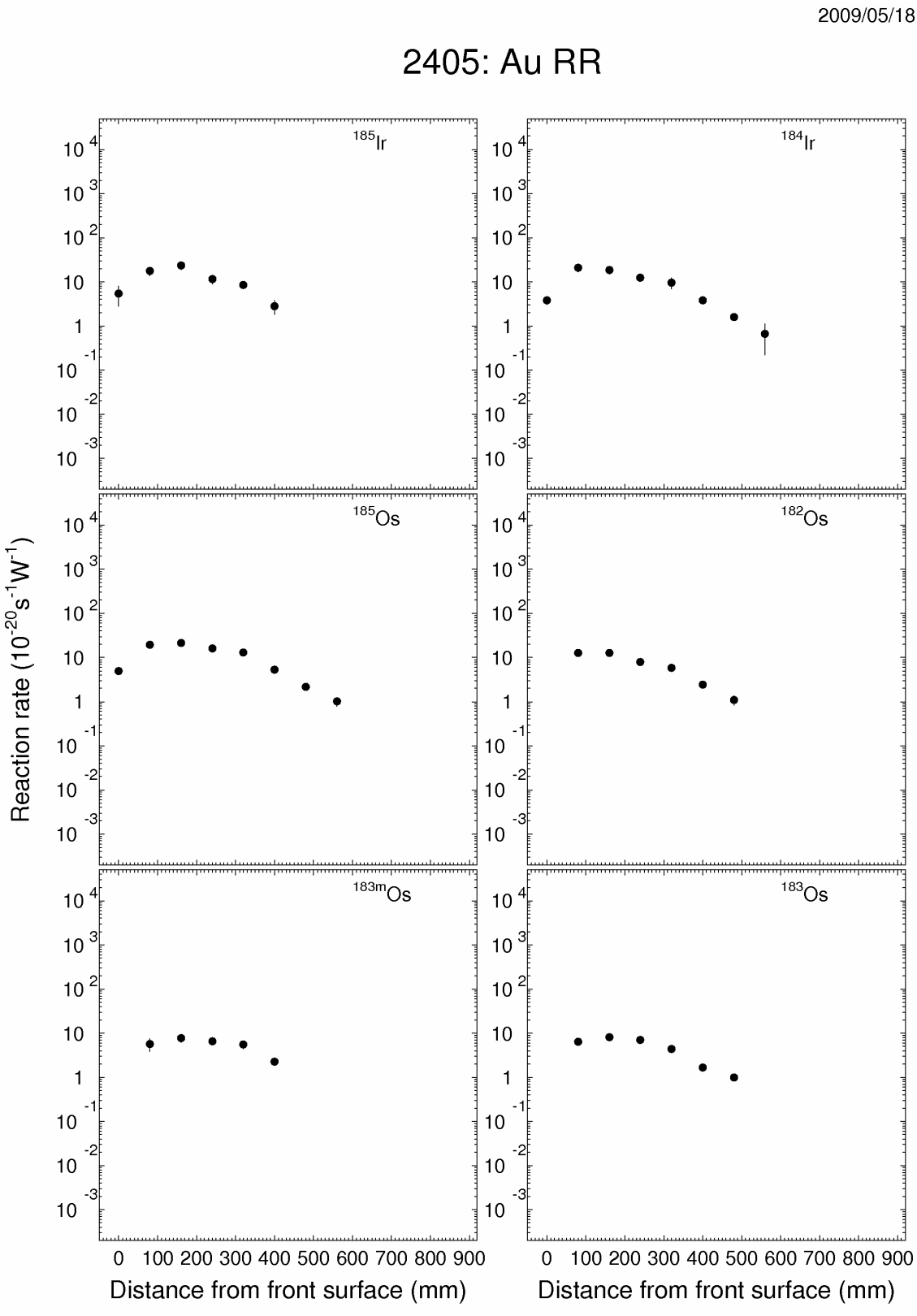

Fig. 20 (cont'd). Experimental and calculated distributions of ^{197}Au reaction products on the surface of the Pb target (line S, ^{185}Ir, ^{184}Ir, ^{185}Os, ^{182}Os, ^{183m}Os, ^{183}Os).

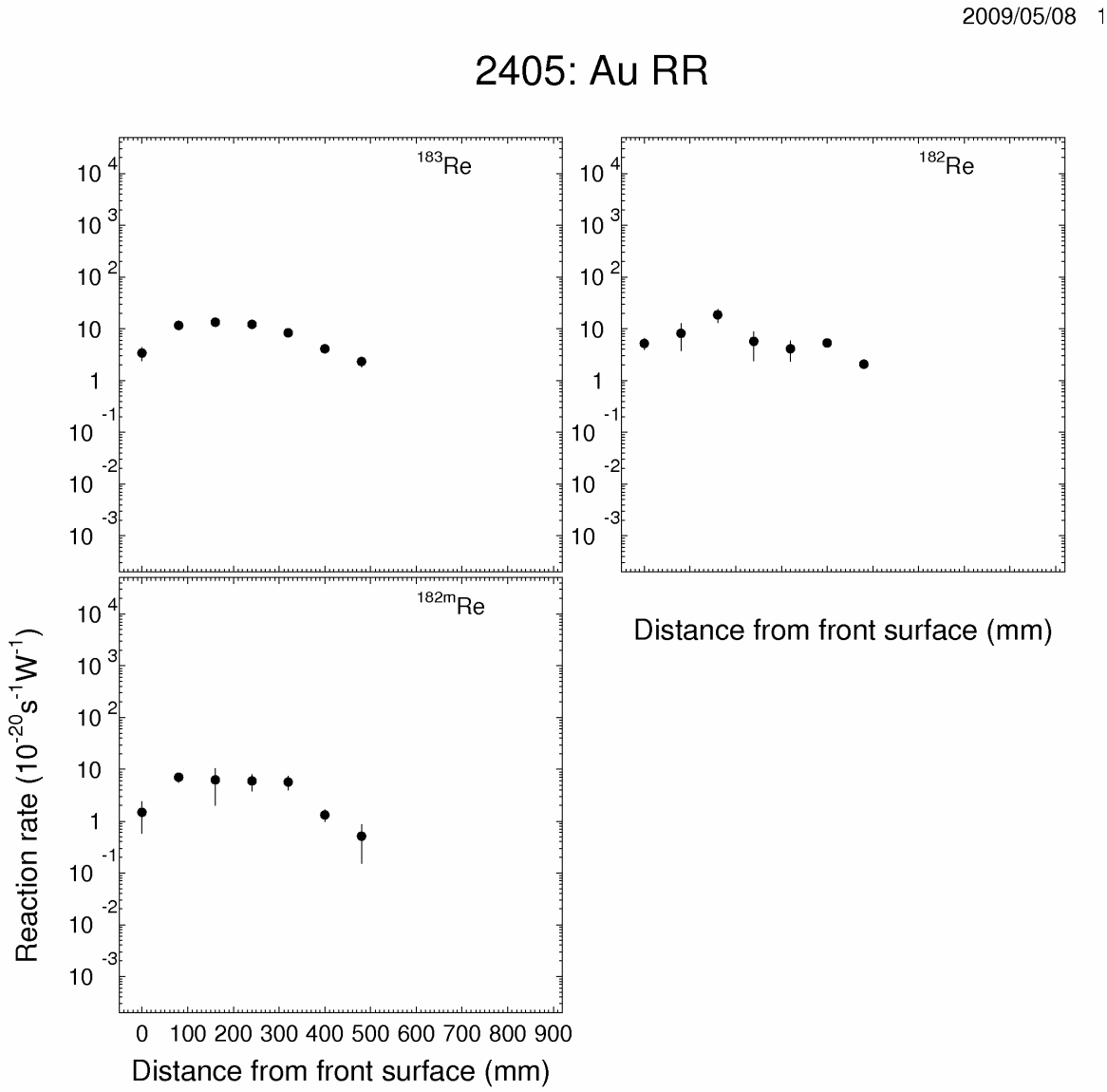

Fig. 20 (cont'd). Experimental and calculated distributions of ^{197}Au reaction products on the surface of the Pb target (line S, ^{183}Re, ^{182}Re ^{182m}Re).

3.8.2.3 Rates of reactions on ^{181}Ta

Table 17 presents the nuclear-physics characteristics of the nuclides produced in twelve ^{197}Au samples in interactions with different-energy neutrons and protons, which are used to calculate reaction rates. Table 18 and Fig. 21 present the rates of residual nuclide production in ^{181}Ta samples irradiated on the surface of the Pb target at 20, 100, 180, 260, 340, 420, 500, 580, 660, 740, 820, and 900 mm from the target front butt end.

Table 17

Nuclear-physics characteristics of nuclides produced in 181Ta sample exposed to high-energy neutrons and protons [4,21].

Nuclide	Half-life	γ- energy (E_γ, keV) and yield (Y_γ, %)
^{182}Ta	114.43d	*1289.2(1.35), 1273.7(0.65), 1257.4(1.49), 1231(11.44), 1221.4(27), 1189.1(16.2), 1157.3(0.59), 1121.3(34.9), 1113.4(0.45), 928(0.62),*

		264.1(3.61), 229.3(3.63), 222.1(7.49), 198.4(1.44), 179.4(3.08), 156.4(2.64), 152.4(6.93), 116.4(0.43), 113.7(1.88),100.1(14.1)
^{180}Ta	8.152h	*103.6(0.81), 93.4(4.51)*
^{178m}Ta	2.36h	*426.4(97), 331.6(31.2), 325.6(94.1), 213.4(81.4)*
^{177}Ta	56.56h	*112.9(7.2)*
^{176}Ta	8.09h	*1862.7(4), 1823.7(4.5), 1722(3.27), 1696.6(4.6), 1643.4(2.4), 1633.7(2.93), 1584(5.3), 1555.1(4), 1357.5(2), 1225(5.7), 1190.2(4.5), 1159.3(24.7), 1157.4(3.4), 1023.1(2.67), 710.5(5.4),521.6(2.43), 521.6(2.43), 201.8(5.7)*
^{175}Ta	10.5h	*1793.1(4.6), 1249.8(2.4),857.7(3.2),475(2), 436.4(3.8), 393.2(2.12), 348.5(12), 288.9(1.48),266.9(10.52), 266.9(10.52), 125.9(8.4).*
^{173}Ta	3.14h	*742(0.1), 172.2(17.5)*
^{181}Hf	42.39d	*482.2(80.5), 133(43.3)*
^{180m}Hf	5.5h	*500.7(14.3), 443.2(81.9), 332.3(94.1), 215.4(81.3)*
^{175}Hf	70d	*343.4(84)*
^{173}Hf	23.6h	*311.2(10.7), 306.6(6.4), 297(33.9), 162(6.5), 139.6(12.7), 135(4.74), 123.7(83)*
^{172}Hf	1.87y	*1093.6(*), 900.7(*), 181.5(*), 125.8(11.3), 125.8(11.3)*
^{171}Hf	12.1h	*852.5(5.0), 739.8(*), 662.0(14.0), 469.5(5.5), 347.5(9.7), 295.8(7.9), 122.1(12.6)*
^{170}Hf	16.01h	*620.7(18), 572.9(15), 481.3(3.7), 164.7(26), 120.2(15)*
^{177}Lu	6.734d	*208.4(11)*
^{172}Lu	6.70d	*1093.6(63.)1002.7(5.25), 900.7(29.8), 181.5(20.6)*
^{171}Lu	8.24d	*839.9(3.04), 780.7(4.36), 739.8(47.8), 689.3(2.37), 667.4(11).*
^{170}Lu	2.012d	*2041.9(6.1), 1512.5(2.55), 1395.7(2.26), 1294.7(2.93), 1225.7(4.99), 985.1(5.5), 193.1(2.14)*
^{169}Lu	34.06h	*1449.7(9.9), 960.6(23.4), 191.2(20.6)*
^{169}Yb	32.026d	*307.7(10.05), 198(35.8), 177.2(22.2), 130.5(11.31), 109.8(17.5)*
^{165}Tm	30.06h	*242.9(35.5)*

Table 18

Rates of residual production in ^{181}Ta samples on Pb target surface. $\left[10^{-20}, \frac{1}{s \cdot nucleus \cdot W}\right]$.

Nuclide	Yield type	$T_{1/2}$	Distance from the target front (mm)											
			20	100	180	260	340	420	500	580	660	740	820	900
^{182}Ta	i(m1+m2+g)	114.43d	1470(130)	1740(160)	1420(130)	1022(93)	692(63)	455(41)	359(33)	333(30)	331(30)	354(32)	398(36)	391(35)
^{180}Ta	i	8.152h	606(69)	718(79)	450(160)	263(89)	134(55)	69(33)	-	-	-	-	-	-
^{178m}Ta	i(m)	2.36h	97.5(9.0)	138(13)	112(10)	77.4(7.4)	47.0(4.4)	21.1(2.1)	7.36(0.78)	3.11(0.54)	1.39(0.41)	-	-	-
^{177}Ta	c*	56.56h	111(27)	177(43)	160(39)	112(27)	67(17)	28.3(7.0)	9.9(2.7)	6.2(2.2)	-	-	-	-
^{176}Ta	c*	8.09h	64.4(7.1)	97.6(9.8)	83.4(8.9)	63.2(7.1)	43.1(4.9)	15.9(2.8)	-	-	-	-	-	-
^{175}Ta	c	10.5h	39.7(3.8)	77.2(7.2)	66.8(6.8)	52.3(5.6)	33.7(3.6)	11.7(2.1)	5.93(0.76)	4.9(1.1)	-	-	-	-
^{173}Ta	c	3.14h	18.8(4.0)	33.2(6.3)	36.6(5.8)	19.6(4.5)	15.7(3.6)	5.2(2.0)	4.4(1.4)	-	-	-	-	-
^{181}Hf	c	42.39d	1.98(0.90)	4.35(0.97)	3.68(0.63)	-	-	-	-	-	-	-	-	-
^{180m}Hf	i(m)	5.5h	3.30(0.40)	4.80(0.67)	4.71(0.54)	3.42(0.56)	1.97(0.35)	0.94(0.27)	-	-	-	-	-	-
^{175}Hf	c	70d	56.1(5.5)	106(10)	98.6(9.6)	70.6(6.9)	48.0(4.7)	18.3(2.1)	7.50(0.87)	3.02(0.44)	2.37(0.61)	-	-	-
^{173}Hf	c*	23.6h	24.1(2.4)	56.0(5.4)	54.3(6.1)	44.5(4.2)	29.2(3.3)	12.4(1.2)	5.69(0.59)	2.48(0.30)	1.52(0.29)	0.515(0.089)	-	-
^{172}Hf	c	1.87y	49(18)	39.9(5.1)	44(23)	31(12)	-	-	-	-	-	-	-	-
^{171}Hf	c	12.1h	5.9(1.2)	17.8(1.9)	19.3(4.8)	28(12)	13.1(2.5)	4.63(0.66)	-	-	-	-	-	-
^{170}Hf	c	16.01h	6.0(1.1)	17.9(3.0)	21.0(3.7)	15.9(2.8)	11.8(2.1)	4.7(1.0)	2.71(0.70)	0.74(0.32)	-	-	-	-
^{177}Lu	c	6.734d	18.4(3.8)	49.9(7.5)	58.9(7.0)	43.7(4.9)	32.2(3.9)	14.3(2.4)	6.7(1.2)	-	-	-	-	-
^{172}Lu	i(m+g)	6.70d	1.57(0.34)	4.71(0.53)	5.5(1.1)	4.93(0.55)	-	-	-	-	-	-	-	-
^{172}Lu	c	6.70d	51(18)	43.3(5.2)	50(23)	36(12)	3.80(0.70)	1.31(0.45)	-	-	-	-	-	-
^{171}Lu	i	8.24d	8(42)	11.6(2.6)	16(13)	15(17)	2.6(6.1)	-	-	-	-	-	-	-
^{171}Lu	c*	8.24d	11.3(1.8)	30.4(2.8)	33.6(3.2)	25.2(3.0)	18.4(1.9)	6.85(0.96)	-	-	-	-	-	-
^{170}Lu	c*	2.012d	15.6(7.3)	23.9(3.5)	29.9(7.0)	17.6(4.9)	13.3(3.7)	-	-	-	-	-	-	-
^{169}Lu	c	34.06h	3.43(0.49)	11.2(1.4)	13.7(1.4)	11.5(1.2)	8.6(1.3)	2.90(0.48)	-	-	-	-	-	-
^{169}Yb	c*	32.026d	8.3(3.0)	16.4(2.6)	18.9(2.6)	16.3(1.7)	11.9(1.3)	3.9(1.4)	3.0(2.4)	-	-	-	-	-
^{165}Tm	c	30.06h	1.14(0.45)	5.79(0.69)	7.80(0.93)	5.97(0.72)	4.20(0.52)	2.33(0.38)	-	-	-	-	-	-

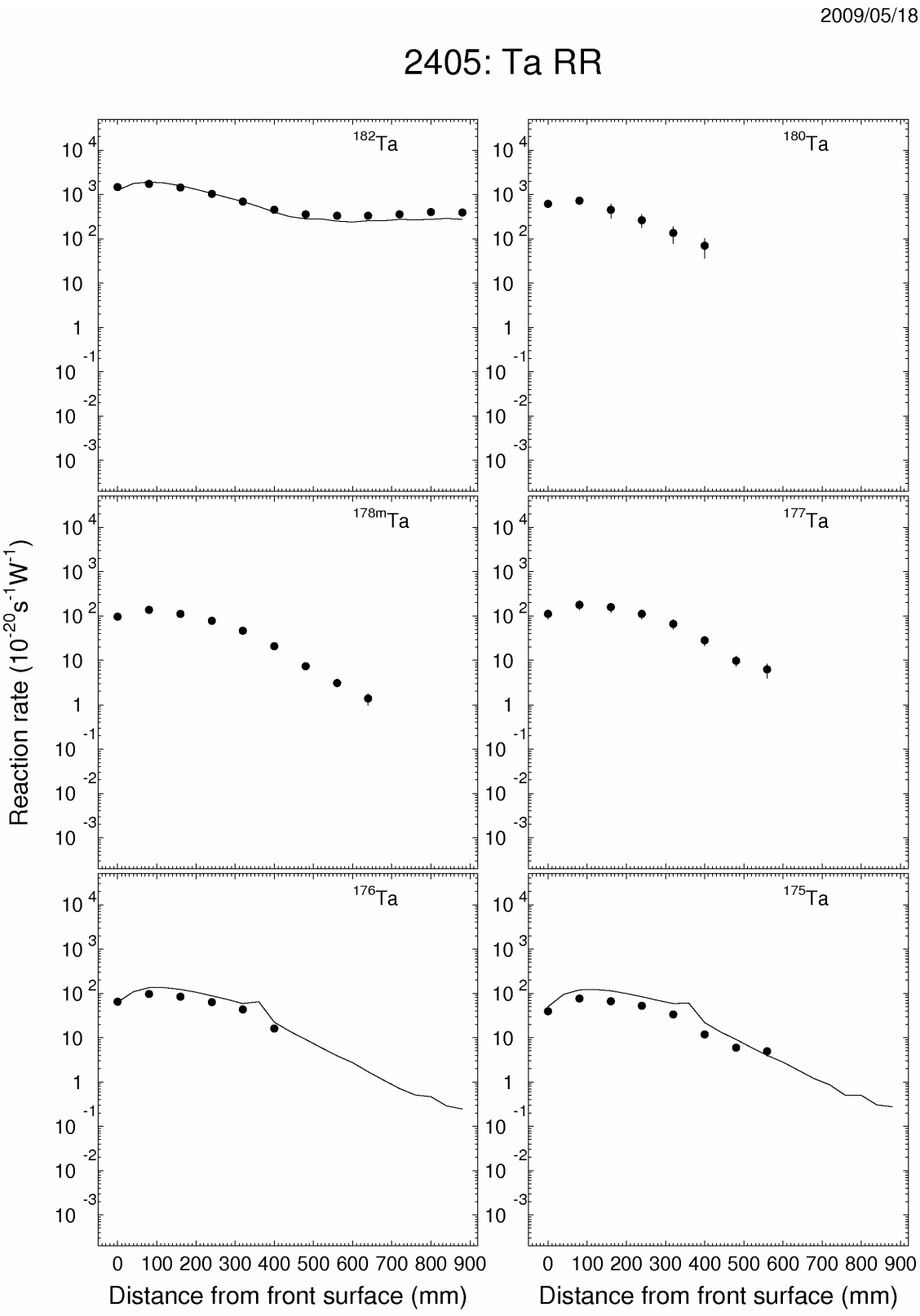

Fig. 21. Experimental and calculated distributions of ^{181}Ta reaction products on the surface of the Pb target (line S, ^{182}Ta, ^{180}Ta, ^{178m}Ta, ^{177}Ta, ^{176}Ta, ^{175}Ta).

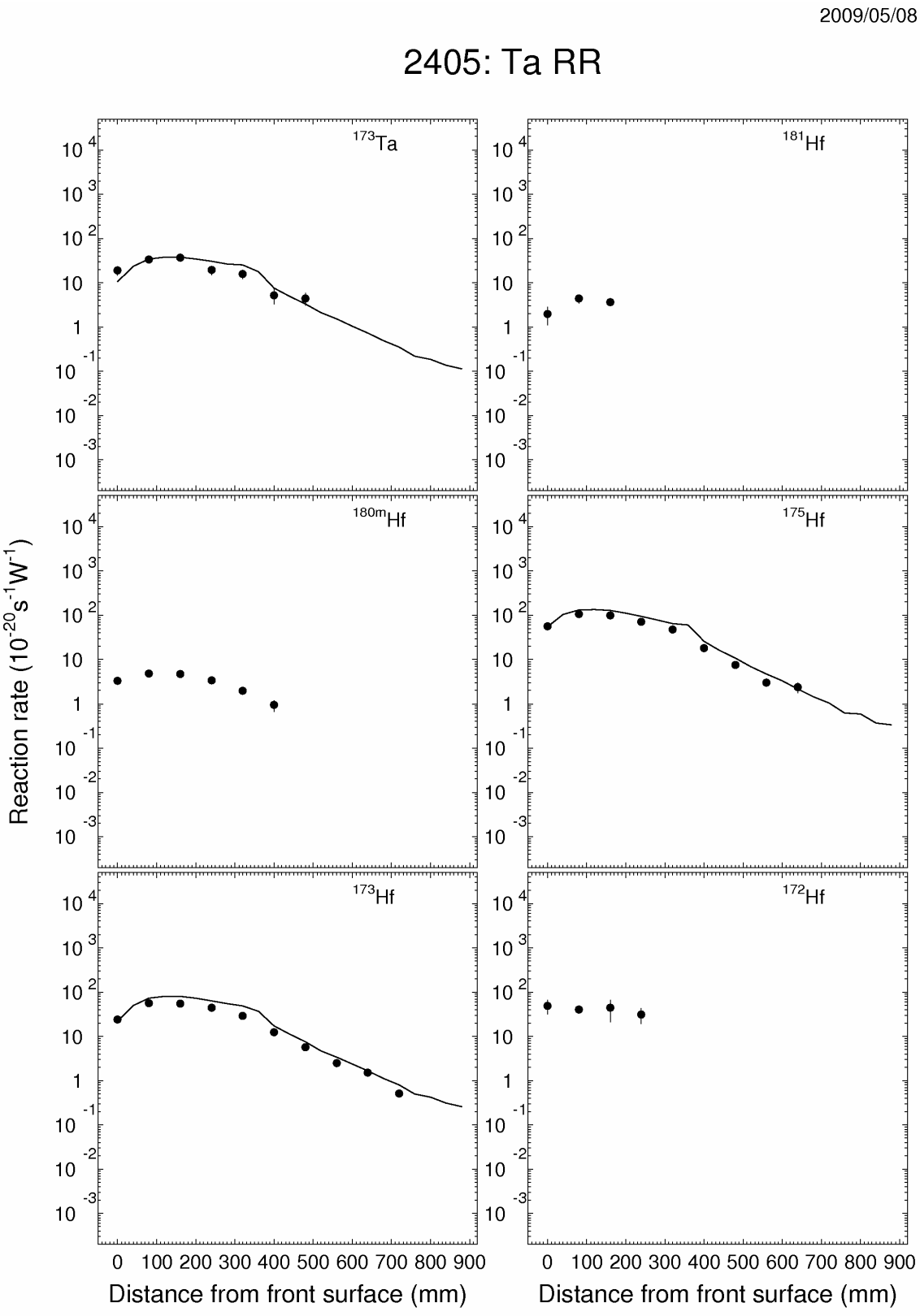

Fig. 21 (cont'd). Experimental and calculated distributions of ^{181}Ta reaction products on the surface of the Pb target (line S, ^{173}Ta, ^{181}Hf, ^{180m}Hf, ^{175}Hf, ^{173}Hf, ^{172}Hf).

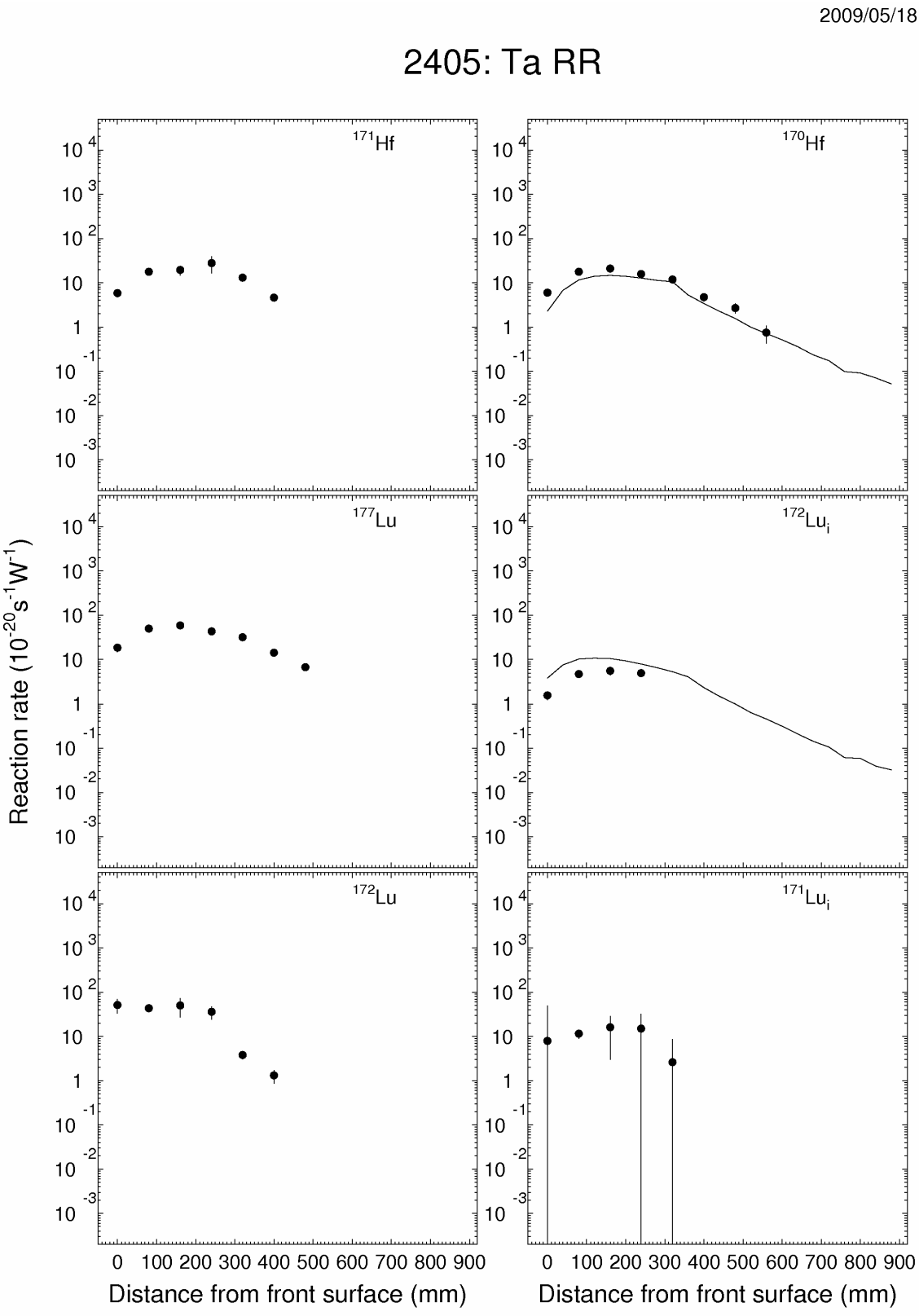

Fig. 21 (cont'd). Experimental and calculated distributions of ^{181}Ta reaction products on the surface of the Pb target (line S, ^{171}Hf, ^{170}Hf, ^{177}Lu, ^{172}Lu$_i$, ^{172}Lu, ^{171}Lu).

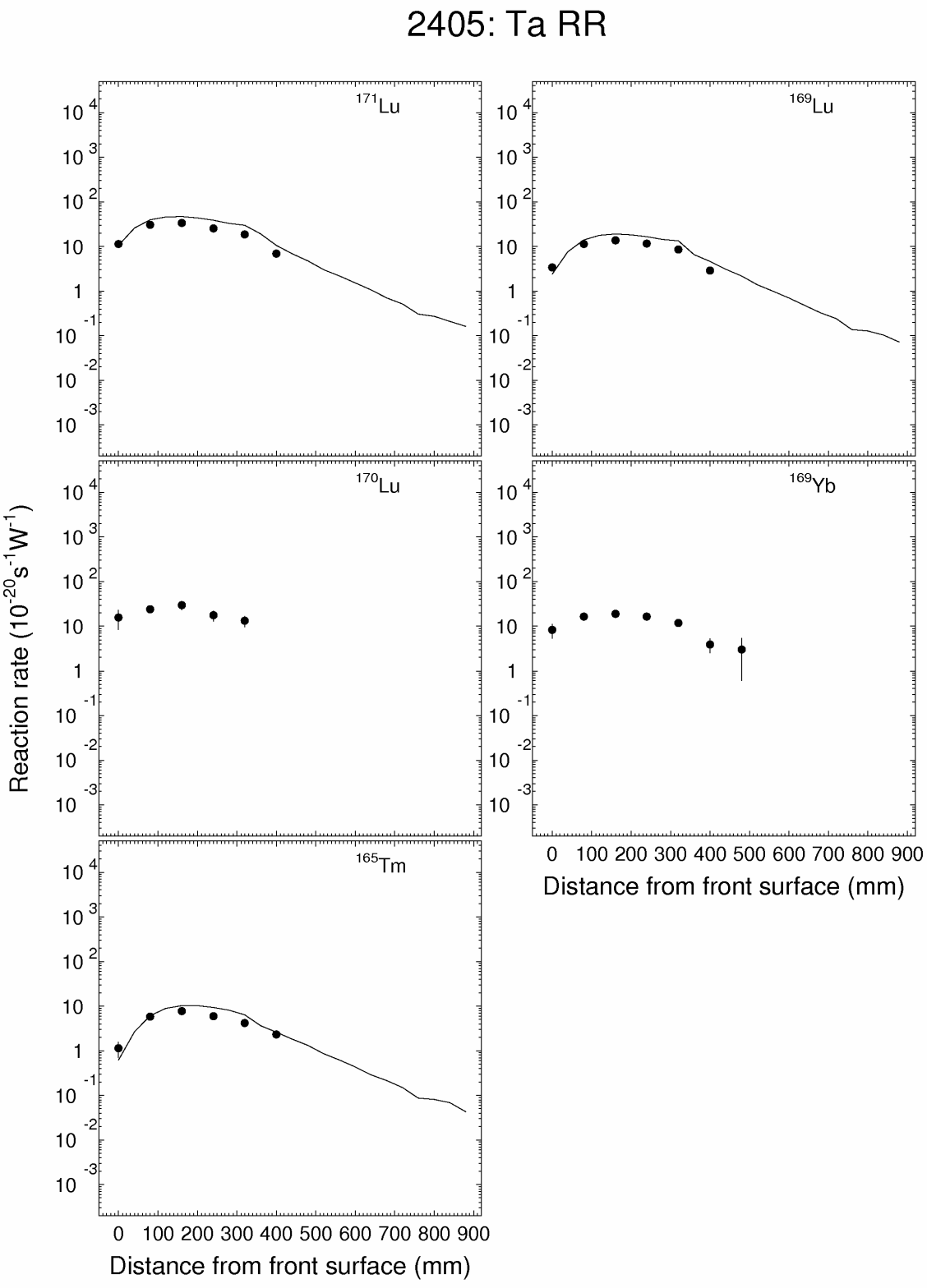

Fig. 21 (cont'd). Experimental and calculated distributions of ^{181}Ta reaction products on the surface of the Pb target (line S, ^{171}Lu, ^{169}Lu, ^{170}Lu, ^{169}Yb, ^{165}Tm).

3.8.2.4 Rates of reactions on ^{nat}In

Table 19 presents the nuclear-physics characteristics of the nuclides produced in twelve ^{197}Au samples in interactions with different-energy neutrons and protons, which are used to

calculate reaction rates. Table 20 and Fig. 22 present the rates of residual nuclide production in ^{181}Ta samples irradiated on the surface of the Pb target at 20, 100, 180, 260, 340, 420, 500, 580, 660, 740, 820, and 900 mm from the target front butt end.

Table 19.

Nuclear-physics characteristics of nuclides produced in ^{nat}In sample exposed to high-energy neutrons and protons [4,21].

Nuclide	Half-life	γ- energy (E_γ, keV) and yield (Y_γ, %)
^{113}Sn	115.09d	391.7(64.97)
^{116m}In	54.29m	2112.1(15.5), 1753.8(2.46), 1507.4(10), 1293.5(84.4), 1097.3(56.2), 818.7(11.5), 416.9(27.7), 138.3(3.29)
^{115m}In	4.486h	497.4(0.05), 336.2(45.8)
^{114m}In	49.51d	725.2(3.2), 558.4(3.2), 190.3(15.56)
^{113m}In	99.476m	391.7(64.2)
^{111}In	2.8047d	245.4(94), 171.3(90.2)
^{110}In	4.9h	1117.4(4.23), 997.2(10.52), 937.5(68.4), 901.5(1.97), 884.7(92.9), 844.7(3.24), 759.9(3.15), 744.3(1.97), 707.4(29.5), 677.6(4.5), 657.8(98.3), 641.7(25.9), 581.9(8.6), 560.3(1.87), 461.8(4.72)
^{109}In	4.2h	1149.1(4.3), 623.5(5.5), 426.2(4.12), 203.5(73.5)
^{115}Cd	53.46h	527.9(27.4), 492.4(8.03), 336.2(*), 260.9(1.94)
^{112}Ag	3.130h	617.4(43)
^{111}Ag	7.45d	342.1(6.7)
^{110m}Ag	249.76d	1384.3(24.9), 937.5(34.2), 884.7(72.7), 763.9(22.62), 706.7(16.33), 677.6(10.56), 657.8(94.3)
^{106m}Ag	8.28d	1572.3(6.6), 1527.7(16.3), 1394.3(1.49), 1222.9(7), 1199.4(11.2), 1128(11.8), 1045.8(29.6), 824.7(15.3), 808.4(4), 804.3(12.4), 748.4(20.6), 717.3(28.9), 703.1(4.47), 680.4(1.54), 616.2(21.6),601.2(1.61), 451(28.2), 429.6(13.2), 406.2(13.4), 391(3.68), 391(3.68), 228.6(2.1), 221.7(6.6)
^{105}Ag	41.29d	1087.9(3.85), 650.7(2.54), 644.5(11.1), 443.4(10.5), 344.5(41.4), 331.5(4.1), 319.2(4.35), 280.4(30.2)
^{101}Pd	8.47h	296.3(19.2)
^{100}Pd	3.63d	2376.0(*), 1929.8(*), 1553.3(*), 1107.2(*), 822.7(*), 539.5(*), 446.1(*), 126.2(7.8)
^{105}Rh	35.36h	318.9(19.1)
^{101m}Rh	4.34d	545.1(4.3), 306.9(81)
^{100}Rh	20.8h	2376(32.6), 1929.8(11.61), 1553.3(20.67), 1362.2(15.39), 1341.5(5.29), 1107.2(13.57), 822.7(21.09), 588.3(5.01), 539.5(80.6), 446.1(11.98).
^{99}Rh	16.1d	353(34.6)
^{103}Ru	39.26d	497.1(91)
^{97}Ru	2.791d	324.5(10.79), 215.7(*)
^{96}Tc	4.28d	849.9(98), 812.5(82), 778.2(99.76)
^{95}Tc	20.0h	765.8(93.8)
^{94}Tc	293m	849.7(95.7), 702.7(99.6)
^{96}Nb	23.35h	778.2(96.45)
^{95}Nb	34.975d	765.8(99.81)
^{90}Nb	14.60h	2319(82), 1129.2(92.7), 141.2(66.8), 141.2(66.8)
^{89}Zr	78.41h	909.2(99.04)
^{87m}Y	13.37h	380.8(78.05)

^{87}Y	79.8h	484.8(89.7), 388.5(82.1)

Table 20

Rates of residual production in ^{nat}In on Pb target surface $\left[10^{-20}, \frac{1}{s \cdot nucleus \cdot W}\right]$.

Nuclide	Yield type	T1/2	Distance from target front (mm)											
			20	100	180	260	340	420	500	580	660	740	820	900
^{113}Sn	i(m+g)	115.09d	1.58(0.22)	3.95(0.58)	6.48(0.78)	4.52(0.53)	3.88(0.49)	0.151(0.062)	-	-	-	-	-	-
^{116m}In	i(m1+m2)	54.29m	1910(180)	2230(210)	1760(170)	1120(100)	743(70)	414(39)	300(28)	268(25)	275(25)	305(28)	283(27)	304(28)
^{115m}In	i(m)	4.486h	2020(210)	2330(240)	1740(180)	1020(100)	579(59)	220(22)	78.3(8.0)	33.0(3.4)	-	-	-	-
^{115m}In	c	4.486h	2020(210)	2320(230)	1730(180)	1020(100)	580(59)	220(22)	78.5(8.0)	33.0(3.4)	16.5(1.7)	11.5(1.2)	6.95(0.72)	5.14(0.54)
^{114m}In	i(m)	49.51d	598(55)	721(66)	553(51)	334(31)	198(18)	84.6(7.8)	36.0(3.3)	19.5(1.8)	14.0(1.3)	14.0(1.3)	11.4(1.1)	11.4(1.1)
^{113m}In	i(m)	99.476m	100.6(9.8)	128(14)	103(15)	58.4(6.3)	32.9(4.1)	13.7(1.2)	-	-	-	-	-	-
^{113m}In	c	99.476m	102.2(10.0)	131(14)	110(15)	63.0(6.6)	36.8(4.4)	13.8(1.3)	5.08(0.61)	2.36(0.26)	0.72(0.21)	0.54(0.16)	0.34(0.11)	-
^{111}In	c	2.8047d	64.6(5.8)	104.0(9.4)	90.3(8.2)	59.2(5.4)	39.9(3.6)	16.5(1.5)	6.62(0.60)	2.91(0.26)	1.36(0.12)	0.747(0.069)	0.327(0.031)	0.180(0.019)
^{110}In	i	4.9h	21.4(1.9)	37.3(3.5)	33.1(3.1)	21.3(1.9)	14.7(1.3)	5.95(0.55)	2.44(0.23)	1.05(0.10)	0.472(0.054)	0.236(0.038)	0.114(0.023)	0.071(0.018)
^{109}In	c	4.2h	11.7(1.3)	23.9(2.3)	21.9(2.2)	15.2(1.4)	11.2(1.1)	4.19(0.40)	1.83(0.19)	0.788(0.093)	0.366(0.048)	0.199(0.048)	0.071(0.031)	-
^{115}Cd	c	53.46h	3.16(0.30)	4.15(0.39)	3.09(0.30)	1.87(0.19)	1.05(0.11)	0.476(0.049)	0.188(0.026)	0.070(0.021)	-	-	-	-
^{112}Ag	i	3.130h	-	5.9(1.6)	3.7(1.2)	3.07(0.72)	1.36(0.53)	1.00(0.24)	-	-	-	-	-	-
^{111}Ag	c	7.45d	4.38(0.61)	6.81(0.97)	6.67(0.86)	4.31(0.55)	2.42(0.38)	1.35(0.23)	-	-	-	-	-	-
^{110m}Ag	i(m)	249.76d	3.67(0.39)	5.99(0.66)	5.21(0.54)	3.26(0.38)	2.36(0.29)	0.71(0.19)	-	-	-	-	-	-
^{106m}Ag	i(m)	8.28d	2.99(0.27)	7.75(0.70)	7.90(0.71)	5.64(0.52)	4.19(0.38)	1.80(0.17)	0.714(0.073)	0.392(0.046)	0.226(0.092)	-	-	-
^{105}Ag	c	41.29d	3.99(0.39)	11.6(1.1)	12.4(1.1)	9.61(0.88)	7.20(0.68)	2.81(0.27)	1.20(0.12)	0.73(0.10)	0.35(0.12)	-	-	-
^{101}Pd	c	8.47h	-	2.22(0.55)	2.80(0.73)	2.29(0.34)	2.03(0.42)	-	0.52(0.14)	-	-	-	-	-
^{100}Pd	c	3.63d	0.208(0.051)	0.714(0.081)	1.26(0.13)	0.355(0.058)	0.762(0.077)	0.188(0.027)	0.132(0.024)	0.099(0.021)	0.033(0.012)	-	-	-
^{105}Rh	c	35.36h	0.68(0.29)	1.25(0.19)	0.89(0.16)	0.81(0.13)	0.60(0.14)	0.206(0.074)	-	-	-	-	-	-
^{101m}Rh	c	4.34d	1.13(0.13)	4.39(0.60)	5.4(1.1)	4.31(0.58)	3.25(0.39)	1.39(0.15)	0.663(0.078)	0.339(0.040)	0.171(0.023)	0.138(0.022)	0.022(0.007)	0.038(0.017)
^{100}Rh	i(m+g)	20.8h	0.353(0.046)	1.97(0.20)	2.22(0.25)	2.34(0.30)	0.873(0.093)	0.554(0.060)	-	-	-	-	-	-
^{100}Rh	c	20.8h	0.617(0.056)	2.70(0.25)	3.01(0.36)	2.64(0.29)	1.62(0.17)	0.740(0.069)	0.263(0.038)	0.087(0.032)	0.033(0.015)	-	-	-
^{99}Rh	c	16.1d	-	0.76(0.10)	0.42(0.19)	0.36(0.11)	-	-	-	-	-	-	-	-
^{103}Ru	c	39.26d	-	0.268(0.081)	0.249(0.083)	-	-	-	-	-	-	-	-	-
^{97}Ru	c	2.791d	0.369(0.040)	1.31(0.12)	1.81(0.16)	1.35(0.12)	0.951(0.091)	0.436(0.039)	0.226(0.025)	0.122(0.018)	0.061(0.009)	-	-	-
^{96}Tc	i(m+g)	4.28d	0.151(0.024)	0.537(0.057)	0.721(0.085)	0.575(0.063)	0.371(0.040)	0.216(0.053)	0.107(0.021)	0.044(0.010)	-	-	-	-
^{95}Tc	c	20.0h	0.085(0.067)	0.78(0.22)	1.07(0.11)	0.856(0.088)	0.552(0.060)	0.305(0.036)	0.152(0.021)	0.081(0.022)	-	-	-	-
^{94}Tc	c	293m	-	0.62(0.16)	0.39(0.25)	0.39(0.12)	0.36(0.12)	-	-	-	-	-	-	-
^{96}Nb	i	23.35h	0.068(0.040)	0.149(0.073)	0.101(0.081)	0.126(0.049)	0.060(0.049)	0.063(0.062)	-	-	-	-	-	-
^{95}Nb	c	34.975d	1.30(0.39)	0.67(0.98)	0.32(0.20)	0.033(0.090)	-	-	-	-	-	-	-	-
^{90}Nb	c	14.60h	0.107(0.045)	0.204(0.060)	0.414(0.085)	0.261(0.056)	0.241(0.058)	0.155(0.036)	0.079(0.030)	-	-	-	-	-
^{89}Zr	c	78.41h	0.124(0.026)	0.290(0.093)	0.314(0.056)	0.241(0.050)	0.315(0.064)	0.089(0.021)	-	-	-	-	-	-
^{87m}Y	c	13.37h	0.156(0.064)	0.229(0.083)	0.207(0.046)	0.166(0.068)	0.149(0.036)	0.115(0.028)	0.096(0.023)	0.056(0.021)	-	-	-	-
^{87}Y	c*	79.8h	0.090(0.022)	0.153(0.023)	0.225(0.042)	0.205(0.051)	0.139(0.037)	0.088(0.013)	0.060(0.011)	0.031(0.020)	-	-	-	-
^{87}Y	c*	79.8H	0.090(0.022)	0.153(0.023)	0.225(0.042)	0.205(0.051)	0.139(0.037)	0.088(0.013)	0.060(0.011)	0.031(0.020)	--	--	--	--

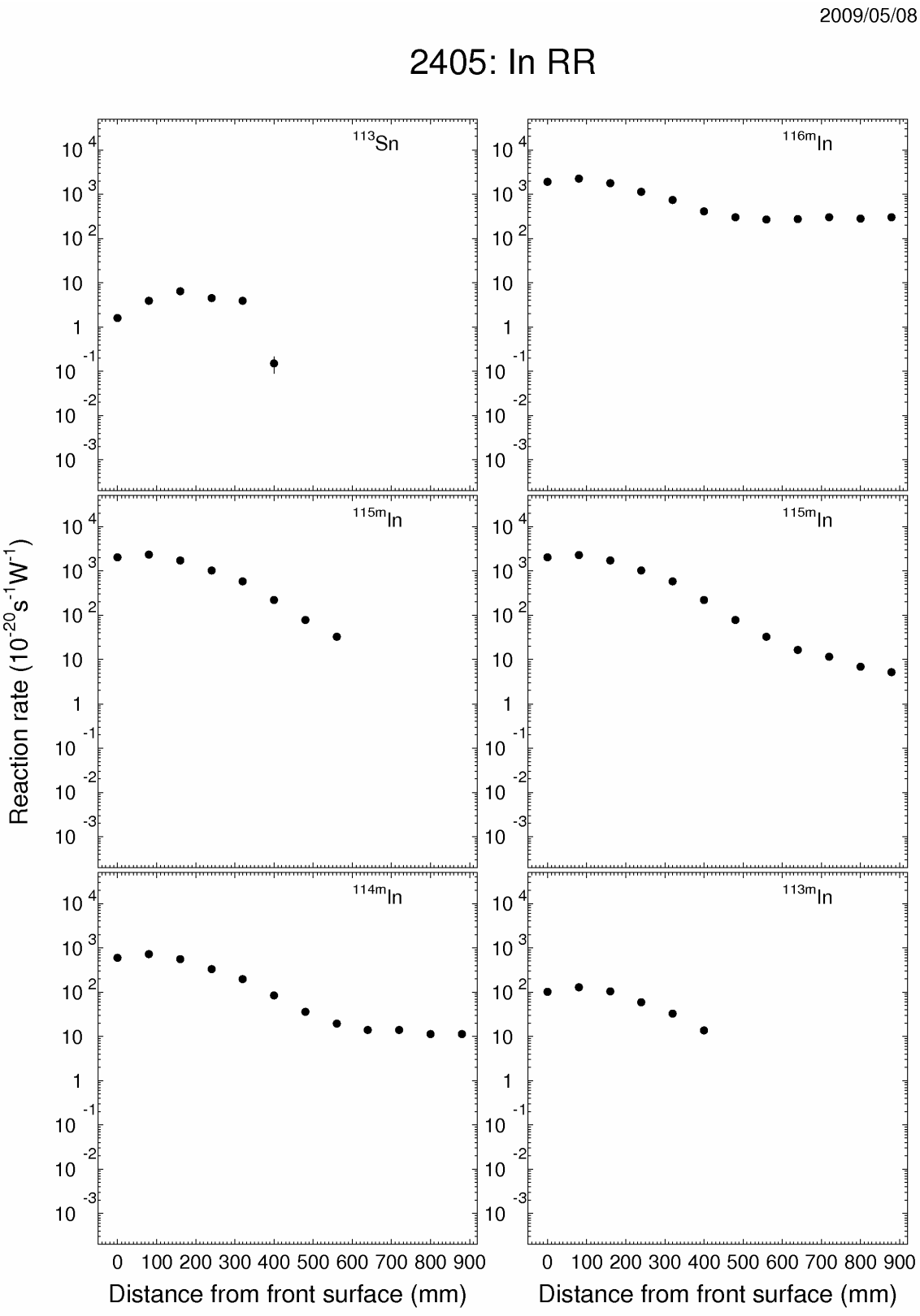

Fig. 22. Experimental and calculated distributions of ^{nat}In reaction products on the surface of the Pb target (line S, ^{113}Sn, ^{116m}In, ^{115m}In, ^{115m}In$_i$, ^{114m}In, ^{113m}In).

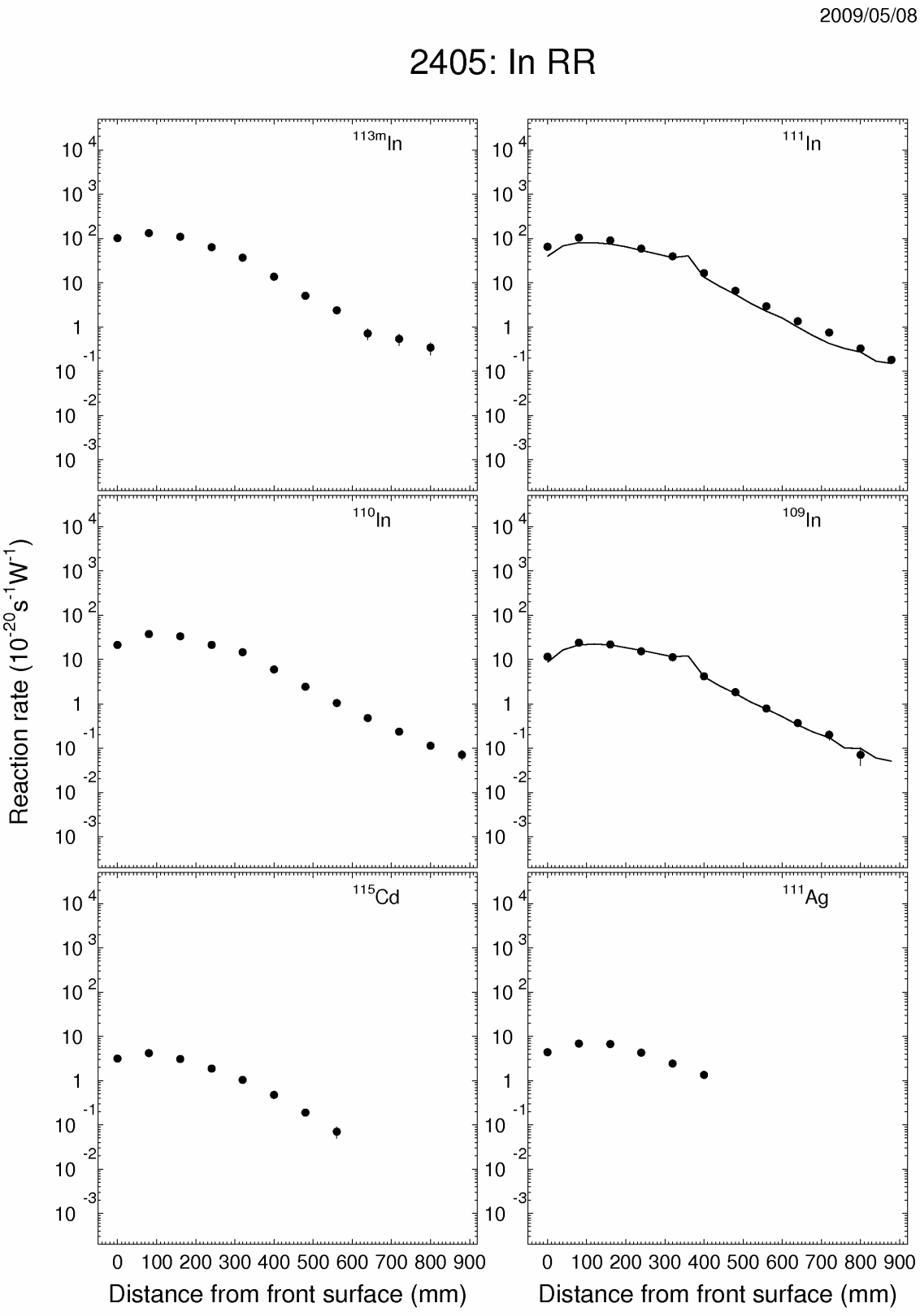

Fig. 22 (cont'd). Experimental and calculated distributions of ^{nat}In reaction products on the surface of the Pb target (line S, ^{113m}Sn, ^{111}In, ^{110}In, ^{109}In, ^{115}Cd, ^{111}Ag).

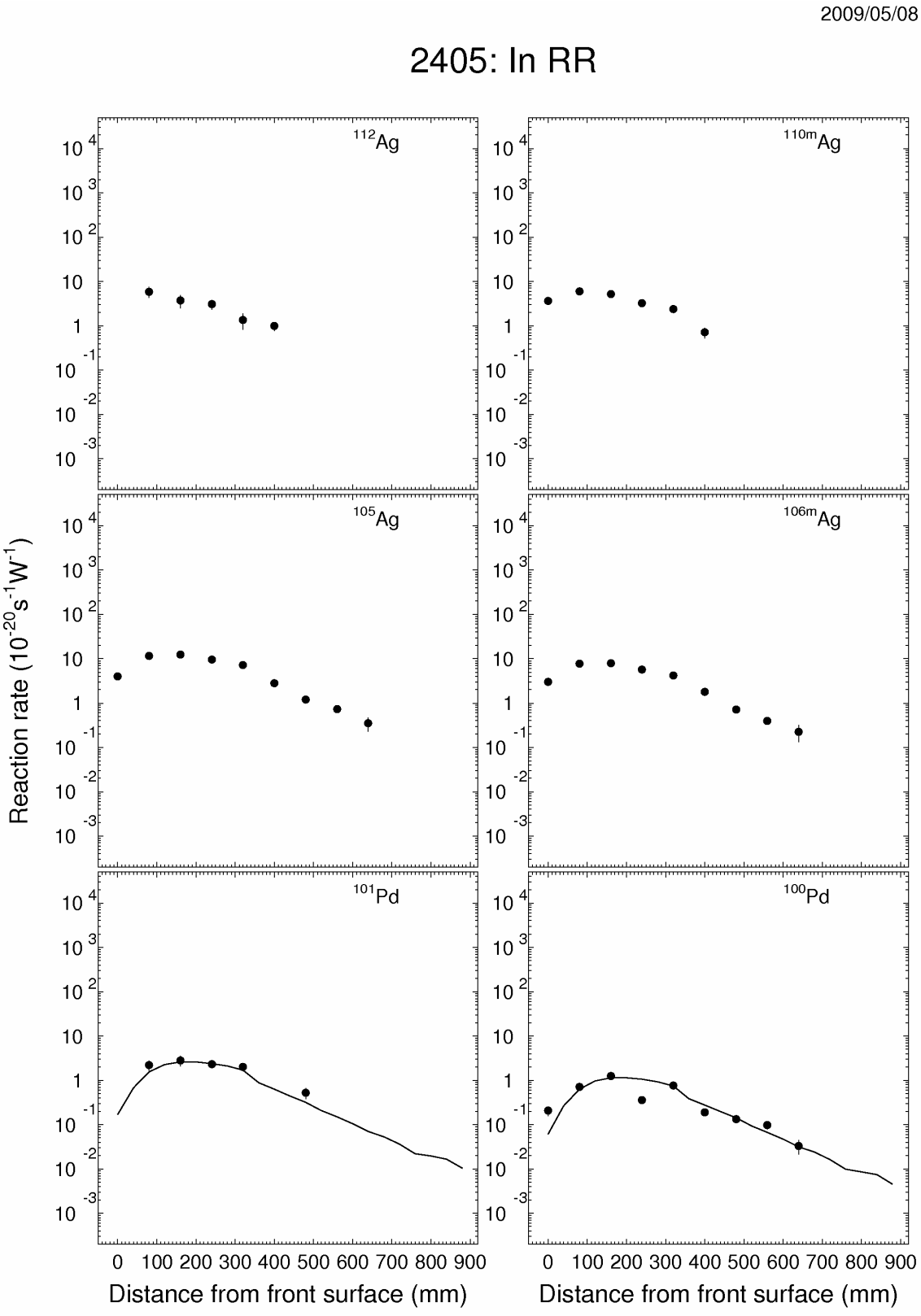

Fig. 22 (cont'd). Experimental and calculated distributions of ^{nat}In reaction products on the surface of the Pb target (line S, ^{112}Ag, ^{110m}Ag, ^{105}Ag, ^{106m}Ag, ^{101}Pd, ^{100}Pd).

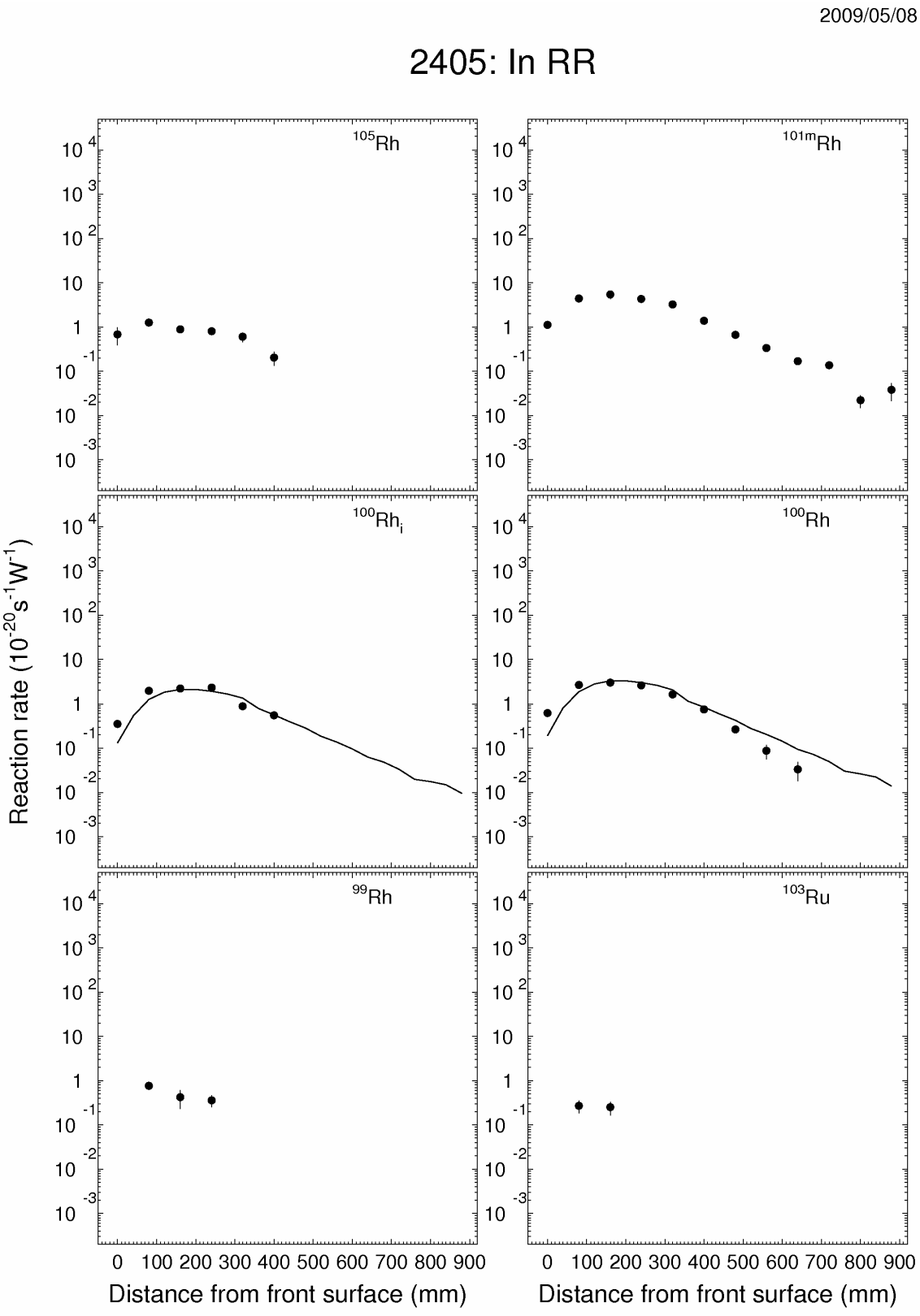

Fig. 22 (cont'd). Experimental and calculated distributions of ^{nat}In reaction products on the surface of the Pb target (line S, ^{105}Rh, ^{101m}Rh, ^{100}Rh$_i$, ^{99}Rh, ^{103}Ru).

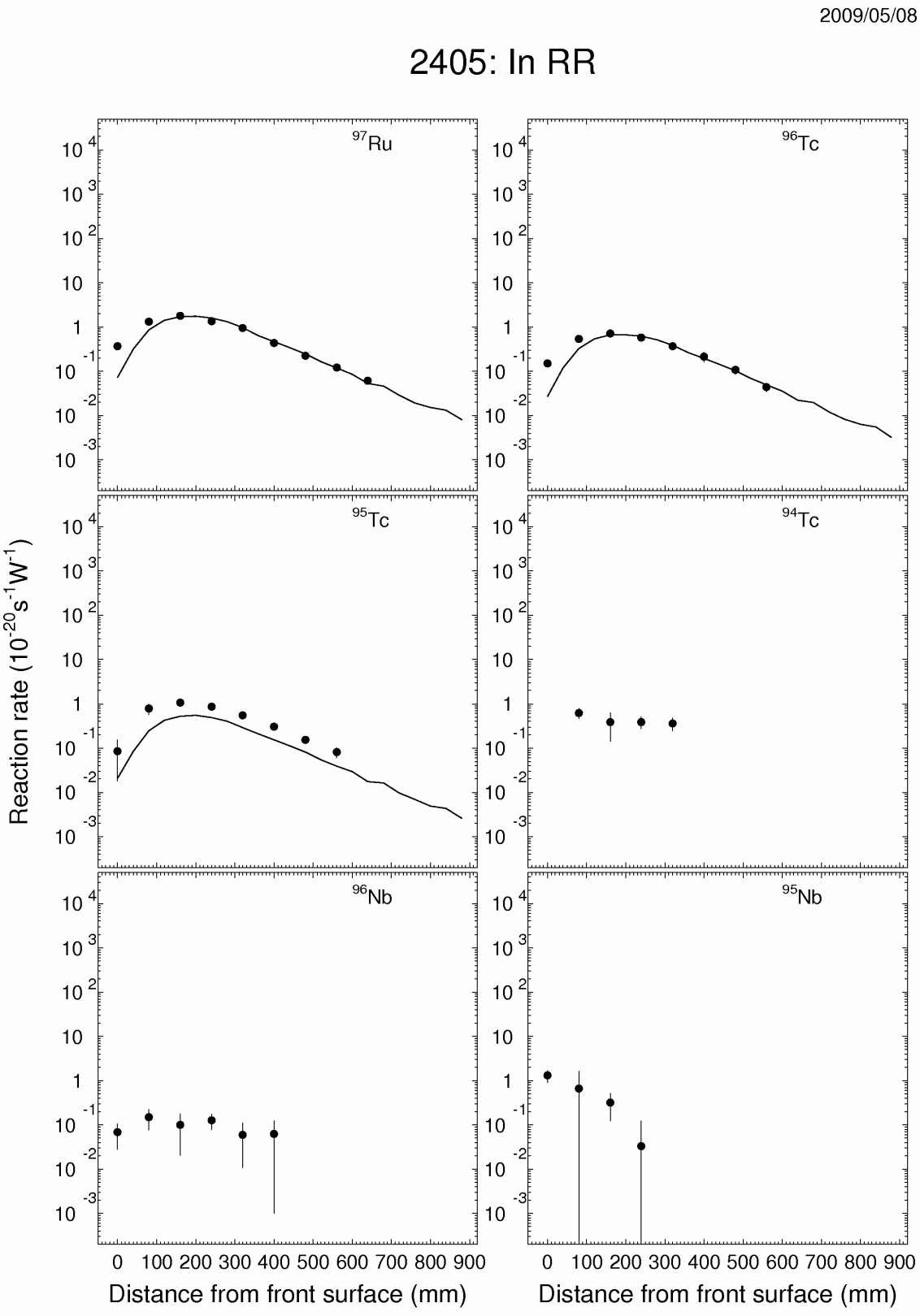

Fig. 22 (cont'd). Experimental and calculated distributions of ^{nat}In reaction products on the surface of the Pb target (line S, ^{97}Ru, ^{96}Tc, ^{95}Tc, ^{94}Tc, ^{96}Nb, ^{95}Nb).

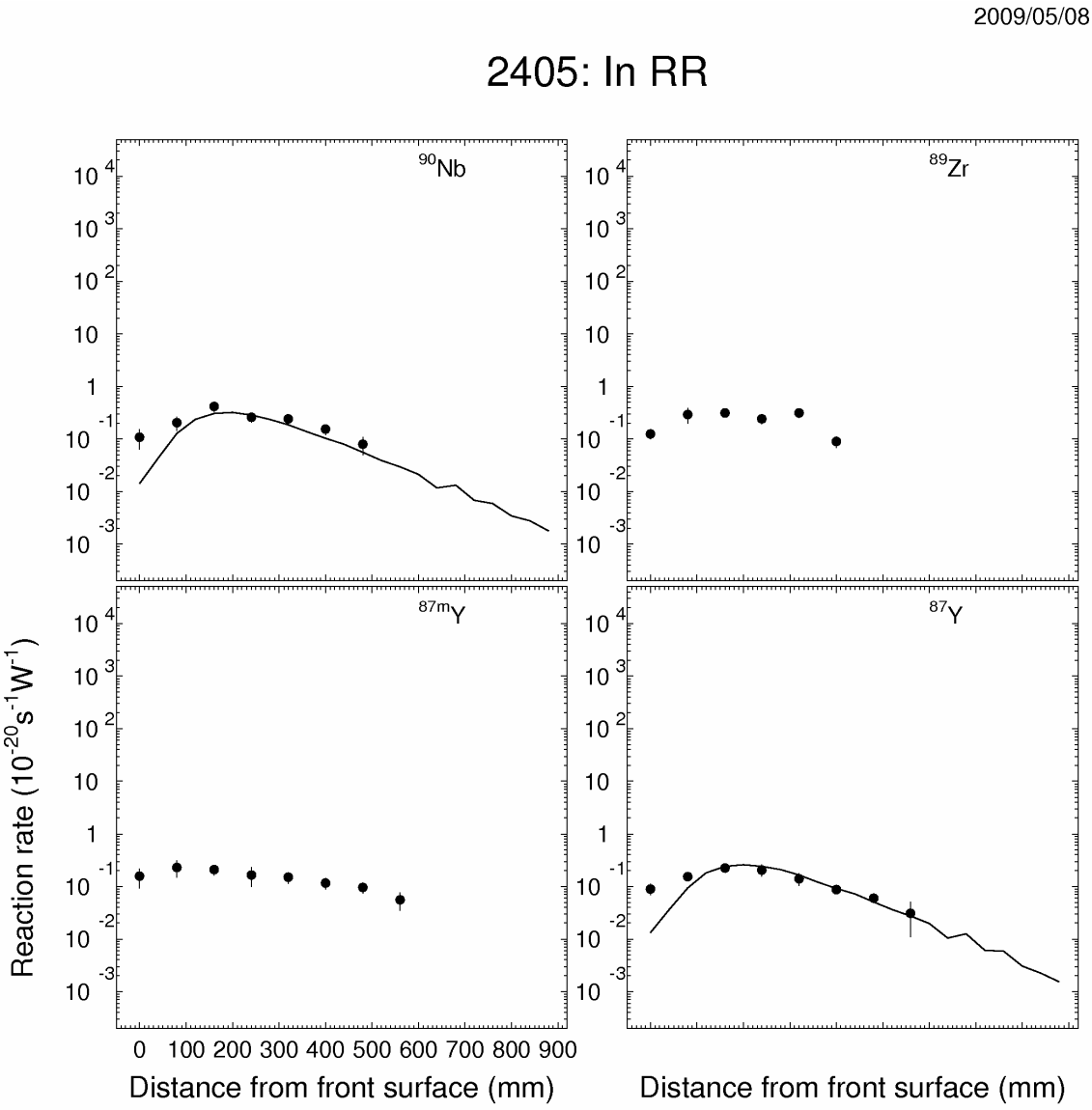

Fig. 22 (cont'd). Experimental and calculated distributions of ^{nat}In reaction products on the surface of the Pb target (line S, ^{90}Nb, ^{89}Zr, ^{87m}Y, ^{87}Y).

3.8.2.5. Rates of reactions on ^{27}Al

Table 11 presents the nuclear-physics characteristics of the nuclides produced in twelve ^{27}Al samples along S lines and in 42 ^{27}Al samples along «I», «J», «K», «L», «M», «N», «O» lines in interactions with different-energy protons, which are used to calculate the reaction rates.

Table 21 and Figs. 23, 24 present the rates of residual nuclide production in ^{27}Al samples irradiated on the surface of the Pb target at 20, 100, 180, 260, 340, 420 500, 580, 660, 740, 820, and 900 mm from the target front butt end. Fig. 25 shows the azimuthal distribution of ^{24}Na in ^{27}Al located on lines S (0° from vertical), M (45° clockwise from vertical), L (90°), K (135°), J (180°), I (225°), O (270°), and N (315°).

Table 21

Rates of residual production in ^{27}Al on Pb target surface $\left[10^{-20}, \frac{1}{s \cdot nucleus \cdot W}\right]$

Posi-tion	Nuclide	Yield type	Distance from target front (mm)											
			20	100	180	260	340	420	500	580	660	740	820	900
S	^{24}Na	c	92.8(16.8)	91.7(15.2)	77.0(14.9)	45.9(5.6)	28.0(2.0)	10.2(0.7)	3.12(0.31)	8.59(0.45)	4.25(0.25)	2.23(0.14)	1.21(0.09)	0.835(0.061)
	^{22}Na	c	53.2(4.8)	82.1(8.2)	58.7(5.2)	34.5(3.2)	20.5(1.8)	8.30(0.84)	3.11(0.28)	1.30(0.12)	0.595(0.056)	0.272(0.029)	0.155(0.016)	0.100(0.011)
	^{27}Mg	c	8.30 (0.87)	8.64(0.95)	12.9 (1.3)	-	5.76(0.73)	4.01(0.60)	-	-	-	-	-	-
I	^{24}Na	c	49.3 (4.4)	-	55.3 (5.1)	-	20.5 (1.9)	-	3.75(0.37)	-	1.26 (0.17)	-	0.411(0.081)	-
J	^{24}Na	c	58.6 (5.2)	-	60.0 (5.5)	-	24.5 (2.3)	-	4.29(0.58)	-	0.882(0.238)	-	0.266(0.068)	-
K	^{24}Na	c	61.2 (6.0)	-	65.4 (5.9)	-	25.6(2.3)	-	3.72(0.53)	-	0.770(0.122)	-	0.313(0.209)	-
L	^{24}Na	c	55.6 (4.9)	-	60.5 (5.4)	-	22.2(2.0)	-	3.59(0.35)	-	0.730(0.069)	-	0.213(0.022)	-
M	^{24}Na	c	52.3 (4.8)	-	57.6 (5.1)	-	21.0 (1.9)	-	3.33(0.33)	-	0.650(0.063)	-	0.176(0.032)	-
N	^{24}Na	c	44.9 (3.9)	-	49.1 (4.4)	-	18.6 (1.7)	-	3.03(0.27)	-	0.644(0.063)	-	0.176(0.022)	-
O	^{24}Na	c	44.9 (4.0)	-	50.3 (4.5)	-	19.2 (1.7)	-	3.31(0.30)	-	0.619(0.067)	-	0.172(0.018)	-

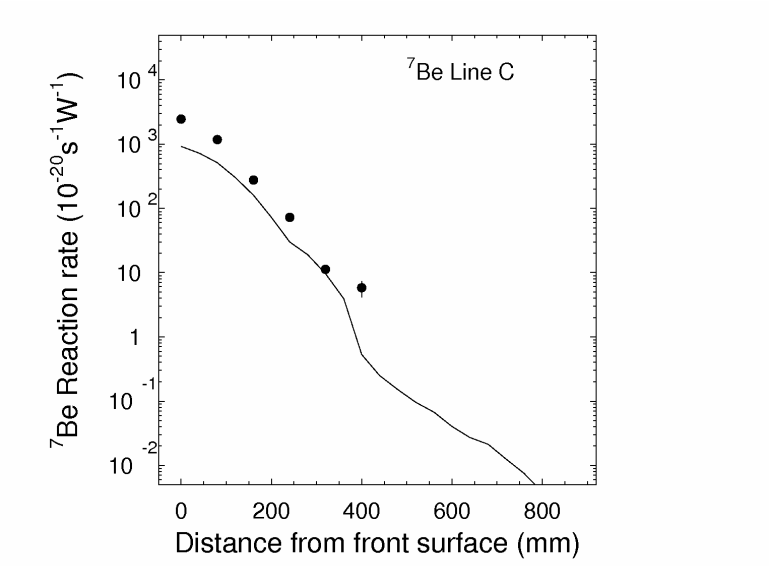

Fig. 23. Experimental and calculated distributions of ^{7}Be in ^{27}Al inside (line C) the target.

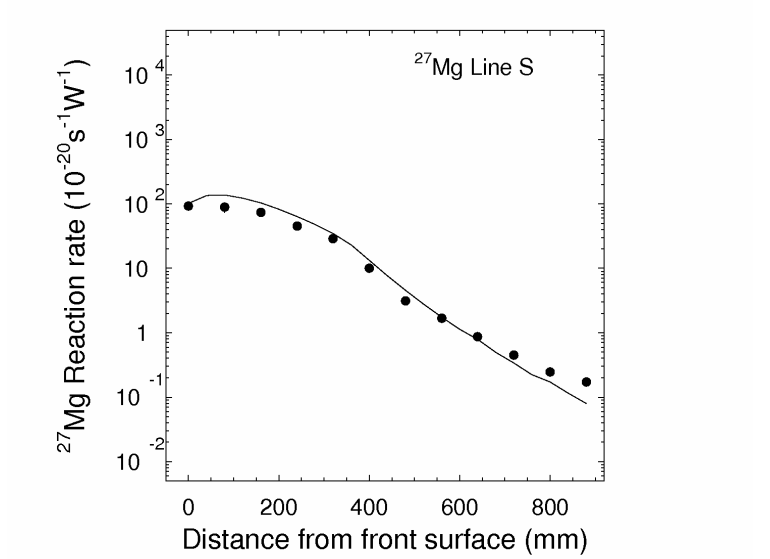

Fig. 24. Experimental and calculated distributions of ^{27}Mg in ^{27}Al outside (line S) the target.

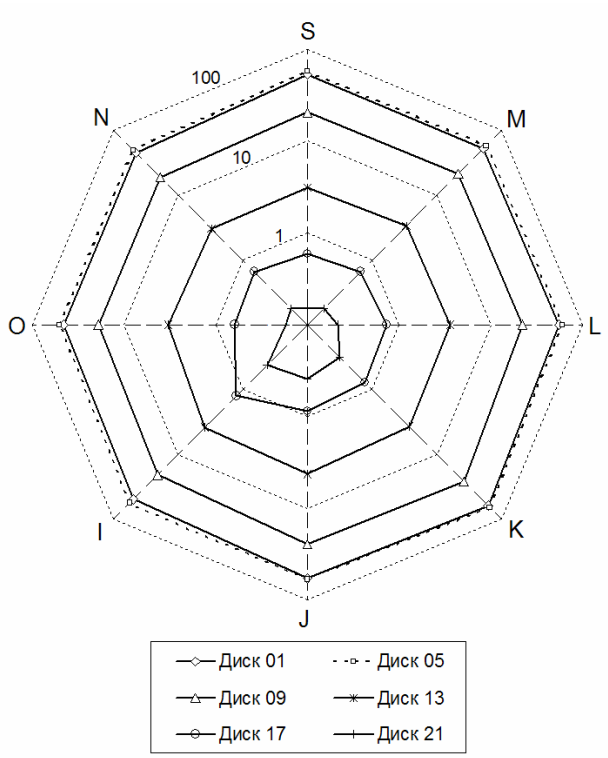

Fig. 25. Azimuthal distribution of ^{24}Na in ^{27}Al located on lines S, I, J, K, L, M, N, O measured on 1-st, 5-th, 9-th, 13-th, 17-th, and 21-th disks.

3.8.3. Nuclide reaction rates on the surface of disc 3 of Pb target.

3.8.3.1. Rates of reactions on ^{169}Tm.

Table 22 presents the nuclear-physics characteristics of nuclides produced in ^{169}Tm by interactions with high-energy neutrons and protons, which are used to calculate the reaction rates. Table 23 and Fig. 26 present the production rates of residuals in ^{169}Tm sample on the surface of disc 3 of Pb target.

Table 22

Nuclear physics characteristics of nuclides produced in ^{169}Tm sample in interactions with high-energy neutrons and protons [4,21].

Nuclide	Halflife	γ-energy (E_γ, keV) and yield (Y_γ, %)
^{166}Yb	56.7h	*2092.1(*), 2079.5(*), 2052.4(*), 1895.1(*), 1867.9(*), 1505(*), 1374.2(*), 1300.7(*), 1273.5(*),1176.7(*), 1152.3(*),875.7(*),785.9(*), 778.8(*), 757.8(*), 712.8(*), 705.3(*), 691.2(*), 674.8(*), 672.2(*), 594.4(*), 459.6(*),215.2(*),184.4(*), 82.3(15.22).*
^{168}Tm	93.1d	*1277.4(1.66), 914.9(3.08), 830(6.89), 816(50.3), 748.3(0.42), 741.4(12.6), 730.7(5.21), 720.4(12), 645.8(1.46), 631.7(9.1), 546.8(2.62), 447.5(23.7), 422.3(0.3), 348.5(0.35), 198.2(53.8), 184.3(17.9), 99.3(4.18)*
^{167}Tm	9.25d	*531.5(1.61), 207.8(42)*
^{166}Tm	7.70h	*2092.1(1.56), 2079.5(6.3), 2052.4(17.2), 1895.1(1.2), 1867.9(4.04), 1505(0.83), 1374.2(5.6), 1347(1.09), 1300.7(1.33), 1273.5(14.9),*

		1235.4(1.85), 1203.9(1.04), 1176.7(9.5), 1152.3(1.55), 875.7(4.06), 810.3(1.09), 785.9(9.9), 778.8(18.9), 757.8(2.33), 712.8(0.41), 705.3(11), 691.2(7.4), 674.8(2.57), 672.2(6.1), 598.8(2.1), 594.4(3.46), 459.6(2.51), 404(0.78), 215.2(5.2), 194.7(0.76), 184.4(16.1)
^{165}Tm	30.06h	*1427.4(0.81), 1380.2(0.39), 1184.4(2.95), 1131.3(1.73), 853.6(0.16), 837.7(0.49), 806.4(9.5), 790.9(0.46), 747(0.18), 698.8(1.29), 665.1(0.38), 610.6(0.48), 608.5(0.45), 589.9(1.82), 564.2(2.31), 542.6(1.43), 527.1(0.94), 513.7(0.24), 487.4(1.04), 472(0.35), 460.3(4.12), 456.5(1.25), 448.6(1.63), 443(0.73), 430.6(0.28), 421.2(0.33), 389.4(2.82), 365.6(0.49), 356.5(2.75), 346.8(0.22), 312.3(0.47), 297.4(12.7), 296.1(3.88), 292.4(1.27), 279.3(0.6), 264.5(0.55), 249(0.4), 242.9(35.5), 218.9(3.34), 210.1(0.84), 195.8(0.58), 162.6(0.06), 150.9(0.56), 113.6(1.56).*
^{163}Tm	1.810h	*241.3(10.9),), 104.3(18.6)*
^{161}Er	3.21h	*826.6(64), 211.1(12.2)*
^{160}Er	28.58h	*966.2(*), 962.4(*), 879.4(22.6),), 872(6.8), 728.2(34), 645.4(18), 538.6(*), 197(15.5)*
^{160m}Ho	5.02h	*966.2(15.4), 962.4(16.6), 538.6(3.6).*
^{157}Dy	8.14h	*326.2(92)*
^{155}Dy	9.9h	*226.9(68.4)*
^{160}Tb	72.3d	*298.6(26.1)*
^{155}Tb	5.32d	*163.3(4.44), 150.6(*), 105.3(25.1)*
^{153}Tb	2.34d	*212(31)*
^{152}Tb	17.5h	*344.3(65)*
^{149}Gd	9.28d	*346.6(23.9), 149.7(48.)*
^{147}Gd	38.06h	*1069.3(7.2)*

Table 23

Production rates of residuals in ^{169}Tm on the Pb target surface $\left[10^{-20}, \frac{1}{s \cdot nucleus \cdot W}\right]$.

Nuclide	Yield type	T1/2	R(ΔR)
^{166}Yb	i	56.7h	5.27(0.47)
^{168}Tm	i	93.1d	902(82)
^{167}Tm	c	9.25d	515(74)
^{166}Tm	i	7.70h	256(23)
^{166}Tm	c	7.70h	264(24)
^{165}Tm	c	30.06h	178(16)
^{163}Tm	c*	1.810h	81(13)
^{161}Er	c*	3.21h	47.3(7.3)
^{160}Er	c	28.58h	29.9(3.0)
^{160m}Ho	i(m)	5.02h	3.4(2.3)
^{160m}Ho	c	5.02h	35.1(5.2)
^{157}Dy	c	8.14h	16.5(1.7)
^{155}Dy	c*	9.9h	8.48(0.83)
^{160}Tb	i	72.3d	13.8(3.0)
^{155}Tb	c*	5.32d	9.1(1.1)
^{153}Tb	c*	2.34d	5.77(0.66)
^{152}Tb	c*	17.5h	4.07(0.57)

^{149}Gd	c	9.28d	2.71(0.59)
^{147}Gd	c	38.06h	14.8(2.3)

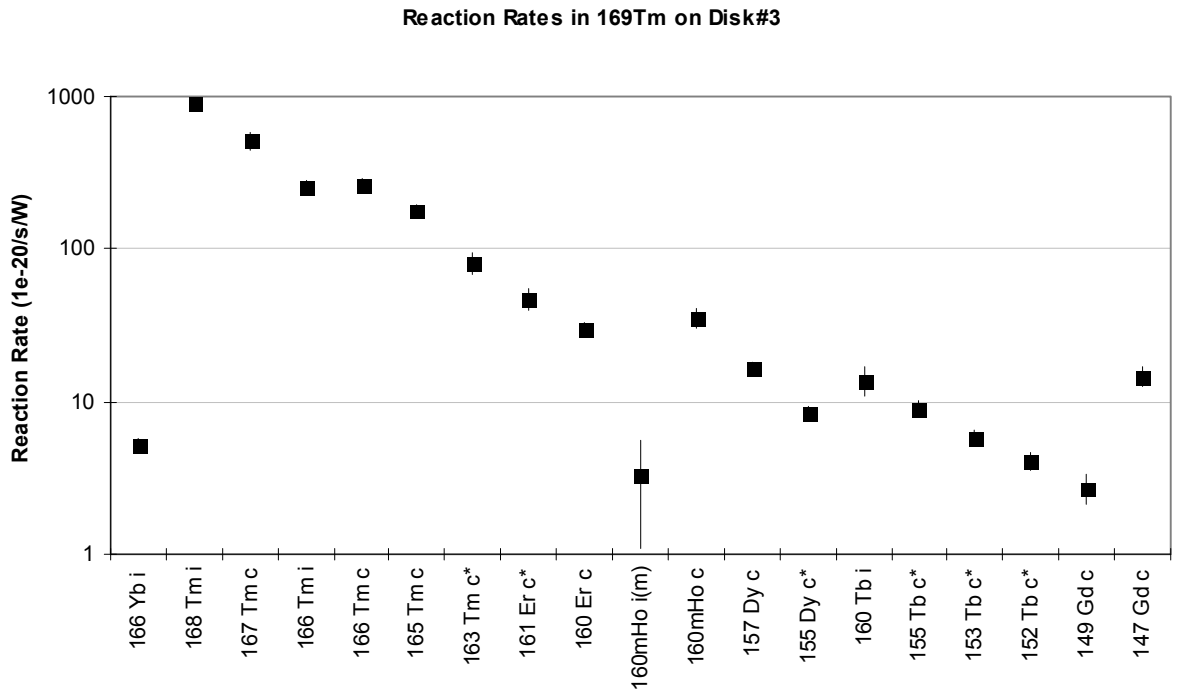

Fig. 26. Experimental production rates in ^{169}Tm sample on the surface of disc 3.

3.8.3.2. Reaction rates in ^{93}Nb

Table 24. presents the nuclear-physics characteristics of nuclides produced in ^{93}Nb by interactions with high-energy neutrons and protons, which are used to calculate the reaction rates. Table 25and Fig. 27 resent the production rates of residuals in ^{93}Nb sample on the surface of disc 3 of Pb target.

Table 24

Nuclear-physics characteristics of nuclides produced in ^{93}Nb sample by interactions with high-energy neutrons and protons [4,21]

Nuclide	Half-life	γ-energy (E_γ, keV) and yield (Y_γ, %)
^{90}Mo	5.56h	*371.3(*),132.7(*)*
^{92m}Nb	10.15d	*1847.5(0.85),934.4(99.07),912.6(1.78)*
^{90}Nb	14.60h	*2319(82),2186.2(17.96),1611.8(2.38), 1129.2(92.7), 890.6(1.8), 371.3(1.8), 141.2(66.8), 132.7(4.13)*
^{89}Zr	78.41h	*1713(0.74),909.2(99.04)*
^{88}Zr	83.4d	*392.9(*)*
^{86}Zr	16.5h	*1920.7(*), 1854.4(*), 1153.1(*), 1076.6(*), 703.3(*), 645.9(*), 627.7(*), 307.0(*), 242.8(95.84)*
^{90m}Y	3.19h	*479.5(90.74),202.5(97.3)*
^{88}Y	106.65d	*1836.1(99.2),898(93.7)*
^{87m}Y	13.37h	*484.8(98.4), 380.8(78.05)*
^{87}Y	79.8h	*484.8(89.7),388.5(82.1)*
^{86}Y	14.74h	*1920.7(20.8),1854.4(17.2),1153.1(30.5),1076.6(82.5),835.7(4.4), 777.4(22.4),703.3(15.4),645.9(9.2),627.7(32.6),580.6(4.78),443.1(16.9), 307(3.47),190.8(1.01)*

^{85m}Y	4.86h	*231.7(22.8)*
^{85m}Sr	67.63m	*231.9(84.4)*
^{85}Sr	64.84d	*514(96)*
^{83}Sr	32.41h	*762.7(30),381.5(14)*
^{82}Sr	25.55d	*776.5(13.4)*
^{83}Rb	86.2d	*552.6(16),529.6(29.3),520.4(45)*
^{82m}Rb	6.472h	*776.5(84.39)*
^{81}Rb	4.576h	*446.1(23.2), 190.5(64.)*
^{82}Br	35.30h	*1317.5(26.5),827.8(24),776.5(83.5),619.1(43.4),554.3(70.8*
^{56}Mn	2.5789h	*846.8(98.9)*
^{54}Mn	312.11d	*834.8(99.98)*
^{52}Mn	5.591d	*1434.1(100),1333.7(5.07),1246.3(4.21),935.5(94.5),744.2(90),511.0(*)*
^{51}Cr	27.7025d	*320.1(9.92)*
^{48}V	15.9735d	*1312.1(97.5),983.5(100)*
^{48}Sc	43.67h	*983.5(100.1)*
^{47}Sc	3.3492d	*159.4(68.3)*
^{46}Sc	83.79d	*1120.6(*),889.3(*)*
^{44m}Sc	58.61h	*1157(98.61),270.9(86.7)*
^{44}Sc	3.97h	*1157(99.9)*

Table 25

Rates of residual production in ^{93}Nb on Pb target surface $\left[10^{-20}, \frac{1}{s \cdot nucleus \cdot W}\right]$

Nuclide	Yield type	T1/2	R(ΔR)
^{90}Mo	c	5.56h	10.2(4.0)
^{92m}Nb	i(m)	10.15d	131(12)
^{90}Nb	i(m1+m2+g)	14.60h	51.0(7.1)
^{90}Nb	c	14.60h	59.6(5.4)
^{89}Zr	c	78.41h	59.0(5.3)
^{88}Zr	c	83.4d	27.0(2.5)
^{86}Zr	c	16.5h	2.80(0.26)
^{90m}Y	i(m)	3.19h	3.85(0.65)
^{88}Y	c	106.65d	20.4(2.5)
^{87m}Y	c*	13.37h	25.8(2.3)
^{87}Y	i	79.8h	1.5(1.5)
^{87}Y	c	79.8h	27.2(2.5)
^{86}Y	i(m+g)	14.74h	12.0(1.3)
^{86}Y	c	14.74h	14.0(1.3)
^{85m}Y	c	4.86h	7.8(1.4)
^{85m}Sr	c	67.63m	4.9(2.5)
^{85}Sr	c	64.84d	16.0(2.2)
^{83}Sr	c	32.41h	4.1(1.5)
^{82}Sr	c	25.55d	44(24)
^{83}Rb	c	86.2d	6.94(0.96)
^{82m}Rb	i(m)	6.472h	2.3(1.3)
^{81}Rb	c	4.576h	3.34(0.41)
^{82}Br	i(m+g)	35.30h	2.5(1.1)
^{56}Mn	c	2.5789h	56.3(5.2)
^{54}Mn	i	312.11d	119(11)

^{52}Mn	c	5.591d	8.10(0.75)
^{51}Cr	c	27.7025d	31.7(3.2)
^{48}V	c	15.9735d	4.41(0.42)
^{48}Sc	i	43.67h	0.12(0.12)
^{47}Sc	c	3.3492d	0.670(0.087)
^{46}Sc	i(m+g)	83.79d	2.24(0.67)
^{44m}Sc	i(m)	58.61h	0.623(0.060)
^{44}Sc	i(m+g)	3.97h	1.62(0.16)
^{44}Sc	i	3.97h	1.01(0.11)

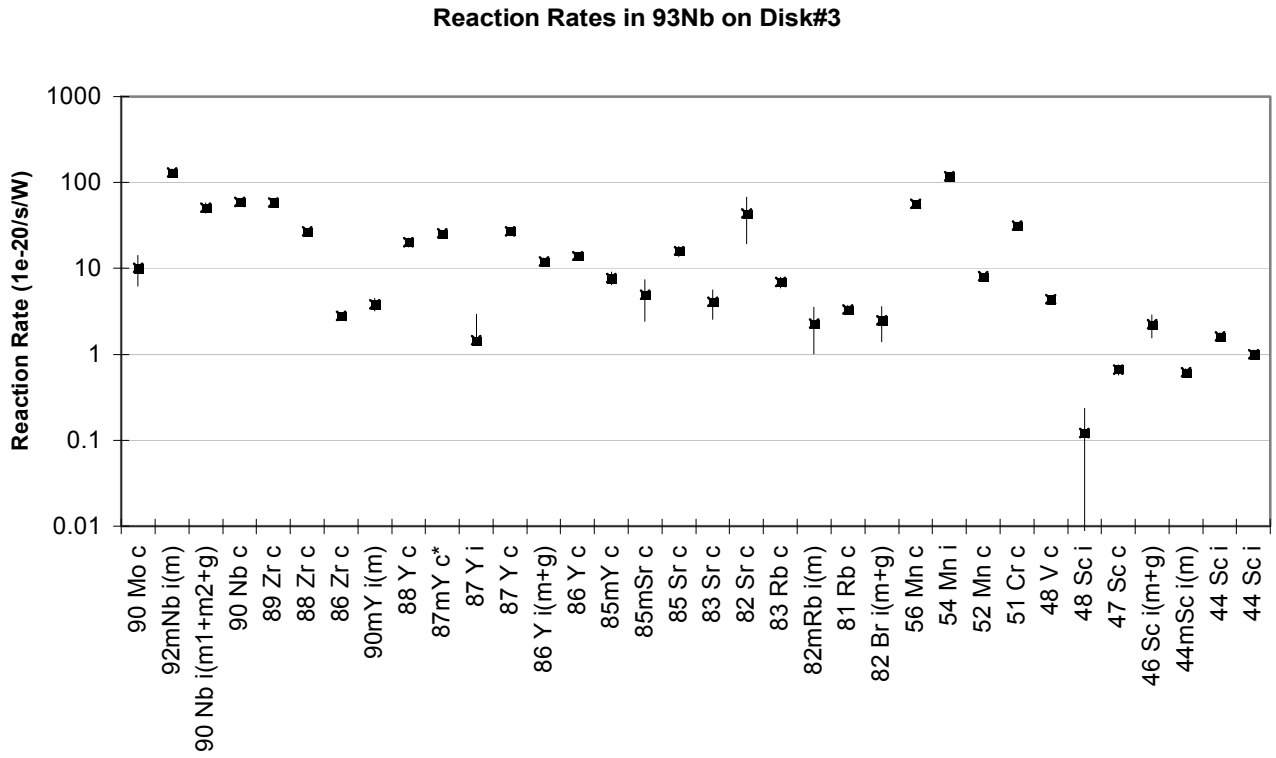

Fig. 27. Experimental production rates in ^{93}Nb sample on the surface of disc 3.

3.8.3.3. Rates of reactions on ^{64}Zn

Table 26 presents the nuclear-physics characteristics of nuclides produced in ^{64}Zn by interactions with high-energy neutrons and protons, which are used to calculate the reaction rates. Table 27 and Fig. 28 present the production rates of residuals in ^{64}Zn sample on the surface of disc 3 of Pb target.

Table 26

Nuclear physics characteristics of nuclides produced in ^{64}Zn sample in interactions with high-energy neutrons and protons [4,21].

Nuclide	Half-life	γ-quantum energy (E_γ, keV) and yield (Y_γ, %)
^{65}Zn	244.26d	*1115.6(50.6)*
^{62}Zn	9.186h	*596.6(26),548.3(15.3),507.6(14.8),394(2.24),246.9(1.9),243.4(2.52)*
^{64}Cu	12.700h	*1345.8(0.47)*
^{61}Cu	3.333h	*1185.2(3.7),908.6(1.1),656(10.8),373(2.1),283(12.2)*

^{57}Ni	35.60h	*1377.6(81.7),127.2(16.7)*
^{58}Co	70.86d	*810.8(99.45)*
^{58m}Co	9.04h	*810.8(*)*
^{57}Co	271.74d	*136.5(10.68),122.1(85.6)*
^{56}Co	77.233d	*2598.5(17.3),1238.3(66.9),846.8(99.94)*
^{55}Co	17.53h	*931.1(75)*
^{54}Mn	312.11d	*834.8(99.98)*
^{52}Mn	5.591d	*1434.1(100),935.5(94.5),744.2(90)*
^{51}Cr	27.7025d	*320.1(9.92)*
^{48}V	15.9735d	*1312.1(97.5),983.5(100)*
^{48}Sc	43.67h	*1312.1(100.1),983.5(100.1)*
^{46}Sc	83.79d	*1120.6(99.99)*

Table 27

Production rates of residuals in ^{64}Zn on Pb target surface $\left[10^{-20}, \frac{1}{s \cdot nucleus \cdot W}\right]$.

Nuclide	Yield type	T1/2	R(ΔR)
^{65}Zn	i	244.26d	211(19)
^{62}Zn	c	9.186h	16.4(1.7)
^{64}Cu	i	12.700h	488(52)
^{61}Cu	c	3.333h	42.5(5.9)
^{57}Ni	c	35.60h	0.79(0.10)
^{58m}Co	i(m)	9.04h	23(12)
^{58}Co	i(m+g)	70.86d	26.3(2.4)
^{58}Co	i	70.86d	3(12)
^{57}Co	c	271.74d	19.0(1.7)
^{56}Co	c	77.233d	4.64(0.50)
^{55}Co	c	17.53h	0.603(0.075)
^{54}Mn	i	312.11d	5.8(1.5)
^{52}Mn	c	5.591d	1.24(0.11)
^{51}Cr	c	27.7025d	2.73(0.78)
^{48}V	c	15.9735d	0.513(0.095)
^{48}Sc	i	43.67h	0.050(0.036)
^{46}Sc	i(m+g)	83.79d	1.44(0.34)

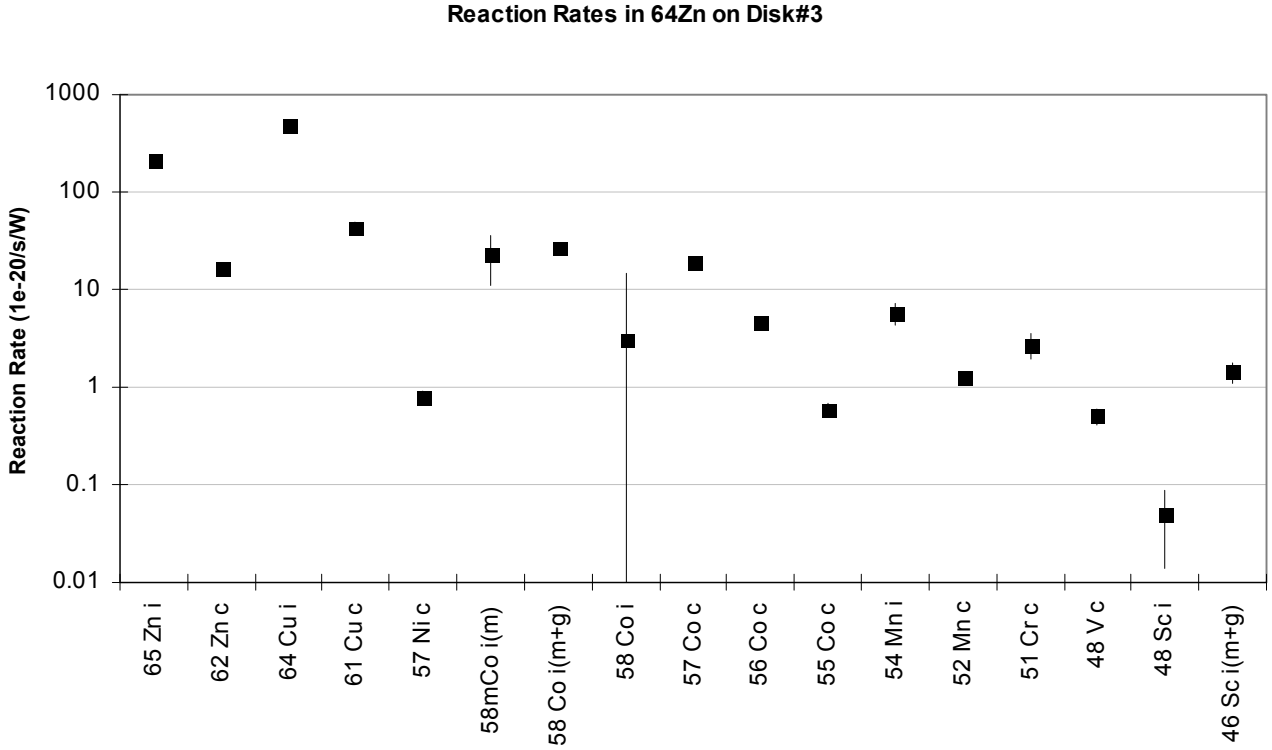

Fig. 28. Experimental production rates of nuclides in ^{64}Zn on the surface of disc 3.

3.8.3.4. Rates of reactions on ^{65}Cu.

Table 28 presents the nuclear-physics characteristics of nuclides produced in ^{65}Cu by interactions with high-energy neutrons and protons, which are used to calculate the reaction rates. Table 29 and Fig. 29 present the production rates of residuals in ^{65}Cu sample on the surface of disc 3 of Pb target.

Table 28

Nuclear physics characteristics of nuclides produced in ^{65}Cu sample in interactions with high-energy neutrons and protons [4,21].

Nuclide	Half-life	γ-quantum energy (E_γ, keV) and yield (Y_γ, %)
^{64}Cu	12.700 h	*511.0 (34.79); 1345.8 (0.47)*
^{61}Cu	3.333 h	*283.0 (12.2); 373.0 (2.1); 529.2 (0.38); 588.6 (1.17); 656.0 (10.80); 908.6 (1.10); 1185.2 (3.70)*
^{65}Ni	2.5172h	*1481.8(23.59), 1115.5(15.43), 366.3(4.81)*
^{57}Ni	35.60 h	*1377.6 (81.70)*
^{60}Co	5.2714 y	*1173.2 (99.97); 1332.5 (99.99)*
^{58}Co	70.86 d	*511.0 (29.80); 810.8 (99.45)*
^{57}Co	271.74 d	*122.1 (85.60); 136.5 (10.68)*
^{56}Co	77.233 d	*846.8 (99.94); 1238.3 (66.90); 1771.3 (15.47)*
^{55}Co	17.53 h	*931.1 (75.00)*
^{59}Fe	44.472 d	*1099.2 (56.50); 1291.6 (43.20)*
^{56}Mn	2.5789 h	*846.8 (98.90)*
^{54}Mn	312.11d	*834.8 (99.98)*
^{52}Mn	5.591 d	*744.2 (90.00); 935.5 (94.50); 1434.1 (100.00);*
^{51}Cr	27.7025 d	*320.1 (9.92)*

^{48}V	15.9735 d	*983.5 (100.0); 1312.1 (97.5)*
^{48}Sc	43.67 h	*983.5 (100.1); 1312.1 (100.1)*
^{47}Sc	3.3492 d	*159.4 (68.3)*
^{46}Sc	83.79 d	*1120.6 (99.99)*
^{44m}Sc	58.61 h	*1157.0 (*) ; 270.9 (86.70)*
^{44}Sc	3.97h	*1157.0(99.9)*
^{47}Ca	4.536 d	*159.4 (*)*

Table 29

Production rates of residuals in ^{65}Cu on Pb target surface $\left[10^{-20}, \frac{1}{s \cdot nucleus \cdot W}\right]$.

Nuclide	Yield type	T1/2	R(ΔR)
^{64}Cu	i	12.700h	409(36)
^{61}Cu	c	3.333h	8.2(1.4)
^{65}Ni	i	2.5172h	18.9(1.9)
^{57}Ni	c	35.60h	0.173(0.036)
^{60}Co	c	5.2714y	25.7(2.6)
^{58}Co	i(m+g)	70.86d	15.5(1.4)
^{57}Co	c	271.74d	7.13(0.66)
^{56}Co	c	77.233d	1.23(0.14)
^{55}Co	c	17.53h	0.107(0.018)
^{59}Fe	c	44.472d	3.64(0.36)
^{56}Mn	c	2.5789h	2.12(0.23)
^{54}Mn	i	312.11d	3.78(0.41)
^{52}Mn	c	5.591d	0.537(0.050)
^{51}Cr	c	27.7025d	1.40(0.21)
^{48}V	c	15.9735d	0.284(0.036)
^{48}Sc	i	43.67h	0.053(0.015)
^{47}Sc	i	3.3492d	0.102(0.013)
^{47}Sc	c	3.3492d	0.129(0.013)
^{46}Sc	i(m+g)	83.79d	0.551(0.092)
^{44m}Sc	i(m)	58.61h	0.039(0.004)
^{44}Sc	i(m+g)	3.97h	24.1(2.2)
^{44}Sc	i	3.97h	24.1(2.2)
^{47}Ca	c	4.536d	0.027(0.007)

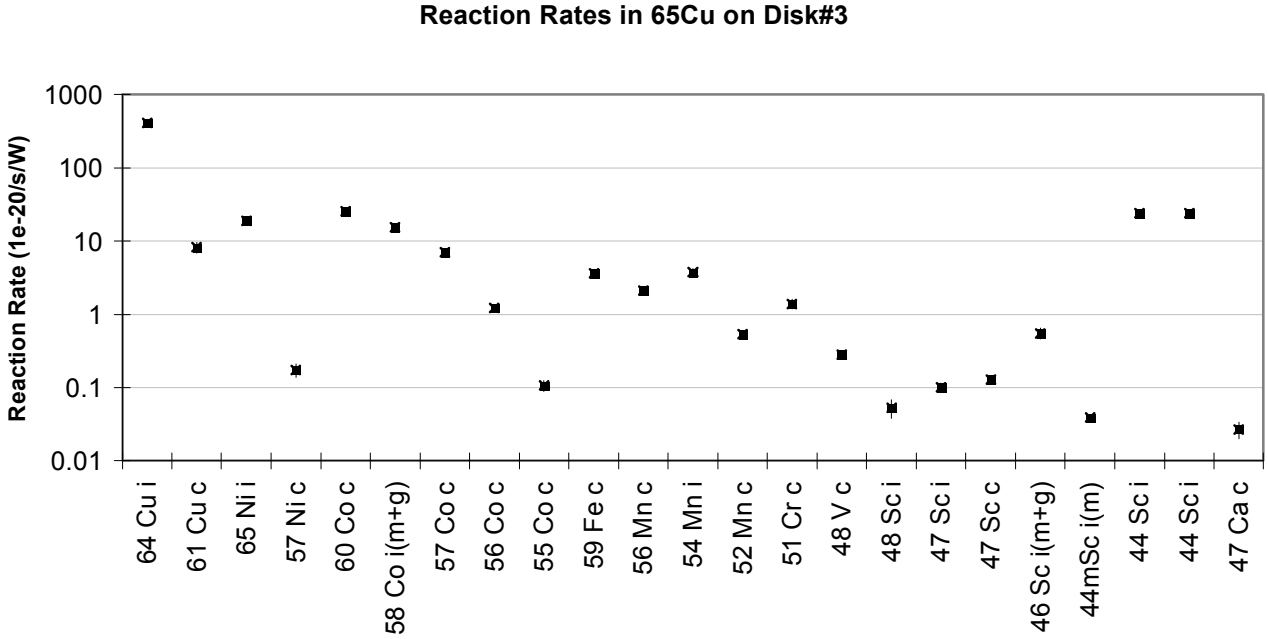

Fig. 29. Experimental nuclide production rates in ^{65}Cu on the surface of disc 3.

3.8.3.5. Rates of reactions on ^{63}Cu

Table 30 presents the nuclear-physics characteristics of nuclides produced in ^{65}Cu by interactions with high-energy neutrons and protons, which are used to calculate the reaction rates. Table 21 and Fig. 30 present the production rates of residuals in ^{63}Cu sample on the surface of disc 3 of Pb target.

Table 30

Nuclear physics characteristics of nuclides produced in ^{63}Cu sample in interactions with high-energy neutrons and protons [4,21].

Nuclide	Half-life	γ-energy (E_γ, keV) and yield (Y_γ, %)
^{62}Zn	9.186 h	*596.6 (26.0)*
^{64}Cu	12.700 h	*511.0 (34.79); 1345.8 (0.47)*
^{61}Cu	3.333 h	*283.0 (12.2); 373.0 (2.1); 529.2 (0.38); 588.6 (1.17); 656.0 (10.80); 908.6 (1.10); 1185.2 (3.70)*
^{57}Ni	35.60 h	*1377.6 (81.70)*
^{56}Ni	6.075 d	*811.8 (86.00)*
^{60}Co	5.2714 y	*1173.2 (99.97); 1332.5 (99.99)*
^{58m}Co	9.04 h	*810.8 (*)*
^{58}Co	70.86 d	*511.0 (29.80); 810.8 (99.45)*
^{57}Co	271.74 d	*122.1 (85.60); 136.5 (10.68)*
^{56}Co	77.233 d	*846.8 (99.94); 1238.3 (66.90); 1771.3 (15.47)*
^{55}Co	17.53 h	*931.1 (75.00)*
^{59}Fe	44.472 d	*1099.2 (56.50); 1291.6 (43.20)*
^{56}Mn	2.5789 h	*846.8 (98.90)*
^{54}Mn	312.11d	*834.8 (99.98)*
^{52}Mn	5.591 d	*744.2 (90.00); 935.5 (94.50); 1434.1 (100.00);*
^{51}Cr	27.7025 d	*320.1 (9.92)*

^{48}V	15.9735 d	*983.5 (100.0); 1312.1 (97.5)*
^{48}Sc	43.67 h	*983.5 (100.1); 1312.1 (100.1)*
^{47}Sc	3.3492 d	*159.4 (68.3)*
^{46}Sc	83.79 d	*1120.6 (99.99)*
^{44m}Sc	58.61 h	*1157.0 (*) ; 270.9 (86.70)*
^{44}Sc	3.97h	*1157.0(99.9)*
^{47}Ca	4.536 d	*159.4 (*)*

Table 31

Production rates of residuals in ^{63}Cu on Pb target surface $\left[10^{-20}, \frac{1}{s \cdot nucleus \cdot W}\right]$.

Nuclide	Yield type	T1/2	R(ΔR)
^{62}Zn	i	9.186h	0.40(0.11)
^{64}Cu	i	12.700h	169(15)
^{61}Cu	c	3.333h	53.2(6.5)
^{57}Ni	c	35.60h	0.413(0.045)
^{56}Ni	c*	6.075d	0.22(0.12)
^{60}Co	c	5.2714y	39.7(4.0)
^{58m}Co	i(m)	9.04h	31.3(8.1)
^{58}Co	i(m+g)	70.86d	39.2(3.5)
^{58}Co	i	70.86d	7.8(7.8)
^{57}Co	c	271.74d	22.8(2.1)
^{56}Co	c	77.233d	4.09(0.38)
^{55}Co	c	17.53h	0.438(0.053)
^{59}Fe	c	44.472d	1.59(0.20)
^{56}Mn	c	2.5789h	1.76(0.21)
^{54}Mn	i	312.11d	7.42(0.78)
^{52}Mn	c	5.591d	1.26(0.12)
^{51}Cr	c	27.7025d	3.32(0.40)
^{48}V	c	15.9735d	0.606(0.063)
^{48}Sc	i	43.67h	0.074(0.020)
^{47}Sc	i	3.3492d	0.117(0.014)
^{47}Sc	c	3.3492d	0.179(0.017)
^{46}Sc	i(m+g)	83.79d	0.84(0.15)
^{44m}Sc	i(m)	58.61h	0.120(0.011)
^{44}Sc	i(m+g)	3.97h	13.2(1.2)
^{44}Sc	i	3.97h	13.1(1.2)
^{47}Ca	c	4.536d	0.062(0.010)

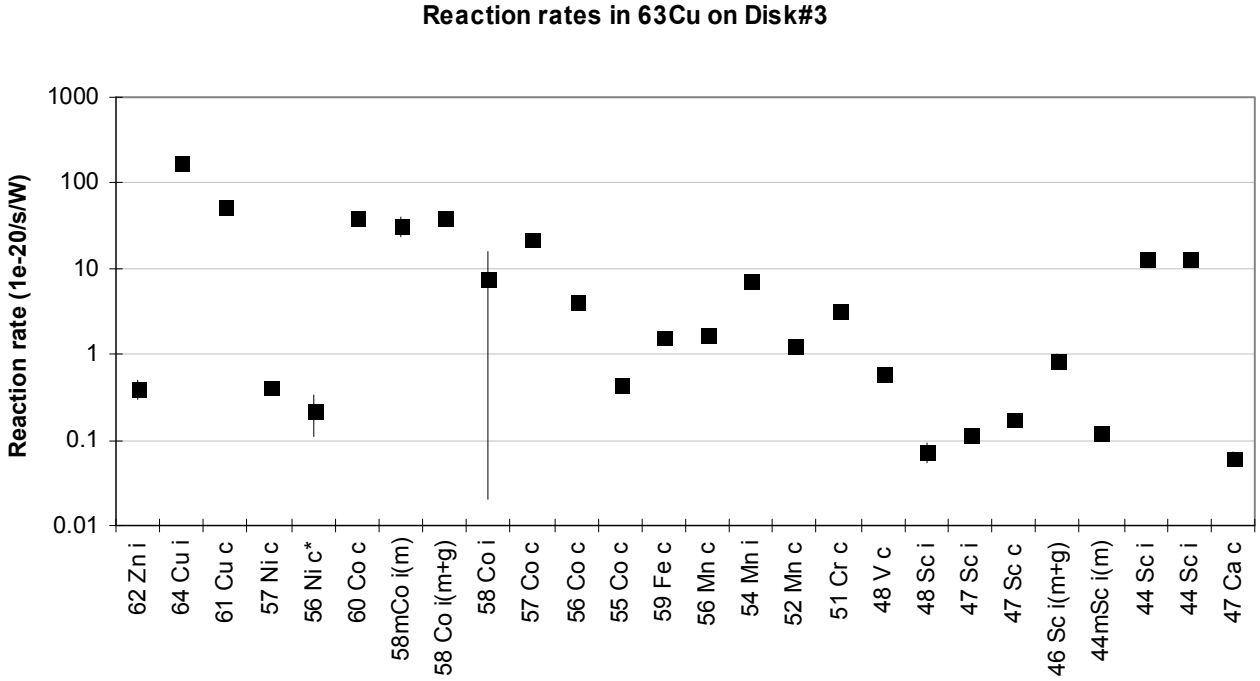

Fig. 30. Experimental nuclide production rates in ^{63}Cu on the surface of disc 3.

3.8.3.6. Rates of reactions on ^{59}Co

Table 32 presents the nuclear-physics characteristics of nuclides produced in ^{59}Co by interactions with high-energy neutrons and protons, which are used to calculate the reaction rates. Table 33 and Fig. 31 present the production rates of residuals in ^{59}Co sample on the surface of disc 3 of Pb target.

Table 32

Nuclear physics characteristics of nuclides produced in ^{59}Co sample in interactions with high-energy neutrons and protons [4,21].

Nuclide	Half-life	γ-energy (E_γ, keV) and yield (Y_γ, %)
^{57}Ni	35.60h	*1377.6(81.7)*
^{60}Co	5.2714y	*1332.5(*),1173.2(*)*
^{58}Co	70.86d	*1674.7(0.52), 864(0.68), 810.8(99.45)*
^{58}mCo	9.04h	*810.8(*)*
^{57}Co	271.74d	*136.5(10.68), 122.1(85.6)*
^{56}Co	77.233d	*2598.5(17.3), 2034.8(7.89), 2015.2(3.04), 1771.3(15.47), 1360.2(4.29), 1238.3(66.9), 1037.8(14.17), 846.8(99.94)*
^{55}Co	17.53h	*1408.5(16.9), 1316.6(7.1), 931.1(75), 477.2(20.2)*
^{59}Fe	44.472d	*1291.6(43.2), 1099.2(56.5), 192.4(3.08), 142.6(1.02)*
^{52}Fe	8.275h	*168.7(99)*
^{56}Mn	2.5789h	*2113.1(14.3), 1810.7(27.2), 846.8(98.9)*
^{54}Mn	312.11d	*834.8(*)*
^{52}Mn	5.591d	*1434.1(100), 1333.7(5.07), 1246.3(4.21), 935.5(94.5), 744.2(90)*

^{51}Cr	27.7025d	*320.1(9.92)*
^{48}Cr	21.56h	*308.2(100)*
^{48}V	15.9735d	*1312.1(97.5), 983.5(100)*
^{48}Sc	43.67h	*1312.1(100.1), 1037.5(97.6), 983.5(100.1)*
^{47}Sc	3.3492d	*159.4(68.3)*
^{46}Sc	83.79d	*1120.6(*),889.3(*)*
^{44}mSc	58.61h	*1157(*), 270.9(86.7)*
^{44}Sc	3.97h	*1157(99.9)*
^{43}Sc	3.891h	*372.8(22.5)*
^{47}Ca	4.536d	*159.4(*)*
^{43}K	22.3h	*372.8(86.8)*

Table 33

Production rates of residuals in ^{59}Co on Pb target surface $\left[10^{-20}, \frac{1}{s \cdot nucleus \cdot W}\right]$.

Nuclide	Type	T1/2	R(ΔR)
^{57}Ni	i	35.60h	0.121(0.017)
^{60}Co	i	5.2714y	106.5(9.7)
^{58m}Co	i(m)	9.04h	228(31)
^{58}Co	i(m+g)	70.86d	355(32)
^{58}Co	i	70.86d	126(25)
^{57}Co	c	271.74d	104.7(9.5)
^{56}Co	c	77.233d	12.6(1.1)
^{55}Co	c	17.53h	0.85(0.11)
^{59}Fe	c	44.472d	42.6(4.3)
^{52}Fe	c	8.275h	0.055(0.015)
^{56}Mn	c	2.5789h	24.2(2.2)
^{54}Mn	i	312.11d	35.6(3.3)
^{52}Mn	c	5.591d	3.89(0.35)
^{51}Cr	c	27.7025d	11.1(1.1)
^{48}Cr	c	21.56h	0.044(0.012)
^{48}V	c	15.9735d	1.99(0.19)
^{48}Sc	i	43.67h	0.110(0.016)
^{47}Sc	i	3.3492d	0.536(0.050)
^{47}Sc	c	3.3492d	0.557(0.051)
^{46}Sc	i(m+g)	83.79d	1.12(0.12)
^{44m}Sc	i(m)	58.61h	0.395(0.038)
^{44}Sc	i(m+g)	3.97h	0.74(0.11)
^{44}Sc	i	3.97h	0.374(0.099)
^{43}Sc	c	3.891h	0.10(0.15)
^{47}Ca	c	4.536d	0.020(0.015)
^{43}K	c	22.3h	0.072(0.019)

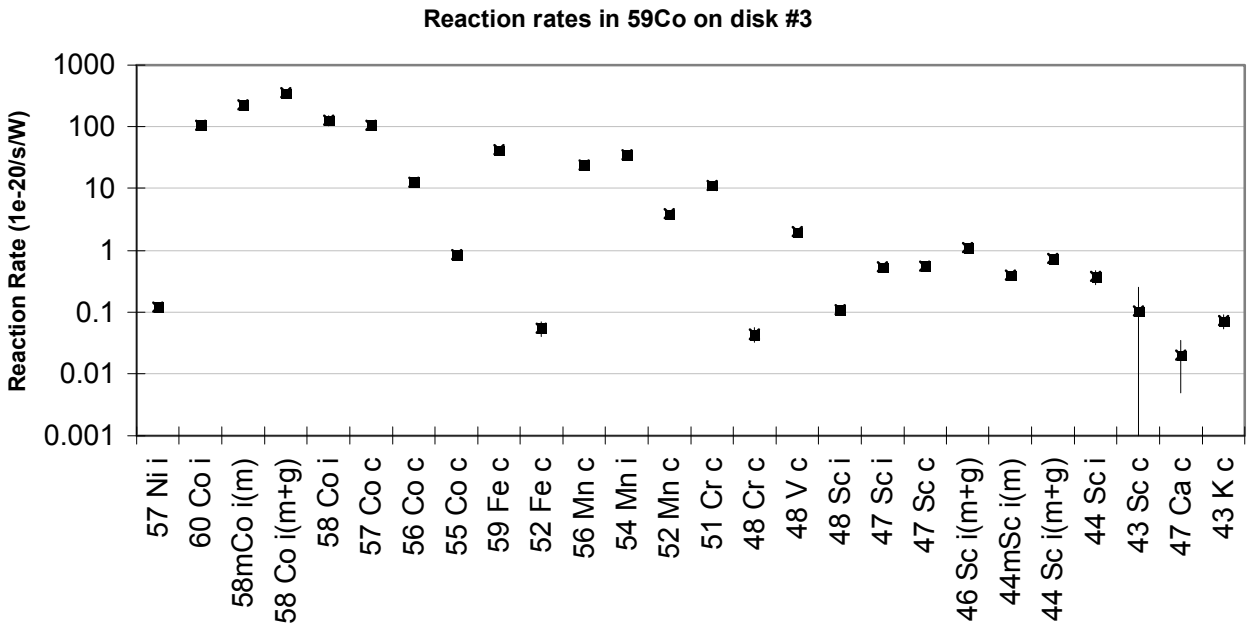

Fig. 31. Experimental nuclide production rates in ^{59}Co on the surface of disc 3.

3.8.3.7. Rates of reactions on ^{19}F

Table 34 presents the nuclear-physics characteristics of nuclides produced in ^{19}F by interactions with high-energy neutrons and protons, which are used to calculate the reaction rates. Table 35 present the production rates of residuals in ^{19}F sample on the surface of disc 3 of Pb target.

Table 34

Nuclear physics characteristics of nuclides produced in ^{19}F sample in interactions with high-energy neutrons and protons [4,21].

Nuclide	Half-life	γ-energy (E_γ, keV) and yield (Y_γ, %)
^{18}F	109.77 m	*511.0 (193.46)*
^{7}Be	53.29 d	*477.6(10.52)*

Table 35

Production rates of residuals in ^{19}F on Pb target surface $\left[10^{-20}, \frac{1}{s \cdot nucleus \cdot W}\right]$.

Nuclide	Type	T1/2	R(ΔR)
^{18}F	c	109.77m	43.7(4.0)
^{7}Be	i	53.29d	19.1(1.8)

3.8.3.8. Rates of reactions on ^{12}C

Table 36 presents the nuclear-physics characteristics of nuclides produced in ^{12}C by interactions with high-energy neutrons and protons, which are used to calculate the reaction rates. Table 37 present the production rates of residuals in ^{12}C sample on the surface of disc 3 of Pb target at 100 mm from the target front butt.

Table 36

Nuclear physics characteristics of nuclides produced in ^{12}C sample in interactions with high-energy neutrons and protons [4,21].

Nuclide	Half-life	γ-energy (E_γ, keV) and yield (Y_γ, %)
^{11}C	20.39 m	*511.0 (199.52)*
^{7}Be	53.29 d	*477.6(10.52)*

Table 37

Production rates of residuals in ^{12}C on Pb target surface $\left[10^{-20}, \frac{1}{s \cdot nucleus \cdot W}\right]$.

Nuclide	Yield type	T1/2	R(ΔR)
^{11}C	i	20.39M	19.6(1.8)
^{7}Be	i	53.29D	5.26(0.53)

3.8.3.9. Rates of reactions on ^{nat}Pb on lines C and S

Tables 38 and 39 present the nuclear-physics characteristics of the nuclides produced in ^{nat}Pb samples on lines S and C in interactions with high-energy neutrons and protons, which are used to calculate the reaction rates.

Tables 40 and 41 and Fig. 32 present the production rates of residuals in ^{nat}Pb samples on lines C and S correspondently.

From Tables 38-41 and from Fig. 32 it is seen that the lists of nuclides measured on lines C and S are somewhat different because the samples from line S began being measured much earlier compared with line C, resulting in loss of short-lived nuclides on line C.

Table 38

Nuclear-physics characteristics of nuclides produced in a ^{nat}Pb sample on line S in interactions with high-energy neutrons and protons [4,21].

Nuclide	T1/2	γ-energy (E_γ, keV) and yield (Y_γ, %)
^{206}Bi	6.243D	1718.7(31.8), 1098.3(13.5), 895.1(15.66), 881(66.2), 803.1(98.9), 620.5(5.76), 537.5(30.5), 516.2(40.7), 497.1(15.31), 398(10.74), 184(15.8).
^{205}Bi	15.31D	1861.7(6.17), 1764.3(32.5), 987.7(16.13), 703.5(31.1).
^{204}Bi	11.22H	984(59), 899.2(98), 374.8(82).
^{203}Bi	11.76H	1679.6(8.8), 820.2(29.6).
^{204m}Pb	67.2M	917.7(90.69), 899.2(99.17), 374.7(89).
^{203}Pb	51.873H	680.5(0.75), 401.3(3.35), 279.2(80.8).
^{202m}Pb	3.53H	960.7(92), 657.5(32.4), 490.5(9.1), 459.7(8.6), 422.1(86), 389.9(6.2).
^{201}Pb	9.33H	1098.5(1.83), 946(7.4), 907.6(5.7), 826.2(2.36), 803.7(1.51), 767.3(3.16), 692.4(4.27), 584.5(3.56), 406(2.01), 361.3(9.9), 331.2(79), 167.4(*).
^{200}Pb	21.5H	1514.9(*), 1362.9(*), 1273.5(*), 1225.5(*), 1205.7(*), 828.3(*), 579.3(*), 450.5(3.33), 367.9(*), 268.4(3.96), 235.6(4.3),

		147.6(37.7), 142.3(3.16).
^{198}Pb	2.4H	1420.6(*), 1312.2(*), 411.8(*), 365.4(19), 173.4(18).
^{202}Tl	12.23D	439.6(91.4).
^{201}Tl	72.912H	167.4(10), 135.3(2.56).
^{200}Tl	26.1H	1514.9(4), 1362.9(3.4), 1273.5(3.31), 1225.5(3.36), 1205.7(29.9), 828.3(10.8), 367.9(87.2).
^{199}Tl	7.42H	455.5(12.4), 247.3(9.3), 208.2(12.3), 158.4(5).
^{198}Tl	5.3H	1420.6(8), 1312.2(4.7), 675.8(10.9), 411.8(82).
^{203}Hg	46.612D	279.2(81.46).
^{197m}Hg	23.8H	134(33.5).
^{195m}Hg	41.6H	779.8(54.2), 560.3(7), 261.8(31).
^{195}Hg	9.9H	779.8(6.8).
^{193m}Hg	11.8H	573.2(26).
^{192}Hg	4.85H	316.5(*), 274.8(50.2)
^{199}Au	3.139D	158.4(40).
^{198}Au	2.69517D	411.8(95.58).
^{196}Au	6.183D	355.7(87).
^{195}Au	186.098D	129.8(0.82), 98.9(10.9).
^{194}Au	38.02H	328.5(61).
^{192}Au	4.94H	316.5(58).
^{191}Pt	2.802D	538.9(13.7), 409.4(8), 359.9(6).
^{188}Pt	10.2D	195.1(18.6), 187.6(19.4), 155.1(*).
^{189}Ir	13.2D	245.1(6).
^{188}Ir	41.5H	155.1(30).
^{185}Os	93.6D	646.1(78).
^{101}Pd	8.47H	296.3(19.2).
^{105}Rh	35.36H	318.9(19.1).
^{103}Ru	39.26D	497.1(91).
^{99}Mo	65.94H	140.5(*).
^{95}Zr	64.02D	756.7(54.46).

Table 39

Nuclear-physics characteristics of nuclides produced in a ^{nat}Pb sample on line C in interactions with high-energy neutrons and protons [4,21].

Nuclide	T1/2	γ-energy (E_γ, keV) and yield (Y_γ, %)
^{207}Bi	31.55Y	1063.7(74.5), 569.7(97.74).
^{206}Bi	6.243D	1718.7(31.8), 1593.3(5.01)1098.3(13.50), 803.1(98.9), 537.5(30.5).
^{205}Bi	15.31D	1861.7(6.17), 1775.8(3.99), 1764.3(32.5), 1208.7(0.51),1190.0(2.26), 703.5(31.1).
^{203}Pb	51.873H	401.3(3.35), 279.2(80.8).
^{200}Pb	21.5H	1205.7(*), 367.9(*), 147.6(37.7).
^{202}Tl	12.23D	439.6(91.4).
^{201}Tl	72.912H	167.4(10.00)
^{200}Tl	26.1H	1205.7(29.9), 367.9(87.2).
^{203}Hg	46.612D	279.2(81.46).
^{195m}Hg	41.6H	560.3(7.0), 261.8(31).
^{194}Hg	444Y	2043.7(3.6), 1468.9(6.4), 364.9(1.51), 328.5(61.00), 293.6(10.4)
^{198m}Au	2.27D	411.8(*).
^{198}Au	2.69517D	411.8(95.98)
^{196}Au	6.183D	426.1(6.6), 355.7(87.0), 333.0(22.9).

^{195}Au	186.09D	129.8(0.82), 98.9(10.9)
^{194}Au	38.02H	328.5(61), 293.6(10.4).
^{191}Pt	2.802D	538.9(13.7), 456.5(3.4), 409.4(8.0) 351.2(3.4), 129.4(3.2).
^{188}Pt	10.2D	1209.8(*), 634.9(*), 478.0(*), 423.3(4.4), 381.4(7.5), 195.1(18.6), 187.6(19.4), 155.1(*).
^{194m}Ir	171D	600.5(62), 482.6(97), 328.5(93).
^{192}Ir	73.827D	316.5(82.71).
^{190}Ir	11.78D	605.1(39.9).
^{189}Ir	13.2D	275.9(0.54), 245.1(6.0).
^{188}Ir	41.5H	1209.8(6.9), 634.9(5.0), 478.0(14.7), 155.1(30).
^{186}Ir	16.64H	773.3(8.9), 434.8(33.9), 137.2(41.4).
^{185}Os	93.6D	874.8(6.29), 717.4(3.94), 646.1(78), 592.1(1.32).
^{183}Os	13.0H	381.8(89.6).
^{182}Os	22.10H	1221.5(58.31), 1189.2(35.27), 1121.4(74.76), 263.3(6.71), 180.2(33.5).
^{183}Re	70.0D	354.0(0.54), 291.7(3.05), 162.3(23.3).
^{182}Re	64.0H	1221.4(17.4), 1189.0(9.0), 1121.3(22.0).
^{181}Re	19.9H	953.6(3.6), 639.0(6.4), 365.5(56).
^{178}W	21.6D	1350.6(1.18), 1340.8(1.03), 1106.1(0.54).
^{177}Ta	56.56H	112.9(7.2).
^{175}Hf	70D	343.4(84).
^{173}Hf	23.6H	123.7(83).
^{172}Hf	1.87Y	2083.4(0.22), 1914.8(0.61), 1724.3(0.44), 1670.5(0.53), 1666.8(0.28), 1621.9(2.18), 1584.1(2.67), 1542.8(1.03), 1488.9(1.16), 1470.4(0.72), 1466.0(0.68), 1440.4(0.61), 1402.5(0.73), 1397.5(0.18), 1387.2(0.88), 1322.7(0.10), 1115.5(0.37), 1093.6(*), 1041.0(0.35), 1022.4(1.42), 1002.7(5.3), 929.1(3.7), 900.7(*), 816.3(1.16), 810.1(*), 709.1(0.83), 703.1(.14), 697.3(6.2), 681.8(0.7), 626.0(0.31), 594.5(0.42), 540.2(1.41), 528.3(4.08), 490.4(1.93), 486.2(0.67), 482.2(0.59), 432.5(1.66), 410.3(1.97), 377.5(3.38), 372.5(2.69), 323.9(1.51), 279.7(1.2), 270.0(1.95), 203.4(5.07), 181.5(20.8), 154.7(0.15), 125.8(11.3), 114.1(2.6), 112.8(1.28).
^{173}Lu	1.37Y	636.1(1.45), 285.4(0.61), 272.1(21.2), 100.7(5.24).
^{172}Lu	6.70D	1093.6(63.), 900.7(29.8), 810.1(16.6).
^{171}Lu	8.24D	853.0(2.55), 839.9(3.04), 739.8(47.8), 689.3(2.37), 667.4(11.0).
^{170}Lu	2.012D	2126.1(5.1), 1512.5(2.55), 1341.2(3.26), 1280.2(8.2), 1054.3(4.76).
^{169}Lu	34.06H	960.6(23.4).
^{169}Yb	32.026D	307.7(10.05), 261.1(1.71), 198.0(35.8), 177.2(22.2).
^{166}Yb	56.7H	2052.4(*), 1176.7(11.0).
^{167}Tm	9.25D	207.8(42).
^{165}Tm	30.06H	242.9(35.5)
^{160}Er	28.58H	728.2(34).
^{155}Tb	5.32D	105.3(25.1).
^{153}Gd	240.4D	103.2(21.1), 97.4(29.0).
^{149}Gd	9.28D	346.6(23.9), 298.6(28.6), 149.7(48).
^{146}Gd	48.27D	747.2(8).
^{154}Eu	8.593Y	723.3(20.11), 123.1(40.6).
^{147}Eu	24.1D	677.5(9.8).
^{146}Eu	4.61D	747.2(99).
^{143}Pm	265D	742.0(38.5).

^{139}Ce	137.640D	165.9(79.89)
^{133}Ba	3848.9D	383.9(8.94), 356.0(62.05), 302.9(18.33), 276.4(7.16).
^{127}Xe	36.4D	375.0(17.2), 202.9(68.3), 172.1(25.5).
^{123m}Te	119.7D	159.0(84.0).
^{121m}Te	154D	573.1(88.6), 212.2(81.4).
^{121}Te	19.16D	573.1(80.3).
^{124}Sb	60.20D	1691.0(47.79), 602.7(98.3).
^{120m}Sb	5.76D	1171.7(*), 1023.3(99.4).
^{117m}Sn	13.60D	158.6(86.4).
^{113}Sn	115.09D	391.7(64.97).
^{114m}In	49.51D	190.3(15.56).
^{110m}Ag	249.76D	1505.0 (13.60), 1475.8(4.17), 1384.3(24.9), 937.5(34.2), 884.7(72.7), 677.6(10.56), 657.8(94.3), 446.8(3.62),
^{106m}Ag	8.28D	1045.8(29.6), 451.0(28.2).
^{105}Ag	41.29D	1087.9(3.85), 443.4(10.5).
^{105}Rh	35.36H	318.9(19.1)
^{102m}Rh	2.9Y	1112.8(19), 1103.2(4.6), 1046.6(34), 766.8(34.0), 607.5(44.0), 631.3(56), 628.0(4.5), 475.1(95.00), 420.4(3.2), 418.5(9.4).
^{102}Rh	207D	628.0(4.5), 475.1(46).
^{101m}Rh	4.34D	306.9(81).
^{101}Rh	3.3Y	198.0(73.00), 127.2(68.00).
^{106}Ru	373.59D	621.9(9.93)
^{103}Ru	39.26D	610.3(5.76), 497.1(91.0).
^{96}Tc	4.28D	849.9(98), 812.5(82).
^{95}Tc	20.0H	765.8(93.8).
^{99}Mo	65.94H	140.5(90.27).
^{95}Nb	34.975D	765.8 (99.81).
^{92m}Nb	10.15D	934.4(99.07).
^{95}Zr	64.02D	765.8(*), 756.7(54.46), 724.2(44.17).
^{89}Zr	78.41H	909.2(99.04),
^{88}Zr	83.4D	1836.1(*), 898.0(*), 392.9(*).
^{88}Y	106.65D	1836.1(99.2), 898.0(93.7).
^{87}Y	79.8H	484.8(89.7), 388.5(82.1).
^{85}Sr	64.84D	514.0(96).
^{86}Rb	18.631D	1077.0(8.64).
^{84}Rb	32.77D	1897.8(0.74), 881.6(69.0).
^{83}Rb	86.2D	552.6(16.0), 529.6(29.3), 520.4(45).
^{82}Br	35.30H	1317.5(26.5), 776.5(83.5), 619.1(43.4), 554.3(70.8).
^{75}Se	119.779D	400.7(11.47), 303.9(1.32), 264.7(58.9), 136.0(58.3).
^{74}As	17.77D	634.8(15.4), 595.8(59).
^{65}Zn	244.26D	1115.6 (50.60).
^{60}Co	5.2714Y	1332.5(*), 1173.2(*).
^{58}Co	70.86D	810.8(99.45).
^{59}Fe	44.472D	1291.6(43.2), 1099.2(56.5).
^{54}Mn	312.11D	834.8(*).
^{46}Sc	83.79D	1120.(99.99), 889.3(99.98).
^{22}Na	2.6019Y	1274.5(99.94).
^{7}Be	53.29D	477.6(10.52).

Table 40

Production rates of residuals in natPb inside Pb target $\left[10^{-20}, \frac{1}{s \cdot nucleus \cdot W}\right]$.

Nuclide	Yield type	$T_{1/2}$	Distance from target front (cm)											
			0	8	16	24	32	40	48	56	64	72	80	88
^{207}Bi	i	31.55y	1130(110)	1150(110)	406(39)	141(14)	43.1(7.0)	56.1(6.1)	-	-	-	-	-	-
^{206}Bi	i	6.243d	1930(190)	2000(180)	714(66)	234(23)	81.9(7.5)	110(10)	0.335(0.049)	0.150(0.034)	-	-	-	-
^{205}Bi	i	15.31d	2630(240)	2650(240)	1015(92)	336(31)	128(12)	200(18)	-	-	-	-	-	-
^{203}Pb	c*	51.873h	16900(1600)	17200(1600)	6850(630)	2360(220)	854(79)	608(55)	29.2(2.7)	11.6(1.1)	5.13(0.48)	2.46(0.23)	1.30(0.27)	0.666(0.069)
^{200}Pb	c	21.5h	8060(720)	8090(730)	3200(290)	1066(96)	392(36)	185(17)	7.81(0.71)	4.00(0.61)	1.63(0.34)	0.80(0.26)	-	-
^{202}Tl	c	12.23d	7380(690)	6090(550)	2080(190)	633(58)	207(19)	37.8(3.5)	6.28(0.58)	2.59(0.24)	1.03(0.10)	0.588(0.064)	0.276(0.043)	0.167(0.021)
^{201}Tl	c*	72.912h	20300(2000)	18800(1800)	7210(720)	2560(240)	960(91)	465(45)	24.2(2.9)	9.4(1.0)	4.32(0.56)	2.35(0.38)	1.88(0.57)	0.57(0.26)
^{200}Tl	i	26.1h	10120(950)	7210(670)	2830(270)	1091(98)	453(41)	47.1(7.2)	8.03(0.98)	-	-	-	-	-
^{200}Tl	c	26.1h	18200(1600)	15300(1400)	6030(540)	2150(190)	843(76)	234(22)	15.9(1.6)	10.3(1.8)	4.70(0.77)	2.46(0.33)	1.17(0.13)	0.635(0.084)
^{203}Hg	c	46.612d	1130(100)	833(76)	275(25)	76.7(7.0)	20.2(1.9)	3.29(0.32)	0.803(0.086)	0.327(0.038)	0.154(0.025)	0.150(0.049)	-	-
^{195m}Hg	i(m)	41.6h	4320(730)	2660(460)	1210(160)	313(50)	78(10)	-	-	-	-	-	-	-
^{194}Hg	c	444y	14800(1600)	11000(1000)	4090(450)	1290(200)	480(140)	-	-	-	-	-	-	-
^{198m}Au	i(m)	2.27d	185(17)	169(15)	41.7(7.5)	9.5(1.1)	2.09(0.50)	0.127(0.011)	0.017(0.001)	-	-	-	-	-
^{198}Au	i(m+g)	2.69517d	682(61)	429(39)	141(14)	37.9(3.5)	8.51(0.88)	0.817(0.074)	0.235(0.021)	-	-	-	-	-
^{198}Au	i	2.69517d	497(45)	260(23)	99(15)	28.4(2.8)	6.4(1.0)	0.690(0.062)	0.219(0.020)	-	-	-	-	-
^{196}Au	i(m1+m2+g)	6.183d	1220(110)	825(83)	271(26)	67.9(6.4)	14.2(1.3)	0.86(0.15)	0.292(0.039)	-	-	-	-	-
^{195}Au	c	186.098d	18100(2400)	14300(2100)	5330(710)	1690(210)	566(68)	21.1(3.3)	7.80(1.30)	3.54(0.71)	-	-	-	-
^{194}Au	i(m1+m2+g)	38.02h	2130(240)	1460(140)	506(51)	117(13)	24.8(3.4)	-	-	-	-	-	-	-
^{191}Pt	c	2.802d	15400(1600)	10400(1100)	3820(400)	1120(120)	237(28)	91(15)	-	-	-	-	-	-
^{188}Pt	c	10.2d	15300(1400)	10070(930)	3370(300)	825(75)	129(12)	3.36(0.57)	1.38(0.18)	0.74(0.27)	-	-	-	-
^{194m}Ir	i(m)	171d	8.8(1.2)	5.05(0.54)	1.36(0.21)	-	-	-	-	-	-	-	-	-
^{192}Ir	i(m1+g)	73.827d	40.9(3.7)	25.3(2.3)	7.08(0.66)	1.06(0.13)	-	-	-	-	-	-	-	-
^{190}Ir	i(m1+g)	11.78d	144(18)	94(11)	28.6(5.9)	-	-	-	-	-	-	-	-	-
^{189}Ir	c	13.2d	17300(2400)	11500(1500)	3510(490)	840(180)	157(22)	-	-	-	-	-	-	-

Nuclide	Yield type	$T_{1/2}$	Distance from target front (cm)											
			0	8	16	24	32	40	48	56	64	72	80	88
^{188}Ir	i	41.5h	880(210)	810(140)	239(59)	79(25)	8.5(5.2)	2.2(1.0)	1.24(0.17)	-	-	-	-	-
^{188}Ir	c	41.5h	17100(1700)	11400(1200)	3770(370)	926(90)	155(15)	5.4(1.2)	2.65(0.37)	-	-	-	-	-
^{186}Ir	c*	16.64h	6130(730)	4340(430)	1200(120)	266(28)	26.2(4.3)	-	-	-	-	-	-	-
^{185}Os	c	93.6d	14300(1300)	9210(840)	2750(250)	556(51)	50.8(4.7)	2.08(0.21)	0.744(0.090)	0.362(0.055)	0.146(0.029)	-	-	-
^{183}Os	c	13.0h	11400(1200)	7030(740)	1980(230)	399(46)	35.3(6.7)	-	-	-	-	-	-	-
^{182}Os	c	22.10h	13000(1200)	7900(720)	2100(190)	341(33)	-	-	-	-	-	-	-	-
^{183}Re	c	70.0d	13800(1300)	8690(810)	2330(210)	400(40)	27.0(2.8)	1.34(0.28)	-	-	-	-	-	-
^{182}Re	c*	64.0h	560(160)	383(67)	57(29)	22.2(4.7)	-	-	-	-	-	-	-	-
^{181}Re	c	19.9h	11300(1600)	5870(860)	1480(230)	231(37)	-	-	-	-	-	-	-	-
^{178}W	c	21.6d	7560(810)	4050(430)	930(100)	-	-	-	-	-	-	-	-	-
^{177}Ta	c	56.56h	11700(3000)	5300(1600)	1180(370)	78(62)	-	-	-	-	-	-	-	-
^{175}Hf	c	70d	8390(810)	3960(380)	742(72)	62.9(6.1)	1.19(0.13)	0.323(0.060)	0.140(0.028)	-	-	-	-	-
^{173}Hf	c*	23.6h	8900(1200)	3650(520)	606(91)	39.4(9.1)	-	-	-	-	-	-	-	-
^{172}Hf	c	1.87y	6290(560)	2510(220)	369(33)	24.4(8.9)	-	-	-	-	-	-	-	-
^{173}Lu	c	1.37y	6870(770)	2910(270)	478(46)	33.4(3.6)	-	-	-	-	-	-	-	-
^{172}Lu	i(m+g)	6.70d	92(36)	247(49)	12(12)	6.2(7.8)	-	-	-	-	-	-	-	-
^{172}Lu	c	6.70d	5730(540)	2570(240)	403(40)	28.6(8.1)	-	-	-	-	-	-	-	-
^{171}Lu	c	8.24d	6170(570)	2500(230)	379(46)	21.8(3.2)	-	-	-	-	-	-	-	-
^{170}Lu	c*	2.012d	6110(660)	2360(250)	236(55)	-	-	-	-	-	-	-	-	-
^{169}Lu	c	34.06h	3610(400)	1530(170)	267(47)	-	-	-	-	-	-	-	-	-
^{169}Yb	c	32.026d	4750(430)	1700(150)	213(20)	8.36(0.94)	-	-	-	-	-	-	-	-
^{166}Yb	c	56.70h	2780(280)	799(98)	-	-	-	-	-	-	-	-	-	-
^{167}Tm	c	9.25d	2910(730)	1390(300)	118(29)	19.4(4.9)	-	-	-	-	-	-	-	-
^{165}Tm	c	30.06h	2710(350)	890(110)	120(21)	-	-	-	-	-	-	-	-	-
^{160}Er	c	28.58h	1180(230)	-	-	-	-	-	-	-	-	-	-	-
^{155}Tb	c	5.32d	571(87)	-	-	-	-	-	-	-	-	-	-	-
^{153}Gd	c	240.4d	251(28)	-	-	-	-	-	-	-	-	-	-	-
^{149}Gd	c	9.28d	205(22)	-	-	-	-	-	-	-	-	-	-	-

Nuclide	Yield type	$T_{1/2}$	Distance from target front (cm)											
			0	8	16	24	32	40	48	56	64	72	80	88
^{146}Gd	c	48.27d	111(11)	23.3(2.3)	2.39(0.23)	-	-	-	-	-	-	-	-	-
^{154}Eu	i(m+g)	8.593y	-	196(23)	-	-	-	-	-	-	-	-	-	-
^{147}Eu	c	24.1d	221(29)	78(21)	-	-	-	-	-	-	-	-	-	-
^{146}Eu	i	4.61d	1050(570)	450(250)	110(19)	-	-	-	-	-	-	-	-	-
^{146}Eu	c	4.61d	1160(570)	470(250)	112(19)	-	-	-	-	-	-	-	-	-
^{143}Pm	c	265d	89(11)	31.6(3.6)	9.5(2.1)	-	-	-	-	-	-	-	-	-
^{139}Ce	c	137.640d	122(11)	53.7(5.1)	13.2(1.3)	2.48(0.27)	0.657(0.080)	-	-	-	-	-	-	-
^{133}Ba	c	3848.9d	119(18)	73.2(7.4)	24.1(8.8)	-	-	-	-	-	-	-	-	-
^{127}Xe	c	36.4d	233(23)	131(13)	39.0(4.1)	6.4(1.7)	1.56(0.40)	-	-	-	-	-	-	-
^{123m}Te	i(m)	119.7d	112(10)	75.5(7.2)	26.9(2.6)	7.42(0.71)	2.13(0.21)	-	-	-	-	-	-	-
^{121m}Te	i(m)	154d	155(14)	98.5(9.1)	31.8(3.0)	7.95(0.74)	1.70(0.17)	-	-	-	-	-	-	-
^{121}Te	c	19.16d	312(30)	180(17)	53.2(5.1)	11.8(1.3)	2.35(0.38)	-	-	-	-	-	-	-
^{121}Te	i(m+g)	19.16d	179(17)	94.7(9.9)	25.8(2.7)	4.86(0.82)	0.82(0.40)	-	-	-	-	-	-	-
^{124}Sb	i(m1+m2+g)	60.20d	24.5(2.7)	19.2(2.6)	6.83(0.69)	2.52(0.29)	0.81(0.12)	0.160(0.053)	-	-	-	-	-	-
^{120m}Sb	i(m)	5.76d	168(27)	111(11)	39.2(5.0)	10.1(1.2)	2.18(0.28)	-	-	-	-	-	-	-
^{117m}Sn	i(m)	13.60d	272(26)	179(18)	59.5(5.7)	17.3(1.7)	3.93(0.41)	-	-	-	-	-	-	-
^{113}Sn	c	115.09d	192(17)	101.5(9.3)	25.8(2.4)	12.3(1.3)	1.19(0.17)	-	-	-	-	-	-	-
^{114m}In	i(m)	49.51d	375(35)	297(28)	85.3(9.0)	19.5(2.0)	4.24(0.48)	-	-	-	-	-	-	-
^{110m}Ag	i(m)	249.76d	418(38)	285(26)	95.6(8.6)	25.7(2.4)	6.47(0.63)	0.171(0.059)	-	-	-	-	-	-
^{106m}Ag	i(m)	8.28d	250(26)	140(20)	39.9(5.3)	6.1(2.1)	-	-	-	-	-	-	-	-
^{105}Ag	c	41.29d	221(23)	111(12)	28.3(3.5)	-	-	-	-	-	-	-	-	-
^{105}Rh	c	35.36h	1370(180)	1220(130)	387(43)	98(16)	32.8(6.7)	-	-	-	-	-	-	-
^{102m}Rh	i(m)	2.9y	473(82)	260(31)	73.4(8.3)	15.3(2.0)	1.58(0.46)	-	-	-	-	-	-	-
^{102}Rh	i	207d	44.3(4.9)	22.2(2.7)	6.25(0.98)	2.8(2.3)	0.46(0.30)	-	-	-	-	-	-	-
^{101m}Rh	c	4.34d	388(53)	196(25)	57.5(7.8)	9.2(1.5)	-	-	-	-	-	-	-	-
^{101}Rh	c	3.3y	137(13)	81.2(7.7)	19.7(2.0)	3.77(0.63)	-	-	-	-	-	-	-	-
^{106}Ru	c	373.59d	354(34)	218(22)	73.7(8.4)	31.4(4.4)	5.5(1.9)	-	-	-	-	-	-	-
^{103}Ru	c	39.26d	1330(120)	965(87)	343(31)	99.0(9.3)	28.3(2.6)	2.98(0.28)	0.174(0.048)	-	-	-	-	-

Nuclide	Yield type	$T_{1/2}$	Distance from target front (cm)											
			0	8	16	24	32	40	48	56	64	72	80	88
^{96}Tc	i(m+g)	4.28d	413(42)	210(21)	56.4(6.6)	9.5(1.8)	-	-	-	-	-	-	-	-
^{95}Tc	i(m+g)	20.0h	596(86)	58(38)	-	-	-	-	-	-	-	-	-	-
^{99}Mo	c	65.94h	1380(150)	870(110)	359(44)	93(10)	25.7(3.0)	3.57(0.53)	-	-	-	-	-	-
^{95}Nb	i(m+g)	34.975d	1120(100)	739(66)	-	62.7(5.7)	14.3(1.4)	-	-	-	-	-	-	-
^{95}Nb	c	34.975d	1920(170)	1320(120)	-	125(11)	33.0(3.0)	-	-	-	-	-	-	-
^{92m}Nb	i(m)	10.15d	125(14)	84.7(8.2)	23.0(2.5)	5.74(0.62)	0.95(0.19)	-	-	-	-	-	-	-
^{95}Zr	c	64.02d	808(72)	587(52)	205(19)	62.4(5.6)	18.8(1.7)	2.40(0.24)	-	-	-	-	-	-
^{89}Zr	c	78.41h	663(64)	340(33)	85(10)	20.2(2.0)	-	-	-	-	-	-	-	-
^{88}Zr	c	83.4d	255(23)	130(12)	30.0(2.7)	5.57(0.50)	0.76(0.21)	-	-	-	-	-	-	-
^{88}Y	i	106.65d	1080(98)	625(59)	181(17)	36.1(3.7)	5.66(0.54)	-	-	-	-	-	-	-
^{88}Y	c	106.65d	1310(120)	754(69)	207(19)	41.6(3.9)	6.44(0.58)	-	-	-	-	-	-	-
^{87}Y	c*	79.8h	870(110)	492(60)	121(17)	22.4(4.1)	2.41(0.95)	-	-	-	-	-	-	-
^{85}Sr	c	64.84d	857(85)	472(47)	124(12)	24.3(2.5)	3.29(0.33)	-	-	-	-	-	-	-
^{86}Rb	i(m+g)	18.631d	1440(130)	891(82)	267(25)	77.1(8.3)	13.4(2.1)	-	-	-	-	-	-	-
^{84}Rb	i(m+g)	32.77d	1160(110)	681(63)	199(19)	47.6(4.8)	-	-	-	-	-	-	-	-
^{83}Rb	c	86.2d	1010(100)	556(55)	145(14)	28.1(2.8)	3.57(0.42)	-	-	-	-	-	-	-
^{82}Br	i(m+g)	35.30h	762(96)	435(56)	167(17)	38.9(4.6)	9.9(1.5)	-	-	-	-	-	-	-
^{75}Se	c	119.779d	387(35)	198(18)	45.6(4.3)	7.07(0.69)	0.86(0.14)	-	-	-	-	-	-	-
^{74}As	i	17.77d	610(130)	320(39)	76(16)	16.0(1.8)	1.93(0.28)	-	-	-	-	-	-	-
^{65}Zn	c	244.26d	116(11)	56.4(5.2)	10.5(1.3)	-	-	-	-	-	-	-	-	-
^{60}Co	i(m+g)	5.2714y	227(21)	111(10)	27.8(2.7)	6.01(0.81)	-	-	-	-	-	-	-	-
^{58}Co	i(m+g)	70.86d	93(12)	32.2(3.5)	5.87(0.83)	-	-	-	-	-	-	-	-	-
^{59}Fe	c	44.472d	259(24)	148(14)	39.4(3.8)	7.27(0.74)	1.12(0.30)	-	-	-	-	-	-	-
^{54}Mn	i	312.11d	87.1(7.9)	41.8(3.8)	8.85(0.86)	1.21(0.21)	-	-	-	-	-	-	-	-
^{46}Sc	i(m+g)	83.79d	67.2(6.5)	29.5(3.0)	6.4(1.0)	1.69(0.82)	-	-	-	-	-	-	-	-
^{22}Na	c	2.6019y	22.1(2.7)	11.7(1.2)	3.89(0.84)	-	-	-	-	-	-	-	-	-
^{7}Be	i	53.29d	338(33)	136(17)	39.9(4.3)	9.6(1.6)	1.96(0.56)	-	-	-	-	-	-	-

Table 41

Production rates of residuals in ^{nat}Pb on the surface of Pb target $\left[10^{-20}, \frac{1}{s \cdot nucleus \cdot W}\right]$.

Nuclide	Yield type	$T_{1/2}$	Distance from target front (cm)											
			2	10	18	26	34	42	50	58	66	74	82	90
^{206}Bi	i	6.243d	0.506(0.055)	2.42(0.23)	2.87(0.26)	2.56(0.24)	1.99(0.20)	0.424(0.053)	0.139(0.027)	-	-	-	-	-
^{205}Bi	i	15.31d	0.73(0.15)	3.85(0.40)	4.88(0.46)	4.11(0.39)	3.28(0.31)	0.64(0.15)	-	-	-	-	-	-
^{204}Bi	i	11.22h	0.736(0.092)	3.44(0.36)	4.42(0.48)	3.67(0.43)	3.24(0.33)	0.469(0.056)	0.129(0.025)	0.064(0.015)	-	-	-	-
^{203}Bi	i(m+g)	11.76h	-	2.66(0.38)	3.32(0.44)	3.38(0.49)	2.93(0.41)	0.65(0.17)	-	-	-	-	-	-
^{204m}Pb	c	67.2m	82.6(7.8)	143(13)	117(11)	84.4(8.0)	52.2(5.1)	22.1(2.1)	8.72(0.83)	3.58(0.36)	1.81(0.20)	0.645(0.081)	0.379(0.063)	0.17(0.10)
^{203}Pb	c*	51.873h	105.6(9.8)	196(18)	176(16)	126(11)	77.9(7.2)	35.0(3.3)	14.3(1.3)	6.07(0.56)	2.73(0.35)	1.36(0.14)	0.678(0.065)	0.372(0.037)
^{202m}Pb	i(m)	3.53h	28.5(2.7)	55.5(5.3)	52.9(5.0)	36.7(3.7)	24.3(2.3)	10.7(1.0)	4.25(0.41)	1.81(0.18)	0.841(0.088)	0.385(0.055)	0.205(0.023)	0.111(0.014)
^{201}Pb	c*	9.33h	34.1(3.4)	81.4(8.5)	77.9(7.6)	60.3(5.6)	40.3(3.8)	16.3(1.6)	6.93(0.67)	2.90(0.32)	1.54(0.15)	0.781(0.091)	0.389(0.045)	0.193(0.024)
^{200}Pb	c	21.5h	19.5(1.8)	51.2(4.7)	50.9(4.7)	37.0(3.5)	24.9(2.3)	11.1(1.0)	4.64(0.44)	2.21(0.22)	1.05(0.10)	0.339(0.080)	0.266(0.028)	0.157(0.017)
^{198}Pb	c	2.4h	0.91(0.33)	35(16)	18.4(6.8)	24.4(8.0)	19.3(6.9)	3.6(2.5)	3.28(0.82)	1.36(0.32)	0.251(0.055)	0.02(0.12)	0.116(0.075)	-
^{202}Tl	c	12.23d	12.1(1.1)	30.1(2.7)	29.8(2.7)	21.9(2.0)	14.2(1.3)	7.06(0.65)	3.13(0.29)	1.42(0.13)	0.677(0.065)	0.336(0.034)	0.194(0.022)	0.095(0.015)
^{201}Tl	i	72.912h	12(10)	10.6(9.1)	15(15)	17(13)	20.0(9.7)	8.4(7.2)	3.8(5.4)	5.3(1.5)	0.811(0.081)	-	-	-
^{201}Tl	c*	72.912h	52.5(5.4)	123(14)	121(12)	87.4(8.9)	60.5(7.3)	26.1(2.7)	10.5(1.2)	5.30(0.56)	2.40(0.24)	-	-	-
^{200}Tl	i	26.1h	8.11(0.82)	21.4(2.1)	23.4(2.3)	18.2(1.8)	13.4(1.5)	5.16(0.54)	2.65(0.26)	1.02(0.18)	0.477(0.076)	0.315(0.068)	0.147(0.020)	0.071(0.014)
^{200}Tl	c	26.1h	27.3(2.5)	71.3(6.4)	72.4(6.5)	54.7(4.9)	37.4(3.4)	16.1(1.5)	7.19(0.65)	3.26(0.30)	1.53(0.14)	0.736(0.069)	0.413(0.038)	0.227(0.021)
^{199}Tl	c*	7.42h	19.1(2.2)	61.9(7.0)	63.7(6.8)	48.2(5.4)	34.8(3.9)	14.7(1.6)	6.22(0.71)	2.89(0.35)	1.29(0.17)	0.70(0.10)	0.306(0.062)	0.221(0.059)
^{198}Tl	i	5.3h	8.2(1.6)	5(12)	15.1(8.4)	21(11)	8.2(6.8)	6.8(1.7)	0.32(0.62)	0.43(0.56)	0.652(0.093)	0.48(0.19)	0.08(0.10)	-
^{198}Tl	c	5.3h	10.9(1.8)	31.8(4.9)	37.4(4.9)	30.6(4.0)	22.9(3.4)	9.4(1.0)	3.19(0.37)	1.80(0.44)	0.903(0.085)	0.508(0.076)	0.195(0.037)	0.156(0.023)
^{203}Hg	c	46.612d	1.95(0.19)	4.16(0.41)	3.95(0.40)	2.88(0.28)	1.87(0.19)	0.93(0.10)	0.431(0.055)	0.150(0.030)	0.108(0.059)	-	-	-
^{197m}Hg	i(m)	23.8h	1.93(0.80)	6.08(0.92)	6.92(0.99)	5.51(0.81)	3.64(0.56)	1.89(0.39)	-	-	-	-	-	-
^{195m}Hg	i(m)	41.6h	-	3.62(0.47)	4.10(0.51)	3.26(0.54)	3.07(0.51)	1.31(0.22)	0.57(0.12)	0.314(0.065)	0.185(0.045)	-	-	-
^{195}Hg	i	9.9h	-	14.8(3.7)	12.5(2.1)	-	-	-	-	-	-	-	-	-
^{195}Hg	c	9.9h	-	17.1(3.7)	14.8(2.3)	12.6(2.9)	6.6(1.4)	3.78(0.69)	2.45(0.44)	1.44(0.33)	-	-	-	-

^{193m}Hg	i(m)	11.8h	-	1.37(0.35)	1.99(0.45)	1.48(0.35)	1.00(0.31)	0.63(0.14)	0.303(0.077)	-	-	-	-	-
^{192}Hg	c	4.85h	0.802(0.088)	6.78(0.71)	7.53(0.73)	6.70(0.74)	5.68(0.84)	2.12(0.21)	1.20(0.11)	0.576(0.072)	0.305(0.047)	0.152(0.020)	-	0.044(0.004)
^{199}Au	c	3.139d	-	0.89(0.18)	0.82(0.14)	0.84(0.19)	0.57(0.12)	0.327(0.069)	-	-	-	-	-	-
^{198}Au	i(m+g)	2.69517d	0.165(0.023)	0.764(0.089)	0.820(0.098)	0.648(0.069)	0.422(0.051)	0.223(0.027)	0.085(0.015)	0.049(0.013)	0.022(0.009)	-	-	-
^{196}Au	i(m1+m2+g)	6.183d	0.221(0.031)	0.747(0.075)	0.994(0.100)	0.852(0.083)	0.553(0.056)	0.300(0.037)	0.122(0.016)	0.078(0.012)	-	0.029(0.009)	-	-
^{195}Au	c	186.098d	6.70(1.30)	58.8(8.7)	71.0(13.0)	52.5(8.5)	33.8(5.6)	15.6(3.3)	6.5(1.5)	2.80(2.40)	-	-	-	-
^{194}Au	i(m1+m2+g)	38.02h	0.213(0.046)	0.99(0.14)	1.37(0.17)	1.17(0.15)	0.78(0.10)	0.426(0.069)	0.203(0.030)	0.102(0.019)	-	-	-	-
^{192}Au	i(m+g)	4.94h	0.900(0.099)	1.0(1.8)	2.3(3.0)	0.9(1.0)	0.43(0.73)	0.32(0.41)	0.171(0.038)	-	0.004(0.091)	0.025(0.015)	-	0.007(0.001)
^{192}Au	c	4.94h	1.70(0.16)	8.3(1.4)	11.9(2.6)	9.3(1.6)	6.43(0.76)	2.89(0.50)	1.40(0.21)	-	0.334(0.070)	0.184(0.029)	-	0.051(0.005)
^{191}Pt	c	2.802d	0.69(0.41)	2.1(1.3)	7.01(0.83)	4.93(0.60)	3.33(0.65)	1.97(0.25)	0.88(0.12)	0.33(0.11)	-	-	-	-
^{188}Pt	c	10.2d	0.670(0.095)	2.63(0.31)	5.15(0.52)	4.25(0.51)	2.52(0.28)	1.21(0.14)	0.85(0.14)	0.35(0.12)	-	-	-	-
^{189}Ir	c	13.2d	-	3.42(0.71)	4.48(0.89)	4.0(1.1)	2.24(0.51)	2.04(0.58)	-	-	-	-	-	-
^{188}Ir	i	41.5h	0.521(0.074)	0.427(0.095)	0.261(0.033)	0.23(0.11)	0.53(0.42)	0.052(0.046)	-	-	-	-	-	-
^{188}Ir	c	41.5h	1.19(0.17)	3.35(0.48)	5.58(0.56)	4.75(0.49)	3.03(0.56)	1.41(0.20)	-	-	-	-	-	-
^{185}Os	c	93.6d	0.254(0.039)	1.03(0.12)	1.77(0.18)	1.66(0.17)	1.10(0.12)	0.615(0.073)	0.356(0.054)	-	-	-	-	-
^{101}Pd	c	8.47h	3.79(0.61)	16.8(2.0)	20.2(2.2)	19.3(2.1)	-	-	-	-	-	-	-	-
^{105}Rh	c	35.36h	-	0.83(0.16)	1.34(0.21)	1.17(0.17)	0.78(0.13)	0.288(0.083)	-	-	-	-	-	-
^{103}Ru	c	39.26d	0.207(0.045)	0.575(0.070)	0.828(0.087)	0.659(0.073)	0.514(0.060)	0.224(0.037)	-	-	-	-	-	-
^{99}Mo	c	65.94h	-	0.95(0.15)	0.96(0.17)	-	0.64(0.13)	0.290(0.067)	-	-	-	-	-	-
^{95}Zr	c	64.02d	-	0.472(0.075)	0.626(0.087)	0.500(0.061)	0.342(0.081)	-	-	-	-	-	-	-

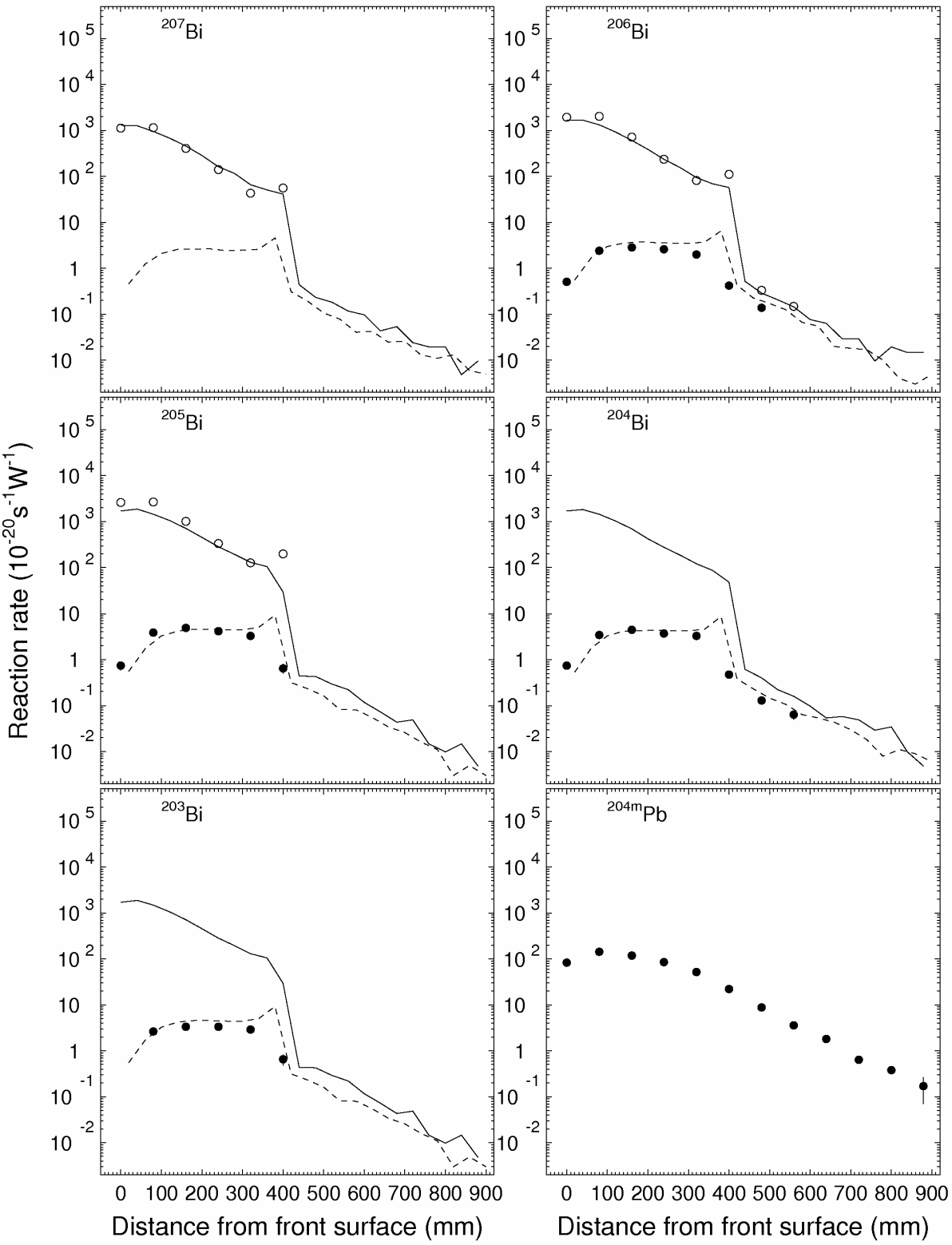

Fig. 32. Experimental production rates in ^{nat}Pb on lines C (light circles) and S (black circles) (^{207}Bi, ^{206}Bi, ^{205}Bi, ^{204}Bi, ^{203}Bi, ^{204m}Pb). The curves correspond to MCNPX simulations on lines C (dashed curves) and lines S (solid curves).

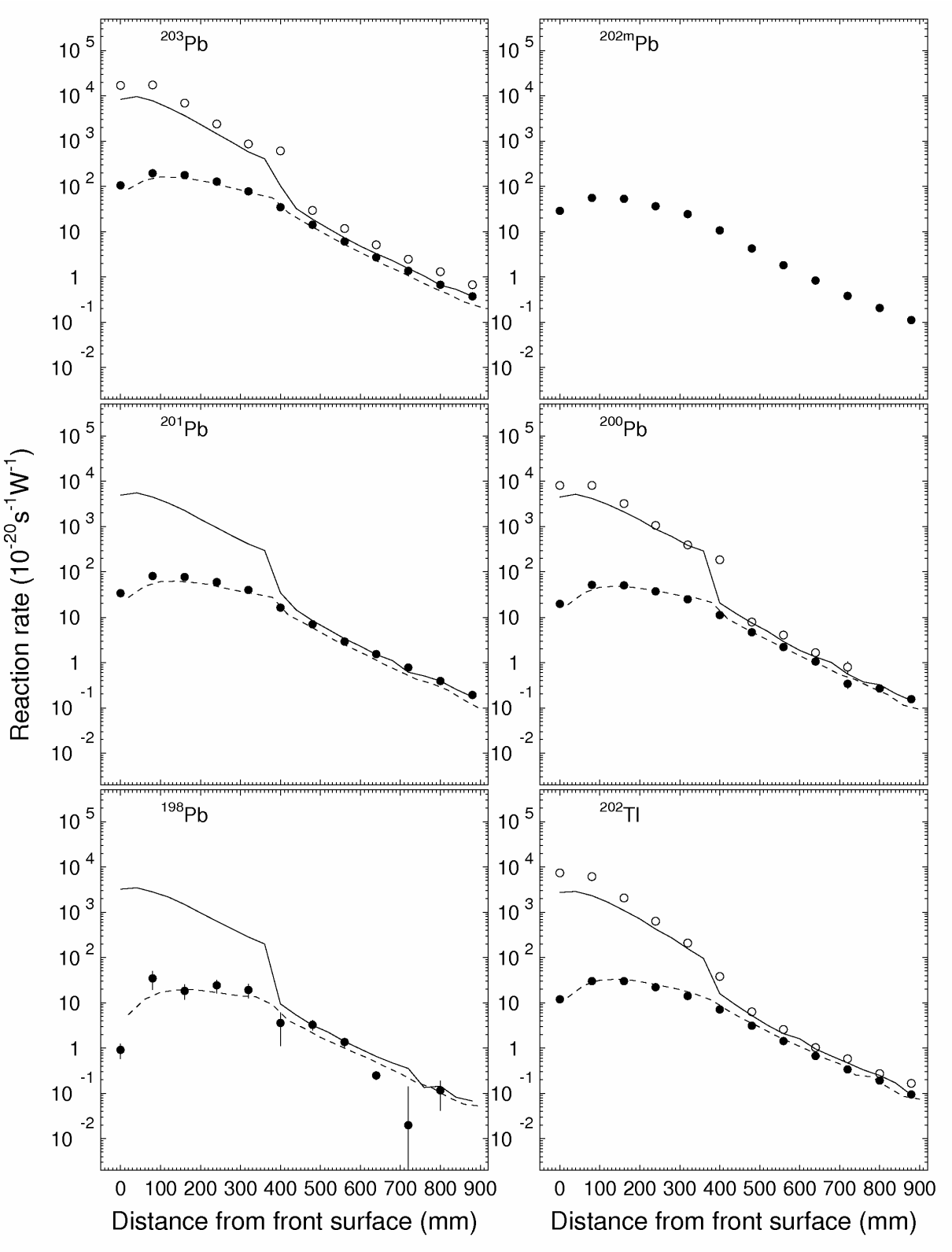

Fig. 32 (cont'd). Experimental production rates in ^{nat}Pb on lines C (light circles) and S (black circles) (^{203}Pb, ^{202m}Pb, ^{201}Pb, ^{200}Pb, ^{198}Pb, ^{202}Tl). The curves correspond to MCNPX simulations on lines C (dashed curves) and lines S (solid curves).

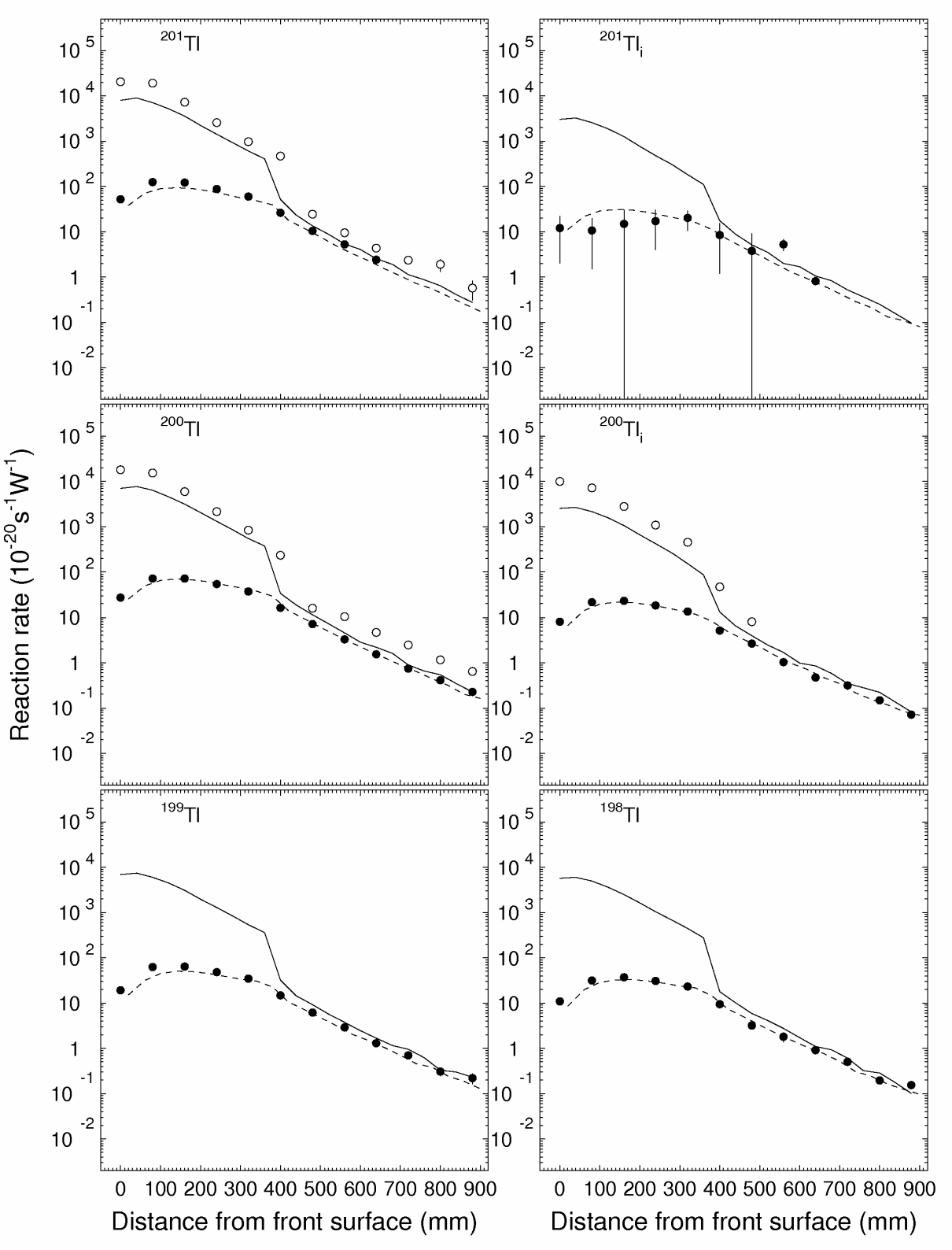

Fig. 32 (cont'd). Experimental production rates in ^{nat}Pb on lines C (light circles) and S (black circles) (^{201}Tl, ^{201}Tl$_i$, ^{200}Tl, ^{200}Tl$_i$, ^{199}Tl, ^{198}Tl). The curves correspond to MCNPX simulations on lines C (dashed curves) and lines S (solid curves).

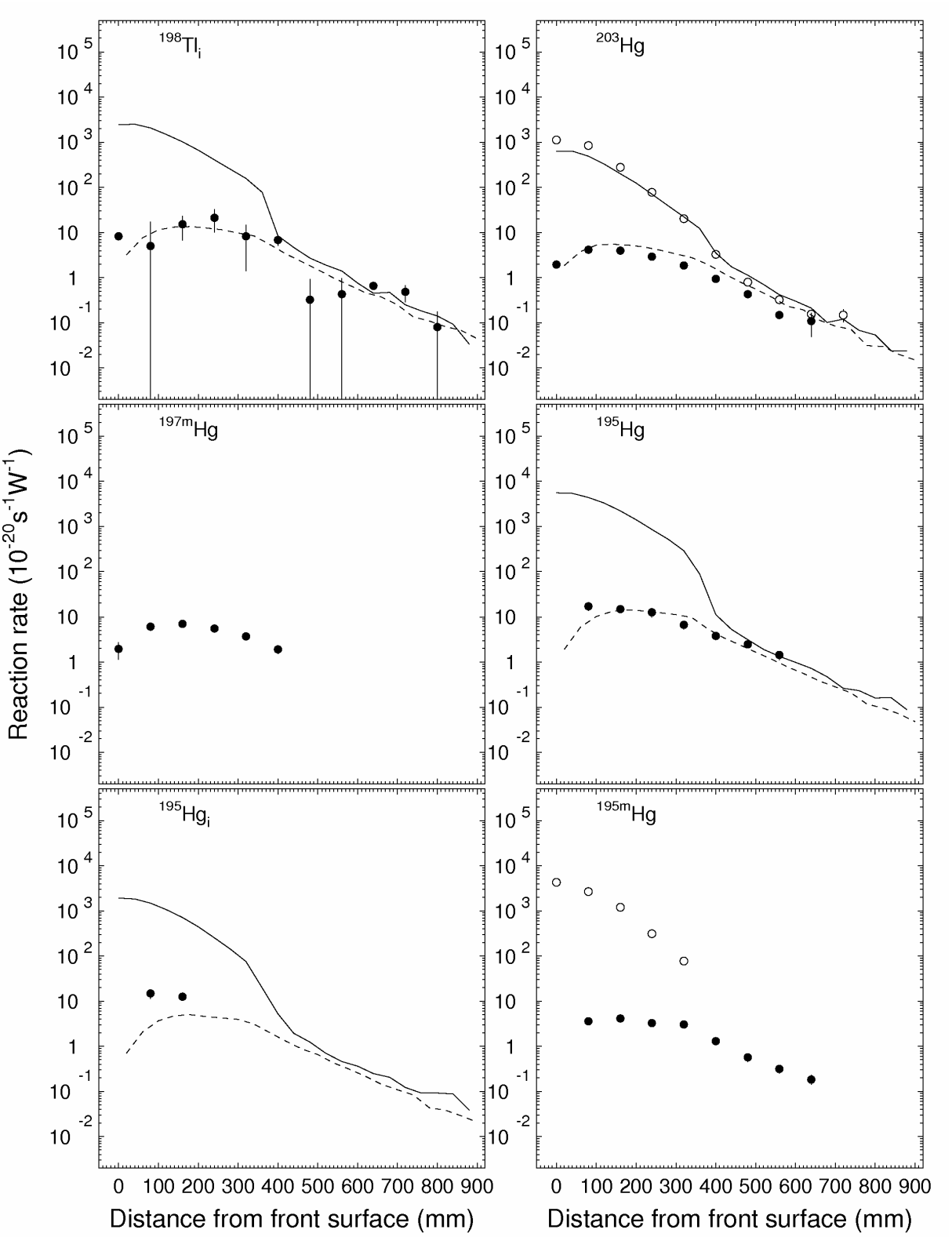

Fig. 32 (cont'd). Experimental production rates in ^{nat}Pb on lines C (light circles) and S (black circles) (^{198}Tl$_i$, ^{203}Hg, ^{197m}Hg, ^{195}Hg, ^{195}Hg$_i$, ^{195m}Hg,). The curves correspond to MCNPX simulations on lines C (dashed curves) and lines S (solid curves).

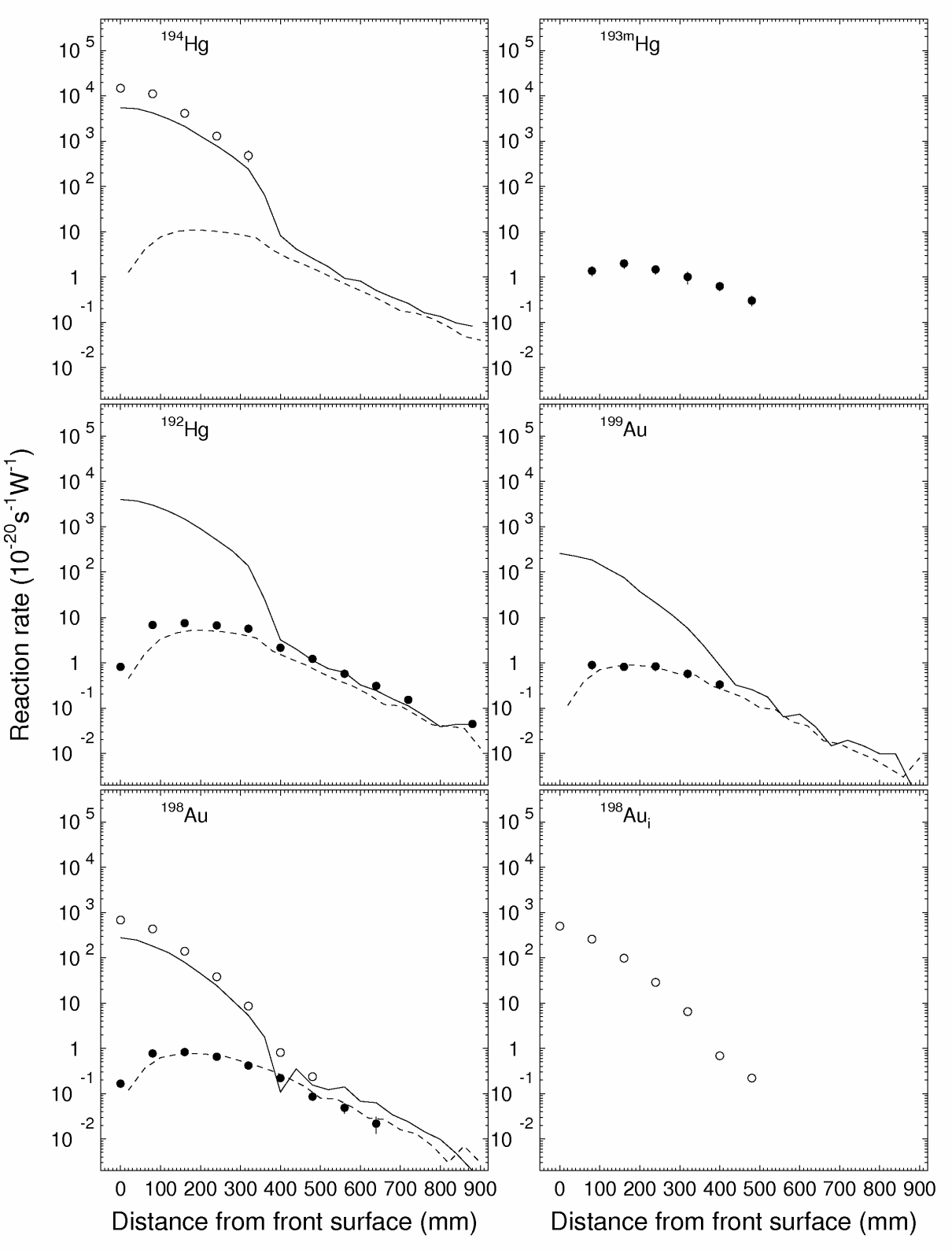

Fig. 32 (cont'd). Experimental production rates in ^{nat}Pb on lines C (light circles) and S (black circles) (^{194}Hg, ^{193m}Hg, ^{192}Hg, ^{199}Au, ^{198}Au, ^{198}Au$_i$). The curves correspond to MCNPX simulations on lines C (dashed curves) and lines S (solid curves).

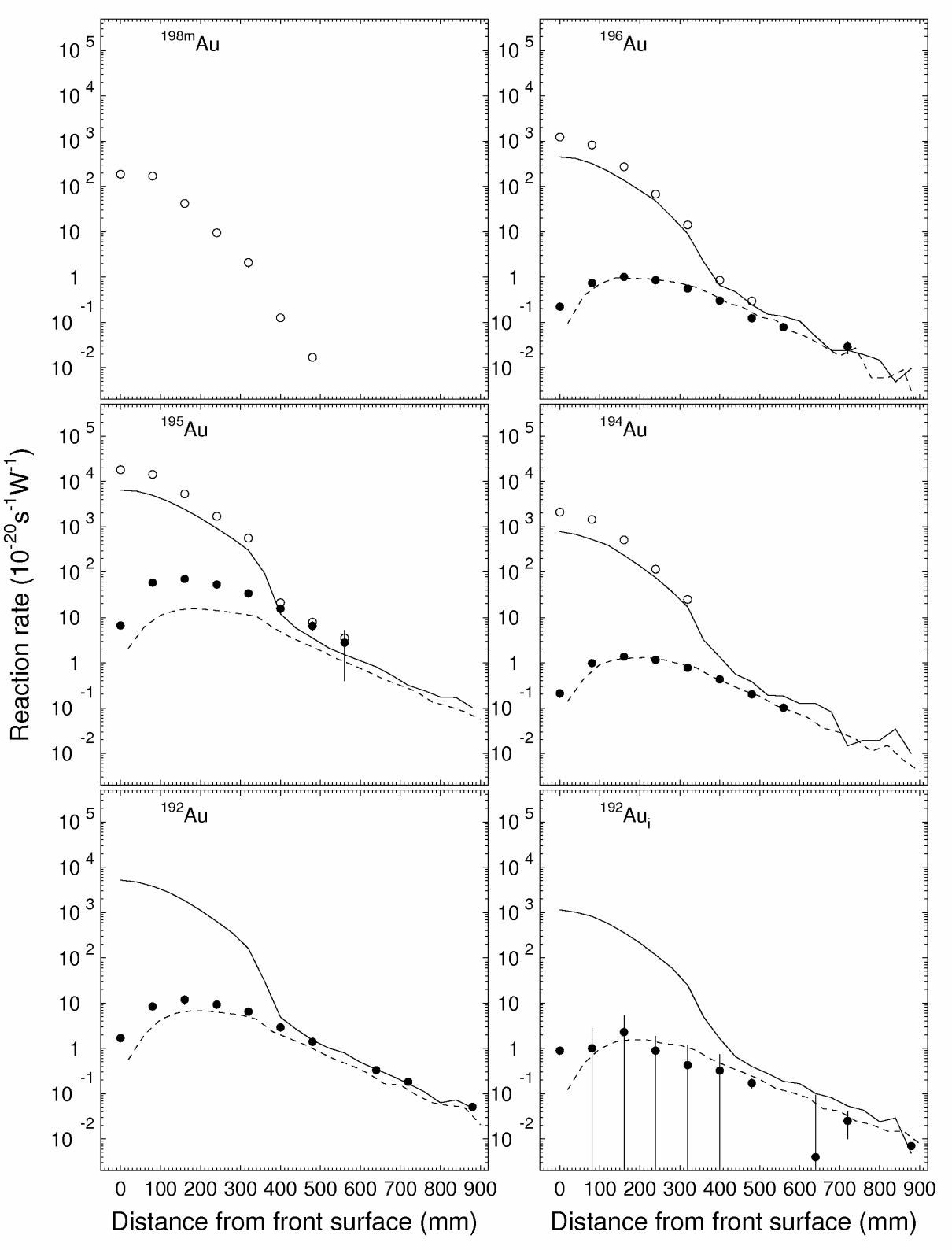

Fig. 32 (cont'd). Experimental production rates in ^{nat}Pb on lines C (light circles) and S (black circles) (^{198m}Au, ^{196}Au, ^{195}Au, ^{194}Au, ^{192}Au, ^{192}Au$_i$). The curves correspond to MCNPX simulations on lines C (dashed curves) and lines S (solid curves).

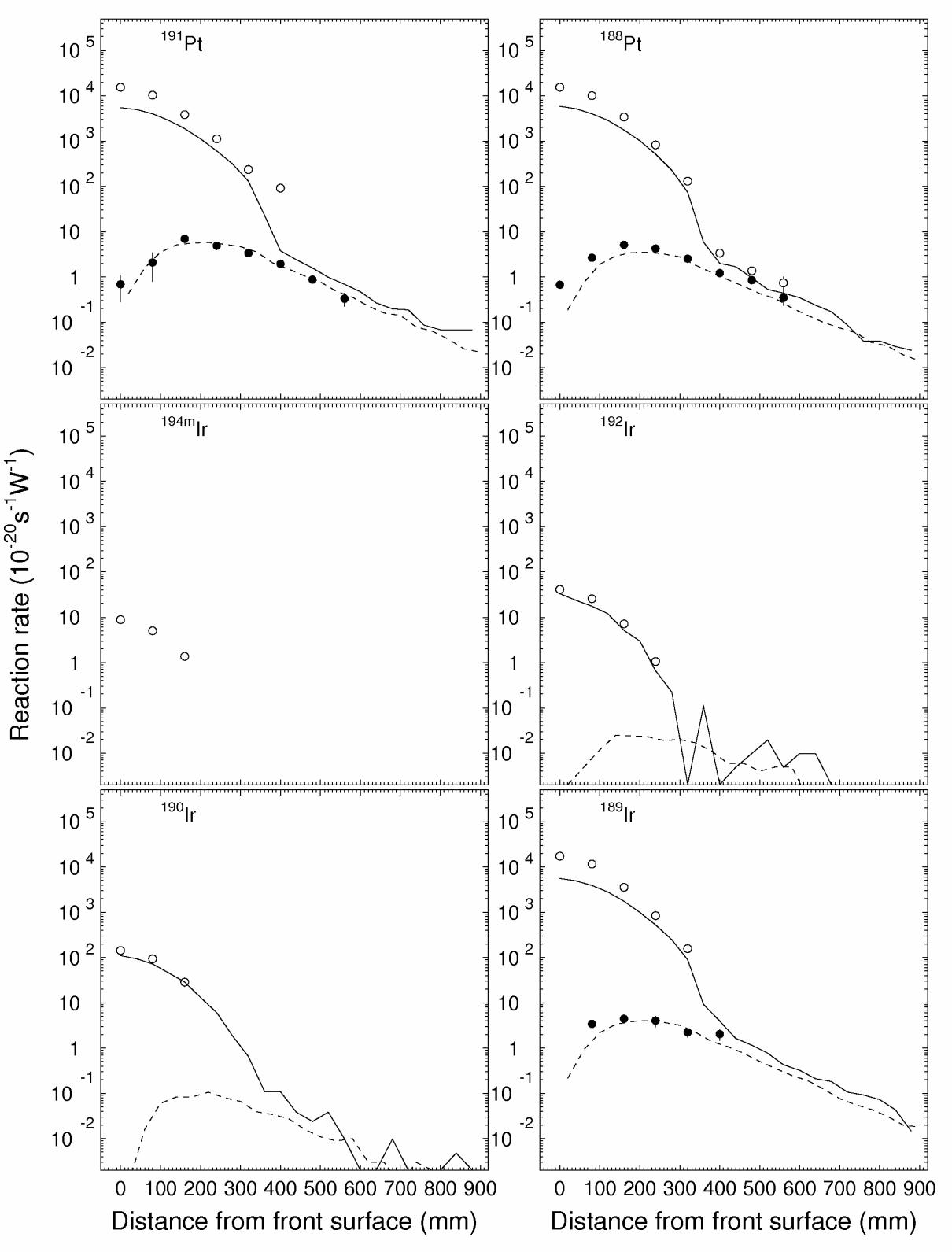

Fig. 32 (cont'd). Experimental production rates in ^{nat}Pb on lines C (light circles) and S (black circles) (^{191}Pt, ^{188}Pt, ^{194m}Ir, ^{192}Ir, ^{190}Ir, ^{189}Ir). The curves correspond to MCNPX simulations on lines C (dashed curves) and lines S (solid curves).

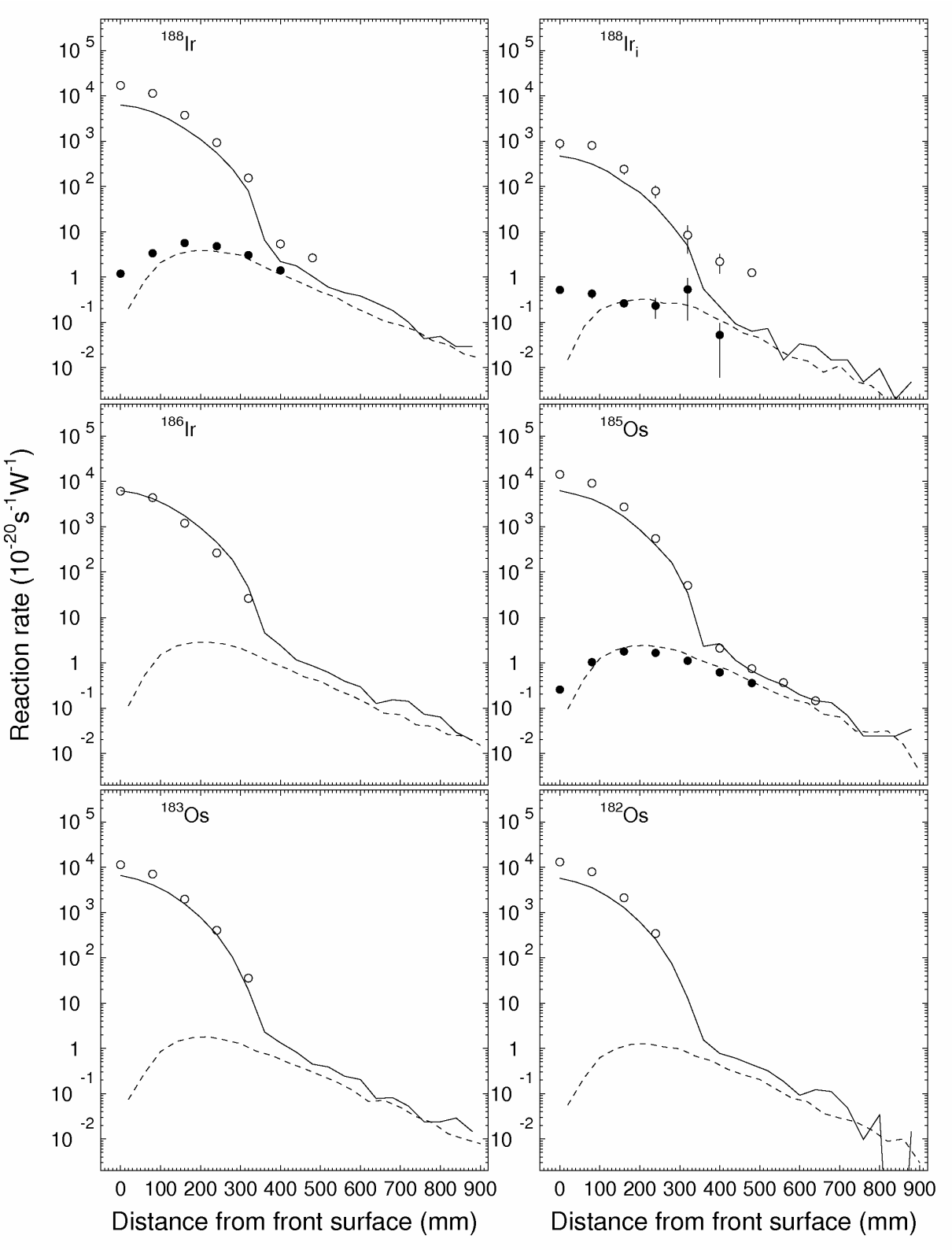

Fig. 32 (cont'd). Experimental production rates in ^{nat}Pb on lines C (light circles) and S (black circles) (^{188}Ir, ^{188}Ir$_i$, ^{186}Ir, ^{185}Os, ^{183}Os, ^{182}Os). The curves correspond to MCNPX simulations on lines C (dashed curves) and lines S (solid curves).

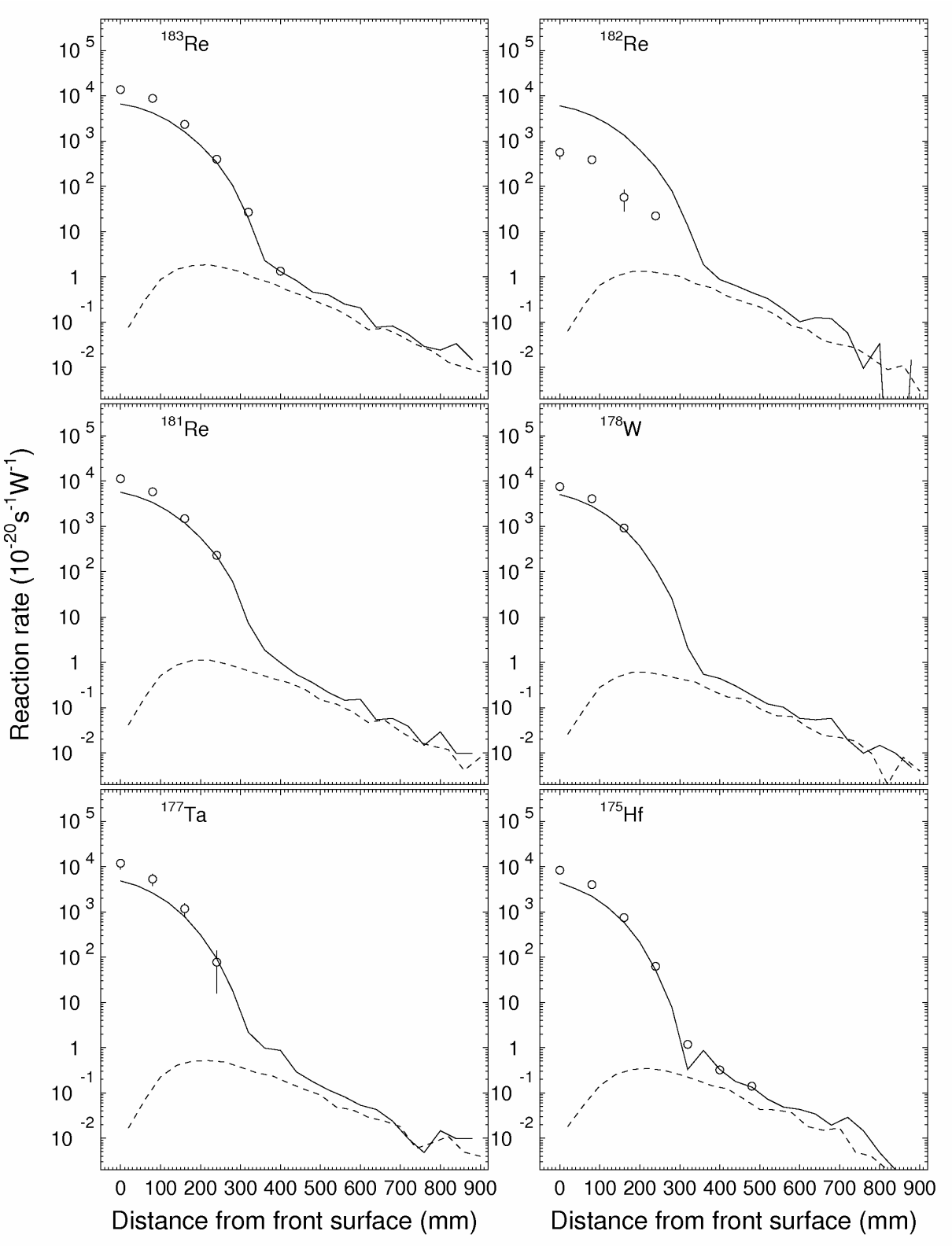

Fig. 32 (cont'd). Experimental production rates in ^{nat}Pb on lines C (light circles) and S (black circles) (^{183}Re, ^{182}Re, ^{181}Re, ^{178}W, ^{177}Ta, ^{175}Hf). The curves correspond to MCNPX simulations on lines C (dashed curves) and lines S (solid curves).

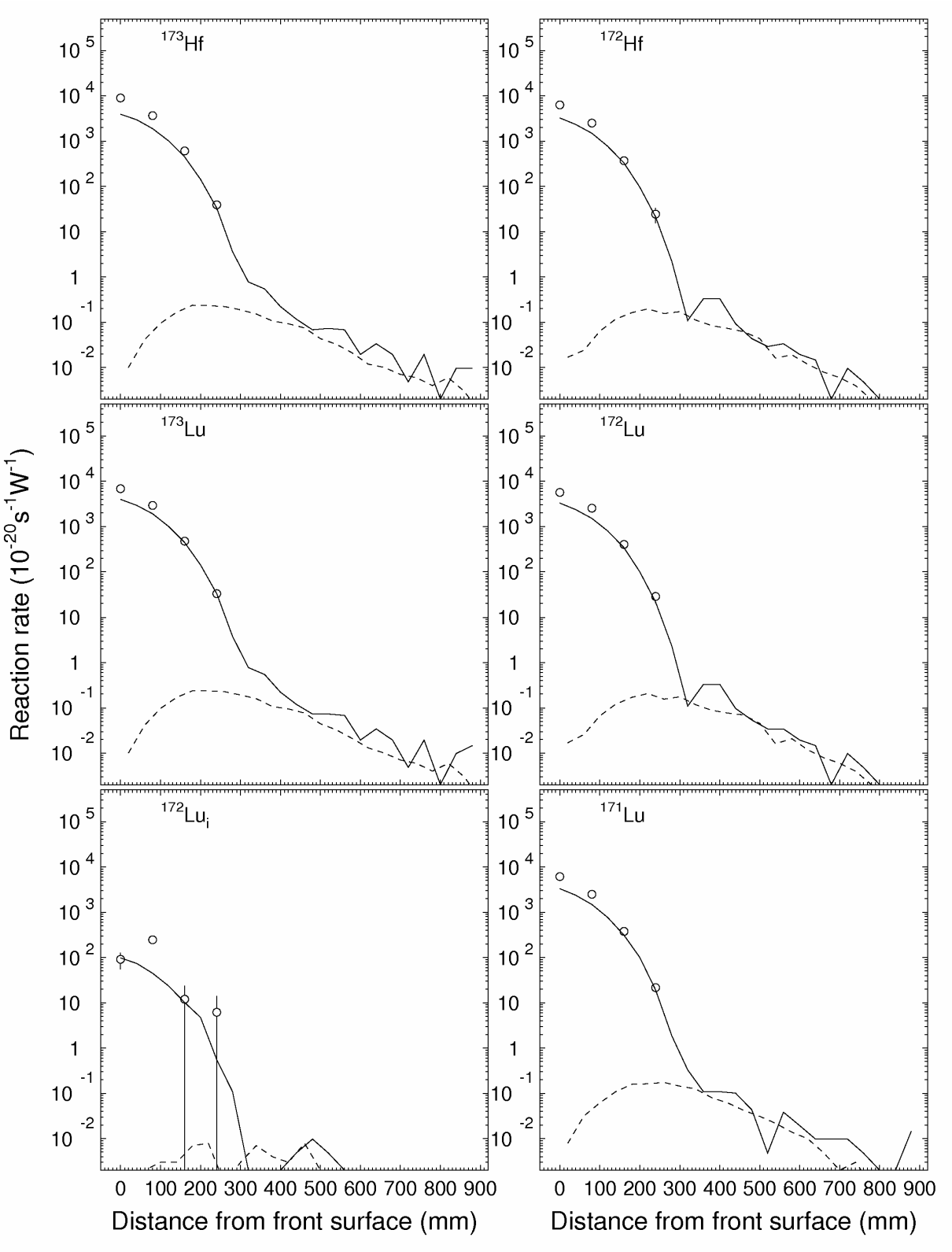

Fig. 32 (cont'd). Experimental production rates in ^{nat}Pb on lines C (light circles) and S (black circles) (^{173}Hf, ^{172}Hf, ^{173}Lu, ^{172}Lu, ^{172}Lu$_i$, ^{171}Lu). The curves correspond to MCNPX simulations on lines C (dashed curves) and lines S (solid curves).

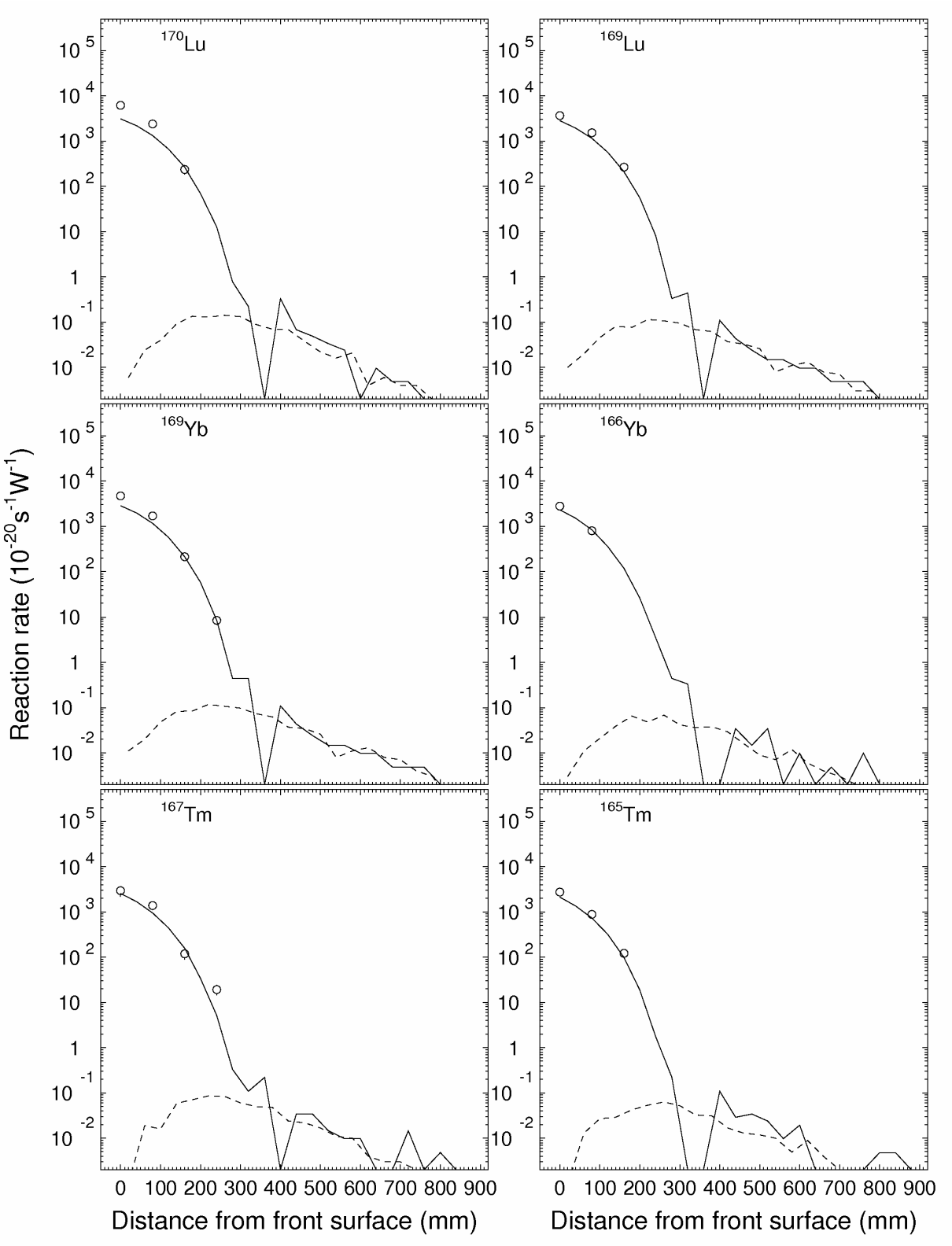

Fig. 32 (cont'd). Experimental production rates in ^{nat}Pb on lines C (light circles) and S (black circles) (^{170}Lu, ^{169}Lu, ^{169}Yb, ^{166}Yb, ^{167}Tm, ^{165}Tm). The curves correspond to MCNPX simulations on lines C (dashed curves) and lines S (solid curves).

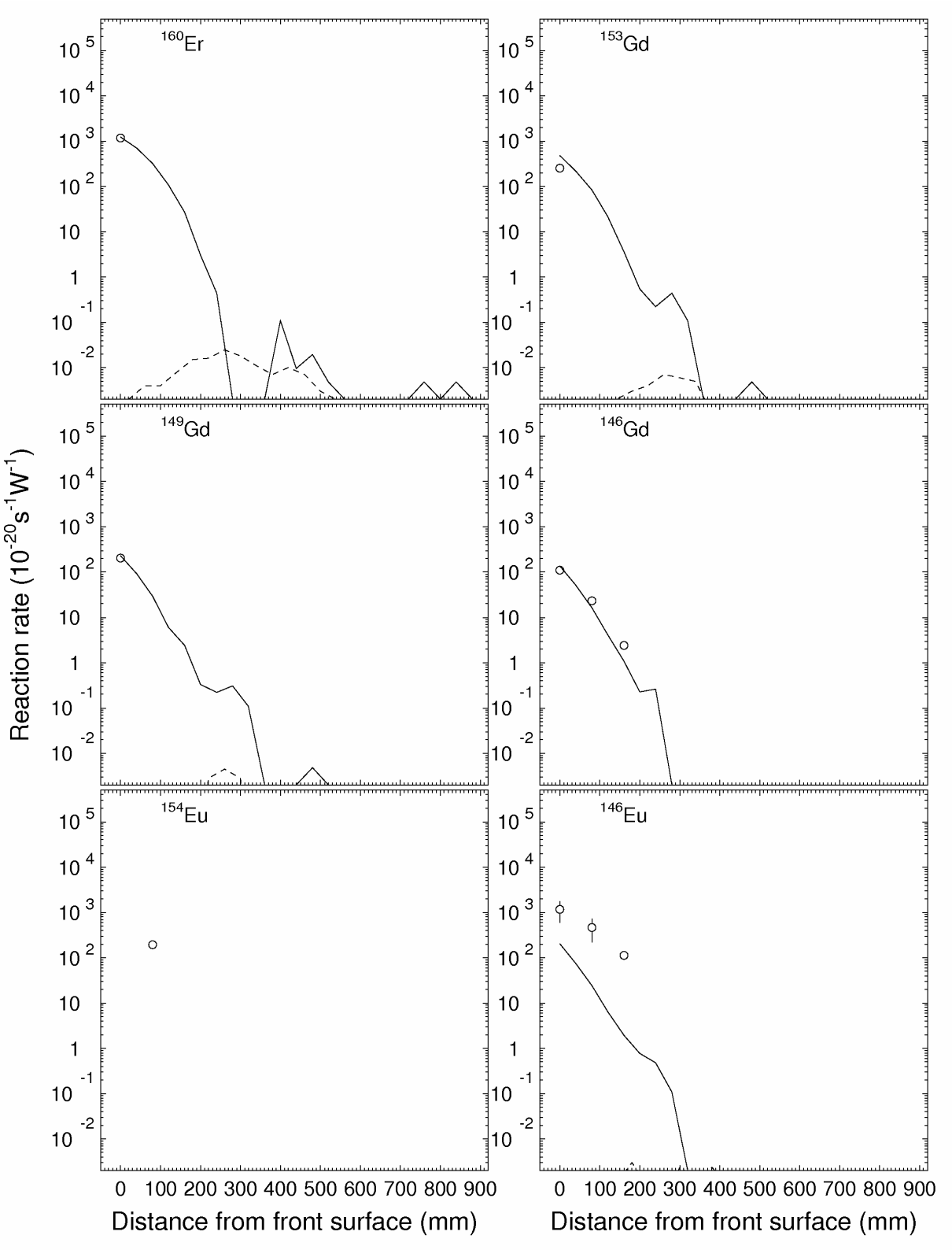

Fig. 32 (cont'd). Experimental production rates in ^{nat}Pb on lines C (light circles) and S (black circles) (^{160}Er, ^{153}Gd, ^{149}Gd, ^{146}Gd, ^{154}Eu, ^{146}Eu). The curves correspond to MCNPX simulations on lines C (dashed curves) and lines S (solid curves).

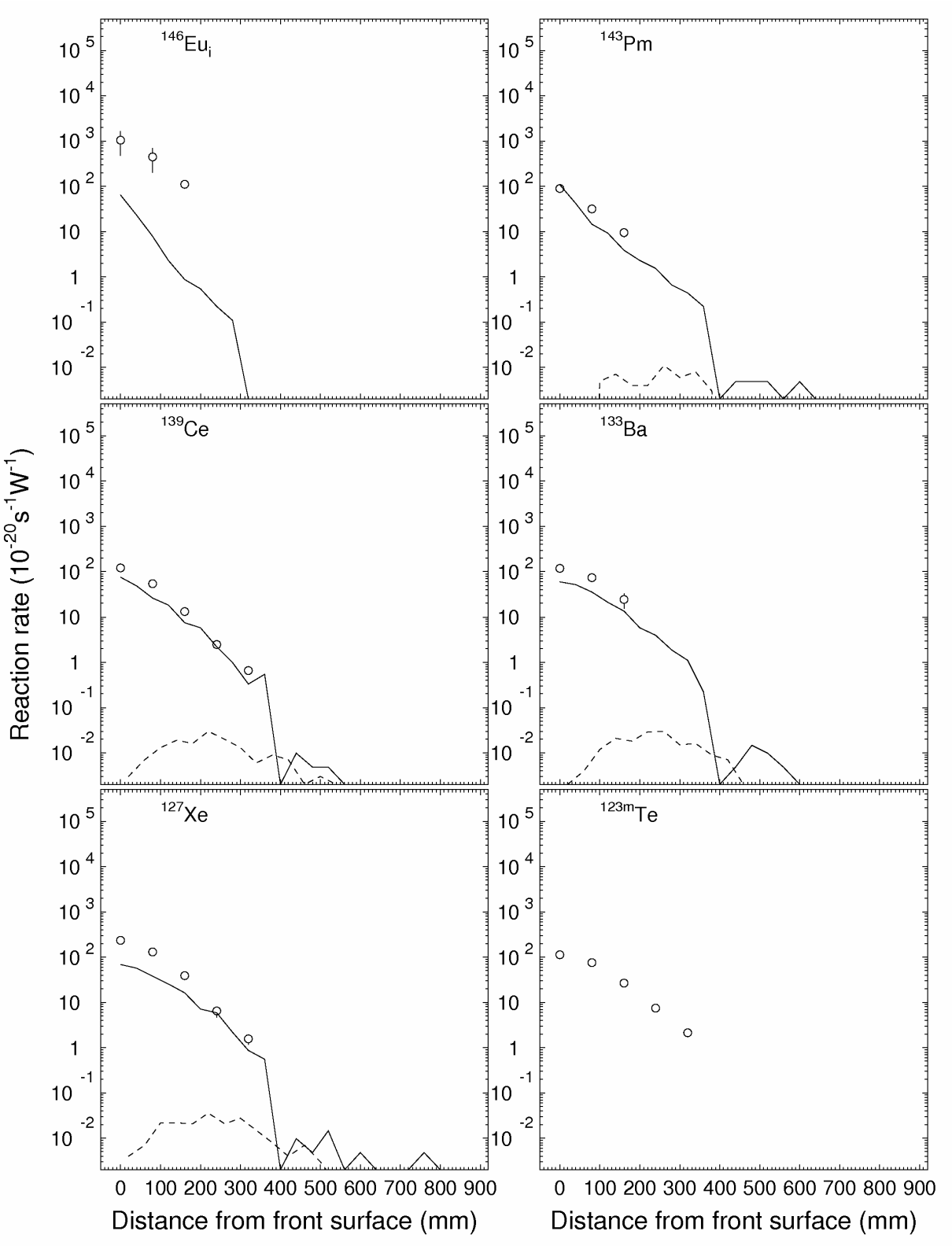

Fig. 32 (cont'd). Experimental production rates in ^{nat}Pb on lines C (light circles) and S (black circles) (^{146}Eu$_i$, ^{143}Pm, ^{139}Ce, ^{133}Ba, ^{127}Xe, ^{123m}Te). The curves correspond to MCNPX simulations on lines C (dashed curves) and lines S (solid curves).

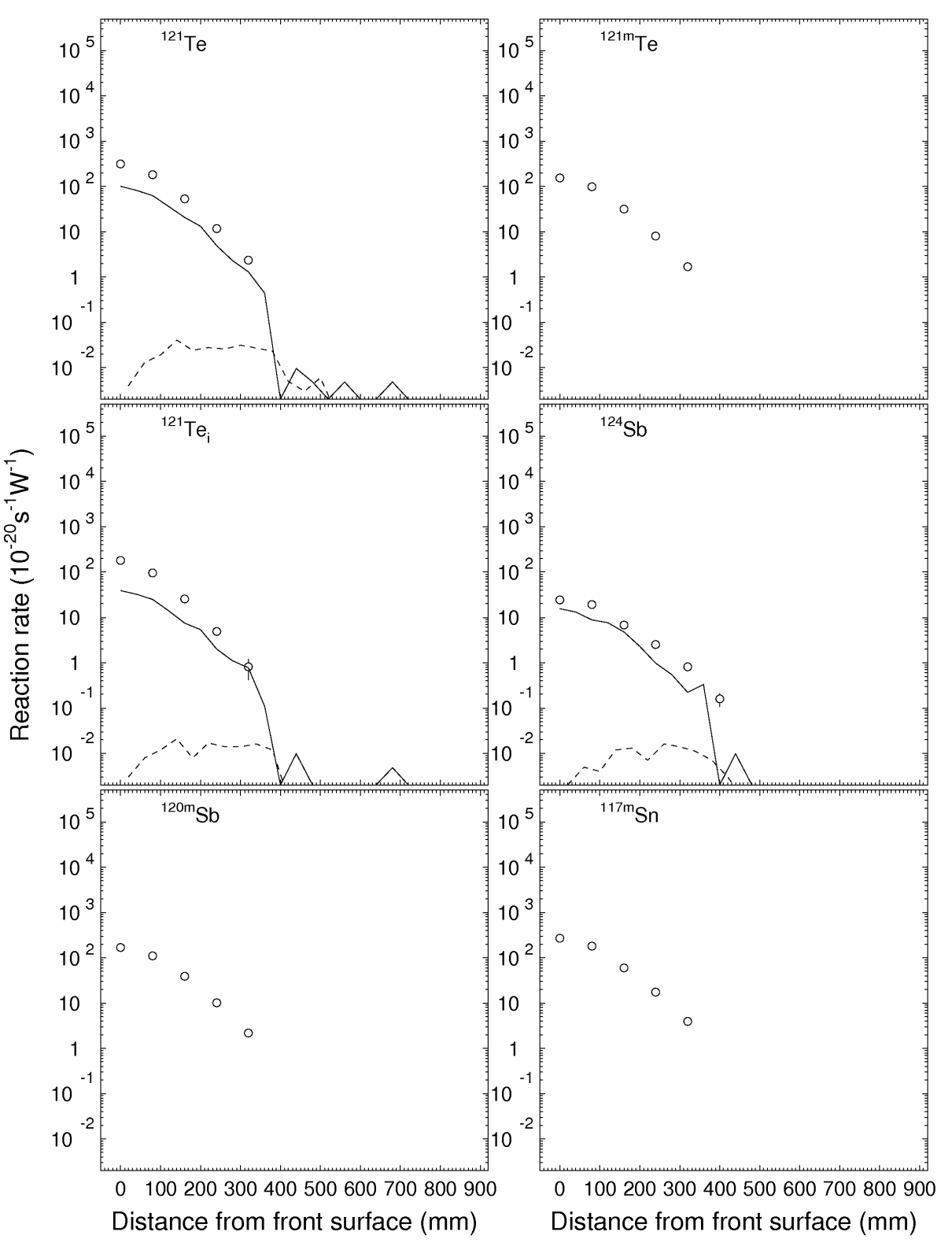

Fig. 32 (cont'd). Experimental production rates in ^{nat}Pb on lines C (light circles) and S (black circles) (^{121}Te, ^{121m}Te, ^{121}Te$_i$, ^{124}Sb, ^{120m}Sb, ^{117m}Sn). The curves correspond to MCNPX simulations on lines C (dashed curves) and lines S (solid curves).

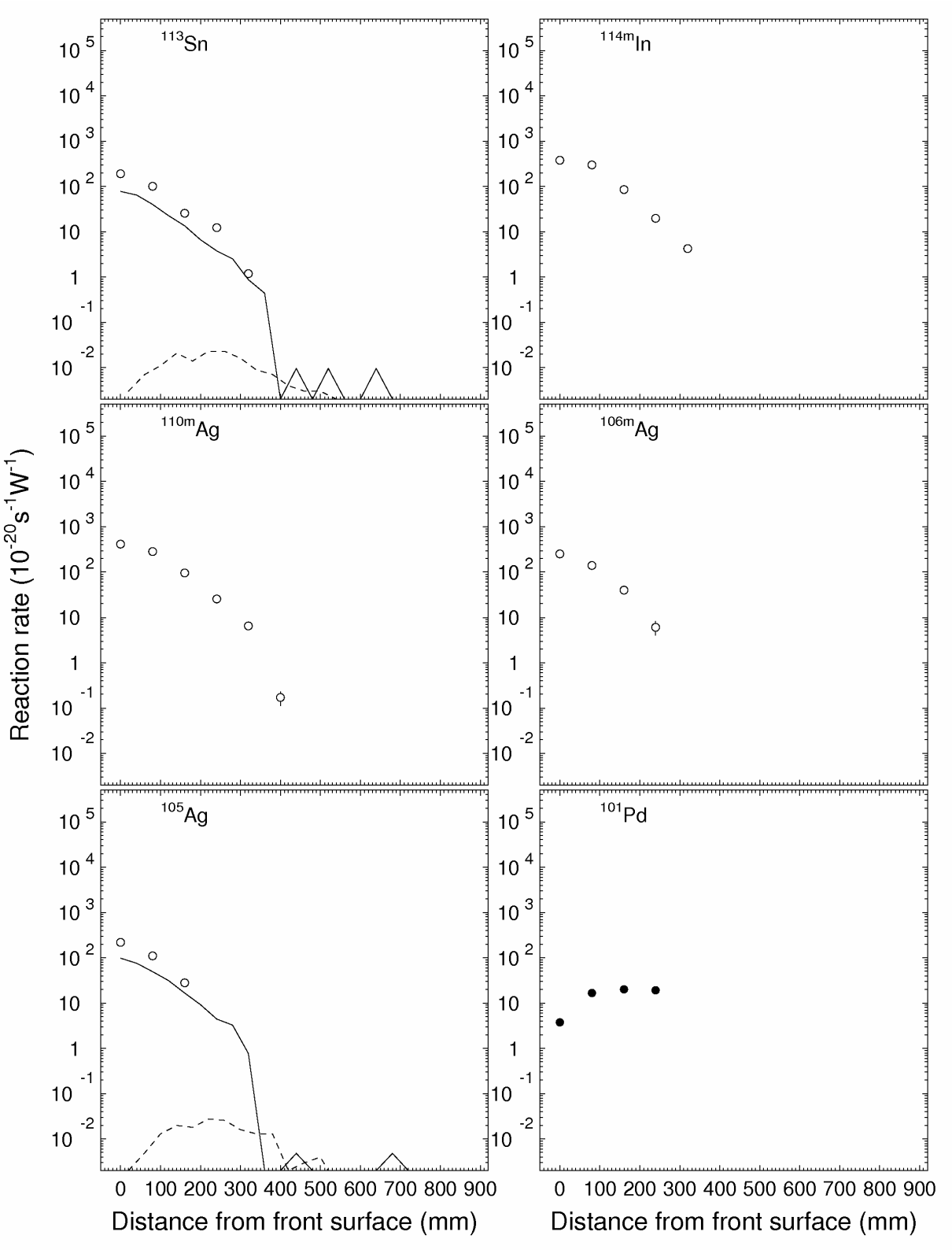

Fig. 32 (cont'd). Experimental production rates in ^{nat}Pb on lines C (light circles) and S (black circles) (^{113}Sn, ^{114m}In, ^{110m}Ag, ^{106m}Ag, ^{105}Ag, ^{101}Pd). The curves correspond to MCNPX simulations on lines C (dashed curves) and lines S (solid curves).

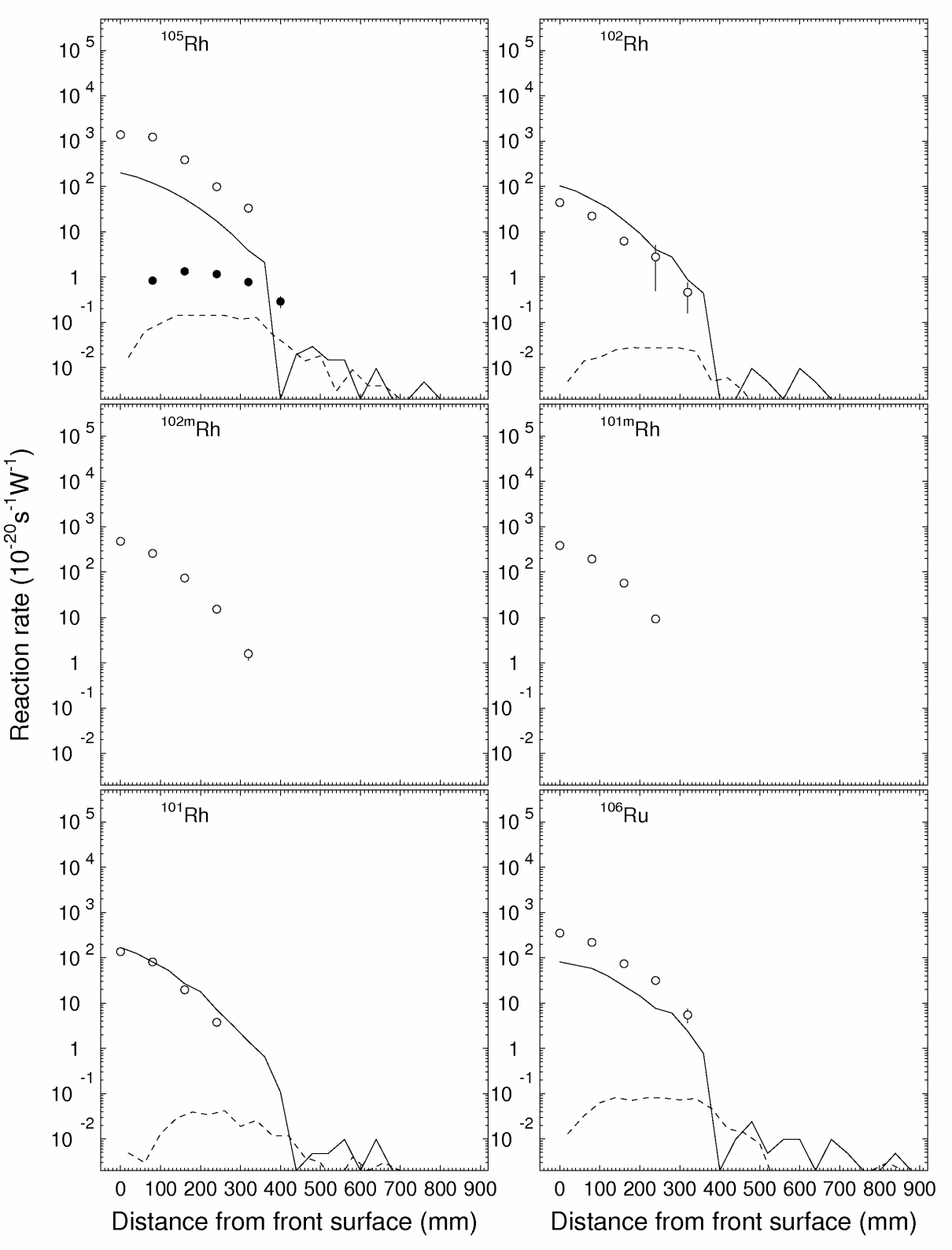

Fig. 32 (cont'd). Experimental production rates in ^{nat}Pb on lines C (light circles) and S (black circles) (^{105}Rh, ^{102}Rh, ^{102m}Rh, ^{101m}Rh, ^{101}Rh, ^{106}Ru). The curves correspond to MCNPX simulations on lines C (dashed curves) and lines S (solid curves).

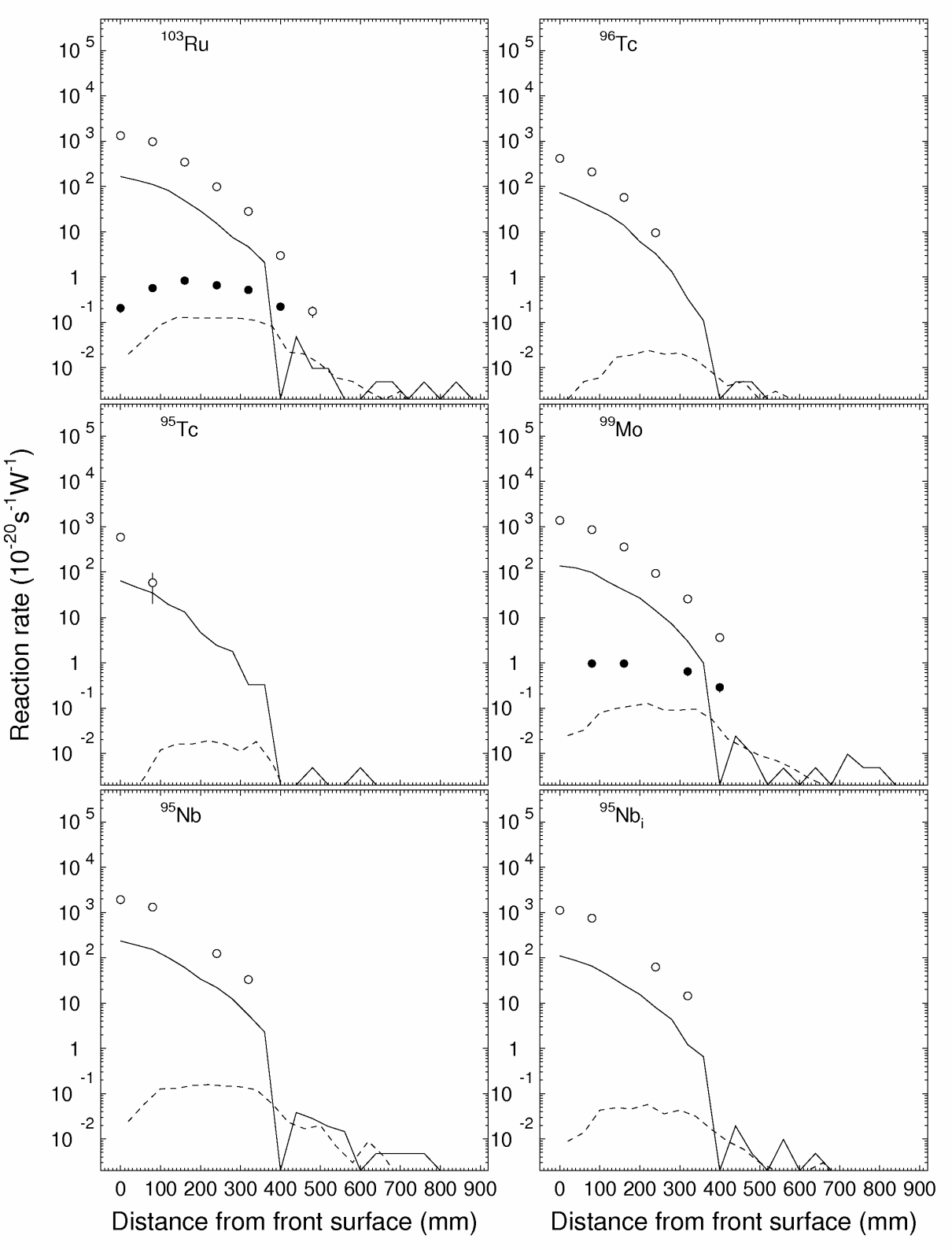

Fig. 32 (cont'd). Experimental production rates in ^{nat}Pb on lines C (light circles) and S (black circles) (^{103}Ru, ^{96}Tc, ^{95}Tc, ^{99}Mo, ^{95}Nb, ^{95}Nbi). The curves correspond to MCNPX simulations on lines C (dashed curves) and lines S (solid curves).

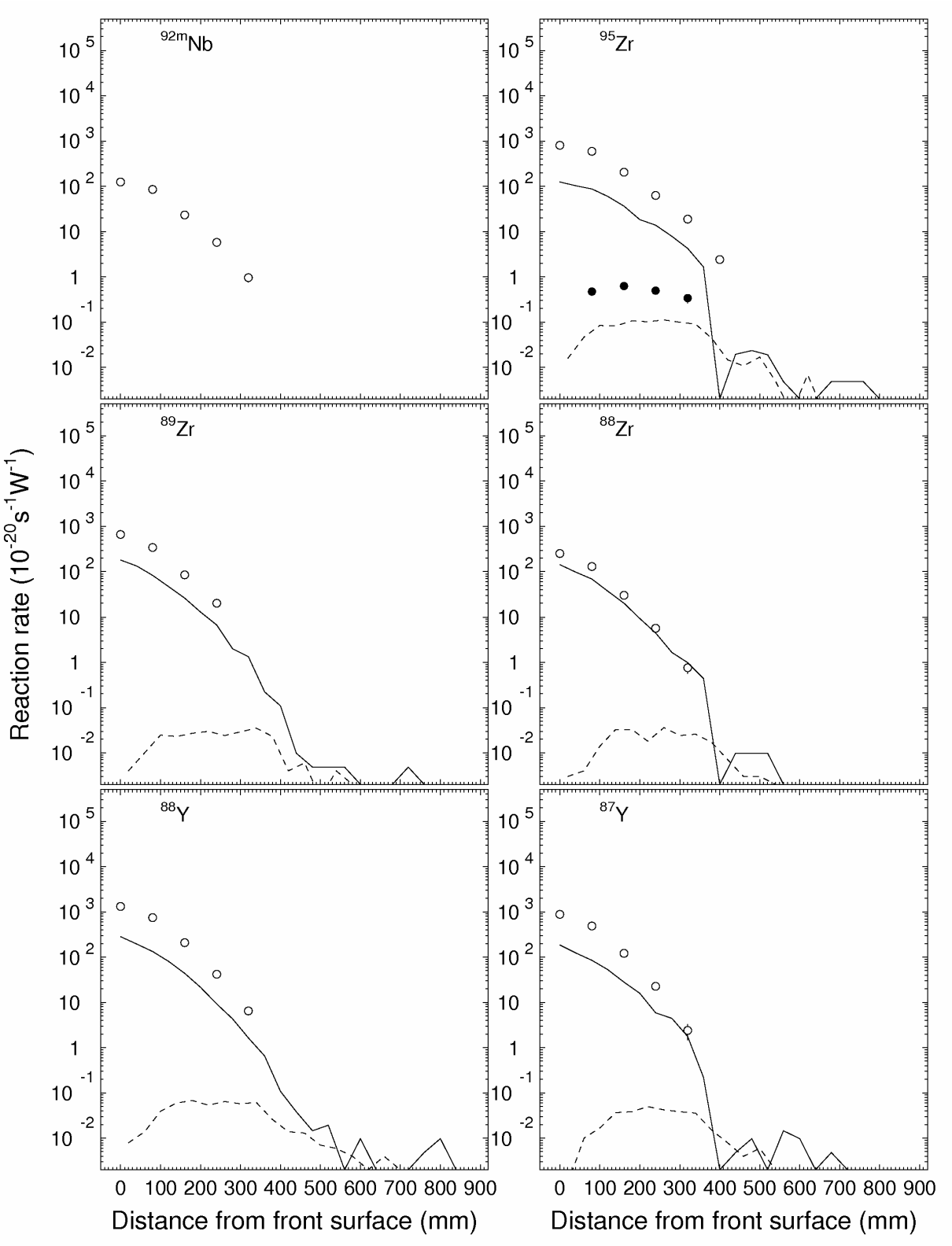

Fig. 32 (cont'd). Experimental production rates in ^{nat}Pb on lines C (light circles) and S (black circles) (^{92m}Nb, ^{95}Zr, ^{89}Zr, ^{88}Zr, ^{88}Y, ^{87}Y). The curves correspond to MCNPX simulations on lines C (dashed curves) and lines S (solid curves).

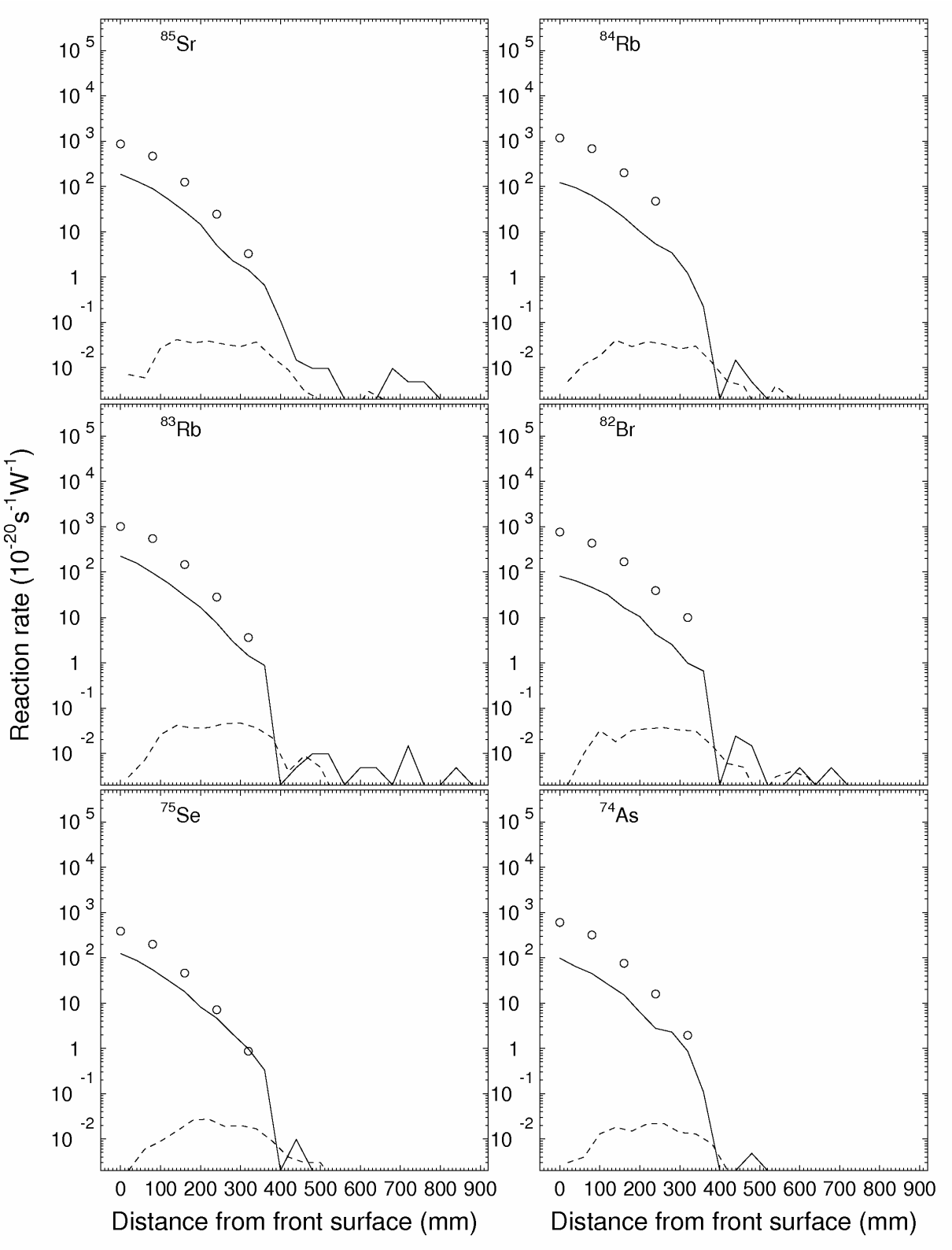

Fig. 32 (cont'd). Experimental production rates in ^{nat}Pb on lines C (light circles) and S (black circles) (^{85}Sr, ^{84}Rb, ^{83}Rb, ^{82}Br, ^{75}Se, ^{74}As). The curves correspond to MCNPX simulations on lines C (dashed curves) and lines S (solid curves).

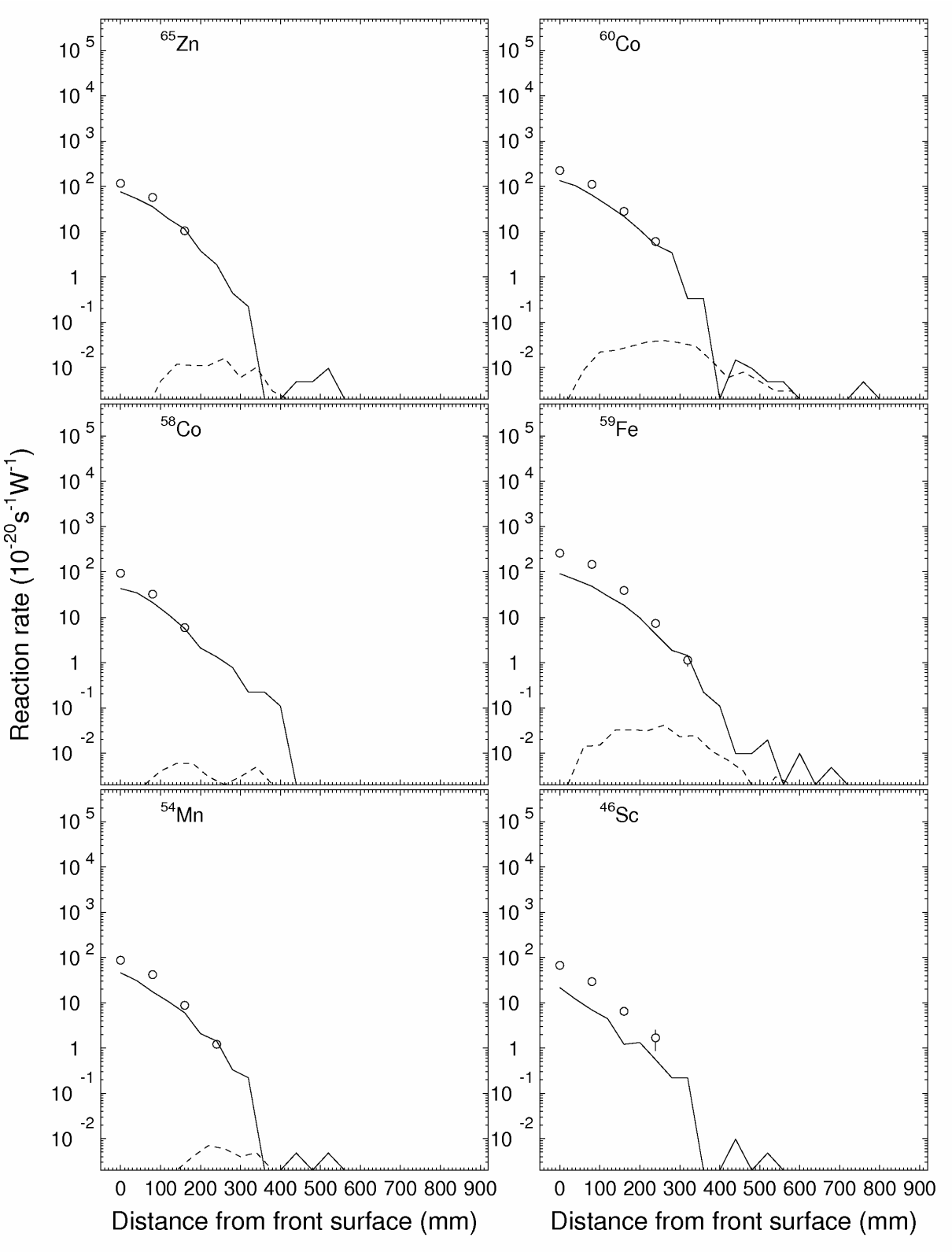

Fig. 32 (cont'd). Experimental production rates in ^{nat}Pb on lines C (light circles) and S (black circles) (^{65}Zn, ^{60}Co, ^{58}Co, ^{59}Fe, ^{54}Mn, ^{46}Sc). The curves correspond to MCNPX simulations on lines C (dashed curves) and lines S (solid curves).

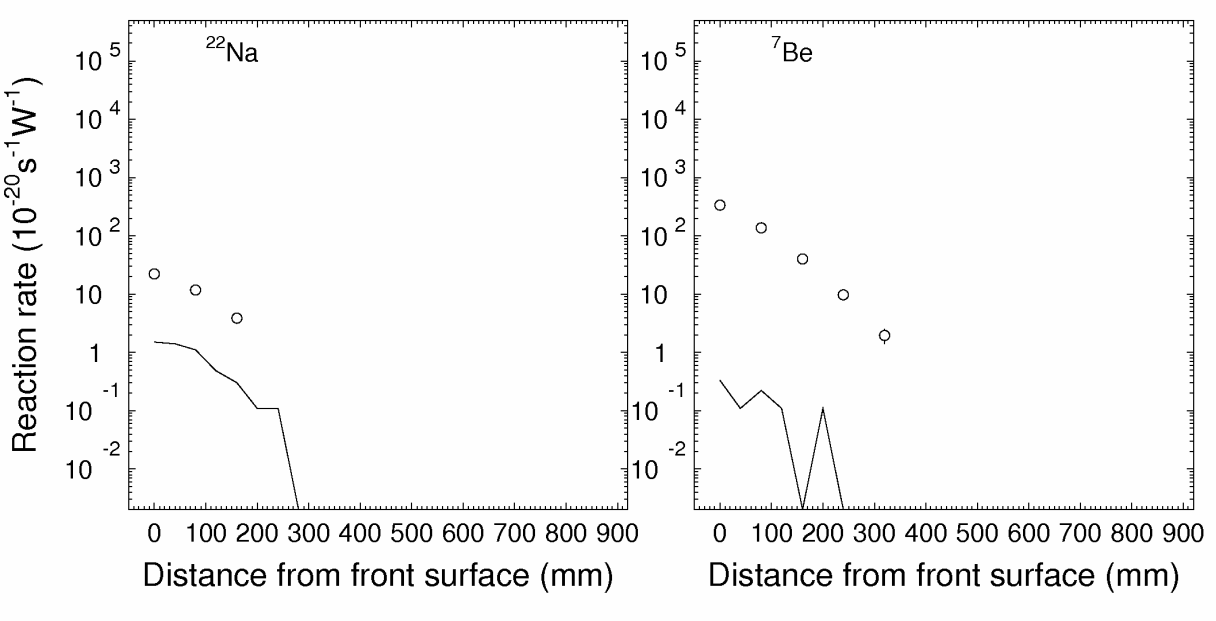

Fig. 32 (cont'd). Experimental production rates in ^{nat}Pb on lines C (light circles) and S (black circles) (^{22}Na, ^{7}Be). The curves correspond to MCNPX simulations on lines C (dashed curves) and lines S (solid curves).

IV. Computational simulation of target parameters

The reaction rates were computer-simulated using MCNPX code [22], which extends the MCNP code with the view to introducing the transport of all the elementary particles, whose lifetimes are significant (34 particles) at all energies. The code incorporates the traits of MNCP-4b code and of versions 2.8 and 3.0 of LAHET code. The high-energy side of the code incorporates also the CEM model to simulate hadron-hadron interactions. The operations with the MCNPX code under the present Project have resulted in the proton and neutron spectra measured on the experimental samples inside and on the surface of the target. Comparison of the results of calculating the neutron spectrum for thin Pb target with experimental data is indicative of a rather high accuracy of the calculations made [23].

4.1. Computational simulation of the measured reaction rates measured

The reaction rates were simulated using the nuclear databases with (p,x)- and (n,x)-cross sections of the reactions measured, including

- the MENDL2 cross section database [24] for the up-to 100 MeV neutron-induced reactions
- the MENDL2P cross section database [25] for the up-to 200 MeV proton-induced reactions.

In the cases when the high-energy range (100<E<800 MeV), which is lacking in the above databases, may contribute much to the measured reaction rates (Al and Co inside the target), cross sections known from experimental works were added to the cross sections taken from the databases.

The sought reaction rates were obtained via integral multiplication of the spectra by the respective reaction cross sections:

$$R = R_{n,x} + R_{p,x} = \sum_{i=n,p} \int \phi_i(E) \cdot \sigma_{i,x} \cdot (E) dE \qquad (57)$$

Fig. 33 shows some examples of the neutron spectra calculated for discs 1 and 9.

The results of computer-aided simulating the reaction rates are shown in Figs. 19-25 together with experimental data.

From Figs. 15-23 it is seen that many of the reaction rates are predicted to within a sufficient accuracy (almost a half of the calculated values differ from the experimental ones by less than 30%). However, some of the figures presented here show also some systematic deviations of the calculated values from experimental data, namely

- all the simulated reaction rates are underestimated by a factor of 1.5-3.0 compared with experimental data at point C1. This fact may arise from the difference between the real lateral distribution of proton beam and the Gaussian with the parameters listed in Table 5;
- the reactions involving a high production threshold (~100 MeV and higher) are as a rule underestimated at point S1 by a factor f up-to 3.

Other differences between calculations and experiment are not systematic and can be explained by but insufficient accuracy of the databases of cross sections used.

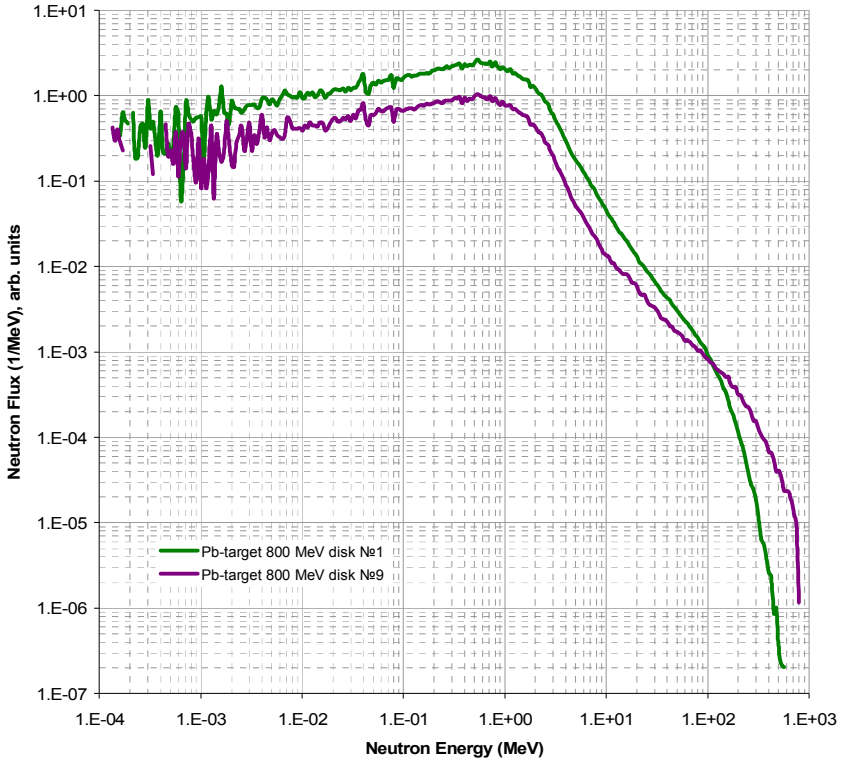

Fig. 33. The neutron spectra from the experimental samples placed on discs 1 and 9 on the surface of the target.

V. Conclusions

The work was aimed at manufacturing, certifying, and proton-irradiating the Pb target and, after that, determining reaction rates in activated samples placed inside and on the surface of the target.

The target was exposed to $6 \cdot 10^{15}$ 800-MeV protons. As a result, 244 samples were irradiated and 1196 γ-spectra were measured and used then to determine 2467 reaction rates.

By now, 64 reaction rates have been simulated, but two reactions ($^{12}C(n,2n)^{11}C$ and $^{115}In(n,n')^{115}In$) were not simulated because their cross sections have not been found in the ENDF/B-V database. The rest reactions are being simulated. The main difficulty in simulating most of the remaining reactions arises from a restricted energy range of the proton and neutron cross sections that can be found in the available MENDL2 and MENDL2P databases. The cross sections in the remaining energy range (above 100 MeV) must be supplied by simulating them via the available codes that simulate high-energy hadron-nucleus interactions.

The results obtained were reported at the Conferences on Nuclear Data for Science & Technology 2007, Nice, 22-27 April 2007 and NUFRA2007, 24-30 September 2007, Kemer, Turkey.

References

[1] Yu.E. Titarenko, V.F. Batyaev, V.M. Zhivun, A.B. Koldobsky, Yu.V. Trebukhovsky, E.I. Karpikhin, R.D. Mulambetov, S.V. Mulambetova, Yu.V. Nekrasov, A.Yu. Titarenko, K.A. Lipatov, B.Yu. Sharkov, A.A. Golubev, A.D Fertman, V.I Turtikov, A.V. Kantsyrev, I.V Roudskoy, G.N. Smirnov, V. S. Barashenkov, K.K. Gudima, M.I. Baznat, S.G. Mashnik, R.E. Prael. Nuclide Production Cross Sections for 59Co and natCu Irradiated with 0.2 GeV and 2.6 GeV Protons and 0.2 GeV/Nucleon Carbon Ions. // Imbedded topical AccApp'03 (Nuclear Applications of Accelerator Technology) 2003 Annual Meeting of the American Nuclear Society (ANS) in San Diego, 1-5 June 2003, California, USA, ANS Proceedings, pp. 535-538;

[2] Yu.E. Titarenko, V.F. Batyaev, E.I. Karpikhin, R.D. Mulambetov, V.M. Zhivun, A.V. Ignatyuk, V.P. Lunev, N.N. Titarenko, Yu.N. Shubin, V.S. Barashenkov, S.V. Mulambetova, K.A. Lipatov, A.V. Belkin, N.N. Alexeev, V.A. Schegolev, Yu.M. Goryachev, V.O. Kudryashov: "Experimental and theoretical studies of the yields of residual product nuclei produced in thin Pb and Bi targets irradiated by 40-2600 MeV protons", Final Technical Report on the ISTC Project #2002, 2005 http://www.nea.fr/html/science/egsaatif/ISTC2002-final-report.pdf

[3] E.Storm, H.I. Israel. Photon cross section from 1 keV to 100 MeV for elements Z=1 to Z=100.

[4] R.B. Firestone, in: Table of Isotope, 8th ed.: 1998Update(with CD ROM) edited by S.Y. Frank Chu (CD ROM Ed.), C.M. Baglim (Ed.) (Wiley Interscince, New York, 1996)

[5]Giredmet Testing Analytical Center. MS&GC Lab. Results of testing mixture compositions №14263.07 - 2007 .

[6] Giredmet Testing Analytical Center. MS&GC Lab. . Results of testing mixture compositions №14269.07 - 2007.

[7] Alfa Aesar. Certificate of Analysis. Stock number: 40761. Lot number: G10D32 – 2006г.

[8] Giredmet Testing Analytical Center. MS&GC Lab. . Results of testing mixture compositions №14264.07 - 2007.

[9] Giredmet Testing Analytical Center. MS&GC Lab. . Results of testing mixture compositions №14267.07 - 2007.

[10] Giredmet Testing Analytical Center. MS&GC Lab. . Results of testing mixture compositions №14262.07 - 2007.

[11] Giredmet Testing Analytical Center. MS&GC Lab. . Results of testing mixture compositions №14266.07 - 2007.

[12] Giredmet Testing Analytical Center. MS&GC Lab. . Results of testing mixture compositions №14265.07 - 2007.

[13] Giredmet Testing Analytical Center. MS&GC Lab. . Results of testing mixture compositions №7336.99 - 1999.

[14] Giredmet Testing Analytical Center. MS&GC Lab. . Results of testing mixture compositions №7333.99 - 1999.

[15] State stable isotope stock. Characteristics of isotope-enriched products. Cerificate 90 – 1988.

[16] State stable isotope stock. Characteristics of isotope-enriched products. Cerificate 135 – 1988.

[17] State stable isotope stock. Characteristics of isotope-enriched products. Cerificate 197 – 1988.

[18] Alfa Aesar. Certificate of Analysis. Stock number: 40182. Lot number: D01P18. – 2006г.

[19] Certificate № 02080, 7У634. State Scientific Center of the Russian Federation "State Scientific Metrological Center" (VNIIFTRI).

[20] J. Tobailem and C.H. de Lassus CEA-N-1466(1)1975; J. Tobailem and C.H. de Lassus CEA-N-1466(5)1981.

[21] R.R. Kinsey, et al., Proc.9th Int. Symp. Of Capture Gamma Ray Spectroscopy and Related Topics, 8-12 October 1996, Budapest, Hungry.

[22] W.S. Waters, MCNPX User manual, version 2.1.5. TPO E83-G-UG-X-00001, November 14, 1999.

[23] Yu.V. Trebukhovsky, Yu.E. Titarenko, V.F. Batyaev, E.I. Karpikhin, R.D. Mulambetov, S.V. Mulambetova, G.N. Smirnov, K.A. Lipatov, A.B. Koldobsky, V.M. Zhivun, V.S. Barashenkov, H. Kumavat, S.G. Mashnik, and R.E. Prael. Double-Differential Cross Sections for the Production of Neutrons from Pb, W, Zr, Cu, and Al Targets Irradiated with 0.8, 1.0, and 1.6-GeV Protons. // Physics of Atomic Nuclei, Vol. 68, No. 1, 2005, pp. 3-15.

[24] Yu.N. Shubin et al., Cross Section Data Library MENDL-2 to Study Activation and Transmutation of Materials Irradiated by Nucleons of Intermediate Energies, IAEA, INDC(CCP)-385, Vienna, May 1995.

[25]Yu.N. Shubin et al., Cross Section Data Library MENDL-2p to Study Activation and Transmutation of Materials Irradiated by Nucleons of Intermediate Energies, Nuclear Data for Science and Technology (Trietse 1997), IPS, Bologna, 1997, v.1., p.1054.

[26] Experimental Nuclear Reaction Data (EXFOR), http://www-nds.iaea.or.at/exfor/exfor00.htm

Nuclear Data Section
International Atomic Energy Agency
Vienna International Centre, P.O. Box 100
A-1400 Vienna
Austria

e-mail: services@iaeand.iaea.org
fax: (43-1) 26007
telephone: (43-1) 2600-21710
Web: http://www-nds.iaea.org